Design, Development and Experimental Validation of a Lab-scale System for Rapid Rotational Molding of Functionally Graded Integral-Skin Cellular Polyethylene Composites

by

Isha K. Raktim

A thesis submitted to the
School of Graduate and Postdoctoral Studies in partial
fulfillment of the requirements for the degree of

Master of Applied Science in Mechanical Engineering

Department of Automotive, Mechanical and Manufacturing Engineering/University of Ontario Institute of Technology/Faculty of Engineering and Applied Science

University of Ontario Institute of Technology

Oshawa, Ontario, Canada

March 2020

THESIS EXAMINATION INFORMATION

Submitted by: **Isha Raktim**

Master of Applied Science in Mechanical Engineering

Thesis title: Design, Development and Experimental Validation of a Lab-scale System for Rapid Rotational Molding of Functionally Graded Integral-Skin Cellular Polyethylene Composites

An oral defense of this thesis took place on March 2, 2020 in front of the following examining committee:

Examining Committee:

Chair of Examining Committee	Dr. Martin Agelin-Chaab
Research Supervisor	Dr. Remon Pop-Iliev
Examining Committee Member	Dr. Ghaus Rizvi
Thesis Examiner	Dr. Sayyed Ali Hosseini, FEAS, University of Ontario Institute of Technology

The above committee determined that the thesis is acceptable in form and content and that a satisfactory knowledge of the field covered by the thesis was demonstrated by the candidate during an oral examination. A signed copy of the Certificate of Approval is available from the School of Graduate and Postdoctoral Studies.

ABSTRACT

An existing lab-scale experimental setup system, originally developed for a patented Rapid Rotational Foam Molding (RRFM) process, was re-designed, built, and its functionality was successfully experimentally verified. The primary objective of the research work presented in this thesis was to provide the physical means to introduce a physical blowing agent (PBA) into RRFM processing operations in order to enable seamless processing of functionally graded polyethylene foamed composites. The quality of the produced specimen were assessed in terms of: foam density, volume expansion ratio, cell density, and cell size. The experimentally obtained rotationally molded foam composites desirably exhibited gradual change in compositional quality and morphology from one region to another, which was correlated with the thermal gradient that exist within the rotational mold during the part cooling process. The newly designed functionally graded cellular composites can have wide applications in automotive, aerospace and marine industries.

Keywords: Rapid Rotational Foam Molding; Functionally Graded Cellular Composites, Physical bowing agent; Chemical blowing agent; Polyethylene;

AUTHOR'S DECLARATION

I hereby declare that this thesis consists of original work of which I have authored. This is a true copy of the thesis, including any required final revisions, as accepted by my examiners.

I authorize the University of Ontario Institute of Technology (Ontario Tech University) to lend this thesis to other institutions or individuals for the purpose of scholarly research. I further authorize University of Ontario Institute of Technology to reproduce this thesis by photocopying or by other means, in total or in part, at the request of other institutions or individuals for the purpose of scholarly research. I understand that my thesis will be made electronically available to the public.

Isha Raktim

YOUR NAME

STATEMENT OF CONTRIBUTIONS

The following experimental apparatus have been used in this thesis: Rotational mold arm assembly & carriage; Rotational mold translation mechanism; Cylindrical mold; Cylindrical mold interface port; Convection oven; and Single screw extruder. These components are part of the patented rapid rotational foam molding experimental setup designed by Remon Pop-Iliev, Christian Kimberly, and Abdalla Emad:

Pop-Iliev, Remon, Kimbery Christian, and Emad Abdalla. Rapid Rotational Foam Molding Process . United States of America Patent US 8,628,704 B2. January 14, 2014.

Skin material formulation for cylindrical mold presented in chapter 4 has been determined by Christian Kimberly as part of her Master's thesis work:

Kimberly, Christian. *Rapid Rotational Foam Molding of Polyethylene Integral-Skin Foamed Core Molding.* Masters Thesis., Univesity of Ontario Institute of Technology: ProQuest Dissertations, 2009, (pg.96).

I performed majority of the work toward re-designing the existing RRFM experimental setup to produce extrusion-assisted physical blowing agent foamed core. All experimental specimen creation and analysis of the same specimen have been conducted by me.

ACKNOWLEDGEMENTS

I am deeply thankful to my supervisor Professor Remon Pop-Iliev for giving me guidance and support for this thesis. His patience, and words of encouragement over the last two years have given me motivation throughout my research project. I would also like to give my deepest appreciation to my supervisor for allowing me to pursue this research topic and providing me with my first employment opportunity right after completing my undergraduate degree. My enrollment into the graduate program would not have been possible without professor Pop-Iliev's help and support. I am also greatly thankful to Professor Pop-Iliev for proving financial support for my research project and allowing me to attend multiple conferences throughout North America to present my research work.

I am also greatly thankful to Professor Ghaus Rizvi and Dr. Carlos Quizano for providing training for polymer characterization equipment. I would also give my thanks to my colleagues in the manufacturing lab, Utkarsh, Pedram Karimipour, Wingyi Pao (Roxana), Muhammad Tariq Abdul Samad, Nabeel Ahmed Syed, and Ashique Baten for always helping me no matter how hard the task.

Finally, I would like to give thanks to my parents Sayeda Banu Moni and Mohammed Kasem for being patient with me throughout my research project. They have given me their unconditional love and support all my life.

TABLE OF CONTENTS

LIST OF TABLES

CHAPTER 3

CHAPTER 4

LIST OF FIGURES

CHAPTER 1

CHAPTER 2

CHAPTER 3

CHAPTER 4

CHAPTER 5

LIST OF ABBREVIATIONS AND SYMBOLS

RRFM	Rapid Rotational Foam Molding
RFM	Rotational Foam Molding
PE	Polyethylene
PP	Polypropylene
LDPE	Low Density Polyethylene
LLDPE	Linear-Low Density Polyethylene
LMDPE	Linear Medium Density Polyethylene
HDPE	High-Density Polyethylene
MFI	Melt Flow Index
SCF	Supercritical Fluids
QFD	Quality Function Deployment
PVDF	Polyvinylidene Fluoride
PTFE	Polytetrafluoroethylene
CFC	Choloroflurocarbon
PLA	Poly(lactic) Acid
HoQ	House of Quality
ΔP	Pressure Drop
VER	Volume Expansion Ratio
ρ_{FOAM}	Foam Density
ρ_P	Pure Polymer Density
CBA	Chemical Blowing Agent
PBA	Physical Blowing Agent
V_{FOAM}	Foam Volume
V_i	Initial Pure Polymer Volume
τ	Shear Stress
$\dot{\gamma}$	Shear Strain Rate
W_s	Sample Weight

V_s	Sample Volume
N	Cell Density
n_{cells}	Number of Cells in 1 cm^2
$D_{average}$	Average Cell Diameter
SEM	Scanning Electron Microscopy
T_g	Glass Transition Temperature
RPM	Revolution per Minute
FGM	Functionally Graded Materials
FGF	Functionally Graded Foam
FGFC	Functionally Graded Foamed Core
η	Polymer Melt Viscosity
Ne	Newton Number
Re_D	Reynolds Number of the Polymer Melt within a Tube with Diameter 'D'
n_{ME}	Number of Mixing Elements
pop	Operating Pressure
D_{ME}	Diameter of Mixing Elements
DTG	Derivative Thermogravimetric
TGA	Thermogravimetric Analyzer
DSC	Differential Scanning Calorimetry
T_M	Melting Temperature
T_C	Recrystallization Temperature
RRFGFM	Rapid Rotational Functionally Graded Foam Molding
TRIZ	Theory of Inventive Problem Solving

Chapter 1. Introduction

1.1 Preamble

Functionally graded integral-skin cellular polymeric composites represent a unique next-generation class of advanced lightweight multi-constituent and multi-phase engineering materials. They can be deliberately engineered with spatially varied gradients of composition that is essentially governed by the inhomogeneous, interchanging, or adjacent solid and cellular macro, micro, or nano morphological structures. The existence of this morphological non-uniformities introduces specific advantageous material properties that vary smoothly and continuously in preferred directions or orientations. Hence, the resulting integral-skin cellular systems can be intentionally designed for specific purposes and practical applications in various scientific and technological fields where having varying properties in different regions of a single component is a requirement, such as aircrafts, combustion nozzles, gas turbines, energy conversion cells, biomaterials, etc. In spite of their obvious importance and wide applicability, the current state of knowledge in materials selection, fabrication, characterization, analysis, modelling and processing methods for functionally graded cellular polymeric composites is quite limited, compared to analog metal-based systems, and further research focusing on identifying the fundamental structure–property relationships and challenges in their fabrication is absolutely necessary.

Rotational molding is a traditional four-step plastic processing technology that is distinguished by its unique capability to fabricate very large-sized, hollow, single-piece, and seamless articles with quite intricate shapes, that can even include minor to moderate undercuts and/or double walls, while using relatively inexpensive molds. It is truly a unique plastic processing technology for which uniqueness direct replacement alternatives do not exist yet. A recently developed and patented melt extrusion-assisted rotational foam molding process, referred to as Rapid Rotational Foam Molding (RRFM), which has been instrumental in significantly reducing the disadvantageously lengthy processing cycle times and the energy consumption of rotational molding operations. RRFM also provides a dramatic improvement of the controllability of the process and widens the window of feasibly implementable materials. By design, in RRFM, the shaping of the solid skin of the integral-skin cellular composite article is completely decoupled and independent from the formation of its foamed layer or core, which is eventually completely encapsulated by the skin. The fundamental innovation of the RRFM technology is the act of direct

introduction of extruded foam in real-time onto the hot internal surface of the non-foamed soft skin layer within a uni-axially rotating hot mold. The foamed core is being injected via a specially designed nozzle-to-mold interface port. It is eventually encapsulated and gradually and simultaneously solidified with the solid skin layer, which creates very strong solid skin-to-foamed core interface bonding between identical or compatible polyolefins. This, combined with the quite large gap in the related research literature reaffirms the urgent need to conduct the presently proposed research.

1.2 Technical Classification

1.2.1 *Functionally Graded Materials*

Functionally graded porous materials are a special class of functionally graded material (FGMs) where the pore size or the cell density have a gradual variation depending on functional requirements. The deliberate production of these types of heterogeneous porous materials have applications in artificial tissue engineering, impact absorption, and in aerospace industries (Sun, et al. 2010, Mahmood and Akinlabi 2017).

Functionally graded materials are characterized by their gradual change in composition from one region to another (Figure1.1a). In traditional composite materials, a distinct boundary interface is present between two different material layers (Figure 1.1b). However, within FGMs the transition in material composition is gradual. The inhomogeneous compositional gradient within FGMs are engineered to meet various functional requirements. Functionally graded materials can also be found in nature in the form of human bones, teeth and plant material. In nature, FGMs are designed to meet multiple functional requirements. For example, in human tooth the outer layer consists of a wear-resistant enamel which gradually changes into more ductile material in the tooth core for better resistance to shock. The human long bone consists of a hard outer layer with a porous inner layer that has a gradual change in pore size toward the core of the bone (Mahmood and Akinlabi 2017).

The need for functionally graded materials originated in the aerospace industry in Japan. A special type of composite material was required which would have been subjected to a substantial temperature gradient. A traditional composite material always failed at this task and the location of failure was usually at the boundary region of two different materials. The failure resulted from

stress concentration and separation between the layers due to differences in thermal properties of the two materials. After modifying the boundary interface into a gradual compositional change from one material to the next, the problem was resolved. In modern engineering application FGMs have expanded to fields beyond thermal shielding. For instance, high impact resistant material in the military to functionally graded foams in the thermoplastics industry (Mahmood and Akinlabi 2017).

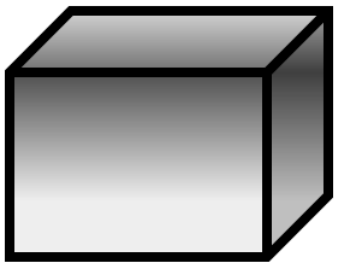

a) Functionally graded material with gradual change in composition.

b) Traditional composite material with distinct boundary interface.

Figure 1.1: Functionally graded material vs Traditional Composite material.

1.2.2 *Functionally Graded Porous Material*

Functionally graded materials can be found with a variety of morphologies, from changing porosity to heterogeneous distribution of microstructure within the bulk volume. The engineered part can be designed for changing chemical, mechanical, and thermal properties. The three major groups within FGMs are chemical composition gradient, microstructure gradient and finally, porosity gradient. Functionally graded porous materials are characterized by its gradual change in porosity across the length of the material (Mahmood and Akinlabi 2017).

The porous structure can be varied according to is shape, size and density within the bulk volume. This non-homogenous structural quality makes this type of FGM ideal for bio-medical application. Artificial tissues can replicate natural tissue structure and promote successful human cell attachment. The porous structure will reduce the weight of the implant while maintaining structural strength (ex. artificial bones, hip replacement). By gradually changing the pore size, shock absorption property is improved from one region to the other. Also the thermal stresses are reduced with improved thermal insulation (Mahmood and Akinlabi 2017).

In the current plastics industries, functionally graded polymeric foam have received increasing attention for its high strength-to-weigh-ratio. The application of functionally graded foams is ideal for automotive, marine and aerospace industries for impact absorption characteristics compared with uniform foam (Sun, et al. 2010). The foams are light-weight with fine cellular and micro cellular structures. It is well suited for absorbing energy when the material goes through plastic deformation. However, the research in polymer foam has been focused on uniform cellular structure under various loading condition. Therefore, there is potential for producing a new class of functionally graded thermoplastic foam with an integral outer skin suitable for impact testing (Cui, Kiernan and Gilchrist 2009).

1.3 Thesis Purpose and Scope

In the plastic processing industries, it is crucial to minimize energy consumption and also at the same time produce articles with improved mechanical properties to remain competitive. In light of this economic reality, rotational foam molding process is not ideal for plastic processing because of long process cycle and high energy consumption. Over the last few years a new processing technique was developed to address the inherent disadvantages of rotational foam molding process. This new technology was named Rapid Rotational Foam molding process (RRFM) presented in Figure 1.2 (Pop-Iliev, Christian and Abdalla 2014). RRFM is a two-step process where the foam and the outer skin are produced through two separate operation. This new processing technique has drastically reduced the cycle time mean while improving foam binding with the outer skin. However, the RRFM process is still open to further improvement. In the current state, the foam is produced through a chemical blowing agent which can produce fine cellular foam. The novelty of the process is that the skin and the foam can be processed simultaneously to reduce the cycle time. An extruder is utilized to rapidly melt the polymer and activate chemical blowing agent premixed with the polymer. At a given set temperature above the melting point of the polymer the chemical blowing agent decomposes and releases gas into the polymer melt to produce the foam within the barrel of the extruder. The foam is directly injected into a hot mold while the outer skin at the mold interface remains soft allowing the foam to penetrate into the skin layer and create a strong bond. This process will be presented with greater details in Chapter 2 (Pop-Iliev 2011).

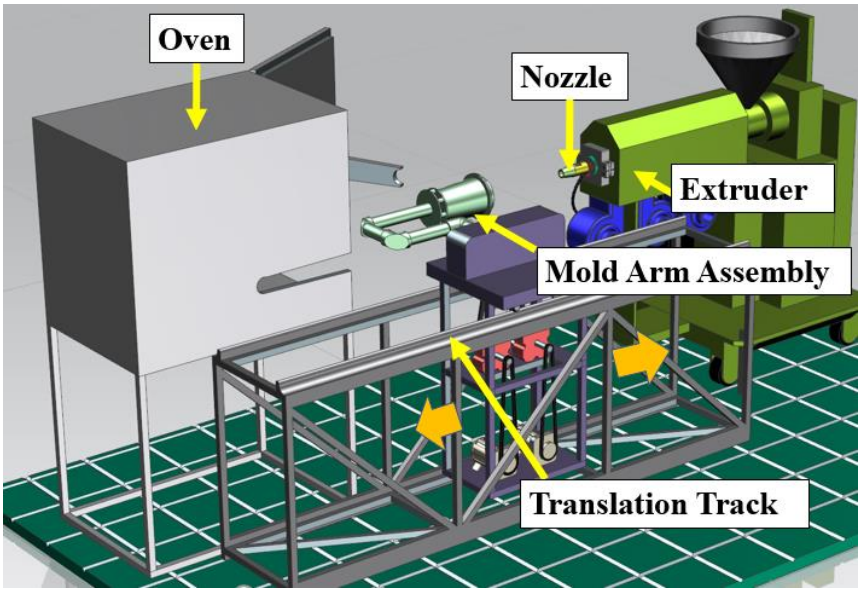

Figure 1.2: Rapid Rotational Foam molded experimental setup.

As it is well known, it is possible to produce microcellular foam utilizing a physical blowing agent (PBA) in extrusion processing (Srinivas, et al. 2002). Thus eventually, functionally graded foam can be produced with both fine and microcellular foam to improve the overall quality of roto-molded foam composites encapsulated with an integral outer solid skin. This thesis describes the undertaken design modifications of the RRFM process that were needed to enable introduction of physical blowing agents in the processing equation of rotational foam molding for the first time ever with a view of eventually enabling and achieving the manufacture of functionally graded integral skin cellular polymeric composites in RRFM.

In this context, the research work focused on the production of functionally graded foam with integral outer skin by modifying the existing RRFM experimental setup. The polymeric materials used for the experiments include various grades of Polyethylene (PE) resins, chemical blowing agent (CBA), PBA and other additives (e.g., talc). The new experimental setup utilizes supercritical carbon dioxide as a PBA to produce polymer foam and the functionally graded foam was produced through a combination of chemically blown foam and physically blown foam, either simultaneously or in series. The successful creation of functionally graded RRFM composites can lead to numerous new industrial applications where lightweight yet strong functionally graded components with unique structural morphologies and thermal and acoustic insulation capabilities are demanded such as in the automotive, marine, and the military sector.

1.4 Thesis Methodology

The design process for the new experimental setup will employ Quality Function Development (QFD) tool. This process will utilize House of Quality to identify the engineering specifications necessary to satisfy a customer's needs for functionally graded foam production. Multiple concepts will be generated for concept evaluation. A purge table will be used to select the most suitable concept for final experimental setup design. After the completion of the experimental setup, feasibility analysis will be performed based on the theoretical knowledge for functionally graded foam production with physical blowing agent.

The new experimental setup has been designed to plasticize various grades of polyethylene resin with a single screw extruder and pump the plastic melt into a heated mixing chamber where pressurized supercritical CO_2 gas is injected to dissolve into the molten polymer. The mixing chamber employs helical blades to enhance the mixing process to form a single-phase gas laden polymer solution. The solubility of the supercritical gas within the polymer resin is maintained through external heaters and a cooling system. The solution pressure is maintained only through the extruder's screw RPM. Rapid pressure drop at the mixing chamber die exit initiates phase separation and creation of the foam. Initially, the extruded foams were rapidly cooled on their own to evaluate the initial design of the experiment setup's ability to produce PBA-based foam. The extruded foams were processed at three different temperatures and at two gas injection rates to systematically compare the differences in cell morphology.

The experimental results revealed that cell density within a given resin can be increased by increasing the gas injection rate. Higher processing temperatures reduce the cell density due to cell coalescence. However, extrusion grade linear low-density polyethylene (LDPE) processed at 135°C with 1wt% and PBA produced the best quality foam with over 1 million cells per cubic cm. The cellular morphology within the foamed core was controlled by varying the CBA content, the content of talc (nucleating agent), the processing temperature and the PBA gas injection rate. High density polyethylene (HDPE), moisture resistant high-density polyethylene sHDPE, & LDPE polyethylene resins have been utilized to produce the foamed core and LLDPE resin was used for the integral outer skin. The quality of the foam was varied by gradually modifying the gas injection from 5 ml/min to 2 ml/min during the extrusion process. A separate attempt was made by gradually increasing talc content within sHDPE resin from 1wt% to 3wt% at different processing

temperatures. A further attempt to modify the cell morphology within LDPE resin was done by gradually increasing the Celogen OT™ content from 0.5wt% to 2wt% while using a physical blowing agent.

1.5 Thesis Contribution

Rotationally molded foam production with a physical blowing agent has never been achieved in previous work. Further, functionally graded foam production for the RRFM process with a physical blowing agent is a completely new processing technique. The successful implementation of the current work will yield highly desirable functionally graded composite material for wide variety of engineering applications.

1.6 Thesis Outline

The preceding sections of this thesis will demonstrate how the tasks presented above have been achieved with the final production of functionally graded PE foam with integral PE outer skin.

In Chapter 2 scholarly literature, previous and current research work along with theoretical background related to rotational foam molding process is presented. Also, this chapter gives detailed description of PE, foaming mechanism with physical blowing agent, and functionally graded foaming process. Along with the design process, and characterization technique of PE foam is also given in detail.

In Chapter 3 the complete design process for the new experimental setup is presented. A detailed House of Quality (HofQ) assessment is conducted determine a set of engineering specification for PBA foam production. In the following sections a decision matrix is utilized to select a concept from the multi-concept generation phase. All analytical and simulation data is presented for the final lab-scale setup. Finally the completed experimental setup is presented with detailed description.

Chapter 4 presents the experimental procedure and the preceding experimental steps for PBA foam production. This chapter also includes the operating conditions and experimental steps for functionally graded foam production utilizing talc as the nucleating agent for the PBA. For comparison this chapter will also present the processing steps for functionally graded foam production with integral outer skin by utilizing CBA and PBA concurrently.

Chapter 5 presents the characterization steps for the PBA foam with X-ray tomography, digital microscope, and scanning electron microscope (SEM). The quality of the rotational molded foam composites are determined according to volume expansion ratio, cell density, average cell size and foam bonding with the integral outer skin.

The final Chapter 6 presents concluding remarks and future desirable improvements of the new experimental setup for future research work.

Chapter 2. Theoretical Background and Literature Survey

2.1 Rotational Molding

2.1.1 *Conventional Rotational Molding Technology*

Conventional rotation molding operation has been utilized to produce large hollow parts unsuitable for injection molding such as water storage tanks. The rotational molding process has four distinct stages: mold charging and closing; mold heating; mold cooling; and mold opening and part removal. The mold rotates simultaneously in two axes, vertical and horizontal. For this reason, the rotation is referred to as bi-axial rotation. Rotation in two axis ensure even coating throughout the interior surface. The plastic articles produced using the rotational molding process are seamless and with uniform thickness. Since the core of the mold is exposed to atmospheric pressure, the mold doesn't have to be designed to withstand high pressure. At an industrial scale, about 85% of all rotomolded parts are produced from PE which includes linear-low density-polyethylene (LLDPE) and high-density-polyethylene (HDPE) (O'Connor 2003).

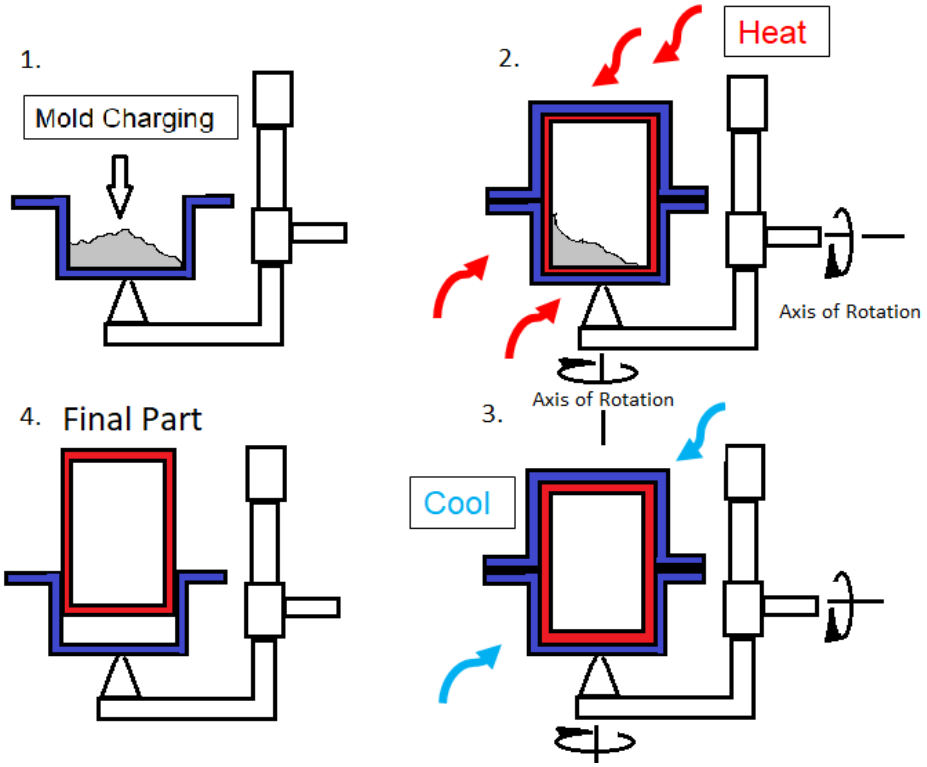

Figure 2.1**:** Rotational molding process for the production of a hollow part.

The rotational molding process was developed to produce hollow plastic parts in the 1940s. The heating, shaping and, cooling process all take place within the mold before the final part is

extracted. As presented in Figure 2.1, the mold is charged with a predetermined amount of polymer powder before the mold is prepared for the heating cycle. Since the entire process is carried out in atmospheric pressure, the cost of mold manufacturing is significantly lower than high pressure molds. In the heating cycle, the mold bi-axially rotates as the powder melts and sinters on the interior mold surface to form the hollow plastic part. After the formation of the hollow part the mold is cooled gradually back to room temperature before the part is extracted. Rotation molding process is ideal for producing parts with complex shapes, large size that are too expensive for injection molding. The process can be very economical for producing low production items (R. Crawford 1996).

The rotational molding process can also be used for the production of thermoplastic foam in conjunction with an integral outer skin. The process will be explained with more detail in the following chapters. In quick summary the foaming process takes place after the formation of the skin to fill the hollow cavity of the mold with foam. It is the focus of the thesis paper to present a novel processing technique for the production of functionally graded foam with the implementation of a modified rotational molding process (R. Crawford 1996).

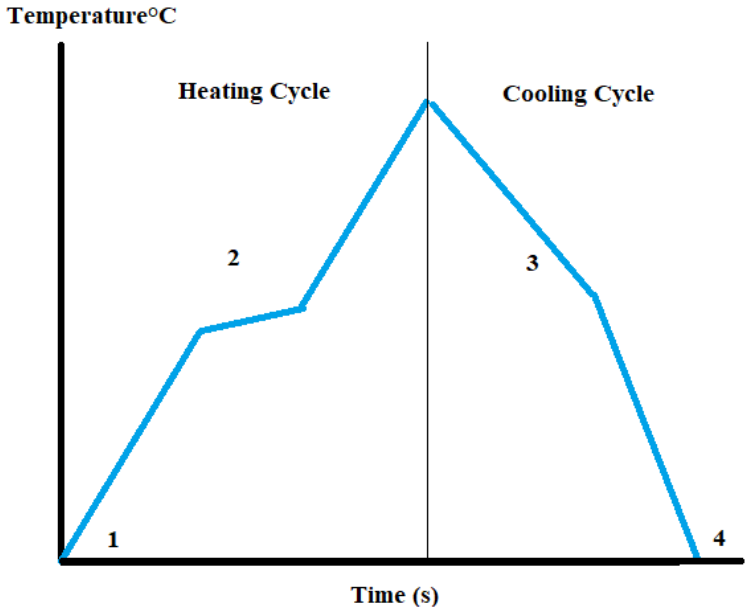

Figure 2.2: The thermograph of a rotational molding temperature cycles (Ogila, et al. 2017).

A typical thermoplastic thermograph is represented in Figure 2.2. Initially the mold is charged with thermoplastic powder at room temperature at point 1. As the temperature increases

the semi-crystalline polymer powder starts to melt which corresponds with the initial plateau at point 2. After the plateau the temperature climbs rapidly as the powder starts sintering and forming the outer skin. Small air bubbles can be observed within the polymer melt at this point. The temperature reaches its peak point after the formation of the outer skin and disappearance of air bubbles. The heating is terminated while the mold maintains bi-axial rotation. The mold can be cooled with variety of methods, however the most popular method for cooling is forced air convection. As the temperature decreases the polymer-melt will start recrystallizing, corresponding with a small plateau on the thermograph. The part solidifies after the completion of recrystallization and the cooling process continues until the mold reaches room temperature when the part can be extracted from the mold. On the average, the entire rotational molding process can require 50 – 90 minutes (Ogila, et al. 2017).

The surface finish of a rotomolded part primarily depends on the particle shape and size, and temperature profile of the mold surface. High quality surface is often difficult to achieve with the rotational molding process since the part has lower thermal stability, making it susceptible to deformation and thermal degradation after long heating cycle. This may result in the onset of thermal degradation, making the part appear brownish in color. However, if the heating cycle is too short it results in reduced mechanical strength due to the presence of air bubbles within the part. It is for this reason that extensive temperature control of the mold is necessary to minimize warping of the part (Ogila, et al. 2017).

A typical rotational mold rpm can vary between 4-20 rpm depending on the size of the mold. The initial flow of the powder within the mold depends on the mold surface roughness and the polymer particle size. Two types of flow are possible within the mold during the heating cycle (Figure 2.3). Initially it was assumed because of the low friction between the mold surface and the particle, the powder can slip easily. As the mold rotates and the friction force can no longer counter gravitational force the entire bulk of powder slips along the interior surface of the mold. However, in a real rotomolding operation the particles that are in contact with the mold surface tend to be lifted due to the rotation of the mold. As the angle increases the particles detach from the surface and tumble down the powder surface of the resin. A variation of this type of flow is referred to as

avalanching when the entire bulk amount of the powder material is lifted by the mold. This type of flow is common for both squared egg particle and disc shaped particles (Ogila, et al. 2017).

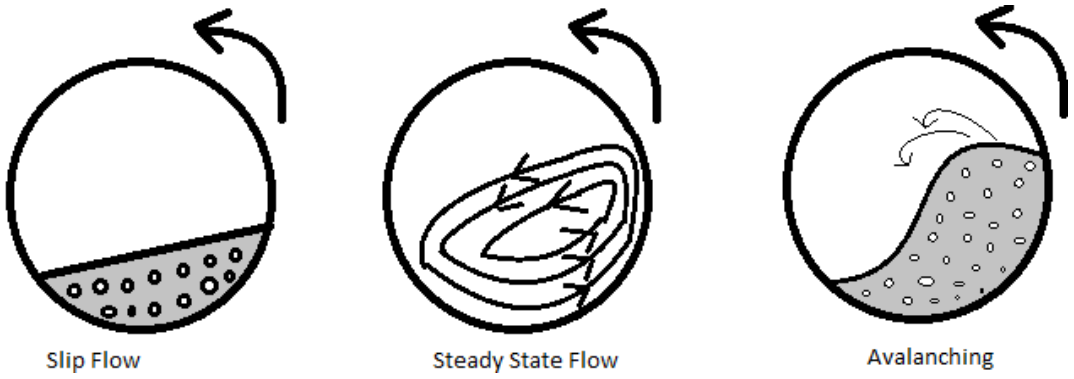

Figure 2.3**:** Powder resin flow within rotational mold (Ogila, et al. 2017).

2.1.2 *Advantage of Rotational Molding Process*

The molds used for the rotational molding operation can be inexpensive since the entire process is carried out at atmospheric pressure. High strength metal is not required and the molds are usually made from cheaper grades of aluminum. It is possible with newer iteration of designs to operate different mold shapes and types simultaneously on a machine with multiple arms. Plastic parts with complex geometry can be produced more easily compared to injection molding process, especially for large complex shaped parts that are too expensive for injection molding operation. It is also possible to manufacture parts with highly detailed surface finish depending on the polymer particle size and the surface polish of the mold (R. Crawford 1996).

2.1.3 *Disadvantage of Rotational Molding Process*

The price can be considerably higher to produce polymer powder rather than pellets. Usually polyolefins like PE can be purchased as pellets not suitable for rotational molding process. Especially designed grinding tools are necessary to convert the pellets to powder. This additional step increases the cost of material for businesses. The rotational molding process is inherently lengthy therefore, large production of smaller parts is not suitable. Also, the unloading process for parts with complex shapes may be cumbersome or labor intensive. Parts that have bosses and solid ribs are difficult to manufacture with rotational molding operation. It is therefore difficult to incorporate geometrical features (e.g., ribs) that can add structural stiffness to the hollow part (R. Crawford 1996).

2.1.4 *Current State of the Art of Conventional Rotational Molding*

Rotational molding technology is favored over other plastic processing techniques for its low capital cost. It is ideal for small businesses to remain competitive and still produce high quality articles. Over the last few decades rotational molding process has matured through improved process control. Most often new technological innovation are observed at research institutions, such as Queen's University in Ireland. Where the temperature of the mold cavity can be monitored directly. This new technology was developed in the 1990s and this system is currently available for purchase through many American industrial suppliers. By directly monitoring the mold air temperature it is possible to control the temperature at a given area of the mold through external heaters (Mapleston 2008).

In the next area of development, a company from Italy Caccia has developed PLCs for direct process control for four caracal rotational mold assembly. Which improves process repeatability to produce parts with identical surface finish and reduce wasted material. Also, through recirculating hot air in the oven improves the hating efficiency of the mold and an improved cooling fan system has reduced the cooling time by 20% (Mapleston 2008).

A company also based in Italy has developed a machine Persico's Leonardo which does not utilize an oven for heating or a traditional cooling system. The mold itself has heating system integrated into the mold walls. The temperature can be controlled through pumping hot or cold oil through the walls of the mold. Even though the mold can be more expensive, greater degree of process control and a more efficient heating and cooling is possible. The entire system is automated with built in vents allow the part to cool down faster after its formation (Mapleston 2008).

2.2 Rotational Foam Molding

There are two major groups of polymer foams: open-cell and closed-cell. In an open cell structure, the cell faces are open allowing air to pass through. Thermoplastic foams are closed-cells, where each cell is completely enclosed with an inner face. The cell walls of closed cells foams are usually stronger than typical open cell foams such as poly-urethane foams. A particular type of foam is identified by its relative density *R*, given in Equation (2.1). Where ρ_f is the foam density and ρ_P is the polymer density. A typical virgin thermoplastic material can have a density range from 900 to 1200 kg m^3. In this context *R* is the volume fraction of only the polymer material

within the foam. Therefore, porosity fraction is defined by 1-*R*. A low-density foam has a porosity fraction less than 0.1. However, through injection molding operation typical foam density can reach between 0.4-0.8 (Mills 2007).

$$\boldsymbol{R} = \frac{\boldsymbol{\rho_f}}{\boldsymbol{\rho_P}} \tag{2.1}$$

The formation of polymer foam initiates while the polymer is in its liquid state. Early stage bubble growth can be observed throughout the bulk volume. The initial bubbles are spherical in shape since the surface energy between the gas bubble and the liquid polymer is the lowest for spherical geometry. As the bubble continues to grow it comes into contact with neighboring gas bubbles distorting its spherical shape. The faces are planer between common cell walls, however curved surfaces are present wherever the bubble is in contact with the liquid polymer. If the faces within the closed cell collapse it becomes an open-cell foam. However, for thermoplastics the cells remain closed as the polymer solidifies (Mills 2007).

Polyolefins are the most commonly used thermoplastic in commercial applications. The two types of polyolefins are polyethylene (PE) and polypropylene (PP). Although PP has a higher melting point, but both are semi-crystalline polymer. Polyolefins have been utilized for foaming application since the 1967. Polyolefin foams can be extruded with fine cells (<100 μm), in sheet or tube form with specially designed dies. It is possible to combine polyolefin foam with rotational molding process to produce a new class of functionally graded foam with integral outer skin (Mills 2007).

2.2.1 *Single-step rotational foam molding process*

Figure 2.4: Schematic of the single-step integral-skin rotational foam molding process to overcome the structural stiffness issue, it is possible to manufacture multilayer rotomolded parts. One popular method is to increase the mechanical strength of the hollow part by introducing a foam layer or core in the empty cavity. Processing of this type of part is referred to as single-step rotational foam molding process. Through this process, it is possible to produce a part with homogenous foamed core (Pop-Iliev and Park 2003). This processing method involves charging the mold with a predetermined amount of non-foamable skin material and foamable resin which already contains the chemical blowing agent (CBA). The mold is transitioned into the oven and heat is applied while the mold rotates bi-axially. When the mold temperature reaches above the melting point of the non-foamable powder, it will sinter together to form the outer skin. The mold temperature is kept constant above the melting point of the non-fomable powder to allow the skin to form without activating the chemical blowing agent (position 2). After the formation of the outer skin the temperature of the mold is raised higher to reach the activation point of the chemical blowing agent. The CBA will release gas inside the foamable resin causing the material to foam and create a layer on top of the solid skin or completely fill the mold cavity. After the foam expands and bonds with the outer skin, the heating process is terminated and the mold is cooled while maintaining bi-axial rotation (position 4). The rotational foam molded article is extracted from the mold after it reaches room temperature.

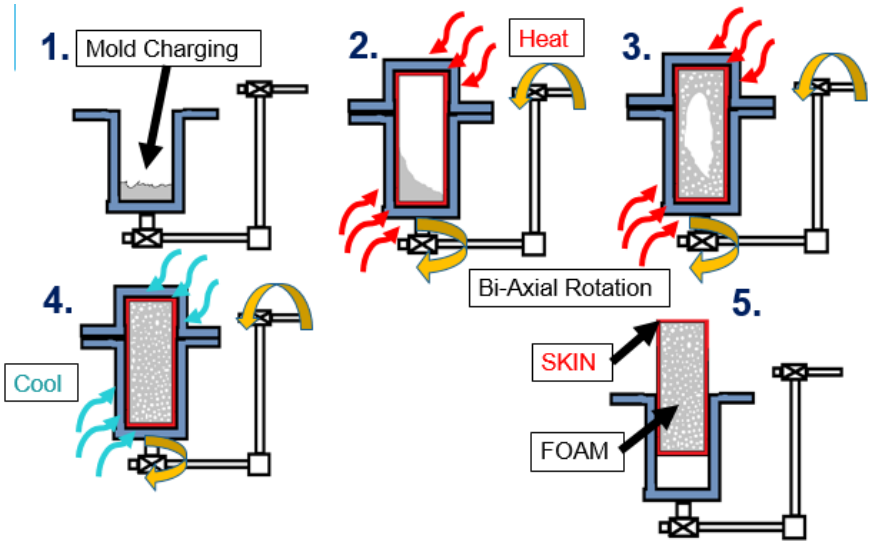

Figure 2.4: Single-step rotational foam molding process of skin encapsulating foamed core.

Over the years, extensive experimentation with single-step rotational foam molding with polyethylene was conducted. For the single step method, a special grade of LLDPE has to be utilized. A foamable resin, which is suitable for the rotational foam molding process, has been produced by extrusion melt compounding it with a CBA (Celogen OT™) using a twin-screw extruder. In their research work, the outer skin material was also rotational grade LLDPE powder. However, the melt compounded foamable resin melts at a higher processing temperature compared with the non-fomable powder. In all experiments uniaxial rotational mold was utilized rather than a biaxial rotational mold (Pop-Iliev and Park 2003).

It was reported that the foam expansion was not simultaneous at every point within the mold cavity. This was due to a temperature gradient within the mold which delayed CBA activation and the foam expansion process. It was also observed that foamable pellets that were near the mold surfaces decomposed and started to foam during the skin formation process. This phenomenon is known as foam skin invasion or penetration and it leads to skin thinning with uneven skin thickness. Foam penetration can be minimized by reducing the mold temperature during the skin formation process. Melt compounded pellets tend to stick to the inner surface during the skin formation process at higher skin processing temperatures. The CBA within the embedded pellets decomposes and can release gas causing premature foaming. It was also crucial to allow the foamed core to expand within reasonable amount of time depending on the mold size. The process is very sensitive to time since the skin material can degrade after long exposure to elevated temperature (Pop-Iliev and Park 2003).

2.2.2 *Thermoplastic Foaming with Chemical Blowing Agent*

A chemical foaming agent (CBA) is a highly refined chemical that will decompose at a given polymer melt processing temperature. Upon decomposition, gas is released causing the polymer to foam. Typical chemical blowing agents only decompose within a narrow temperature range. The development of various types of chemical blowing agents started in the 1950s. An ideal chemical blowing agent has the following properties: gas is released over narrow temperature range; residue from the decomposition is colorless and non-staining; residue should not be corrosive to metal processing tools and equipment; the chemical should not react with the polymer melt (Throne 1996).

2.2.3 *Visualization of Polyethylene Foaming with CBA*

The foaming mechanism of polyethylene can be visualized using a hot stage microscope. The chemical blowing agent utilized with polyethylene foaming experimentation is Celogen OT™ with particle size of 6 μm which decomposes between 150°C-160°C. In the experiment, Celogen OT™ was added to linear low-density polyethylene (LLDPE) in two ways: first method involved sandwiching CBA between two LLDPE films; the second method involved dry blending CBA with LLDPE resin before making a film with a compression molding machine. The two types of samples were heated and all the consecutive phases of the foaming process were visualized and recorded using the experimental setup that included a digital camera, an optical microscope equipped with the hot stage (Pop-Iliev, Dong, et al. 2007).

It was shown from the research work that there are four distinct phases for bubble formation, they are: prenucleation; bubble nucleation; bubble growth; and finally bubble shrinkage. In the prenucleation phase, the CBA particles start to decompose and tiny bubbles appear and disappear instantaneously. These initially short-lived bubbles had a size of 5-10 μm. It was observed that higher decomposition temperature can lead to longer lifespan for the short-lived tiny bubbles. As the gas concentration within the polymer melt increases bubble nucleation process initiates. The tiny bubbles that are sustained at the regions where CBA particles are closely packed together, serve as the primary sites for gas diffusion from the CBA decomposition. These growing bubbles cause the polymer to be stretched and resist the bubble growth. In the bubble growth phase, the decomposed gas diffuses into the growing bubble due to a pressure difference. However, eventually the bubble will start to shrink later during its life after a growth peak has been reached. It was determined from these observations that at higher processing temperatures the lifespan of the bubbles was shorter. Also, higher CBA concentration resulted in a longer life span and larger bubbles (Pop-Iliev, Dong, et al. 2007).

A mathematical model has also been developed to predict the effects of diffusion, viscosity, surface tension, and elasticity on cell growth and shrinkage. The model predicts that bubble life should decrease with increase in diffusion. The gas loss accelerates and therefore high rate of diffusion reduces bubble life. However, when the surface tension decreases it increases the bubble lifespan. Since surface tension resists bubble growth, the reduction in surface tension lowers the gas pressure in the bubble. The negative pressure within the bubble reduces gas diffusion into the

polymer melt. The model also predicts that by increasing the melt viscosity, the growth of the bubble and its eventual collapse is impeded (Xu, et al. 2005).

2.2.4 *Rotational Foam Molding of Fine Celled Foams*

Fine celled foam production with the rotational foam molding process was also investigated. Fine-cell foams are identified by their cell size being less than 100 μm. In previous experiments, Celogen OT™ was used as the chemical blowing agent for PE. The samples were prepared with 3 wt % Celogen OT™ melt compounded with LLDPE. The foam generation was observed under a hot stage microscope. From the observation it was evident that at certain regions CBA particle decomposition can immediately lead to the bubble formation. However, in other regions the decomposition of CBA particles increased the gas concentration within the polymer melt hindering the growth of neighboring bubbles. This phenomenon was short lived and the growth of the bubbles after the initial decomposition phase was governed by the viscoelastic effect of the polymer enclosing the bubbles. However, as the pressure decreased within the growing bubble the viscoelastic resistance was overcome through gas diffusion. After the CBA decomposition phase the bubble volume would reach its peak by depleting the gas in the polymer melt. This would create a pressure gradient and promoting gas diffusion out of the growing bubble. Eventually the bubbles would shrink and disappear unless they were frozen in place by lowering the temperature and solidifying the plastic. In single step-rotational foam molding process the long heating cycles can last longer than the lifespan of fine–cellular bubbles. This makes it difficult to produce fine cellular foam with roto-molding (Pop-Iliev, Xu and Park 2004).

2.2.5 *Polypropylene Foam Production with Rotational molding*

On the other hand, the processing technique for Polypropylene (PP) foam with rotational molding has been investigated. The PP resins for the foaming process are prepared by grinding the pellets into powder before dry blending with a suitable CBA (Celogen AZ™). The CBA/PP mixture was then melt compounded to disperse the CBA particle through-out the polymer melt. The extruded compounded material was immediately quenched underwater and pelletized to prevent premature CBA decomposition. However, for this rotational molding process the foam was produced without an un-foamed integral outer skin. The rotational mold is only charged with

a predetermined amount of melt-compounded CBA/PP pellets before starting the heating cycle (Pop-Iliev and Park 2002).

As the mold is heated, the pellets in direct contact with the mold surface will begin sintering to the wall. This process will continue as more pellets sinter together to form a layer of polymer melt on the mold wall. After the sintering process, CBA decomposition takes place as the mold reaches the CBA activation temperature and gas is generated within the polymer matrix. Bubble nucleation at the site of CBA decomposition initiates the foaming process. The nucleated bubbles continue to grow until the gas within the polymer melt starts to deplete. The bubbles eventually stabilize as the viscosity of the polymer is increased by lowering the temperature. The rotational mold is cooled after the foam has completely filled the cavity. Although the PP foam did not yield fine cellular structure for 3 and 6-fold of volume expansion, the foam quality compared to prior results was improved through the melt compounding method since the CBA particles were more evenly distributed (Pop-Iliev and Park 2002).

2.2.6 *Production of Integral Skin Polypropylene Rotational Foam Composite*

Rotational foam molded PP composites are advantageous in certain engineering application for having higher service temperature compared to PE. The production of single-charge integral skin polypropylene foam composites demonstrated an uninterrupted interface between the foam and skin layer. These types of composites are durable and much stiffer compared with polyurethane filled foam. Therefore, PP foam composites are suitable for harsh-weather resistant applications such as marine buoys and road barriers. The experimental study utilized high-melt strength PP resin for the production of low-density foam. Celogen AZ™ was used as the blowing agent since it has a decomposition temperature higher than the melting point of PP resins. However, unlike PE skin and foam combination, PP skin foam combination does not require two different temperature profiles. The increase in rotation speed of the mold is sufficient for providing different heating rate for the skin and the foam material. Therefore, PP skin formation is completely separate from the foam production process (Pop-Iliev, Lee and Park 2006).

2.3 Rapid Rotational Foam Molding Process

This patented process utilizes extrusion assisted foaming in conjunction with rotational molding to produce polyolefin rotational foam molded composites. The produced plastic article contains a foamed core encapsulated by an unfoamed solid outer skin layer (Figure 2.5) (Pop-Iliev, Christian and Abdalla 2014).

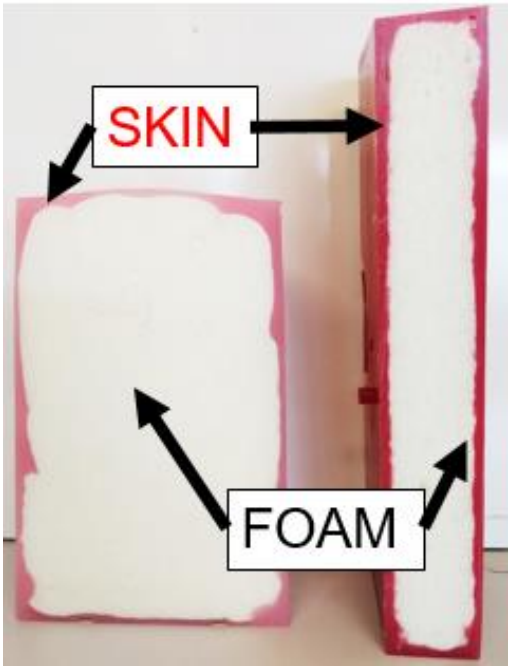

Figure 2.5: Rapid Rotational Foam Molded Composites.

2.3.1 *The Rational for Developing RRFM Technology*

The goal of any polyolefin foam production is to achieve high cell density with uniform cell size. In rotational molding process, foam production with CBA can be challenging. Where fine cells are difficult to retain due to the lengthy production cycle of the single charge rotational molding process. Another negative aspect of the single charge technique is that the skin material is exposed to higher temperature for long duration to ensure CBA decomposition is complete within all the foamable pellets. Long exposure to high temperature leads to the degradation of the skin material. The presence of a temperature gradient toward the center of the mold causes the foam within the core to reach the recrystallization temperature few minutes after the initiation of the cooling process. Which can lead to high degree of cell coalescence and cell shrinkage and

disappearance before reaching the freezing point of the polymer. This results in low cell density and larger cells toward the center of the foam. Bubble disappearance is further aggravated as the oxygen within the trapped air-pockets start dissolving into the polymer as the mold reaches high enough temperature. The dissolved oxygen reduces bubble diameter which contain nitrogen gas. As the bubble diameter decreases, pressure within the bubble increases creating a pressure difference between the bubble and the polymer matrix. This leads to nitrogen diffusion out of the bubble until the bubble disappears (Pop-Iliev, Christian and Abdalla 2014).

2.3.2 *Rapid Rotational Foam Molding Process*

The RRFM process by design forms the skin independent from the foaming process. In the initial step, the mold is charged with a predetermined amount of resin powder (Figure 2.6). The mold is then sealed and bi-axial rotation is initiated as the mold is translated into a preheated oven. The outer skin is allowed to form in an un-interrupted manner. Meanwhile, for the foam processing step, CBA powder is dry blended with plastic resin to ensure even distribution of blowing agent particles. After the dry blending step, the mixture is added into the extruder hopper for the foam extrusion process. The resin/CBA mixture is fed into the extruder chamber by the extruder screw. The processing temperature of the mixture is controlled by band heaters attached to the exterior surface of the barrel of the extruder. Rapid melt formation is achieved through a combination of frictional forces and heater elements. In a single screw extruder, the gap between the screw surface and the barrel decreases as the material moves further toward the extruder exit. This change in cross-section increases friction and generates heat to rapidly melt the plastic. The processing temperature across the length of the extruder is maintained in a manner to ensure that the plastic resin completely melts before the CBA decomposition. The decomposition of CBA takes place in the metering section of the extruder barrel. The release of gas produces a cellular structure within the polymer melt therefore producing plastic foam (Pop-Iliev, Christian and Abdalla 2014).

To receive the foam, the mold is translated out of the oven while the skin is soft. A specially designed interface port on the mold is removed. Since the skin coats all of the interior surface of the mold, a portion of the skin material remains attached to the interface port after the mold is opened. The interface port is placed inside the oven to ensure the skin material does not solidify on the port surface for the duration of mold filling. The foam is injected into the mold cavity through a nozzle as the mold rotates uni-axially. The injected foam bonds well with the soft outer skin to form an uninterrupted skin/foam interface. After a predetermined amount of time, the nozzle is translated out and the interface port is resealed to completely encapsulate the foamed core by the outer skin. The mold is cooled by forced convection as it rotates bi-axially. The finished RRFM composite is extracted after the mold temperature drops below the recrystallization point of the plastic (Pop-Iliev, Christian and Abdalla 2014).

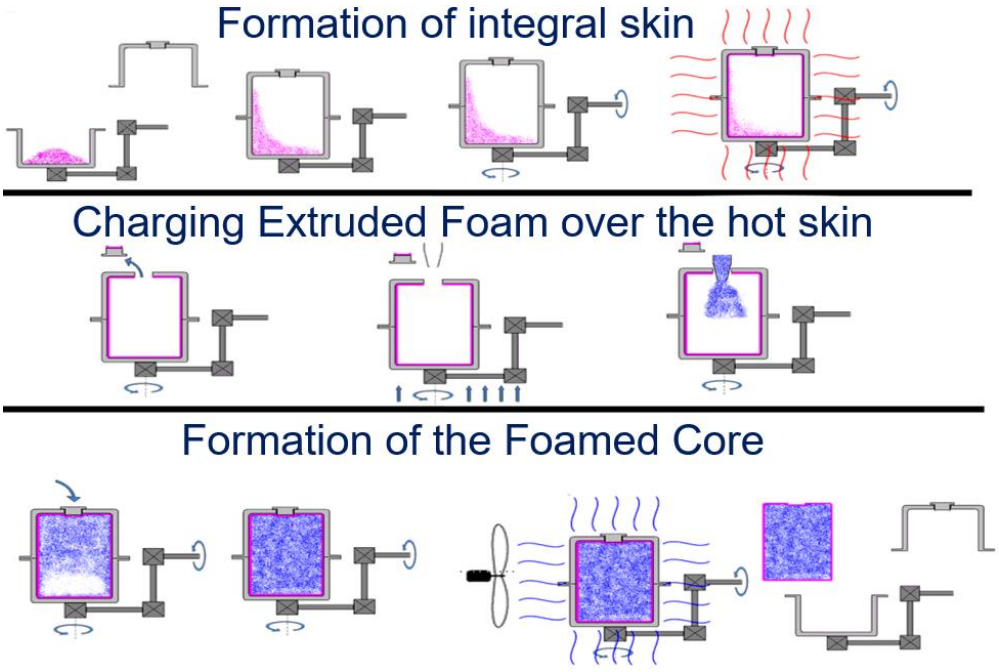

Figure 2.6**:** Rapid Rotational Foam Molding process (Pop-Iliev, Christian and Abdalla 2014).

2.3.3 *Rotational Molding Apparatus*

The primary apparatus of the RRFM experimental setup is the rotational mold assembly and the linear translation mechanism (Figure 1.2). The rotational arm carriage is supported on the track with rail wheels. The entire carriage can be translated linearly to bring the rotational arm from the oven to the extruder nozzle to receive the foam. The bi-axial motion of the rotational arm is individually controlled by two separate AC motors (Figure 2.7). The rotation about the x-axis is

accomplished by connecting the external hollow shaft to one of the motors with a chain and socket. However, independent gear boxes are used to reduce the input RPM from the motor to the external shaft. Rotation of the mold about the y-axis is achieved by connecting the secondary motor to an internal shaft housed within the external shaft through a separate chain and socket. Similarly to the first gear box, a separate gearbox is used to reduce the RPM from the second motor to the internal shaft. The drive system for the rotation about the y-axis utilizes three bevel gears to transfer the power through the arm assembly to the mold. The internal shaft assembly is concentric with the external shaft assembly (Pop-Iliev, Christian and Abdalla 2014).

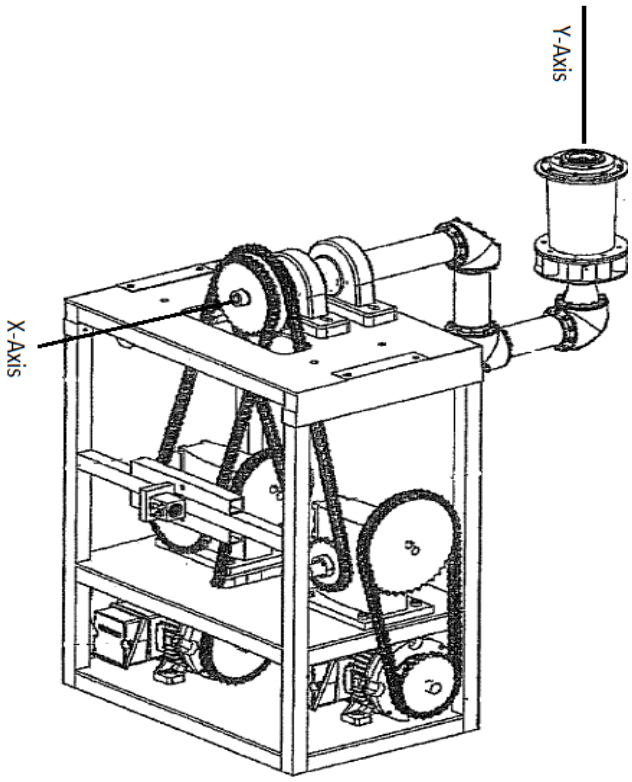

Figure 2.7: The rotational arm assembly and the drive system carriage (Pop-Iliev, Christian and Abdalla 2014).

2.4 Supercritical Fluids

2.4.1 *Physical Blowing Agent*

In previous sections, polymer foam was produced from the decomposition of CBA, which released gas into the polymer matrix as a result of its decomposition triggered by heat. In contrast, physical blowing agents are permanent gases, and certain volatile liquids. Permanent gases are considered natural foaming agents, for example carbon dioxide and nitrogen. Volatile liquids are manufactured from halogenated hydrocarbons or other petroleum byproducts (Throne 1996).

One of the most commonly used physical blowing agent for foam production is supercritical CO_2 for being a low-cost alternative to many volatile liquids. It is chemically inert, readily available, and environmentally friendly. Carbon dioxide is soluble in polymer melt at elevated temperature and pressure. Supercritical CO_2 is especially suitable for producing high density foam. Compared with other atmospheric gases, it has a low critical point (31°C and 1200 psi) and above this critical value, CO_2 exists as a vapor. Phase changes can affect the flow rate of the fluid and therefore, specialized pumping equipment is necessary to maintain the correct metering conditions (Throne 1996).

2.4.2 *Supercritical Fluids*

Supercritical fluid (SCF) exist as a gas or a liquid above the critical temperature and pressure of that particular fluid. At this state, the fluid has properties similar to both gas and a liquid. SCFs have a gas-like viscosity and a density similar to a liquid. The diffusion characteristic of the fluid is somewhere between a gas and a liquid. A SCF can easily diffuse into pours material and it can also act as a solvent and dissolve materials. The density of a SCF can be varied with pressure and therefore, the solubility of a dissolved substance within the fluid can be changed. Through this process separation of a substance from the solvent can easily be achieved. SCF are environmentally friendly compared to ozone depleting volatile organic compounds like chlorofluorocarbon (CFC). Supercritical fluids are also safe for the user and cost of disposal is cheaper compared to strong organic solvents (Adxchiri, et al. 2002, Goodship and Ogur 2004).

SCFs have many practical industrial applications in extraction, drying and cleaning. Extraction is a process where solid particles can be separated by utilizing a supercritical solvent. In this process supercritical gas extracts components from within a solid bed of substrate as it flows

over the material. The dissolved components within the SCF can be precipitated out by reducing the pressure and temperature. Sesame oil can be extracted from sesame seeds through this process without the risk of flavor loss. The active components of the sesame oil (sesamoline, sesamine, stances) are all soluble in CO_2 and they can be extracted at a significantly lower temperature compared to the traditional method. Supercritical CO_2 is also excellent for cleaning and drying porous materials. In conventional drying process heating can cause the narrow gaps within the porous material to collapse because of the capillary forces of the liquid. Since a supercritical fluid does not have any surface tension, it can easily pass through the gaps and remove unwanted residue without damaging the delicate cellular structure. Fatty acids can be removed from rice grain through this process and thereby shortening the cooking time by 30 percent (Brunner 2010, Zhang, Heinonen and Levanen 2014).

2.4.3 *Polymer Processing with Supercritical Fluids*

Supercritical carbon dioxide is used in the polymer processing industry for having a low critical temperature and high purity at relatively low cost. In atmospheric condition CO_2 is exist as a gas therefore, it can be easily removed after its intended use in plastic processing at atmospheric pressure. The critical point of CO_2 is well below the processing condition for injection molding and extrusion. This ensures that CO_2 always remains at supercritical state during extrusion and injection molding operation. However, it should be noted that supercritical CO_2 interact differently with amorphous polymers compared to semi-crystalline polymers. Amorphous material can dissolve a greater quantity of CO_2 than semi-crystalline materials. This is because CO_2 can only be absorbed into the amorphous region and not into the highly organized semi-crystalline region. Higher SCF concentration will also increase the melting temperature of the plastic and change its mechanical properties (Goodship and Ogur 2004).

This increase in SCF concentration results in greater amount of plastication leading to the reduction in melt flow viscosity. This is highly desired for very viscous material with high molecular weight. The viscosity can be reduced by increasing the temperature. However, at higher processing temperature material degradation is more likely. The rapid dissolution of supercritical CO_2 into the polymer melt reduce the viscosity while maintaining lower processing temperature. Therefore, material degradation can be avoided with the use of supercritical fluids (Nalawade, Picchioni and Janssen 2006).

Dissolved CO_2 within the polymer can also facilitate the uptake of catalyst and other modifiers during processing. Supercritical CO_2 is used as the particle carrier for modifying the material during batch processing or in extrusion. Research work is being carried out on polypropylene and poly(tetrafluroethylene) (PTFE) to modify the hydrophilic property. Monomers such as maleic anhydride has been successfully integrated onto PP by utilizing supercritical CO_2. The SCF does not act as a reaction modifier but rather it serves to distribute the reactive monomers more evenly throughout the matrix (Nalawade, Picchioni and Janssen 2006).

A major application of SCF is in the production of microcellular foam. The foam can be produced through batch processing, extrusion, injection molding, extrusion blow molding, and thermoforming. In relation to the quality of the foamed article, the strength of microcellular foam do not diminish significantly as the weight of the part decreases. This is advantageous for plastic manufacturers, as they save material cost without compromising quality. Currently research work is being done on solid state foaming processing. Which involves saturating a solid plastic article in a high-pressure CO_2 environment for few days at room temperature. After those few days the part is extracted and given a hot oil bath to generate microcelluar foam (Matuana 2008). The clear advantage of this process is that greater quantities of CO_2 can be dissolved into the core of the polymer matrix to give high cell density in the final product (Tomasko, et al. 2009).

2.4.4 *Solubility of Physical Blowing Agent within Polyethylene Melt*

Microcellular foam quality is dependent on the amount of dissolved gas present within the polymer melt prior to the bubble nucleation process. It is therefore important to determine the solubility of supercritical carbon dioxide in polymer melt at a given pressure and temperature. The earliest experimentation for solubility measurements involved observing the pressure drop within the polymer due to gas absorption. Later, vibrating reed method was developed to indirectly measure gas solubility as it is being absolved into the polymer melt. However, much more direct measurement of solubility was possible utilizing graviometric methods, which utilize a sensitive weight balance and quartz springs to measure the change in mass of a sample after gas uptake. It is also possible to use the graviometric method to observe the change in density of a gas/polymer solution. A platinum plate is submerged into the gas/polymer solution and the buoyancy force is measured. This buoyancy force represents the weight of the gas/polymer solution which has been displaced by the platinum. Therefore, the mass and the volume of the plate can be used to

determine the density of the solution (Funami, Taki and Ohshima 2007). It is also possible to measure solubility during foam extrusion. The melt pressure and temperature can be controlled between the die and the extruder and by observing bubble formation through an optical window to evaluate gas solubility (Chaudhary and Jhons 1998).

A novel method was developed by Chaudhary and colleagues to determine PBA solubility in polymer melt (Chaudhary and Jhons 1998). This method utilizes a magnetic suspension device (MSD). The equipment is highly sensitive to change in mass and it can operate at temperatures above 250°C and pressure of 4300 Psi. The high operating conditions allowed the researches to analyze solubility of three blowing agents (isobutene, nitrogen and carbon dioxide) in LDPE from temperature ranging from 110°C to 200°C and pressures up to 3000 psi. The results of the solubility experiments revealed that nitrogen has lower solubility in LDPE compared to carbon dioxide and isobutene at the same processing conditions. The solubility of carbon dioxide increased by increasing the pressure, and solubility decreased with increasing temperature. However, the decrease in solubility due to increase in temperature was not significant for carbon dioxide (Chaudhary and Jhons 1998). In fact, nitrogen also has lower solubility in high-density polyethylene (HDPE) at any given pressure and temperature compared with carbon dioxide (Sato, et al. 1999).

2.5 Microcellular Foaming Process with Physical Blowing Agent

2.5.1 *Rapid Single-Phase Polymer-Gas Solution Formation*

The production of microcellular foam was successfully accomplished at Massachusetts Institute of Technology (MIT) in the mid 1980's. Microcellular foams have cell density between 10^9- 10^{15} cells per cubic centimeter and average cell size of 0.1-10 µm. Microcellular foams can have improved impact strength and toughness compared with solid plastics. However, the continuous production of microcellular foam can present its unique challenges unlike the traditional batch processing method (Jacobs, Kemmere and Keurentjes 2008, Park and Suh 1996).

In batch processing, similar to solid state processing the polymer sample is saturated with high pressure carbon dioxide gas. After a certain period of saturation time the chamber is depressurized and the temperature is increased, leading to bubble nucleation and foam formation. As discussed in the previous sections, the gas solubility decreases when the sample temperature is

raised. This thermodynamic instability causes phase separation between the gas and polymer and micro-scale bubble formation. However, before the thermodynamic instability is initiated, it is crucial to form a single-phase solution between the gas and the polymer. In continuous foam extrusion processing the single-phase solution formation and the eventual cell nucleation process are integrated into one step (Park and Suh 1996).

In a typical batch processing method, the diffusion of gas is slow. However, for continuous foaming process gas diffusion has to be rapid. The nature of rapid solution formation through convective diffusion for continuous microcellular foam production was investigated by Park. The formation of microcellular bubbles with the extrusion process involves plastication, solution formation and microcellular nucleation. The extruder, through its screw motion and external heaters, completely melt the plastic before it enters the solution formation section. Carbon dioxide or nitrogen is injected in the melt polymer after the plastication section. In the single-phase solution formation section, mixing blades attached to the main screw shaft generate shear field as the screw rotates. This promotes gas diffusion into the polymer melt by convective flow. Also, a static mixer is used to further enhance the mixing operation which is placed downstream from the metering section of the extruder. Finally, thermodynamic instability is initiated after the static mixer as the gas/polymer solution pass through a rapid-heating nucleation device and eventually through a filament die (Park and Suh 1996).

The critical step for continuous foam production is the creation of a single-phase solution between the polymer and the gas. When gas is injected into the extruder, two phase polymer/gas mixture is observed. Eventually, the gaseous phase is stretched and separate into smaller bubbles due to the motion of the screw. This type of mixing is known as shear mixing and through this process single phase solution can be formed. The diffusion of gas into the polymer melt can be compared with heat transfer. Similar to high rate of heat transfer by forced convection, diffusion can also be increased through mass transfer. In the barrel of the extruder, recently plasticized polymer melt is brought into close contact with bubbles, which contain high gas concentration at the metering stage. The concentration gradient between the bubble and the polymer melt promote high rate of diffusion. This process is further enhanced since the diffusion sources (gas bubbles) are also in motion as the polymer melt is pushed through the barrel. When the mixture is moving toward the extruder exit it is replaced by newly plasticized material that continuously maintains

the concentration gradient and thereby promoting high rate of diffusion. The mixing blades on the screw shaft bring the gas bubbles close to the shear fields of the polymer by wiping action produced by the screw. Eventually all gas bubbles shrink and completely diffuse into the polymer matrix forming the single-phase solution. The solution will then enter the nucleation section, where thermodynamic instability is created by rapidly increasing the solution temperature and reducing the gas solubility resulting in the formation of micro bubbles. The microbubbles continue to grow in size until the polymer reaches its recrystallization temperature (Park and Suh 1996).

After the cell nucleation stage, the bubble will continue to expand and neighboring cells can merge and produce a more stable bubble with larger diameter. To overcome cell coalescence and maintain high cell density, the polymer melt has to be cooled to increase the melt strength before reaching the die. The extruded foam will continue to expand unless it is rapidly frozen. In order to minimize gas loss, the surface of the extrudate is cooled to its freezing point. However, the cooling rate has to be maintained in a manner to allow the bubbles to expand and grow to achieve the desired final foam quality. It is the increase in material stiffness that counters the growth and merging of neighboring bubbles (Sauceau, et al. 2011).

2.5.2 *Experimental Setup Design for Continuous Foaming with PBA*

Similar to the experimental setup presented by Park, Siripurapu and his colleagues designed an experimental setup for continuous foaming of polyvinylidene fluoride or polyvinylidene difluoride (PVDF) with supercritical carbon dioxide. A specially designed single screw extruder was utilized for the foaming process. The supercritical gas was directly injected into the barrel of the extruder at the metering section through an injection port. A pressure relief valve ensured constant gas flow from the syringe pump. The deep flights at the injection point maintained a region of low pressure and promoting gas flow into the barrel. The extruder was mainly involved in dissolving the gas into the polymer. However, a Saxton static mixer was placed after the extruder to increase gas/polymer homogeneity (Srinivas, et al. 2002).

The microcellular foaming was accomplished by utilizing a cooler, a nozzle, and static mixers within the die adapter. The complete dissolution of gas within the die adapter section was promoted by increasing the melt temperature above the extruder exit point. The cooling section was integrated into the experimental setup to lower the melt temperature and maintain uniform

cooling. At a lower temperature the melt strength of the polymer increases and minimizes cell coalescence and prevents gas loss during de-pressurization (Tsivintzelis, Angelopoulou and Panayiotou 2007). Thermodynamic instability is initiated at the die exit through rapid pressure drop and cell nucleation (Srinivas, et al. 2002).

It is also common to use tandem extrusion system for the foaming process, as presented by Wang and his colleagues for poly(lactic acid) (PLA) foam extrusion. In this setup the first extruder is used for plasticizing the PLA and later to disperse the gas into the polymer melt. A gear pump positioned between the first and second extruder provides melt flow rate control at a given temperature and pressure. The second extruder provides further vigorous mixing to promote complete gas dissolution into the polymer matrix. The heat exchanger lowers the mixture temperature before the filament die. The die provides enough resistance to maintain the desired solubility pressure to maintain single phase solution (Wang, et al. 2012). An alternative to the design is to position the gear pump after the second extruder to compensate for pressure losses from the extrusion line (Chauvet, Sauceau and Fages 2017).

In continuous PBA foaming operations, it is very common to directly inject the supercritical fluid into the extruder barrel. However, it is possible to directly inject the supercritical fluid after the extruder in a separate mixing chamber. Such work has been presented by Selvakumar and Bhatnagar on the production of polypropylene/carbon fiber composite foams. The experimental setup consisted of a single screw extruder followed by a mixing chamber and an injection nozzle. A syringe pump was used to inject pressurized gas into the mixing chamber through a metallic flow restrictor. The gas is dispersed into the melt polymer with the use of two SMK mixing elements positioned after the gas injector. A pneumatically controlled shut off valve remains closed to maintain the appropriate level of pressure during the gas metering stage (Selvakumar and Bhatnagar 2009).

2.5.3 *Die Design for PBA Foam Extrusion*

The purpose of a foam extrusion die is to control the pressure drop and pressure drop rates through its geometrical shape. The flow channel is designed to maintain uniform velocity at the die exit. Stagnation point must be minimized or eliminated, because melt stagnation increases residence time which leads to material degradation. Pressure drop across the length of the die

should also be minimized. As the friction forces from the viscous dissipation generate heat, it increases melt temperature and reduces melt strength. To overcome excessive pressure losses, the extruder has to provide greater drive force which may increase the equipment cost (Walter 2003). The pressure drop across the length of a capillary die is given by Equation 2.2. The residence time is given by Equation 2.4 and the pressure drop rate is obtained by dividing Equation 2.2 by Equation 2.3 (Lee, et al. 2008).

$$\Delta P = -2m\frac{L}{R^{3n+1}}\left[\left(3+\frac{1}{n}\right)\frac{Q}{\pi}\right]^{n} \tag{2.2}$$

$$t_{residence} \sim \frac{\pi R^2 L}{Q} \tag{2.3}$$

$$\frac{\Delta P}{t_{residence}} \sim -2m\left(3+\frac{1}{n}\right)^{n}\left(\frac{Q}{\pi R^2}\right)^{n+1} \tag{2.4}$$

In Equation 2.2 '*L'* represents the length of the die channel and '*R'* is the radius of the channel. The power law parameters for shear thinning of pure polypropylene (PP) are determined from a capillary rheometer at 190°C. This power law parameter can be found in the research work conducted by Lee et al. on die geometry on foaming behavior (Lee, et al. 2008).

Lee and colleagues conducted research work on the foaming behavior of gas laden PP at three different pressure points and three different pressure rates. The analysis was carried out by varying the pressure drop from 7- 21 MPa on a die with the same cross-section. However the die length varied for each pressure drop test. Overall nine different geometrical designs were used in three groups. Each group had the same die channel cross section which ranged from roughly 1 to 2 mm. The channel length was varied from 13 to 39 mm for the first group and 25 to 75 mm for the second group and 71 to 144 mm for the final group. This variation in length produced residence time ranging from 4.4E +1 to 1.93E +3 ms. The volume expansion and the cell nucleation process was observed at different CO_2 contents (1- 5wt%) (Lee, et al. 2008).

From the analysis four main conclusions were reported. The volume expansion ratio due to temperature was dependent on gas loss and melt stiffening, for gas concentration between 3-5wt%. The die pressure had less of an effect on the volume expansion. Nucleation within the same die group was negligible, as long as the pressure remained above the solubility pressure of the gas. It was also observed that the cell density increased as the pressure drop rate increased. However, the

cell nucleation behavior and volume expansion were similar within the same die group (Lee, et al. 2008).

In a similar fashion, Lee and colleagues investigated the nucleation behavior with various die geometry with polystyrene foam produced with carbon dioxide. Three die groups were used with pressure drop ranging from 14-27 MPa within each group. However, each die group had a constant channel cross-section from 0.5 mm for the first set, 0.8 mm for the second set, and 1.2 mm for the final set. In the first die set, the length varied from 3.4-7 mm. In the second die set, the length varied from 10-22 mm. In the final set, the length varied from 25-50 mm. The residence time varied due to the changing die length. However, the pressure drop rate remained constant for each die group (Xiang, Donglai and Pop-Iliev 2003).

The analysis of the die geometry revealed that regardless of CO_2 or talc content the cell density improved when the pressure-drop rate was higher. A large thermodynamic instability was critical factor for inducing large amount of cell nucleation and eventually leading to high cell density. However, when the die channel cross-section cannot be reduced any further due to manufacturing limitation, the gas content, talc content, and the melt flow rate needs to be modified to achieve high cell density. The nature of the melt flow and the variation in die pressure was controlled by the melt temperature and the channel geometry. However, the change in melt temperature and the change in die cross-section does not significantly change cell density. It was also common to observe large bubbles and phase separation if the die pressure was below the solubility pressure (Xiang, Donglai and Pop-Iliev 2003).

To further understand the pressure drop across the length of a die, Zhang and colleagues carried out experimental analysis on HDPE/ wood fiber mixture foamed with supercritical carbon dioxide gas. Pressure transduces were positioned across the length of a slit die to record the pressure drop across a die. The CO_2 content was varied between 1 to 3wt% percentages for the foam extrusion test. The operating pressure was kept above the saturation pressure at 135°C, 140°C, and 145°C to prevent phase separation at those operating temperatures. The reduction in pressure across the length of a die was linear regardless of CO_2 content. The initial pressure at the entry point of the die was highest for the mixture with the lowest CO_2 content. Also, with higher gas content in the solution shear viscosity was reduced. However, the shear viscosity increased as the operating temperature was decreased (Zhang, Rizvi and Park 2011).

2.5.5 *Microcellular Foaming Strategy with Polyethylene*

2.5.5.1 Challenges with Low-Density Foam production

The production of low-density microcellular foam (density: 50 kg/m^3) with inert gas can be difficult. The primary challenge is to control the initial cell nucleation process. In the nucleation stage, rapid drop in pressure initiates the formation of billions micro cells throughout the polymer matrix. The cell density can be improved by increasing the number of nucleation sites which is accomplished by maximizing the pressure drop rate. The next critical step is to control the cell density during the bubble growth stage. Cell coalescence reduce the overall cell density and this is suppressed during the growth stage by increasing the melt strength. This involves lowering the die temperature which increases the resistance to extensional flow of the cell wall as the gas diffuses into the individual cells. However, this process is not guaranteed to preserve the micro cell structure uniformly during extrusion. Therefore, uniform cooling is necessary to eliminate hot spots within the polymer matrix (Park, Behravesh and Venter 1998). Even though the die temperature plays an important role during the cell nucleation process, single phase solution must be created before the mixture reaches the die to ensure a homogenous distribution of nucleation sites (Kim, et al. 2010).

The final step is to control the volume expansion to produce the desired foam density. Low density microcellular foam is difficult to produce with CO_2 since it has high rate of diffusion due to its small size compared with long chain volatile hydrocarbons. As the cells grow within the extruded foam the cell walls become thinner and speed up gas diffusion out of the foam. This is further exacerbated at higher processing temperature. The growth of the foam is reduced as less gas is available for cells to expand. This causes the growing cells to collapse leading to foam contraction before polymer recrystallization. One method to prevent gas loss is to freeze the skin of the extruded foam. The lower temperature increases the melt stiffness and prevents foam contraction. Therefore, cooling the polymer melt will not only reduce cell coalescence but also reduce the rate of gas diffusion out of the foam (Park, Behravesh and Venter 1998).

2.5.5.2 Foaming Strategy with LDPE

In any given continuous PBA foaming operation, it is crucial to induce rapid thermodynamic instability at the die exit. As previously summarized in the previous sections, supercritical carbon

dioxide is an excellent blowing agent for microcellular foam production. It is advisable to dissolve the highest quantity of CO_2 into the polymer matrix just below the solubility limit at a given temperature and pressure. This will ensure maximum amount of nucleation sites after the thermodynamic instability. It is equally important to achieve a high degree of mixing between the gas and the polymer melt in the mixing chamber with adequate mixing time and high pressure to dissolve the CO_2. After which the single-phase solution is subjected to high pressure drop rate at the die to produce the foam (Park, Lee, et al. 2006).

Park and colleagues discovered that the cell population can be increased by utilizing talc. Talc is the common name for hydrated magnesium silicate $Mg_3Si_4O_{10}(OH)_2$ (Park, Lee, et al. 2006). It is most commonly used as a nucleating agent for polymer foaming process (Shakoor and Thomas 2014). The cell nucleation takes place at the boundary layer between the talc particles and polymer melt. In the boundary interface the activation energy for bubble formation is lower and therefore, cell nucleation is more likely to occur at these regions (Park, Lee, et al. 2006). Talc particles have an added benefit of increasing the thermal stability of the polymer (Wang, et al. 2013). However, with increasing the talc content gas loss also increases at elevated temperature (Naguib, Park and Lee 2003).

In previous research work, Park and colleagues reported that high CO_2 concentration doesn't improve the cell density significantly even by increasing the talc content. Therefore, the talc content should not exceed 2wt%. Beyond this point the quality of the foam doesn't change drastically. From their experiments on LDPE, it was discovered that microcellular foaming can be achieved with CO_2 content as high as 12-15wt% with crosslinking agent blended in with the polymer (Park, Lee, et al. 2006).

2.5.6 *Static Mixers*

2.5.6.1 Definition

Static mixers can have many types of geometrical blade design but they are all fixed in position and motionless. In industrial application they are used as agitators for being cheaper to operate compared to mechanical agitators. Static mixers provide an excellent method for homogenizing a mixture in a short period of time. A typical static mixer has multiple identical static blades placed in series called elements. Each element within a series of elements can be

offset from one another by a predetermined angle which depend on the functional requirements. The elements can be positioned inside a pipe or a reactor chamber. These elements redistribute the fluid flow toward the radial and tangential direction and later recombines the separated flow. The degree of the mixing and redistribution depends on the type of static mixer. Commercially available mixing elements can have variety of geometrical shapes. From simple helical elements to more complex X-grid type of mixing elements (SMX). Helical elements are used for homogenizing the polymer melt in laminar flow and gas-liquid dispersion in turbulent flow. X-grid type mixers are used for high viscosity liquids and also for homogenizing polymer melt (Thakur, et al. 2003).

The performance of static mixers is evaluated based on their length and the pressure drop for viscous liquids. The mixing efficiency is also determined from the interfacial stretch generated between two different liquids. Since helical elements have less resistance to flow, the pressure loss per element is lower compared with x-grid (SMX) type element. However, the degree of interfacial stretching is higher per element with x-grid type elements. Therefore, higher degree of mixing is possible with x-grid static mixers (Meijer, Singh and Anderson 2012).

2.5.6.2 Dispersive & Distributive Mixing

The two main types of mixing operations include dispersive mixing and distributive mixing. In dispersive mixing operations the larger close-knit components are reduced in size into smaller components (Figure 2.8), whereas the homogeneous distribution of minor particulates within a solid or a liquid without the reduction of particulate size constitutes distributive mixing (Figure 2.9) (Rauwendaal 1998). A mixing element with its close arrangement of blades provide narrow flow passages. A mixing element with its close arrangement of blades provide narrow flow passages. A complex network of flow passages are present as the immiscible fluids move past elements that are offset from one another by some given angle. These series of closely packed blades split the bulk fluid into layers as the stream pass through the network of passages. The layers keep multiplying with each passing element. The formation of each layer is accompanied by shear rate on cross-sectional shear plane perpendicular to the blade surface. When the shearing plane area decreases as the fluid flows across the blade surface, shear rate and viscous shear stress increases. This results into a higher degree of dispersive mixing. Other contributor of dispersive

mixing is elongation flow, and squeezing flow. The distributive mixing capacity of a static mixer is directly proportional to the number of mixing elements (Soman and Madhuranthakam 2017).

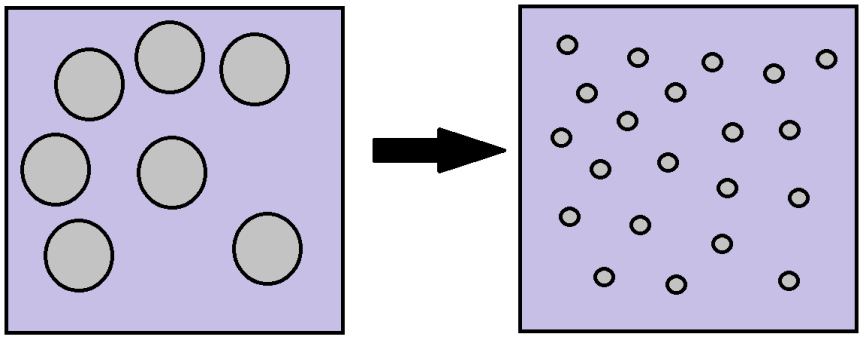

Figure 2.8: An illustration of dispersive mixing (Rauwendaal 1998).

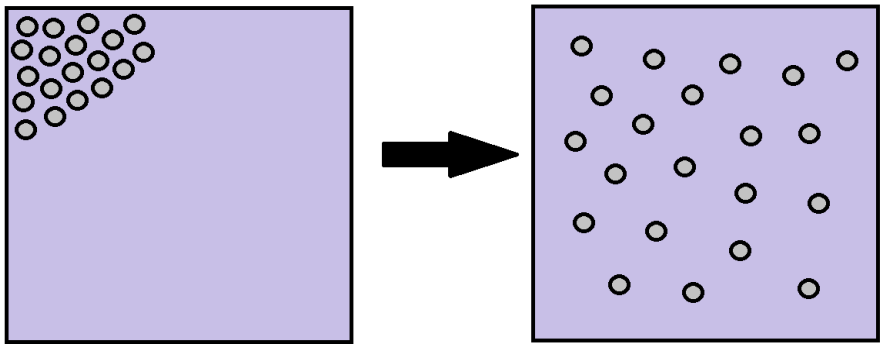

Figure 2.9: An illustration of distributive mixing (Rauwendaal 1998).

2.5.6.3 Dispersion of Gas in Viscous Liquids using Static mixers

Dispersion of gas in viscous liquids involves the breakdown of a large bubble into smaller bubbles and this process is repeated until the interfacial tension on the bubble wall can no longer support further reduction in size (Fradette, et al. 2006). The mixing of gas in polymer is promoted through shearing and stretching the melt. The diffusion of gas through this process into the polymer melt is the primary purpose of the static mixer. The mixing elements are usually offset by 90° or 180° from one another, this splits the stream toward the radial direction and later recombines the stream toward the axial direction. This mixing process is repeated with each successive element and the polymer melt is stretched and sheared which enhances gas diffusion (Rizvi 2016).

2.6 Functionally Graded Foam Production

2.6.2 *Functionally Graded Material Manufacturing*

The manufacturing of FGMs involves the production of a structure with spatial inhomogeneity. In powder metallurgy, porosity gradient structures can be formed by layering a powder mix with different particle shape or by varying the rate of powder deposition. Varying the chemical composition in a single-phase material involves the deposition of powder with gradual change in composition. After the sintering process, the material appears to have a single-phase solid material structure but with gradual change in concentration of an element depending on a spatially varied solubility within the composite. In sheet lamination, sheets with gradual change in composition are produced either by powder rolling or tape casting. In slip casting, porous materials are submerged in a series of slurries with varying powder composition. The uptake of liquid within the pores produces a surface layer with stepwise gradient. In die compaction the gradient is formed by layering powder with varying composition within the compacting die (Kieback, Neubrand and Riedel 2003).

2.6.3 *Functionally Graded Polyethylene Foam Production*

In the field of polymer foam production, functionally graded foaming process can be achieved through variety of methods. One of the popular production methods utilizes compression molding with thermally graded plates. For instance, Yao and Barzegari have produced density graded linear medium density polyethylene (LMDPE) foam by using different temperature on the top and bottom plate of a compression molding machine. In the foaming process synthetic microbeads were used to vary the cell morphology from one region to another and thereby creating density graded foam. The bead arrangement along with mold plate temperature and the processing time produced foam with changing cell size and cell density. From their analysis it was reported that the gradual variation in cell morphology can be produced with a combination of temperature gradient and microbead content. The flexural modulus of the inhomogeneous cell density depends on how a load is applied to the sample. However, the value tends to be higher in the regions with higher cell density (Yao, Barzegari and Rodrigue 2011, Barzegari, Yao and Rodrigue 2009).

Density graded polyethylene foam can also be produced by utilizing chemical blowing agent. Yao & Rodrigue, carried out foaming experiments with a compression molding machine by

controlling the temperature in the top and bottom plate. The CBA content, temperature gradient and processing time are key factors that control the production of the graded foam. From their study it was reported that the blowing agent concentration in conjunction with the temperature gradient had a substantial effect on the foam morphology. However, uniform foam quality can be achieved if both top and bottom plates are maintained at the same processing temperature. The density gradient is not only strongly dependent on the temperature profile, but also the processing time through the rate of heat transfer within the polymer melt (Yao and Rodrigue 2012). The primary method of visually characterizing the internal structure of porous material is through scanning electron microscopy (El-Desouky, et al. 2013).

2.7 Polymeric Material Formulation & Characterization

2.7.1 *Polyethylene*

Polyethylene is a long chain of ethylene monomers with a common formula of $C_{2n}H_{4n+2}$, the *n* represents the degree of polymerization. However, all polyethylene resins do not exhibit identical molecular structure. A resin type can have a wide range of branching length and backbone length. The backbone length depends on the degree of polymerization. Which can range in excess of 200, 000. There are there main types of polyethylene which are characterized by their branching structure. They are, high density polyethylene (HDPE), low density polyethylene (LDPE), and linear low density polyethylene (LLDPE) (Peacock 2000).

High density polyethylene has a structure very similar to a pure long chain polyethylene (Figure 2.10). The structure mainly consists of unbranched molecules with slight bend in its linearity. High degree of crystallinity is possible with HDPE because very few kinks are present to disrupt the organization. The density of HDPE can range from 0.94 to 0.97 g/cm^3. Unlike HDPE low density polyethylene contain high degree of branching (Figure 2.11). For this reason, LDPE exhibit a lower degree of crystallinity due to the presence of large number of branches on its backbone. The branches mainly consist of ethyl and butyl groups and various lengths of long chains. The density of a typical LDPE resin ranges from 0.90 to 0.94 g/cm^3. Linear low-density polyethylene (LLDPE) consist of a linear backbone with short branches of ethyl, butyl, and hexyl groups (figure 2.12). The branches are usually separated by 25-100 carbon atoms. However, the branching complexity is less than that of LDPE. The degree of crystallinity of LLDPE is not as

high as HDPE, but it is significantly higher than LDPE. Structurally LLDPE molecules are thought of as chemically in between the extremes of HDPE and LDPE (Peacock 2000).

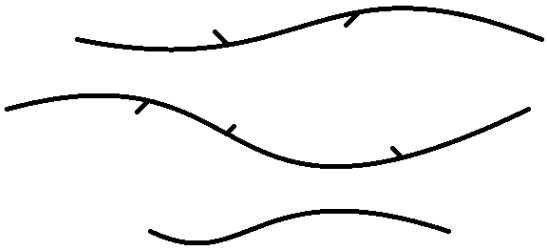

Figure 2.10: Molecular structure of HDPE (Peacock 2000).

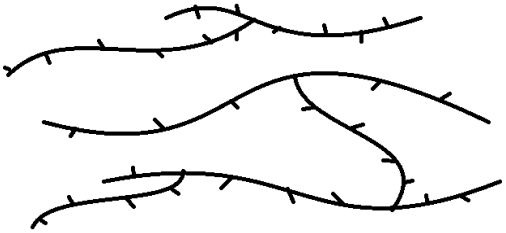

Figure 2.11: Molecular structure of LDPE (Peacock 2000).

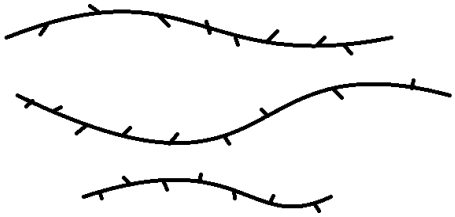

Figure 2.12: Molecular structure of LLDPE (Peacock 2000).

2.7.2 *Material Formulation*

The amount of resin powder needed to form the outer un-foamed skin is determined from the desired skin thickness. The skin volume is dependent on the rotational mold shape and size. The skin material (m_{SKIN}) can be obtained by multiplying the skin volume with the given resin density:

$$\boldsymbol{m_{SKIN} = V_{SKIN}\rho_{PE}} \tag{2.5}$$

Foam Material Formulation with CBA: Formulation for the foam resin quantity has been reported by Kimberly. Initially, the foam volume (V_{FOAM}) is obtained by subtracting the skin volume (V_{SKIN}) from the total mold volume. To fill the interior cavity of the mold, the foamable

resin has to expand up to the V_{FOAM}. The expansion ratio of the polymer resin needed to fill the mold is known as the volume expansion ratio (VER). VER is obtained by dividing V_{FOAM} by the initial resin volume V_i, given in Equation 2.6. After determining the initial resin volume, the resin material (m_{FOAM}) can be calculated from Equation 2.5 (Kimberly 2009).

$$\boldsymbol{VER = \frac{V_{FOAM}}{V_i} = \frac{\rho_{PURE}}{\rho_{FOAM}}} \tag{2.6}$$

The CBA content can be determined from the desired VER and the gas yield. The gas yield of the chemical blowing agent is given by the manufacturer (φ_{STP}). The corrected gas yield ($\varphi_{corrected}$) is obtained from Equation 2.7, where T_C represents the crystallization temperature and T_{room} is the room temperature (Kimberly 2009).

$$\boldsymbol{\varphi_{corrected} = \varphi_{STP}\frac{T_C}{T_{room}}} \tag{2.7}$$

The mass of the CBA can be obtained from Equation 2.8 with the corrected gas yield (Kimberly 2009).

$$\boldsymbol{m_{CBA} = \frac{V_{FOAM} - V_i}{\varphi_{corrected}}} \tag{2.8}$$

2.7.3 *Polymer Melt Characteristics*

When a liquid is under stress, the ratio of shear stress 'τ' by shear strain rate '$\dot{\gamma}$' is known as the shear viscosity 'η'. For Newtonian fluid like water this value is constant regardless of shear-strain rate (Figure. 2.13). However, for Non-Newtonian fluids like polymer melt, the shear viscosity is dependent on stress, shear rate, temperature, and pressure. If the viscosity of a material decreases with increasing shear rate, it is known as a pseudoplastic. Majority of liquid polymers behave like a pseudoplastic (shear-thinning) (Strong 2006, R. Crawford 1998).

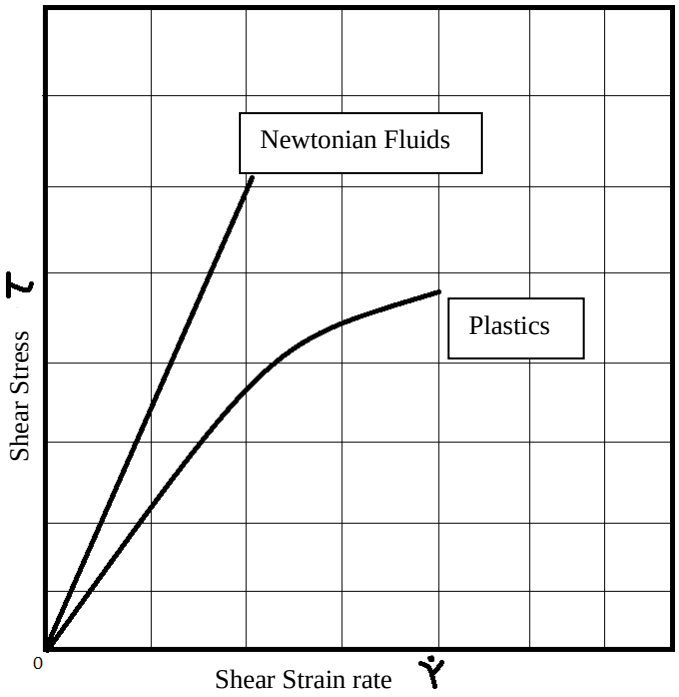

Figure 2.13: Shear stress and shear rate relationship (R. Crawford 1998).

In contrast, the reduction in viscosity for a gas laden polymer melt is achieved through free volume mechanism. The dissolved gas causes the polymer melt to swell and thereby disentangling the long chains, which increases the free volume and chain mobility. Nobelen and colleagues have demonstrated that the injection of 1wt% CO_2 into the PE melt can reduce the viscosity of the solution by 15%. Upon injection of 2wt% CO_2 into the PE melt the viscosity reduce by 25%. However, by increasing processing pressure and lowering the temperature, the free volume within the melt decreases reducing and cell mobility and increasing viscosity (Nobelen, et al. 2006).

2.7.4 *Melt Flow Index*

The flow of polyethylene is defined by the melt flow index (MFI). The value for MFI is determined by the grams of polymer melt that flows out of a standard orifice at a given temperature in ten minutes due to a standard weight being placed on top of the polymer melt. The MFI value for some grades of PE can be in excess of 100. However, with a higher MFI value, impact strength, ductility, resistance to cracking, and resistance to chemicals decrease. The MFI value gives an indirect measurement of PE's molecular weight and chain length. A resin with a high MFI value has short chains with low molecular weight. The lower molecular weight gives the polymer low

strength characteristics. However, the strength characteristic is also dependent on pressure, temperature, and dissolved solvents within the polymer melt (Ogila, et al. 2017).

2.7.5 *Melt Strength*

The melt strength of a polymer is the measurement of its extensional viscosity or, resistance to stretching. The melt strength value is obtained by determining the maximum tension that can be sustained by a polymer melt without breaking when a load is applied. Polyolefins are known to have low melt strength. This is because the long molecular chains of the resin get stretched and aligned and can easily slide past one another without entangling. In contrast, polymers with greater degree of branching exhibit higher melt strength since the branches get entangled. LDPE for instance is much stiffer than LLDPE in shear but softer in extension. In relation to polymer foaming process, low melt strength has a negative effect on bubble stability. However, during the bubble growth stage it is desirable to have lower melt strength to allow the foam to expand. The melt strength can be increased either by lowering the temperature of the melt or by blending fillers to increase viscosity (Viachopoulos 2015).

2.7.6 *Single Screw Extrusion*

A single screw extruder can be fed with solid polymer pellets or liquid polymer. In the context of this thesis the discussion will be limited to plasticizing extruders, which are only fed with solid plastic particles. The plastic particles must meet the size requirements of an extruder screw for effective melt conveying. A plasticating extruder has three major sections: solid conveying; melting; and metering (Rauwendaal 1998).

Solid Conveying: After being loaded into the feeder, the polymer resin encounters frictional forces on the barrel wall. This frictional force is the driving force for moving the material forward as the screw rotates. The resin is exposed to increasing temperature and pressure as it is conveyed forward. This results in the formation of a solid bed of resin that moves in plug flow through the groove of the screw. The solid bed is subjected to exponential increase in pressure as it moves forward. The increase in pressure is accompanied with increasing temperature. The sources of the heat are frictional forces and heaters placed on the extruder barrel. As the polymer starts to soften due to the increasing temperature, the pressure will stabilize followed by the onset of polymer melting (Rauwendaal 1998).

Melting: The onset of melting initiates at the barrel surface due to higher frictional forces on the wall because the polymer experiences higher velocity on the barrel surface compared with the screw surface. Also, the barrel surface is heated by band heaters unlike the screw surface, which is not heated by any electrical heaters. The solid bed eventually reduces in size as it moves down the length of the screw. A transition layer known as the melt film is present between the hot barrel surface and the solid bed. Melting occurs in the interface between the melt film and the solid bed. As molten material enters the melt film, the top layer of the film is dragged away due to the rotation of the screw. The newly molten material pools in front of the solid bed, pushing it against the blade of the screw. This type of melting is referred to as drag induced melting or contiguous solid melting (Rauwendaal 1998).

Metering: After the completion of the melting process, the polymer melt is conveyed and pumped out of the extruder. The polymer melt experiences viscous drag due to its relative motion in the gap between barrel and the screw. The melt flow rate is directly proportional to the screw RPM. The flow rate is the total combination of pressure flow, drag flow and leakage flow. Pressure flow depends on the pressure gradient across the length of the melt conveying region. The flow rate can be increased by maintaining a negative pressure gradient from the beginning of the melt conveyer section to the extruder exit. Leakage flow occurs at the clearance between the flank of the screw and the barrel wall. It is usually negligible however, if the clearance increases due to screw surface wear over time, the total flow rate will decrease (Rauwendaal 1998).

2.7.7 *Thermal Analysis*

Thermal analysis is used for measuring the material property while the sample is heated, cooled or held in an isothermal state. The specific material response can be observed and recorded at a given temperature. The most common thermal analysis instruments include the differential scanning calorimeter (DSC) and the thermogravimetric analyzer (TGA). Thermal analysis is a very useful research tool to determine processing parameters for manufacturing polymeric materials (Menczel, Prime and Gallagher 2009).

2.7.7.1 Thermogravimetric Analyzer

In thermogravimetric analysis, the change in mass of a sample is compared against temperature or over time. The change in sample weight is measured by a thermogravimetric

analyzer (TGA). The TGA apparatus utilized in the experimental work presented in this thesis is shown in Figure 2.14. A TGA device has very sensitive weight scale that can resolve up to 1- 0.1 µg. The sample material can be analyzed in a variety of inert atmospheres, such as nitrogen or argon gas. The TGA instrument is mainly employed to determine the decomposition temperature of a material. The output data from a TGA instrument shows the initial onset of mass loss with a downward dip in the curve, which is indicative of the decomposition point. However, in most cases a reliable qualitative and quantitative evaluation of the thermogravimetric (TG) curve is impossible without having its first derivative (i.e. DTG curve). A DTG graph can be generated from the derivative of a TG trace, which plots the change in mass over temperature and/or time. The peak point from the DTG graph identifies the temperature/time at which maximum mass loss is evident (Greenwood 2001, Speyer 1994).

Figure 2.14: TA instrument's Q series Thermogravimetric Analyzer (TGA).

2.7.7.2 Differential Scanning Calorimeter

A differential scanning calorimeter can measure the heat flux of a sample against temperature or time. The DSC apparatus utilized in the experimental work presented in this thesis is shown in Figure 2.15. Similar to the TGA, the analysis can be carried out in an inert atmosphere with nitrogen or argon gas. Inside a DSC furnace chamber the heat flux is compared against an

empty pan to generate the DSC plot. The sample pan and the empty reference pan are subjected to the same temperature and atmosphere at the same time. As the transformation takes place within the sample pan, the temperature deviates from the reference pan. This change is detected by the instrument and it increases heat input to the sample pan while reducing heat input to the empty pan to maintain zero temperature difference. The energy input that must be added to maintain this zero difference is assumed to be the heat released by the sample. This is represented by a dip on the DSC curve. For polymer characterization a DSC trace can be used to find the glass transition temperature, melting and recrystallization temperatures of a polymer (Greenwood 2001, Speyer 1994).

Figure 2.15: TA instrument's differential scanning calorimeter (DSC).

2.8 Foam Characterization

2.8.1 *Analytical Characterization*

In this thesis, the morphology of rotationally foam molded composites and extruded foam samples will be evaluated and characterized by its: foam density; average cell density; and average cell size. The foam density (ρ_{FOAM}) will be evaluated according to the procedure described in ASTM D1622-08. The foam sample must not be less than $1in^3$ in volume and it should be weighed on a scale with a precision of $\pm$0.1%. The dimension of the foam should be measured with a caliper

to a precision of ±0.1%. The final foam density is calculated with Equation 2.8. Where the sample weight is represented by $'W_s'$ and the sample volume is represented by $'V_s'$ (ASTM-D1622-08 2008).

$$\boldsymbol{\rho_{FOAM} = \frac{W_s}{V_s}} \tag{2.9}$$

The cell density (*N*) is determined from Equation 2.10, where n_{cells} represents the number of cells within a 1cm^2 area. The value for n_{cells} is obtained by observing the sample under a scanning electron microscope (SEM), or a digital microscope to visually count the cells (< 100 μm). The volume expansion ratio (*VER*) is predetermined from Equation 2.6 for CBA produced foam. For PBA foam the VER is obtained from the volume of injected gas (Pop-Iliev, Lee and Park 2006).

$$\boldsymbol{N = (n_{cells})^{\frac{3}{2}} \bullet VER} \tag{2.10}$$

Finally, the average cell density is determined from Equation 2.11 (Pop-Iliev, Lee and Park 2006).

$$\boldsymbol{D_{average} = \sqrt[3]{(VER - 1) \bullet \frac{6}{\pi \bullet N}}} \tag{2.11}$$

2.8.2 *X-Ray Computed Tomography (X-ray CT)*

Characterization of cellular morphology along with interfacial bond quality between the foam and the outer skin layer will be done with micro-computed X-ray tomography. This is a non-destructive analysis technique to visualize internal cellular structure. High resolution images are captured from a sample with x-ray beams. The 2-D images are taken at each angular step while the sample rotates 360 degrees. A 3-D reconstruction of the actual object is produced from all the 2-D images captured by the x-ray machine. The internal structure can be analyzed at any region within the sample from the 3-D reconstruction (Utkarsh, et al. 2018).

2.8.3 *Scanning Electron Microscopy (SEM)*

Scanning electron microscopy is a destructive analysis technique. The rotational molded foam samples will be cryogenically frozen below the glass transition temperature (T_g) of the

polymer. Below its T_g, a polymer becomes brittle and behaves like a glass. The sample is fractured at this point to preserve the delicate internal cellular morphology. The exposed surface is gold sputter-coated up to a thickness of ~50 nm. The gold coated samples are placed inside a scanning electron microscope to capture the backscatter electron images (Todd and Kuznetsova 2011).

2.9 Quality Function Deployment Tool

2.9.1 *House of Quality (HofQ)*

The house of quality (HofQ) matrix ensures that a new design or a re-design of an existing product satisfies customer requirements. In the customer requirements section (Figure 2.16), the customer needs are ranked according to their importance from a customer marketing survey. Through this customer-oriented design process, a list of engineering specifications can be identified to meet the customer demands. The engineering specifications must be measurable and it should be directly linked with one or multiple customer requirements. The roof of the house determines positive or negative interaction between the engineering specifications. It is the goal of a designer to minimize these interactions as much as possible, however, interactions cannot be completely eliminated. Competition assessment compares how existing technologies satisfy the customer needs against the potential new technology. The heart of the HofQ matrix is the deployment matrix where each engineering specifications are scored based on the intensity of the relationship to each customer requirement. In the bottom of the house, target values are tabulated to prioritize the most important engineering specifications for customer satisfaction (Ramirez, Cisternas and Kraslawski 2017).

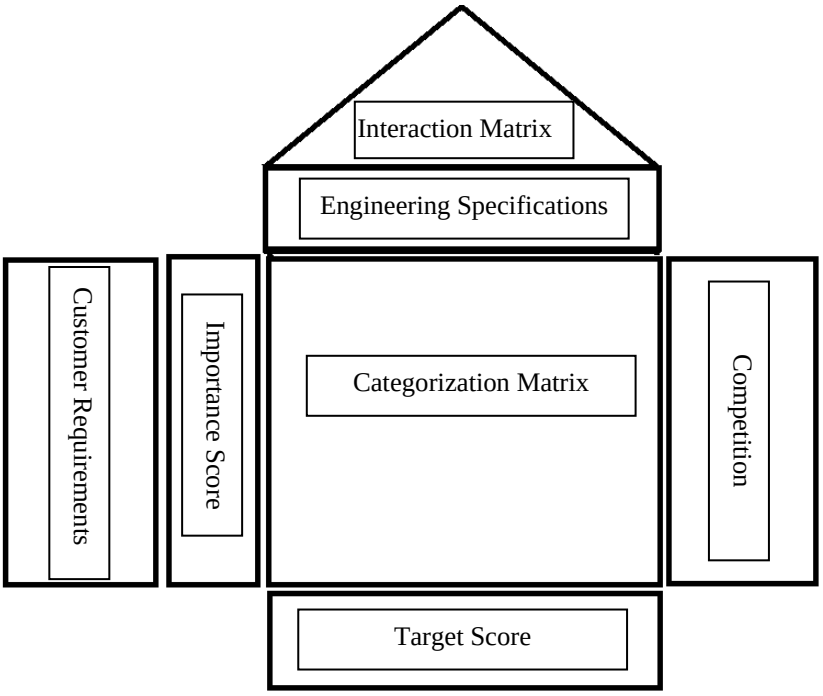

Figure 2.16: House of Quality Matrix for a new product design (Ramirez, Cisternas and Kraslawski 2017).

2.9.2 *Pugh Decision Matrix Method*

The identified engineering specifications are implemented to generate multiple competing design concepts. A Pugh matrix (decision matrix) is utilized to select the best design from a group of concepts. The concept is selected based on its overall function as a whole, rather than the operation of its individual components. The importance of a selection criteria is given a value from 1 to 10, where 1 is the least important and 10 being the most important criteria. One of the design concepts is used as the datum to compare against the alternative designs. A positive symbol is given if the alternative design concept satisfies the selectin criteria. A negative symbol is assigned if the alternative design does not satisfy the criteria. The total score is tabulated for each alternative design by multiplying the symbols to each criterion rating and then adding them together. The concept design with the highest score is selected as the final design for the prototype (Raktim and Pop-Iliev 2018).

2.9.3 *Summary*

The theoretical background and the survey of the relevant literature presented and discussed in this chapter clearly indicated that for successfully conducting and accomplishing the present

research, which is aiming towards eventually achieving the means for fabrication of functionally graded rotationally molded integral-skin cellular composite artifacts by using the rapid rotational foam molding technology, it would be necessary to redesign and modify the existing RRFM experimental setup. These modifications will allow the production of foam by implementing supercritical carbon dioxide in extrusion, which would represent the very first time of implementing a physical blowing agent (PBA) in the context of rotational foam molding. For this reason, and among many other components, a mixing chamber will be necessary to be designed and built into the system to enable the production of a single-phase polymer/gas solution. From this solution, various morphology qualities of microcellular and fine cellular foams having seamless and smooth transition of morphologies will be possible to be created using the modified RRFM process. In the following chapter, engineering specifications for supercritical fluid -based foam production will be designed by utilizing the Quality Function Deployment design engineering tool.

Chapter 3. Experimental Setup Redesign: Concept Generation and Evaluation

3.1 Introduction

The goal of this chapter is to present and evaluate new concepts for modifying the existing RRFM experimental setup to produce functionally graded rotationally molded integral-skin cellular polyethylene (PE) composites. The initial step was to outline the design problem along with the desired outcome upon the completion of the new experimental setup. Through this process, potential design requirements for the new experimental setup were identified and implemented during the concept generation phase. After conducting a feasibility analysis, the most promissing concept was selected for the final design. A detailed description with technical specification of the new experimental setup will be presented in the final sections of this chapter.

3.2 Problem Statement

The patented Rapid Rotational Foam Molding (RRFM) (Pop-Iliev, Christian and Abdalla 2014) process was developed to: (i) significantly improve the control of the processing variables; (ii) reduce the processing time, and (iii) lower the energy consumption needed for fabricating rotationally foam molded composite artifacts that are fully encapsulated with an outer solid skin. This was accomplished by completely decoupling the skin formation from the foam production processing steps by practically implementing the “separation in time” and “separation in space” TRIZ inventive principles (Theory of Inventive Problem Solving 2011). Thus, unlike the single-charge technique, where both the skin foam formation take place simultaneously within the rotating mold, in RRFM a single screw extruder is used to rapidly melt a foamable polymeric resin and activate its pre-mixed or pre-compounded CBA content to produce foam and later pump/inject the foam into the mold’s cavity to bond with the already prepared soft outer skin in a separate conventional rotational molding operation. Through this extrusion assisted foaming process, fine cellular foam morphology was achieved. The foam morphology was dependent on the amount chemical blowing agent (CBA) content within the foamable resin and the extruder processing temperature. However, the foam morphology can vary slightly from the center of the core to the skin interface due to the temperature gradient within the mold. Although this phenomenon indirectly determines the final cell morphology, the intent of the RRFM process was to produce a homogeneous cellular morphology within the foamed core (Pop-Iliev 2011).

In its original state, the RRFM process was not deliberately designed to provide systematic and deliberate control of the cell morphology after the foam is injected into the mold. Further, the RRFM process was not designed to gradually change the quality of the foam as it is being injected into the mold cavity. In addition, the original RRFM process was not designed to facilitate the injection of a physical blowing agent (PBA) into the existing extrusion system with a goal of achieving production of microcellular foams. Therefore, it was necessary to undertake a redesign of the existing RRFM experimental setup so that the modified system would allow the production of functionally graded (FG) integral-skin cellular composites by utilizing CBA or PBA separately or concurrently. If successful, the redesigned RRFM process, referred further as Rapid Rotational Functionally Graded Foam Molding (RRFGFM) process, would represent the first and only processing technology based on rotational molding that would be able to incorporate PBAs in the fabrication of functionally graded composites.

The flowchart presented in Figure. 3.1 represents the key elements consisting the RRFGFM production process. The first step of this new process is to charge a mold with predetermined amount of skin material before translating the mold into the oven. The mold rotates bi-axially in the heated oven to form the outer skin. While the skin is forming, the extruder is charged with either foamable resin based on a CBA or pure resin for PBA injection, or both. The mold is translated out of the oven to receive CBA-based or PBA-based polymeric foam or a mixture of both through a specially designed openable interface to create the functionally graded foam (FGF) core as desired on top of the already formed polymeric soft skin. After the foam has been injected, the mold is cooled back down to room temperature and the part is extracted. The key expected feature that the RRFGFM process will uniquely provide include the possibility to implement and combine at least three different polymeric resins (for solid skin, for CBA foam, and for PBA foam) with at least two kinds of blowing agents (CBA and PBA) within the same processing cycle. Thereby, by deliberately varying the quantities of the said material ingredients along with varying

the processing parameters countless combinations of functionally graded cores deliberately designed for a variety of applications would become achievable in RRFGFM.

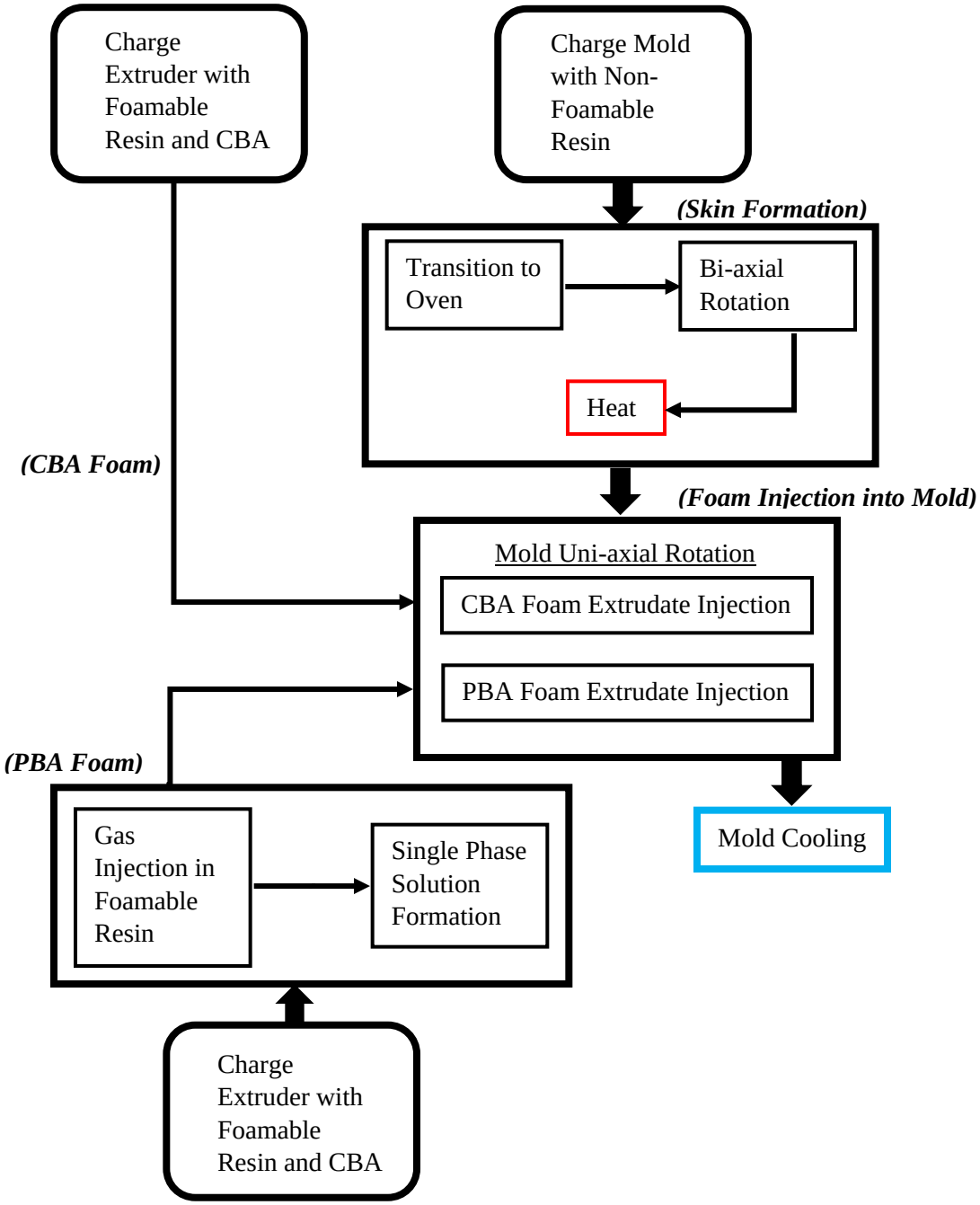

Figure 3.1: Proposed flowchart of the RRFGFM production process.

The successful production of RRFGFM composites can lead to wide application in construction, automotive, and marine industry. The quality of the functionally graded foamed core

will determine its application. The non-homogeneous distribution of gradually changing foam morphologies will introduce specific physical properties depending on direction and orientation.

3.3 RRFM Experimental Apparatus

Extruder: A laboratory scale refurbished single screw extruder from the Wayne Machine and Die Company was used for all experiments (Figure 3.2). It is a single screw extruder with 32 mm diameter screw and a length to diameter compression ratio of 24:1. The drive motor of the extruder is capable of providing 7.5 HP to the screw to produce a maximum RPM of 100. The extruder has three temperature zones which can be monitored and controlled from an extruder control panel. The screw RPM can also be controlled from the same control panel. The extruder exit temperature and pressure can be monitored with a Gefran melt pressure transducer positioned at the metering section of the extruder (Kimberly 2009).

Figure 3.2**:** Single screw extruder with control panel.

Oven: A forced convection oven is used to heat the mold to form the outer skin (Figure 3.3). It is capable of reaching a max temperature of 300°C at a rate of 15°C/min. The internal dimension of the oven is 0.609x0.609x0.609 m^3. The oven required slight modification to allow the biaxial mold to enter and exit laterally. A slotted section was removed from the side of the oven facing the mold carriage. The slot cut allowed the rotational arm to pass through easily. The slotted cut section was re-attached to the door of the oven to seal the side after the rotational arm is translated into and out of the oven (Kimberly 2009).

Figure 3.3: Oven for the rotational mold.

Rotational Arm: The bi-axial rotation arm is presented in Figure 3.4. The mold is mounted on the end of the arm on a mounting plate which is attached to the inner shaft responsible for rotating the mold on its central axis. The rotational motion is transferred from the motor to the inner shafts by bevel gears. The external mold rotation shaft rotates on its central axis causing the entire rotational assembly to rotate 360 degrees (Kimberly 2009).

Figure 3.4**:** Rotational mold arm assembly.

Motor Carriage and Frame: A skeleton box frame made with stainless steel is used to support the two DC motors and transmission gears for the bi-axial rotational arm (Figure 3.5). The two DC motors are supplied with 220 V to operate at a maximum RPM of 1725. Each motor

transfers power through a gearbox to the rotational arm assembly. For the external rotational arm, a gearbox reduces the rotational speed by a ratio of 60:1 from one of the motors. However, since the rotation of the mold must be faster than the rotational arm, the input rotational speed from the second motor is reduced by a ratio of 40:1 by a separate gearbox. The higher rotational speed of the mold results in a uniform outer skin thickness. From initial experimentation with the rotational arm by Kimberly, it was determined that the ideal motor RPM should be 1600. The final gear and socket arrangement achieved 3.94:1 rotation ratio between the mold and the arm (Kimberly 2009).

Two motors and two gearboxes were housed in a carriage made from steel tubing and 1/4" steel plates. The rotational arm is mounted on top of the carriage with two bearing support housing to ensure that the arm can rotate along its central axis. On the underside of the top steel plate of the carriage, metal wheel assemblies were attached to allow the carriage to move on an L-shaped track. The movement of the carriage is facilitated by ball screw mounted on the side of the external frame. The manual rotation of screw allows the carriage to move between the oven and the extruder. The entire carriage is supported on the track of the frame. The height of the frame is adjustable to align the mold with the nozzle of the extruder (Kimberly 2009).

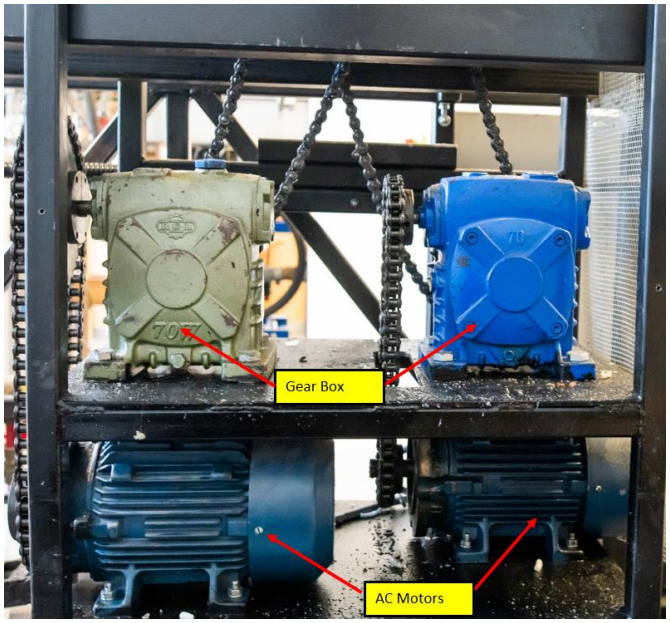

Figure 3.5: Motor carriage and frame for the rotational arm.

Cylindrical Mold: The mold components are made with Aluminum 2014 with thermal conductivity of 192 W/m•K. This material was selected for its high rate of heat transfer. The

cylindrical mold assembly is composed of three components: The main cylinder section; pressure tube support; and the mold connection adapter plate (Figure 3.6). The main cylindrical section has a draft angle of 2° to easily remove the plastic part. On either side of the cylinder, two flanges containing mounting holes are present for attachment with the rotational arm and the mold connection adapter plate (Kimberly 2009).

Figure 3.6**:** Cylindrical mold assembly.

3.4 New Experimental Setup Design for PBA Foam Production

3.4.1 *Evolution of Rotational Molded Foam Composite Technology*

The potential future innovations for rotational foam molding technology are represented on an S-curve in Figure 3.7. At the bottom this S-curve, the single charge manufacturing process represents the earliest version of the technology. The steep rise in the slope of the curve corresponds with rapid evolution and future improvement to the manufacturing processes. Eventually, the system reaches its ideal state at the plateau of the S-curve with completely automated manufacturing process and shortest possible production time.

In recent years, development of the RRFM technology has led to drastic improvements in the quality of the foamed core. The extrusion assisted process reduces cycle time and produces fine cellular foamed core with CBA (Kimberly 2009). By decoupling the foaming process from the single charge method, new design opportunities are being realized. Through the extrusion assisted foaming operation, it is now possible to produce foamed core with PBA, and functionally graded foamed core moldings with PBA or CBA (RRFGFM). In upcoming future iteration of the RRFGFM technology, co-extrusion foam production methods and injection molding technology will be employed to produce with integral outer skin.

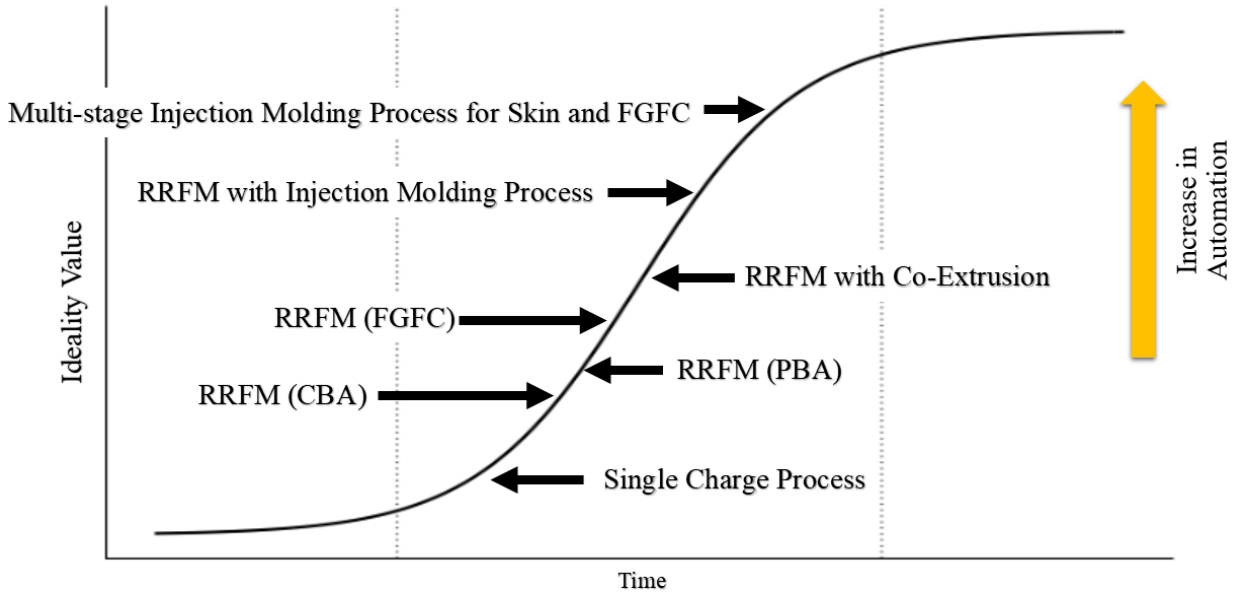

Figure 3.7: Stages of development in the field rotational molded foam composites.

3.4.2 Governing Processing Variables for RRFGM.

The development of a PBA based foam extrusion process is the first step towards developing the RRFGFM processing framework. It should enable utilizing supercritical carbon dioxide as the blowing agent. It is envisioned that by varying the injection rate of the blowing agent content and other processing parameters, the quality of the foam will be possible to be deliberately varied.

Extrusion Variables: Extrusion of polymeric material begins with loading the extruder hopper with a predetermined amount polymer resin. However, it is common to dry blend agents with the polymer resin to provide sites for bubble nucleation. The nucleating agent content dispersed within the polymer resin directly controls the final cell population density of the foam.

By gradually increasing or decreasing the nucleating agent weight percentage in the bulk material, the cell morphology can be varied.

While being conveyed through the barrel of the extruder, the polymeric resin is heated until it melts. The flow characteristics of the polymer melt and its viscosity are influenced by temperature and pressure. Although the temperature also influences melt pressure, the pressure can be increased or decreased by modifying the extruder's screw RPM. After the polymer has reaches its molten state in the extruder barrel, the extruder's screw pumps the polymer melt towards the gas injection port and the subsequent mixing sections.

Supercritical Gas Injection and Mixing Variables: Pressurized carbon dioxide (CO_2) gas (super critical state) is pumped directly into the polymer melt. The dissolution rate of the supercritical gas is determined by the processing temperature and pressure. By increasing the pressure of the bulk fluid, the solubility of the given gas is increased, which will allow for higher quantity of supercritical fluid to be dissolved into the polymer melt. The diffusion of gas into the polymer melt is further aided by controlling the melt temperature. At a higher processing temperature, the diffusion rate of CO_2 increases and thereby forming the single-phase solution faster.

Along with temperature and pressure the other key factors for forming a single-phase polymer-gas solution are the gas injection rate, and the geometry of the mixing blade(s) of the static mixer. The initial gas injection pressure and flow rate are controlled with a syringe pump. When the gas flow rate is increased, larger size gas bubbles are introduced into the polymer melt. Bigger bubbles can increase the overall gas diffusion time in the mixing chamber because more time is required for larger bubbles to break down into smaller bubbles for faster diffusion. On the other hand, the geometry of the mixing blade(s) of the static mixer and its overall length can aid in the diffusion process through distributive and dispersive mixing operation.

Foam Extrusion Die Variables: In the final phase, the gas laden polymer melt will experience thermodynamic instability as it flows out of the die orifice. The rapid depressurization decreases gas solubility within the polymer melt resulting in micro bubble nucleation throughout the polymer. The nucleated bubbles continue to grow until they stabilize in the final foam structure. The final cell morphology is dependent on pressure drop and the die temperature. By lowering the melt temperature, the polymer melt strength is increased to resist excessive cell growth and cell

coalescence to preserve microcellular bubbles within the solid foam. The overall cell density can be increased by decreasing the diameter of the die orifice. This increases resistance to flow and thereby, making it possible to induce a higher pressure drop. When the pressure drop is higher the number of bubble nucleating sites increases resulting into foams having a higher cell density.

3.4.3 *House of Quality for a PBA Foam Extrusion*

A complete House-of-Quality for PBA foam extrusion is included in Appendix A1. The analysis in the present section addresses only the customer requirements for PBA based foam extrusion. It is defined in three main categories, experimental setup, process control, and final foam quality. The primary customers for the new extrusion process are the equipment operator, and potential plastic parts manufacturing company interested in the RRFGFM production process. In the RRFM process the polyethylene foamed core is produced with CBA, whereas the new experimental setup will be capable of completely replacing the use of CBA with a PBA or to entertain both chemical blowing agents concurrently.

Who & What: The customer requirements are listed in the '*What'* section of the matrix. Each of the customer requirement is scored from 1-100, and for each customer the sum of each column is 100. The operator can be identified as a researcher conducting experiments in a laboratory environment. The production of PBA foam will involve injecting CO_2 gas into polymer melt, and precise temperature and pressure control of the mixture. From the perspective of an operator, operational control of these variables is critical to varying the cellular morphology of the foam. Therefore, in the operator column, customer requirement for temperature, pressure and CO_2 injection control are scored higher for greater design priority.

Since PBA of any type have never been utilized to produce foam for rotational molding process, the major customer requirements for a plastic manufacturer company is the strength of the foam. Even though pressure and temperature control received higher priority score. The final quality of the foamed core is more important. This includes average bubble size, cell density, and mechanical property for market applications.

How: In this section, non-specific customer requirements are translated into measurable engineering specifications. When the relationship is strong between an engineering specification and a specific customer requirement, it receives a score of "9". However, a lower degree of

relationship (e.g., medium) receives a score of "3", whereas a weak relationship receives a score of "1", and no relationship receives a score of "zero". In Table 3.1, the formulation for identifying the critical engineering specifications for customer satisfaction is presented.

A cell within the customer requirement section is represented by A_n or B_n. As described previously, the importance score for a specific customer requirement for each customer type are given in these cells. In the "*How*" section, each column represents a single engineering specification (C_n, Dn, E_n, F_n), where each cell horizontally intersects with a single cell of a specific customer type, represented by the curved arrows. The numerical value from each of these intersecting cells is multiplied with the corresponding cell of the customer requirement section. This process is repeated from n = 1 to the last cell of a column for every engineering specification. The summation of all the multiplication operation gives the importance score for each engineering specification to the customer. Higher value indicates greater importance to a specific customer type. A percentage value can also be assigned to outline the relative importance of a design parameter.

From this analysis, it was determined that the pressure drop at the die exit is the critical design consideration for both customer types. In contrast, the ability to control fluid injection pressure, heat flux, and melt flow pressure control through the extruder's RPM are more important for the operator. Finally, a plastic manufacturer gives higher importance to the process time and the overall material property of the finished RRFGFM composites.

Now: This section represents the current market solutions and how well the new solution might meet customer needs. In these cases, the current technology is the patented RRFM process utilizing CBA, which can produce fine cellular foamed core encapsulated by an unfoamed solid outer skin. The new process aims to produce functionally graded foamed core with position dependent cell morphology.

Table 3.1: Identification of critical engineering specifications for customer satisfaction.

Customer Requirements		Engineering Specifications (**How**)			
A_1	B_1	C_1	D_1	E_1	F_1
A_n	B_n	C_n (Intersecting Cell)	D_n (Intersecting Cell)	E_n (Intersecting Cell)	F_n (Intersecting Cell)
		$\sum C_n \bullet B_n$	$\sum D_n \bullet B_n$	$\sum E_n \bullet B_n$	$\sum F_n \bullet B_n$
n = 1, 2, 3 …..		$\sum C_n \bullet A_n$	$\sum D_n \bullet A_n$	$\sum E_n \bullet A_n$	$\sum F_n \bullet A_n$

Roof: The roof of the house identifies positive and negative interaction between engineering specifications. For instance, by increasing the process temperature, the melt viscosity is reduced and by association the pressure drop value also decreases. This relationship can be characterized as a negative interaction (i.e., a trade-off type of technical contradiction). However, pressure drop can be increased by increasing the extruder screw RPM. The positive and negative interaction are presented in Figure 3.8 for key design parameters for the foaming operation. The goal of a designer is to minimize interactions as much as possible for a good design. However, interaction between engineering specifications cannot be completely eliminated.

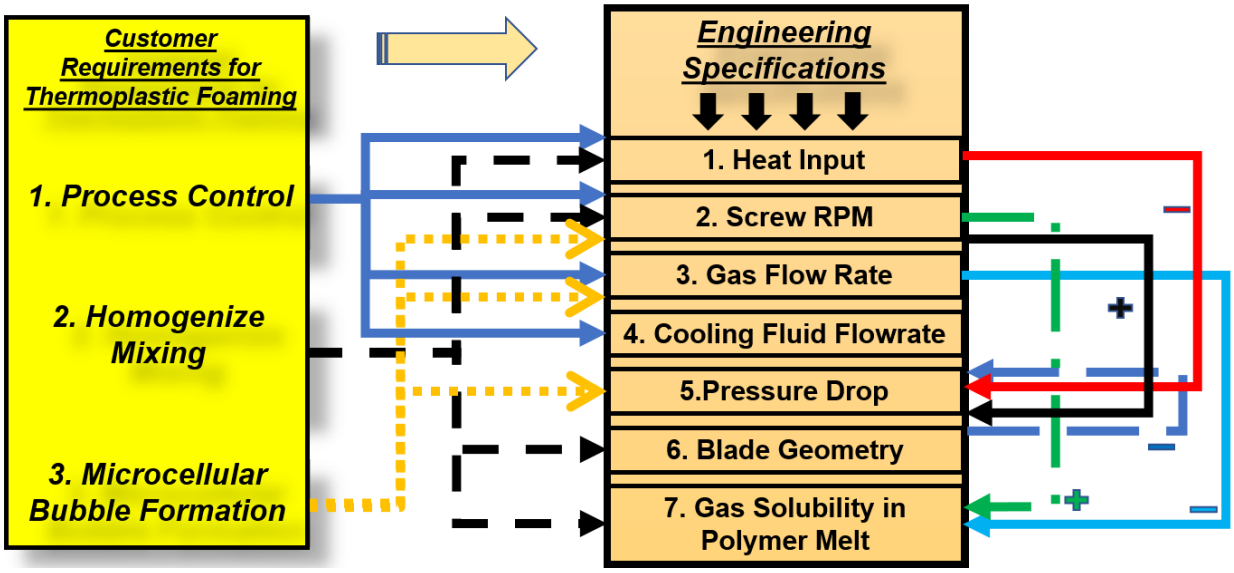

Figure 3.8: Positive and negative interaction between engineering specifications.

3.4.4 *Concept Generation*

From the HofQ analysis, the important engineering specifications were identified for customer satisfaction. Now, these specifications will be implemented in the concept generation phase. A decision matrix (Pugh chart) will be used to select the best concept for final experimental setup design. In the decision matrix, the concepts are evaluated based on their overall function, and not for individual components. Similar to the HofQ scoring system, the importance of each selection criteria is given a value from 1 to 10. Where a score of 10 gives the highest importance. For comparing each concept with one another, one of the concepts is chosen as the datum. A positive symbol is given if a concept satisfies the selection criteria and a negative symbol is assigned if the selection criteria isn't satisfied. The weighted total is determined for all the concepts from the criteria rating in combination with the positive and negative sign. The concept with the highest score is chosen as the final design.

The individual components for each concept is represented in a simplified block diagram. Each concept presents different methods for achieving high degree of mixing between the polymer melt and the supercritical fluid to produce a single-phase polymer-gas solution before inducing thermodynamic instability. The inspiration for the proposed designs came from research work on continuous PBA foam extrusion (Park and Suh 1996), (Srinivas, et al. 2002), (Wang, et al. 2012) and, (Selvakumar and Bhatnagar 2009).

***Concept 1*:** In the experimental setup presented in Figure 3.9, the molten polymer is directly fed into the static mixer from the metering section of an extruder. The flowrate, and back pressure are controlled by the screw RPM. In this setup the gas is directly injected into the static mixer barrel to initiate the mixing process. As the gas laden polymer moves through the mixer barrel, it encounters static mixing blades. The stationary blades split the melt flow and later recombine it to completely disassociate the gas into the polymer matrix. The processing temperature is maintained with band heaters and cooling oil jacket located on the external surface of the static mixer barrel. After leaving the static mixer, the polymer/gas solution experiences rapid thermodynamic instability at the die exit and this is why foam is produced (Raktim and Pop-Iliev 2018).

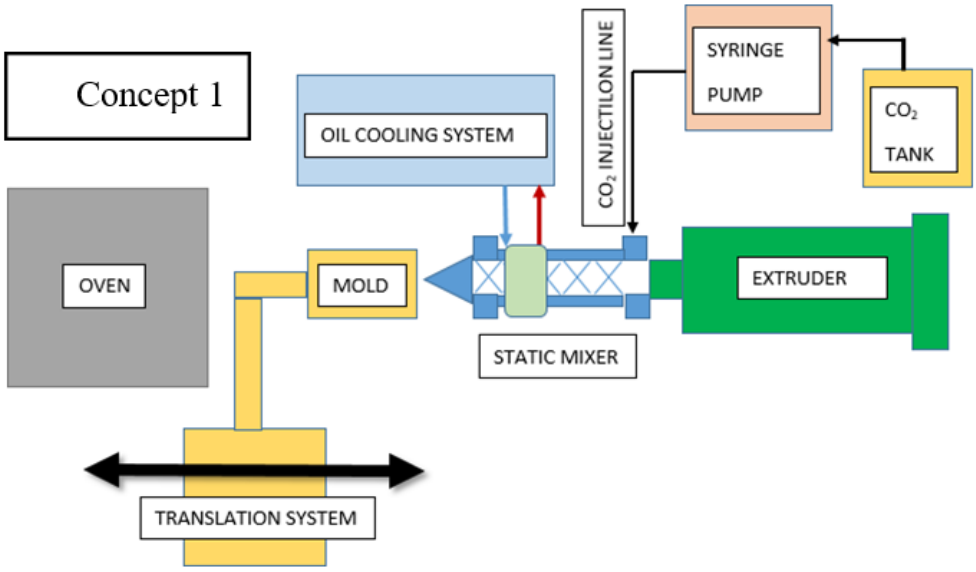

Figure 3.9: Concept 1, new experimental setup design for PBA foam production (Raktim and Pop-Iliev 2018).

***Concept 2*:** This experimental setup consists of two extruders placed in tandem arrangement (Figure 3.10). The first extruder serves to plasticize the plastic resin while the second extruder is utilized for mixing supercritical CO_2 into the polymer melt. In the second extruder, vigorous shear mixing can be achieved through the rotation of the screw. The pressure and melt flow rate are also controlled with the screw RPM of the second extruder. The first extruder only controls the material feed-rate into the second extruder. The temperature is maintained with PID controlled band heaters, located on the exterior surface of the extruder barrel. The gas is injected in the special

mixing zone of the second extruder where the geometry of the blade surface promotes rapid gas diffusion (Raktim and Pop-Iliev 2018).

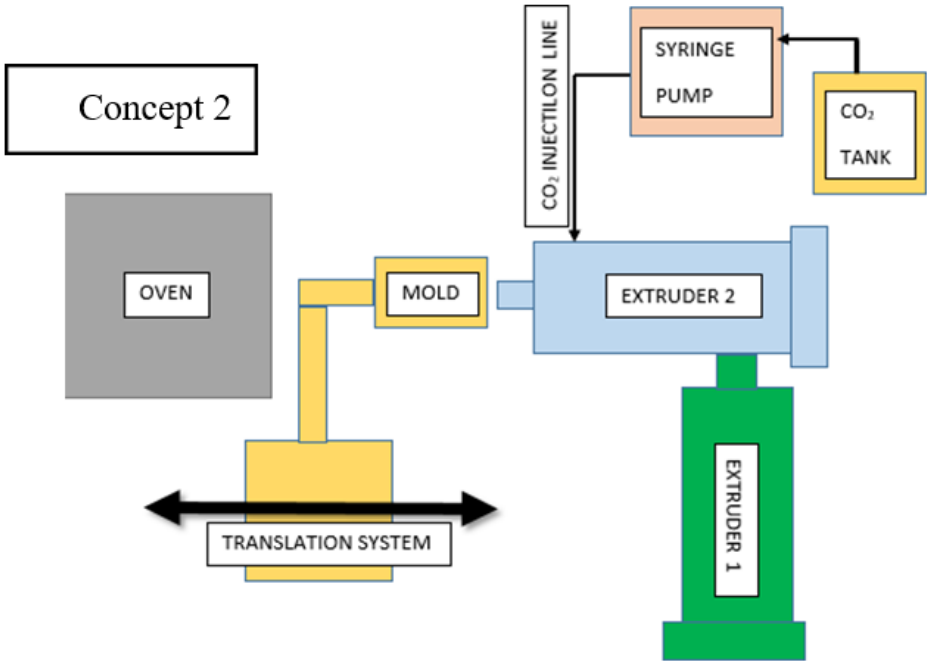

Figure 3.10: Concept 2, new experimental setup design for PBA foam production (Raktim and Pop-Iliev 2018).

***Concept 3*:** This experimental setup is a modified version of concept 1 with greater process control capabilities (Figure 3.11). In this proposed design, a gear pump is introduced after the static mixer. With a gear pump, it is possible to use mixing blades with greater surface area for enhanced mixing. The increase in pressure loss due to friction on the blade surface can be compensated with the gear pump. However, the flow into the static mixer and the melt pressure within is controlled from the extruder. The gear pump can maintain the processing pressure and flow rate before the gas laden polymer enters the die zone. In this setup, a closed loop water cooling system is utilized rather than an oil cooling system (Raktim and Pop-Iliev 2018).

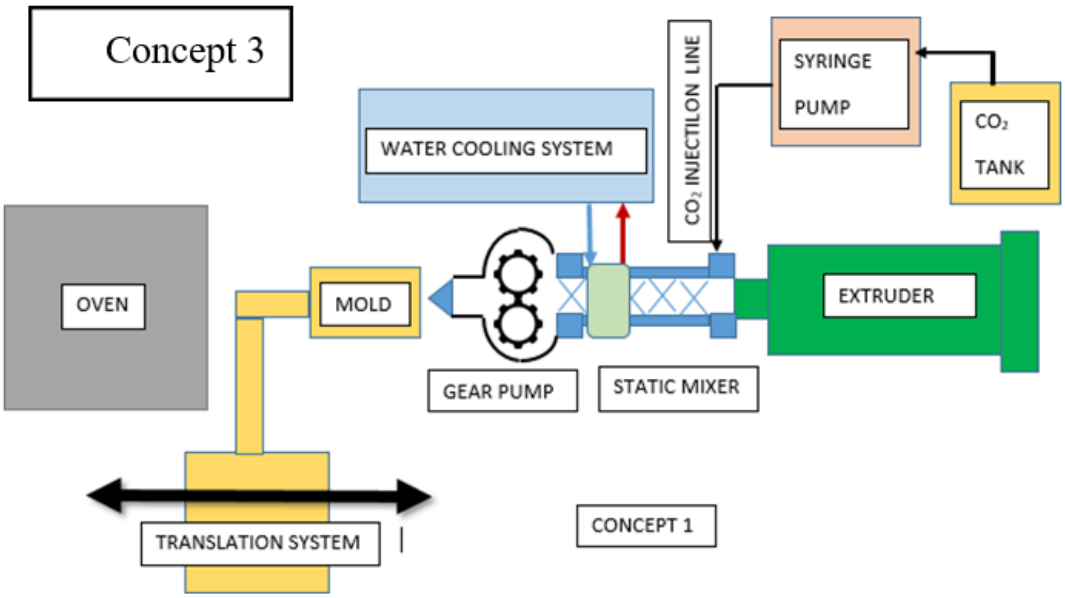

Figure 3.11: Concept 3, new experimental setup design for PBA foam production (Raktim and Pop-Iliev 2018).

The selection criteria and their importance scores are presented in Table 3.2. The first selection criterion is design complexity. A complex and unique design require longer development time therefore, the overall experimental setup design has received the highest importance priority. The second most important selection criteria are the process controllability and fabrication complexity. In order to control the quality of the injected foam, the process variables require modification when necessary. For this reason, an operator needs the ability to modify as many processing parameters as possible. However, with greater process control, fabrication complexity may increase as well. A researcher has to keep mindful of this fact especially with limited budget and time. Therefore, it is a good practice to buy as many standard and off-the-shelf parts to ease assembly as much as possible. For some components this may not be feasible but, it is the goal of the designer to minimize the fabrication time and assembly time (Raktim and Pop-Iliev 2018).

The final two selection criteria are specific to the lab environment. They are: space required for components, and safety. The safety concerns are mainly for the operators of the equipment. The operator will be exposed to moving mechanical components, high temperature heaters, pressure vessel housing the mixer, and chemicals used for the process. Although protective gear must be worn during the experiment, the health and physical safety of the operator should be given important consideration during the design process to minimize and/or eliminate exposure to

hazards. Finally, the least important selection criteria is the area required for the components. Since, the new experimental setup must integrate with the existing RRFM setup, it is important that all new components fit in the space between the extruder and the oven and still allow enough room for the mold translation system to bi-axially rotate outside the oven (Raktim and Pop-Iliev 2018).

Table 3.2: Concept feasibility for PBA foam production with RRFM technology.

Criteria	*Importance*	*Criteria 1*	*Alternative*	
			Criteria 2	***Criteria 3***
Design Complexity	10	Datum	-	-
Process Controllability	9		+	+
Space Required for Components	7		-	-
Safety	8		+	-
Fabrication Complexity	9		-	-
Weighted Total		0	-9	-25

The final weighted totals for concept 2 & 3 are negative, therefore, concept 1 will be used as the design for the new experimental setup design. Even though concept 1 has limited process control compared against the alternatives, it is more desirable for having significantly reduced design and fabrication complexity. In terms of safety for the operator, concept 2 is ideal for having the heating elements housed within the outer shell of the extruder. This eliminates exposure to hot surfaces during typical experimentation process. However, concept 2 require more lab space to place two extruders in tandem arrangement. This will further limit the work space for the operator and making it difficult to access other equipment. In regards of safety, concept 3 is not desirable for utilizing a water-based cooling system. Since polymer processing temperature is well above 100°C, the risk of water converting to steam during the cooling process is extremely dangerous

for the operator. It is for this reason an oil with a smoke point above the polymer processing temperature will be used in the cooler (Raktim and Pop-Iliev 2018).

3.4.5 *Summary of Developed Design Guidelines*

The new RRFGFM experimental setup will consist of a single mixing chamber where supercritical carbon dioxide will be injected at pressure ranging from 20-30 MPa to initiate the mixing process. The static mixer (mixing chamber) is going to be positioned at the output flange of a single screw extruder. The complete dissolution of gas into the polymer melt will be aided by static mixing blades housed within the chamber. The specially designed blade will regenerate shear fields to promote gas diffusion into the polymer matrix. The gas laden polymer solution will go through a rapid pressure drop at the die exit to induce phase separation between the gas and polymer and creation of the foam. An integrated cooling shell will be positioned at the exit of the static mixer barrel to provide temperature control.

3.4.6 *Static Mixer Design*

3.4.6.1 Static Blade Selection

Inside the chamber of a static mixer, the static blade surface replicate shear fields to thoroughly mix supercritical fluid into the polymer matrix. The geometry of the blade elements reorients the flow toward the radial direction to enhance the mixing process. The orientation of the mixing element also eliminates temperature gradients in the radial direction and recombines stagnant wall creep material into the main bulk flow. In light of all these advantages one major disadvantage is that the static blades impede melt flow due to friction on the blade surface. The pressure loss across the length of a static mixer channel is considerably higher than in a hollow pipe. Therefore, it is crucial to determine the acceptable blade type and length for a given extruder. The extruder has to provide enough force to push the polymer melt past the mixing elements. Currently, there are many different types of mixing blade design available in the market place. The differences in design dictate the application of the element type in polymer processing. Industrial applications of static mixers are prominent in blow molding, foam sheet extrusion and blow film co-extrusion (Schneider n.d.).

The purpose of a static mixer is to homogenize the polymer melt with the supercritical fluid to create a single-phase polymer-gas solution before the melt flow enters the die section. By design each mixing element is offset by 90° from the adjacent element. This way, the flow is split toward the radial direction and later recombined toward the axis of the mixer barrel. The pressure loss across the length of the static mixer directly depends on the viscosity of the polymer melt, Reynolds number, mixing element geometry, process temperature, and the polymer grade (Schneider n.d.).

$$\boldsymbol{\Delta P} = \left(\frac{\boldsymbol{4}}{\boldsymbol{\pi}}\right) \boldsymbol{Ne\ Re_D} \left(\frac{\dot{\boldsymbol{V}}}{\boldsymbol{D^3}}\right) \boldsymbol{\eta} \left(\frac{\boldsymbol{n_{ME}}}{\boldsymbol{2}}\right) \tag{3.1}$$

$$\boldsymbol{\eta = (\dot{\gamma}, T, (type, grade), p_{op}} \tag{3.2}$$

$$\boldsymbol{\dot{\gamma} = (V\,, D_{ME}, geometry)} \tag{3.3}$$

The pressure loss across the length of the mixing element is obtained from Equation 3.1. The number of mixing elements is represented by the term n_{ME} and Ne is the newton number and Re_D is the Reynolds number of the polymer melt inside a pipe with diameter D. The volumetric flow rate is represented by $\dot{V}$ and the melt viscosity is represented by η. The melt viscosity of the polymer is dependent on temperature, shear rate ($\dot{\gamma}$), polymer type and, operating pressure (p_{OP}) (Equation 3.2). The shear rate ($\dot{\gamma}$) in Equation 3.3 is a function of flow rate, pipe cross section, and mixing blade geometry. The two major types of commercially available mixing elements are helical blade and X grid. The combined value of $NeRe_D$ for helical mixer can vary between 200 & 400. However, for an X grid type of mixer the $NeRe_D$ value can vary from 1200 to 2000 (Schneider n.d.).

A parametric analysis was conducted to determine the most suitable blade design and overall length for PBA foam production. The analysis was carried out on helical and GX grid mixing elements from Stamixco Company presented in Figure 3.12. The melt flow viscosity was varied from 500 Pa•s to 3000 Pa•s to determine pressure loss across the length of various types of mixer blade arrangement. It should be noted that the supercritical fluid acts as a plasticizer and reduces polymer viscosity at a given processing temperature.

The GX type mixer have greater blade surface area and this leads to higher degree of mixing compared to helical elements. However, with greater surface area, pressure loss is also

significantly higher than helical mixers. The helical mixing elements are sold in six blades increment and the GX-grid mixers are sold in four element increment. For this reason, pressure loss is analyzed for 12 helical blades with 16 GX elements, since they are close in length. Also, 12 helical elements were being considered during the early phase of the design process. From the analysis, pressure loss remained well below 10 MPa for helical mixing elements. However, pressure loss is only acceptable for GX grid mixer when the melt viscosity is below 1000 Pa•s. Therefore, the final design will utilize helical mixers to form the single-phase solution.

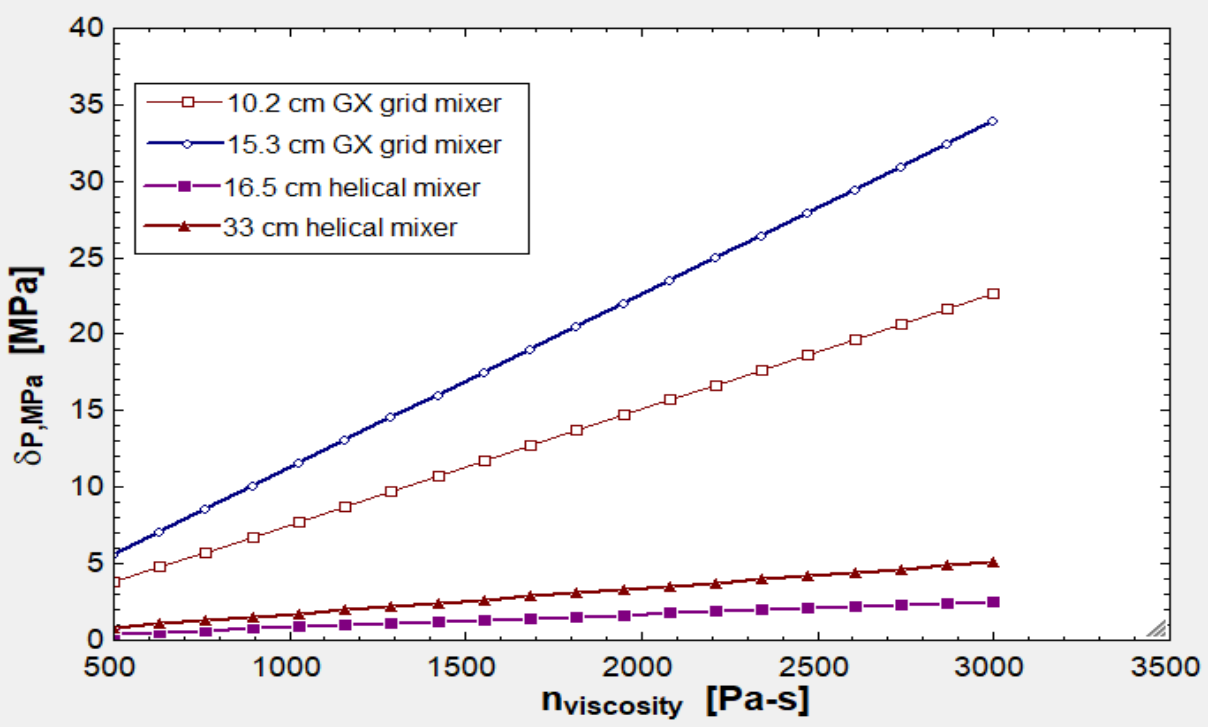

Figure 3.12: Pressure loss for GX-grid and helical blades (Raktim and Pop-Iliev 2018).

3.4.6.2 Static Mixer Chamber Design

The Static mixer chamber and 10 helical mixing blades were manufactured by Stamixco. The internal diameter of the barrel is 1.9 cm and the outer diameter is 2.9 cm. The chamber was machined from 17-4 PH stainless steel and it was designed to operate at a maximum temperature of 170°C with allowable pressure of 31 MPa. This has been determined from ASME section 8 Division II pressure vessel code. The upstream extruder adapter flanges shown in Figure 3.13 was custom machined to have a draft angle of 60° for a 'V' shape clamp. When torque is applied to the

nut of a clamp, radial force is created which wedges the extruder flange and extruder adapter flange together for a pressure tight seal.

The injection port after the flange has been designed for a spring activated check valve supplied by Stamixco. A detailed description of the check valve will be given in the preceding section. The cooling shell near the exit of the static mixer provides temperature control by reducing melt temperature during the extrusion process. The inner section of the cooling shell contains fins to enhance heat transfer. The cooling fluid flow through the channels between the fins from the inlet to the outlet port. Two additional ports are positioned after the cooling shell. The top port is for a melt pressure transducer with ½-20 UNF thread. The bottom port is for a rupture disc with ½-20 UNF thread as well. The output section of the mixing chamber is also flanged to attach to a die. However, the draft angle is only 51° for a smaller 'V' clamp. The Static mixer chamber contains three major sections: Gas Injection; Homogenization; and the cooling section (Figure 3.14). The 2-D drawings of the static mixer are included in Appendix A2.

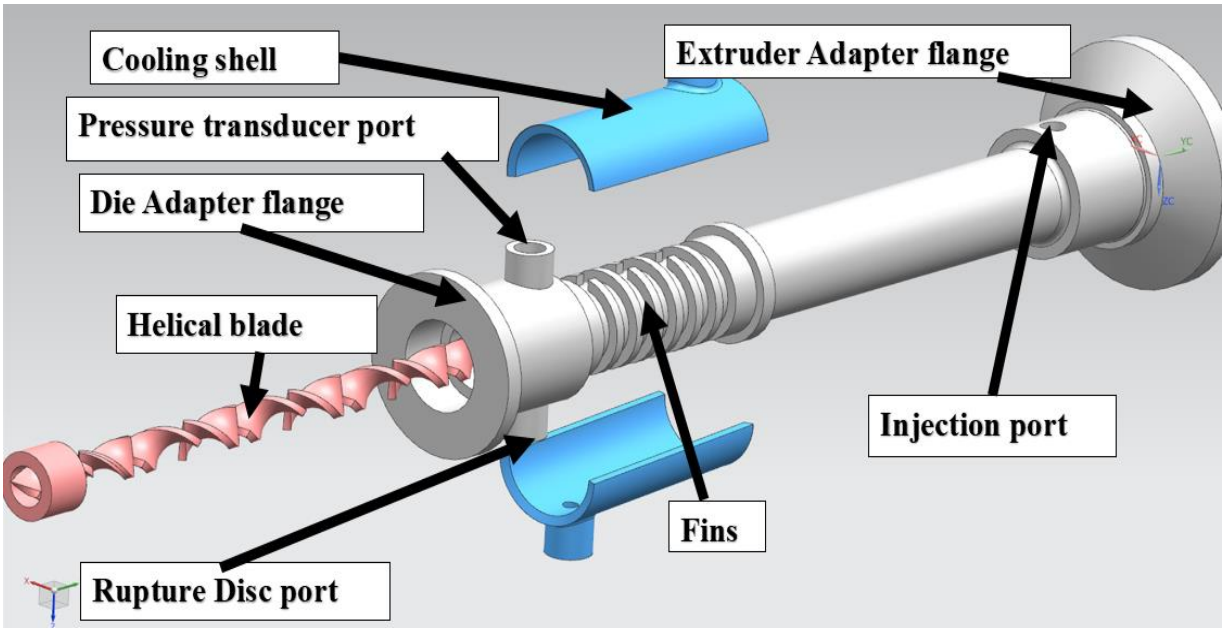

Figure 3.13: CAD representation of the static mixer chamber design.

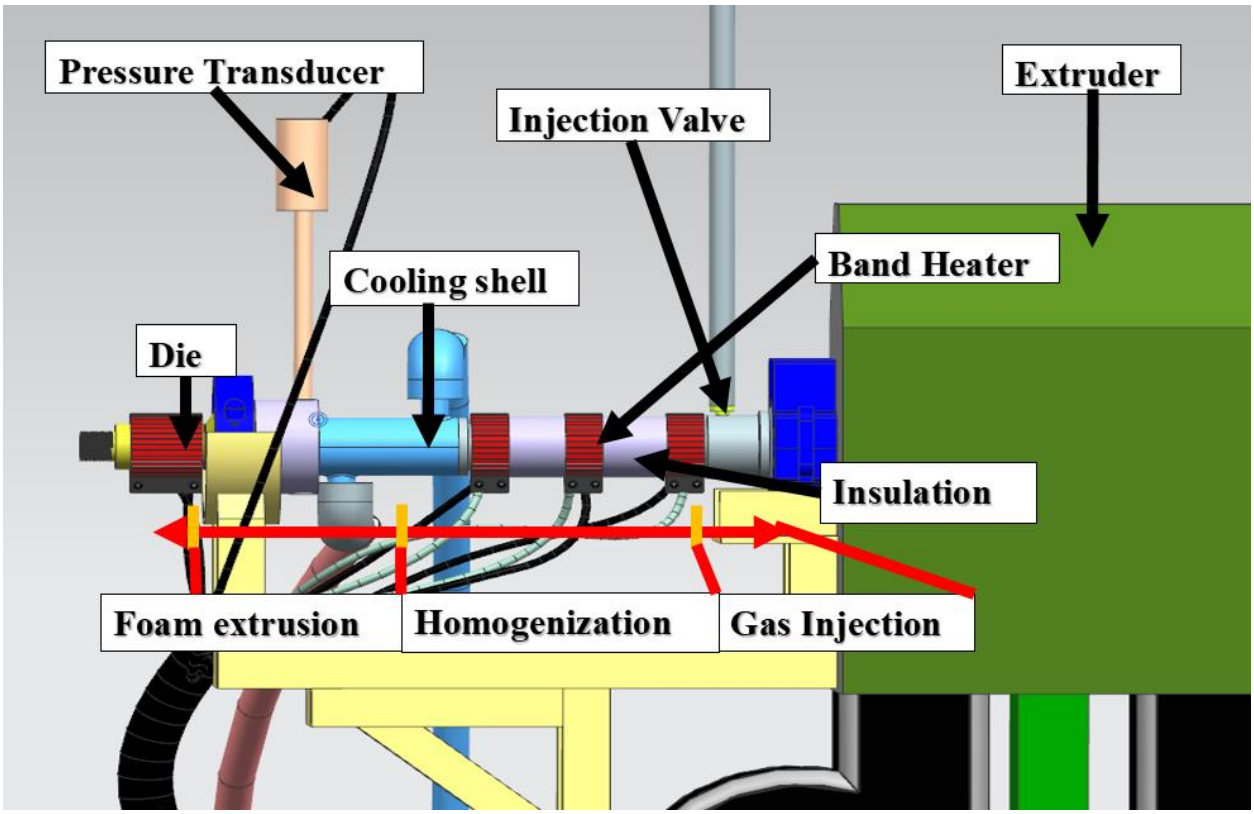

Figure 3.14: CAD representation of PBA based experimental setup.

Gas Injection Section: Supercritical gas is directly injected into the mixing chamber from a syringe pump. The gas is supplied to the syringe pump inlet from a CO_2 gas cylinder. The gas within the cylinder is pressurized at 6.2 MPa (900 psi) and it is 99.1 % pure Bone Dry grade carbon dioxide (Figure 3.15). When the CO_2 cylinder valve is open, the gas flows through 1/8" SS tubing into the syringe pump piston chamber. A separate two-way shutoff valve at the syringe pump inlet control the flow into the piston chamber (Figure 3.16). This valve remains closed during the gas injection process to prevent backflow into the CO_2 cylinder. In case the inlet line to the syringe pump becomes over pressurized, a pressure relief valve is present on the CO_2 cylinder to vent gas above 10 MPa.

Figure 3.15: Carbon Dioxide cylinder.

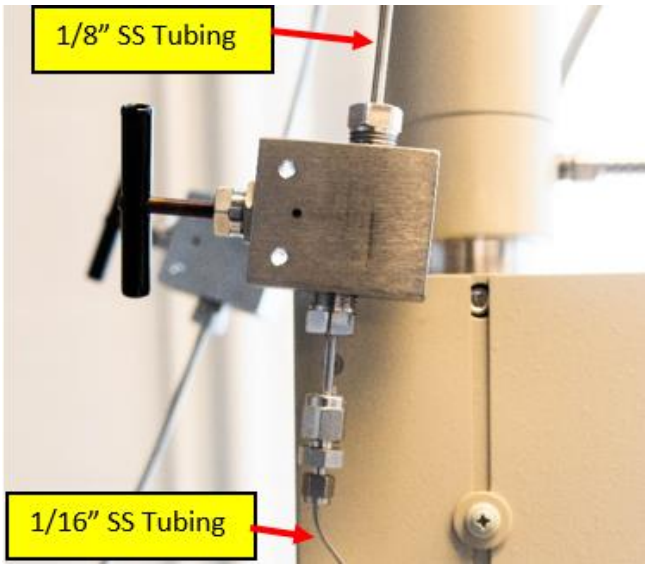

Figure 3.16: Two-way shutoff valve at syringe pump inlet.

The syringe pump is manufactured by Teledyne USA, a company specializing in supercritical gas extraction. In all experiments, the 260D variant was utilized for PBA injection (Figure 3.17). The pump chamber capacity is 266 ml with a refill time of 2.5 minutes. The displacement resolution is 16.63 nl/step and, the flow rate resolution is 1 µl/min. The pressure range of the equipment is 0.6895 to 517.1 bar. The piston is designed to operate from 1.0 µl/min to 107 ml/min. A pressure transducer positioned at the top of the piston chamber measures the

pressure at the outlet port of the pump. The pressure reading along with flowrate and current chamber volume is displayed on the controller (Teledyne 2020).

In a similar fashion to the inlet port, another two-way shut off valve is present at the outlet port. This valve can be used to isolate the piston chamber from the injection line. However, unlike the inlet port the outlet port SS tubing is reduced from 1/8" to 1/16" SS after the two-way valve. The 1/16" and 1/8" 316L SS tubing are manufactured by Autoclave for low pressure application (< 69 MPa, 10 000 Psi) (Autoclave 2020). The tubes are connected to all fittings by compression. Where a ferrule is compressed on the tube when a nut is tightened, creating a pressure tight seal (Valco 2019).

To monitor the pressure at the inlet of the check valve, an Aschroft oil filled general service pressure gauge was utilized (Figure 3.18). The span accuracy is ASME Grade 1A $\pm$ 1% and the outer casing is constructed from 316 stainless steel. The pressure gauge range is from 0 to 5000 Psi (Ashcroft 2012). The pressure gauge is connected to a threaded capsule diaphragm to provide protection against high temperature heaters located near the static mixer inlet line (Figure 3.19). The diaphragm material is constructed from 316 stainless steel and the inner PTFE gasket between the bottom housing and the diaphragm provide corrosion resistant seal (Ashcroft 2011). The pressure gauge diaphragm assembly is connected to the injection line through a 1/16" tee connector. Where one line splits toward the diaphragm and the other junction connects directly with the check valve (Figure 3.20).

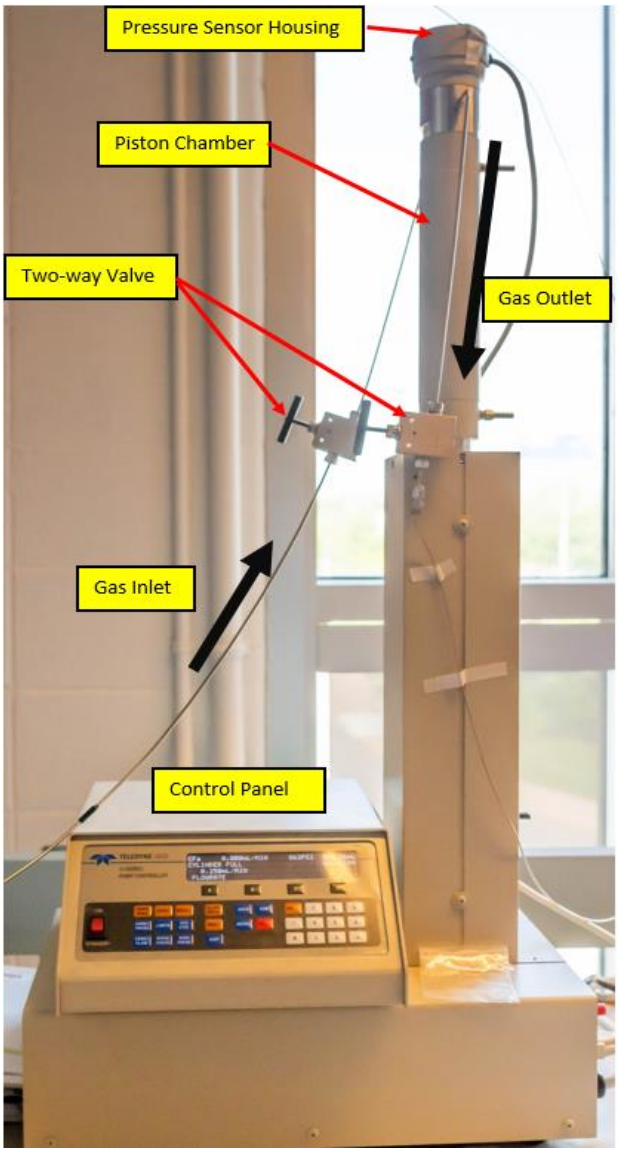

Figure 3.17: 260D Teledyne Syringe Pump.

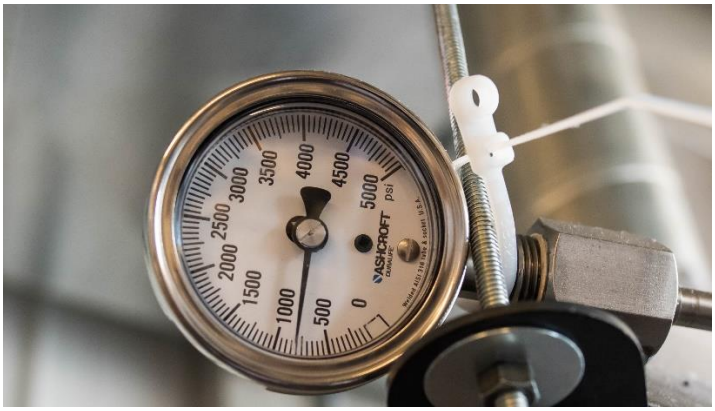

Figure 3.18: Oil filled pressure gauge.

Figure 3.19: Diaphragm assembly.

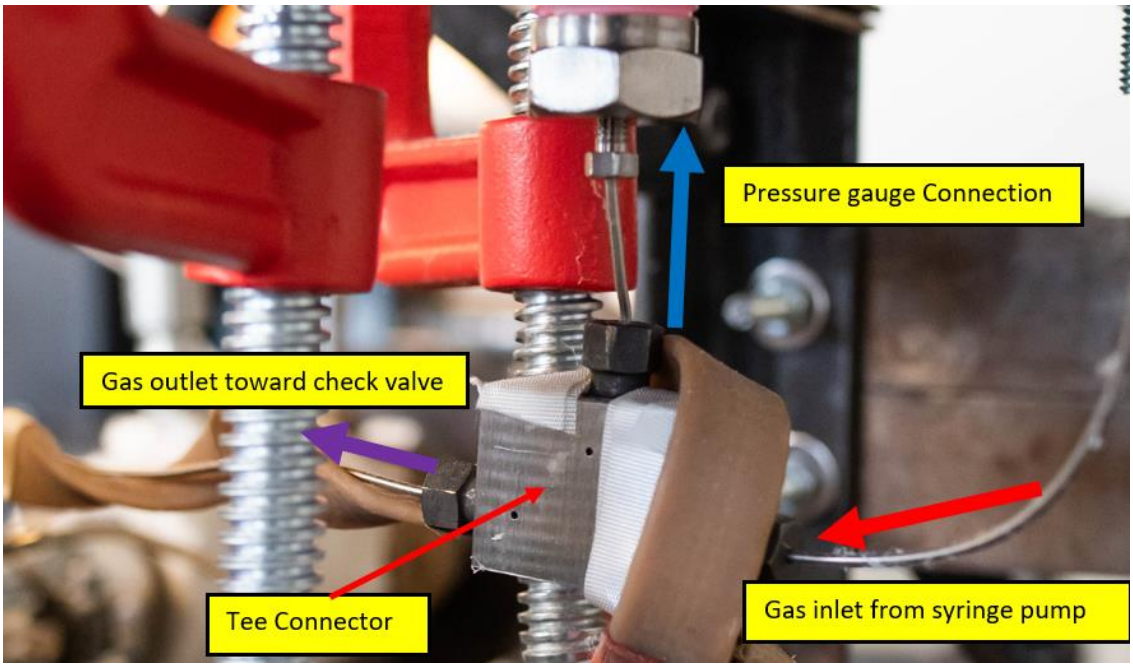

Figure 3.20: Tee connector.

The pressurized fluid is preheated to 90°C to ensure supercritical state as the fluid enters the static mixer chamber. A constant wattage cable heater is wrapped around the tee connector and the tubing to raise the fluid temperature (Figure 3.21). Unidirectional fluid injection into the polymer melt is maintained with a spring activated check valve shown in Figure 3.22. By design the spring mechanism is isolated from the fluid flow by copper O-rings to prevent the melt polymer from breaching the spring housing during back flow. The opening pressure can be changed by adjusting the degree of spring compression which can be done by turning the adjustment knob at the top of

the valve. When the opening pressure is reached, the needle connected to the spring actuate inward into the valve chamber to allow the fluid to enter the mixer chamber. In case of sudden drop in injection pressure, the spring return to the reset position and the needle tip moves outward to reseal the valve outlet port.

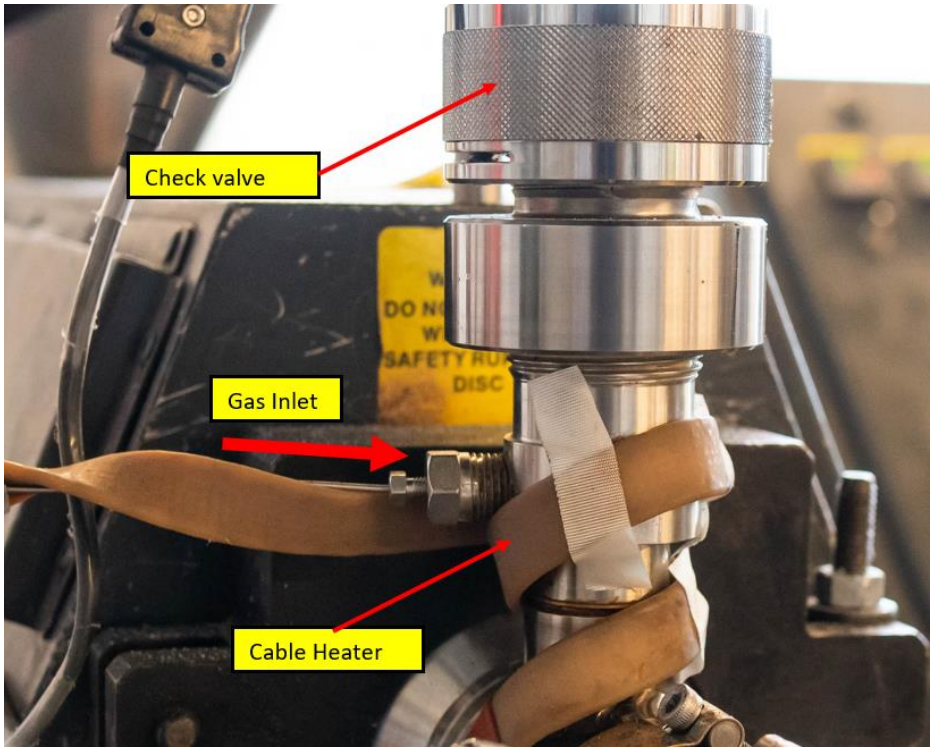

Figure 3.21: 120-volt cable heater.

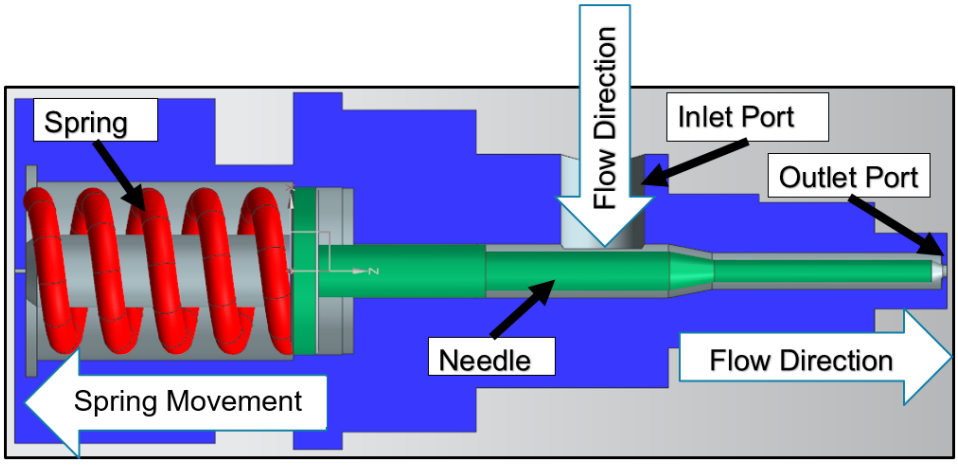

Figure 3.22: Stamixco spring activated check valve.

Homogenization Section: In this section, the chamber is heated to the desired processing temperature to promote gas diffusion into the polymer matrix. On the exterior surface, two-piece band heater is utilized as the primary heat source (Figure 3.23). Each half of the heater insulated is 5" long and designed for 1.5" barrel diameter. The combined heat output from the band heater is 600 watts and each half is rated for 120 VAC. The power is supplied to the heater by the extruder from a disconnect twist lock plug NEMA L6-15P. The maximum operating voltage is 230 VAC and maximum supply current is 5 Amp. The heat output is controlled with a J-type thermocouple in a closed loop feedback system. The temperature can be regulated on the extruder control panel along with any additional heaters.

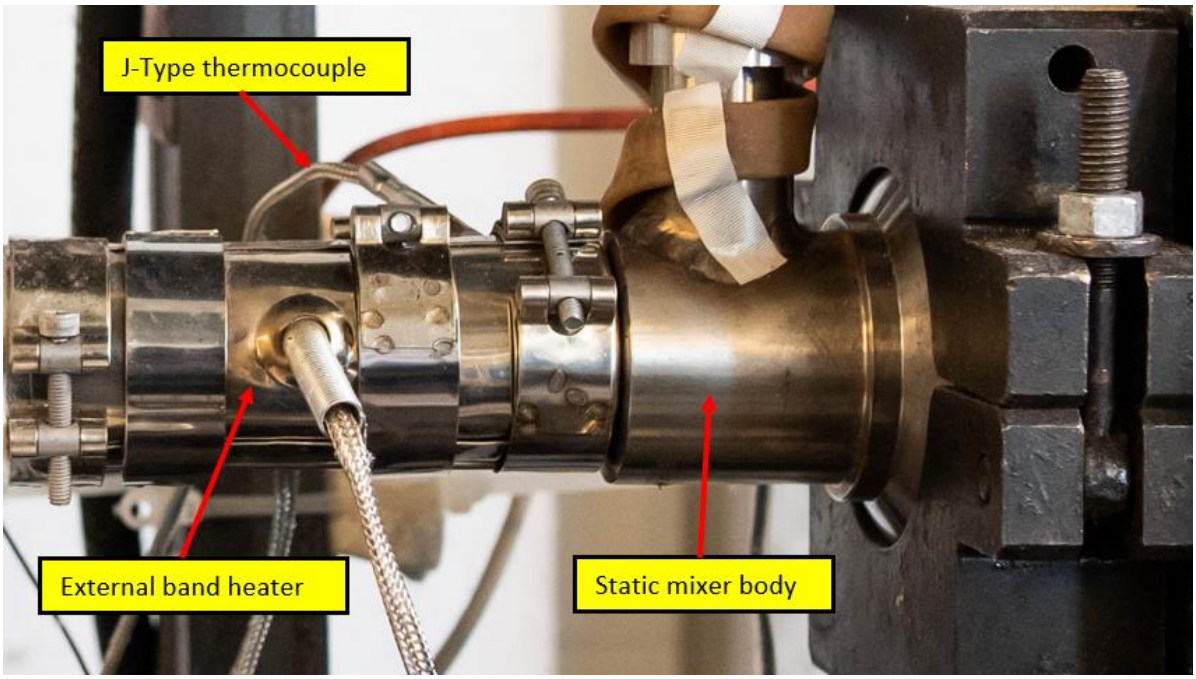

Figure 3.23: Band heater surrounding the external barrel of the staticmixer chamber.

The helical blades with in the mixer barrel are positioned after the spring activated check valve. The blades are manufactured by twisting metal strip under heat and pressure. However, it is also possible to produce the blade by machining a solid piece of stainless steel rod. A detailed drawing of the helical blade assembly is given in Appendix A3. In the assembly, each blade is 1.25" long and 0.65" wide. The surface of the blades is polished with a surface finish of Ra <= 32 micro-inches. Each blade thickness is 3 mm and the leading and trailing edges are knife edged. The blades are offset by 90° from each other. This offset splits the flow in the radial direction and

enhance the degree of mixing. The blade surface generates shear fields and disperse the large injected gas bubbles into smaller ones for faster diffusion into the polymer matrix.

The exposed external surfaces of the static mixer chamber is insulated to minimize heat loss (Figure 3.24a). Insulation is also used to protect heater controllers located near hot surfaces on the main support stand (Figure 3.24b). The insulation material is silica aerogel with thermal conductivity of 21 (mW/m•K) with a maximum operating temperature of 650°C (Aerogel 2020).

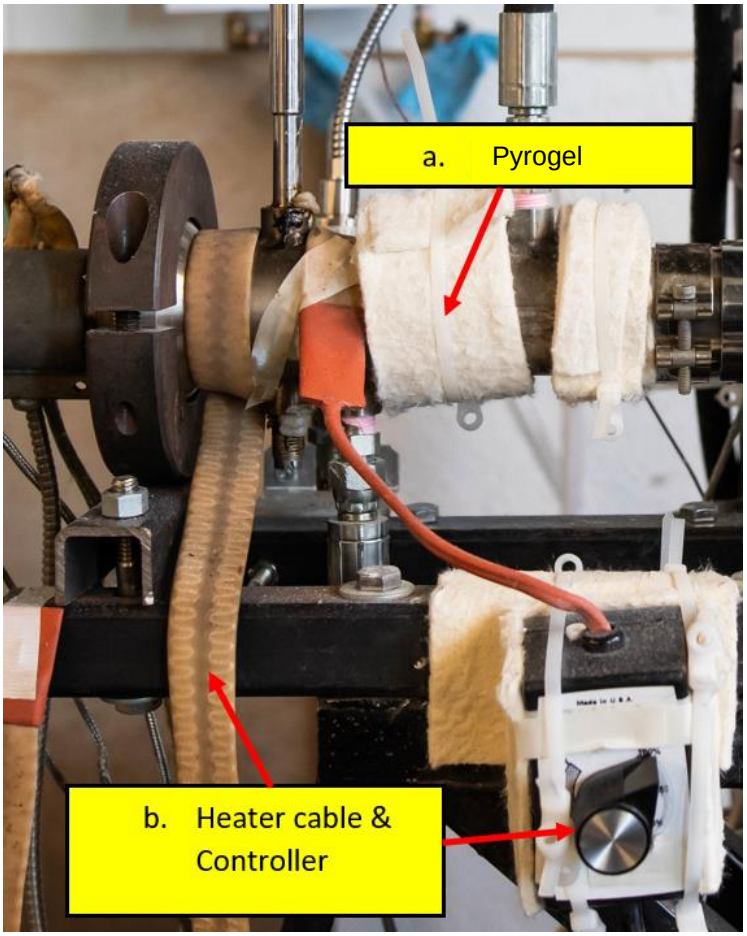

Figure 3.24: a) Pyrogel insulation b) 120VAC heater controller on the support stand.

The cooling shell serves to control the melt temperature during the extrusion process. The cooling fluid is pumped intermittently to cool the melt temperature when required. A 3-D representation of the pumping system is represented in Figure: 3.25. A double acting hydraulic lifting system was used to pump the hydraulic fluid through the cooling shell. The pump is operated with 12 V power supply. The fluid is pumped at 500 Psi with a constant flowrate of 1.32 GPM (Princessauto 2020). A hydraulic hose assembly connects the pump with the cooling shell and the

radiator fan (Figure 3.26). In the experimental setup, the lifting system requires 100 amps to pump the fluid at 1.32 GPM. The power supply unit for the hydraulic lifting system is an 110V AC to 12V DC 100 Amp power converter (Figure 3.27) (Amazon 2020). For the high Amp requirement, copper clad aluminum 0 gauge cable has been used. A pressure gauge mounted at the outlet valve displays the pressure during the operation of the pump.

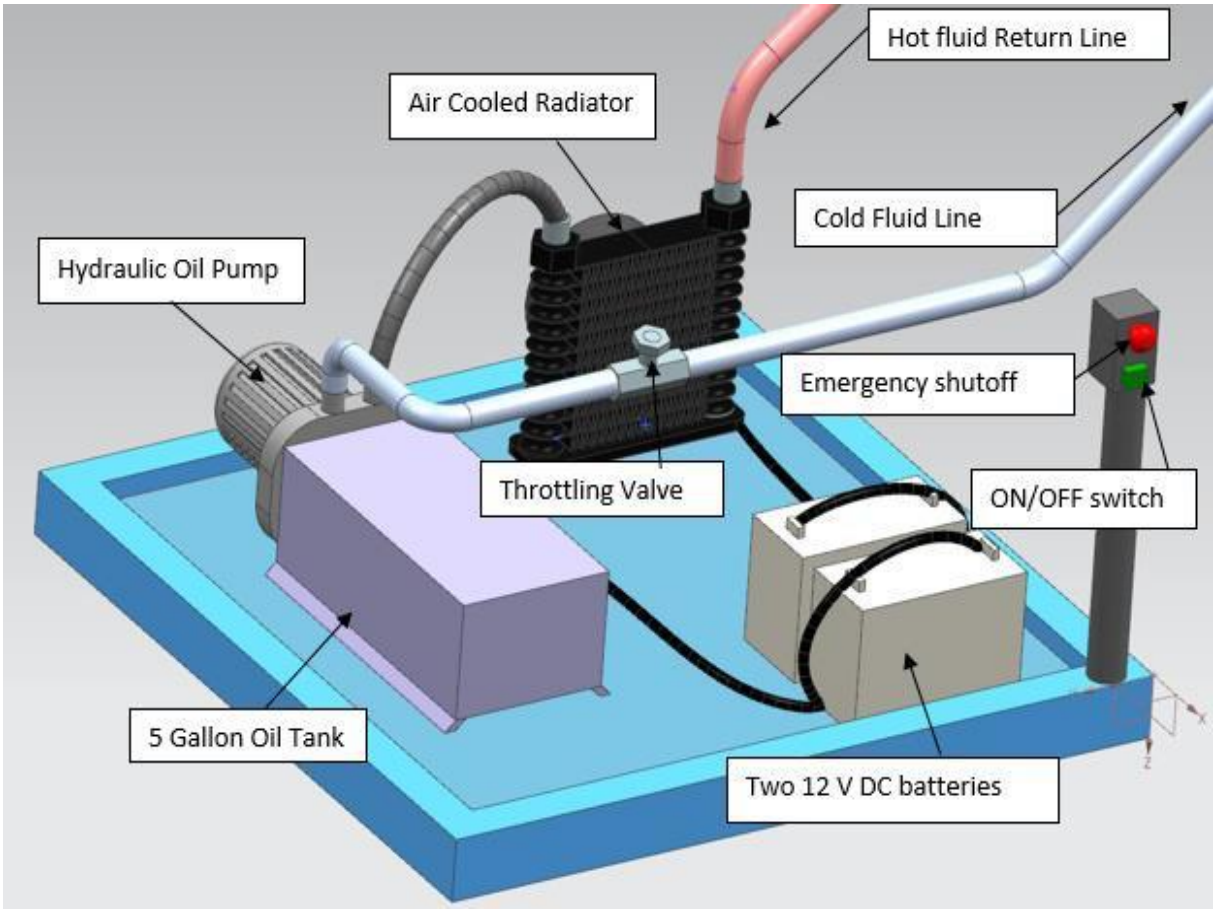

Figure 3.25: Static mixer cooling system assembly (Raktim and Pop-Iliev 2018).

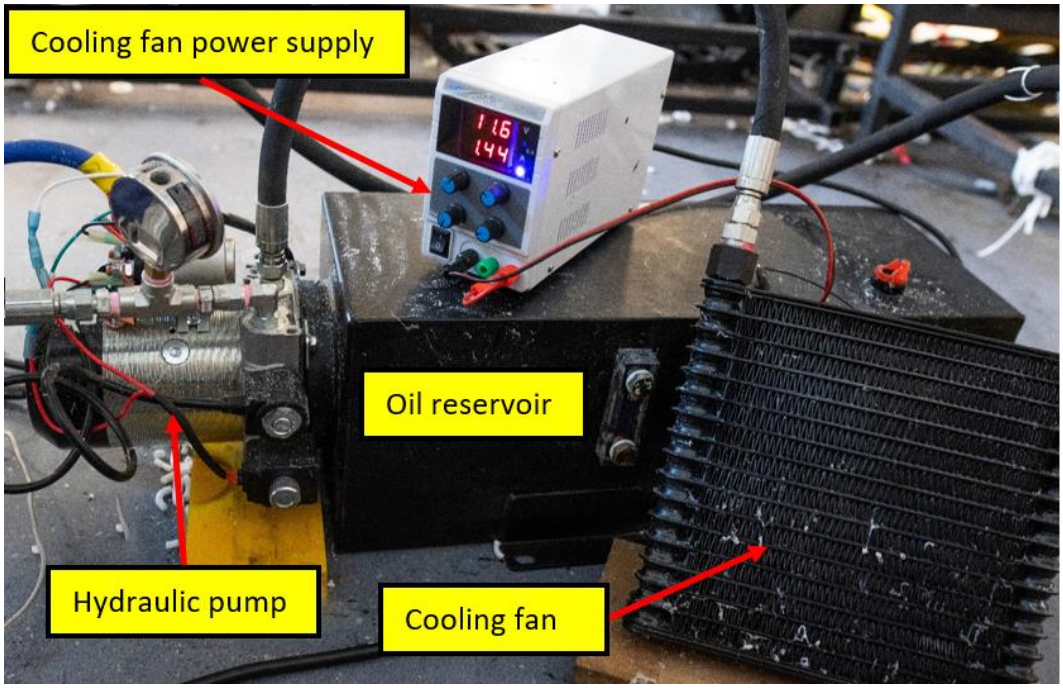

Figure 3.26: Hydraulic cooling system.

Figure 3.27: PowerMax AC to DC converter for hydraulic lifting system.

A forced air cooled radiator is used for the cooling fluid before the hydraulic oil returns to the reservoir tank. The radiator can remove 4 HP of heat at a continuous flowrate of 2.6 GPM. The airflow at the recommended fan current of 1.7 amp is 266 CFM (cubic feet per minute). The fan is operated with a variable DC power supply. The maximum voltage rating for the radiator is 12 V with 5 Amps. The hydraulic oil used in the cooling system is of ISO AW 45 grade. The smoke point of this particular oil was tested to be at 190°C.

Foam Extrusion Section: From the end of the cooling shell to the tip of the die nozzle constitutes the foam extrusion section. The processing temperature at the exit of the static mixer

is monitored with a Gefran melt pressure transducer (Figure 3.28a). The sensor signal is transmitted through a six-pin bayonet cable. The pressure cable is connected to a six-digit Gefran LED panel (Figure 3.28b). The pressure transducer can display pressure up to 690 bar. The signal from the J-type thermos couple is sent through OSTW standard male connector. The port size for all melt pressure transducer is ½-20 UNF connection (Gefran 2020). The exposed mixer surface at the melt pressure transducer port is heated with constant wattage heater cable. A temperature control dial is used to control the heater output.

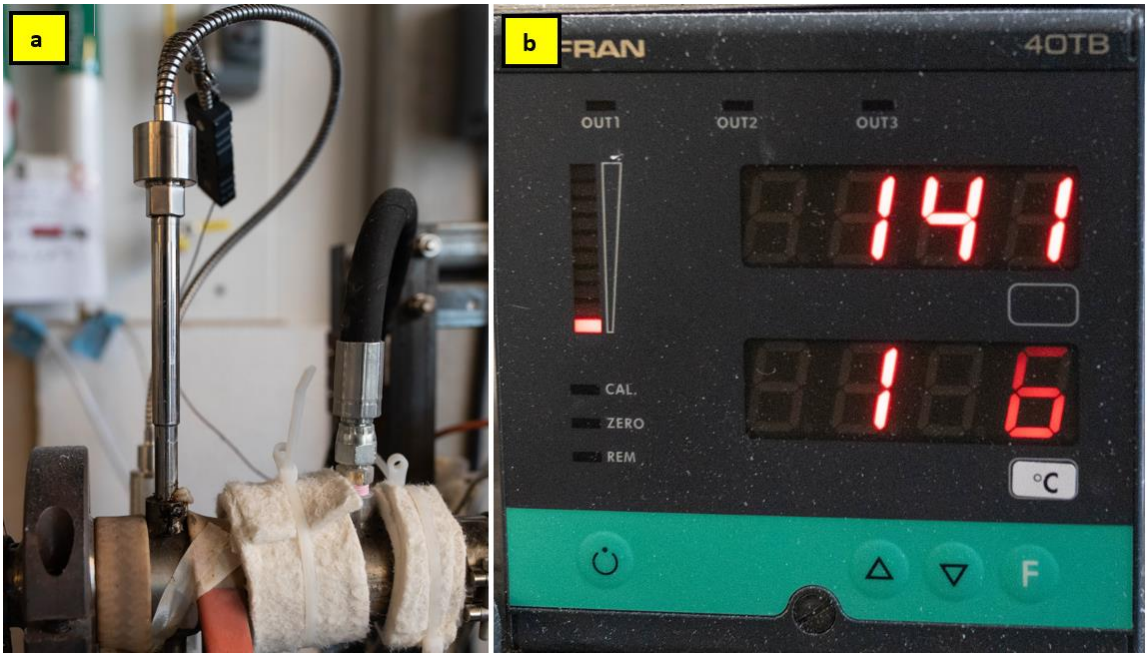

Figure 3. 28: a) Gefran melt pressure transducer and constant wattage heater. b) Temperature and pressure display panel.

The final region of the extrusion section is the die zone, where PID controlled band heaters maintain the die zone temperature. The die nozzle has been designed to inject foam into a cylindrical mold cavity. The interior geometry of the nozzle is gradually reduced to a 3 mm cross-section at the die exit (Figure 3.29). The nozzle is machined from 17-4PH stainless steel rod and its overall length is 10 cm. The complete final experimental setup is presented in Figure 3.30.

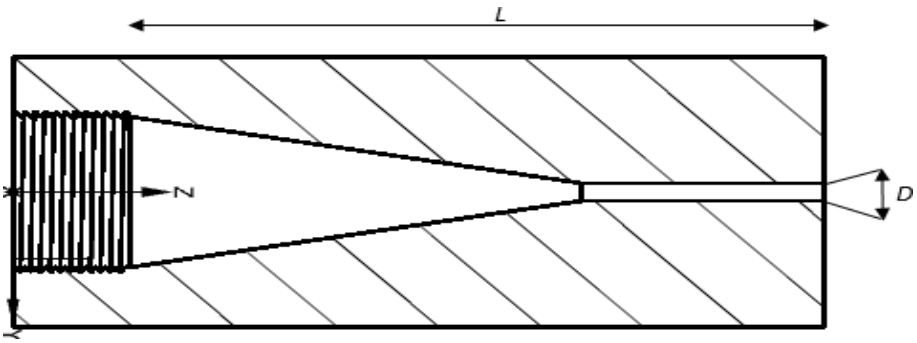

Figure 3.29: Interior geometry of the nozzle.

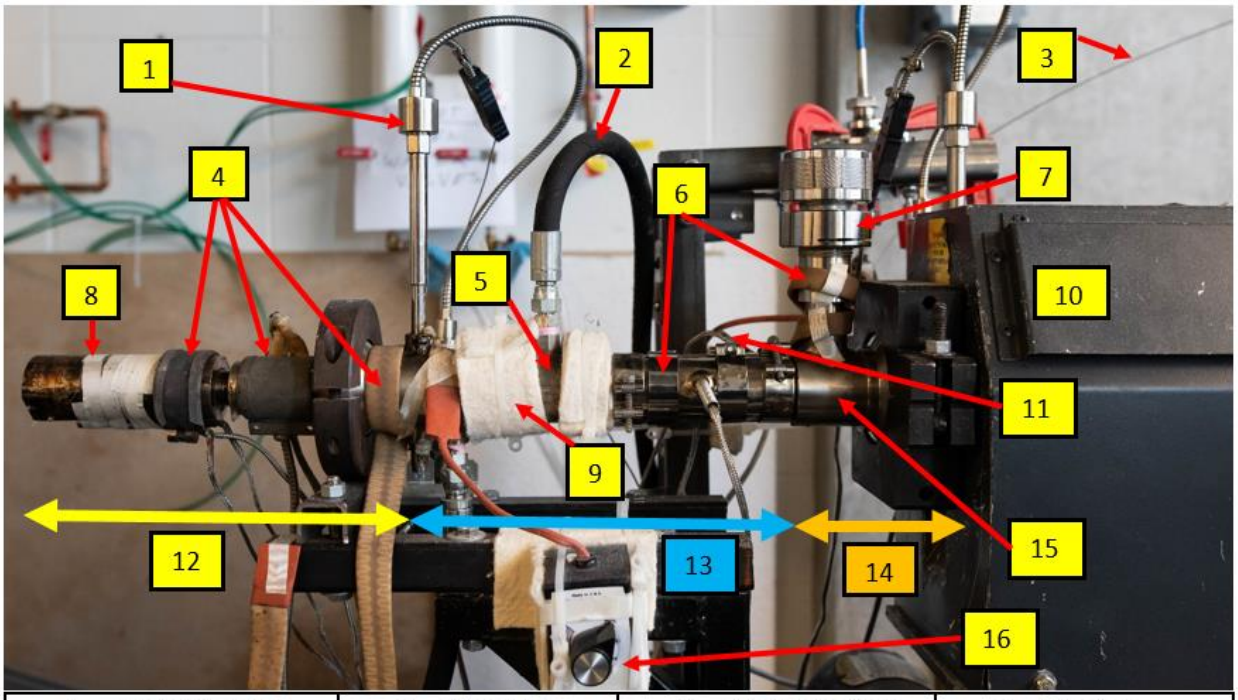

1. Melt Pressure Transducer	2. Cooling Hose	3. Gas Injection Line	4. Heaters
5. Cooling Shell	6. Barrel Heater & Cable Heater	7. Check Valve	8. Die Nozzle
9. Pyrogel Insulation	10. Extruder	11. J-Type Thermocouple	12. Foam Extrusion Section
13. Homogenization Section	14. Gas Injection Section	15. Static Mixer Barrel	16. Cable Heater Controller

Figure 3.30: Complete experimental setup for PBA foam extrusion.

Chapter 4. Experimental Validation of the Designed & Built RRFGFM Experimental Setup

4.1 Introduction

This chapter presents the experimental process to determine the feasibility of the new experimental RRFGFM setup to produce functionally graded foamed core with polyethylene (PE). The experimental trials revealed that, among the other governing variables, foam quality can vary drastically depending on the grade of the material being used. A detailed description of all the processing parameters for all foaming experiments are given in the upcoming sections of the present chapter.

4.2 Experimental Materials

The material property of all polymer resins used in the subsequent foaming experiments are listed in Table 4.1 (NovaChemicals 2020). NOVA chemicals was the primary resin supplier for extrusion grade PE and, Equistar provided the rotational molding grade LLDPE resin. Furthermore, the foaming experiments were conducted with extrusion grade HDPE and MHDPE, foam extrusion grade LDPE, and rotational molding grade powder sHDPE. Equistar supplied LLDPE was exclusively used to produce the outer skin of the composite materials (MatWeb n.d.).

The extrusion grade PE 19C is a homo-polymer manufactured for film extrusion. The secondary extrusion grade PE used in the experiment was MHDPE, which is manufactured from hexane co-monomer for pipe extrusion. However, the LDPE resin supplied by NOVA chemicals was exclusively manufactured for foam production. Similar to the extrusion grade PEs, the LDPE is also a homo-polymer but the flexure modulus is well below the extrusion grade HDPEs. The rotational molding grade sHDPEs supplied by NOVA were also utilized for foam extrusion as well. It should be noted that sHDPE is a special type of HDPE used for moisture barrier application in food industries (Aubee, Lam and Marshall 2006). Both grades of sHDPE were produced from octane co-monomers (NovaChemicals 2020).

Table 4.1: Material property of PE resin from NOVA chemicals & Equistar.

Resin Properties	ASTM Test	19C (HDPE)	HE-Y499-AC (MHDPE)	LA-0522-A (LDPE)	RMS-245-UG (sHDPE)	RMS-341-UG (sHDPE)	GA625662 (LLDPE)
MFI (g/10min)	D1238	0.95	0.3	4.5	1.7	3.5	5
ρ (g/cm^3)	D792	0.958	0.949	0.920	0.945	0.941	0.935
Flexure Modulus (MPa)	D790	840 (ASTM D882)	1 140	276	1 030	827	601
Yield Strength (MPa)	D638	25 (ASTM D882)	24	9.4	23	20.2	17.2

The CBA selected for the experimental process is Celogen OT™. This material was purchased from Crompton Chemicals. The activation temperature for Celogen OT™ is above the melting point of all grades of PE. However, Celogen AZ™ activation temperature is also above all grades of PE. Unlike Celogen AZ™, Celogen OT™ can be used at lower processing temperatures since the decomposition temperature for Celogen AZ™ is 170°C. The material properties of Celogen OT™ are presented in (Kimberly 2009).

Table 4.2: Celogen OT™ material properties (Kimberly 2009).

CBA Properties	Celogen OT™
Chemical Composition	p,p'=oxybis(benzenesulfonylhydrazide)
Gas Composition	Nitrogen (91%), steam (9%)
φ_{STP} (cc/g)	125
Decomposition Temperature (°C)	160
Density (kg/m^3)	496

To increase the cell density of the foam produced with physical blowing agent (PBA), talc was utilized. It is also known as hydrous magnesium silicate and it is commonly purchased in its powder form. For foaming experiments talc was purchased from MiliporeSigma. Unlike chemical blowing agents, talc is inert and does not go through chemical decomposition at typical PE melt processing temperatures. It can be utilized as a nucleating agent for all types of polyolefin

including polypropylene resins. The material properties of talc are listed in Table 4.3 (MilliporeSigma 2020).

Table 4.3: Talc material properties (MilliporeSigma 2020).

Nucleating Agent Properties	Talc
Chemical formula	$3MgO•4SiO_2•H_2O$
Particle size	< 10 µm
Molecular Weight	379.27 g/mol

4.3 Thermal Characterization of Experimental Materials

Thermal gravimetric analysis has been conducted to determine the decomposition temperature of the CBA and the onset of thermal degradation of all the resin types. At the degradation point the polymer backbone experiences bond scission and eventually complete breakdown of the molecular structure. The DTG curve identifies the temperature where maximum mass loss is present. The respective onset of degradation temperatures and the respective DTG traces for each resin type is presented in Figures 4.1-4.6. The decomposition temperature of Celogen OT™ is given in Figure 4.7. The degradation temperatures are summarized in Table 4.4.

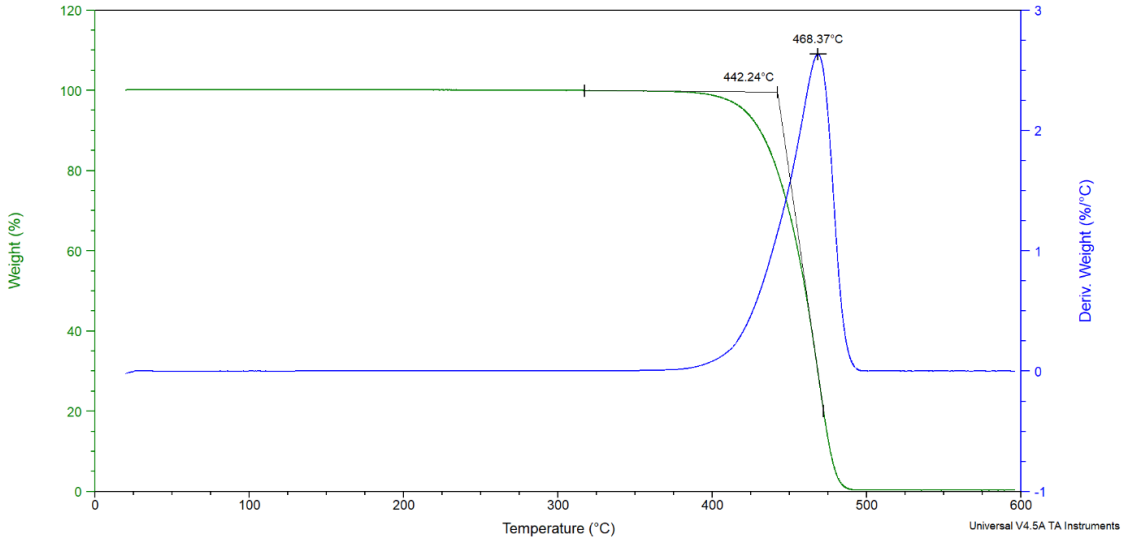

Figure 4.1: TGA thermograph for 19C (HDPE), heating rate 10°C/min.

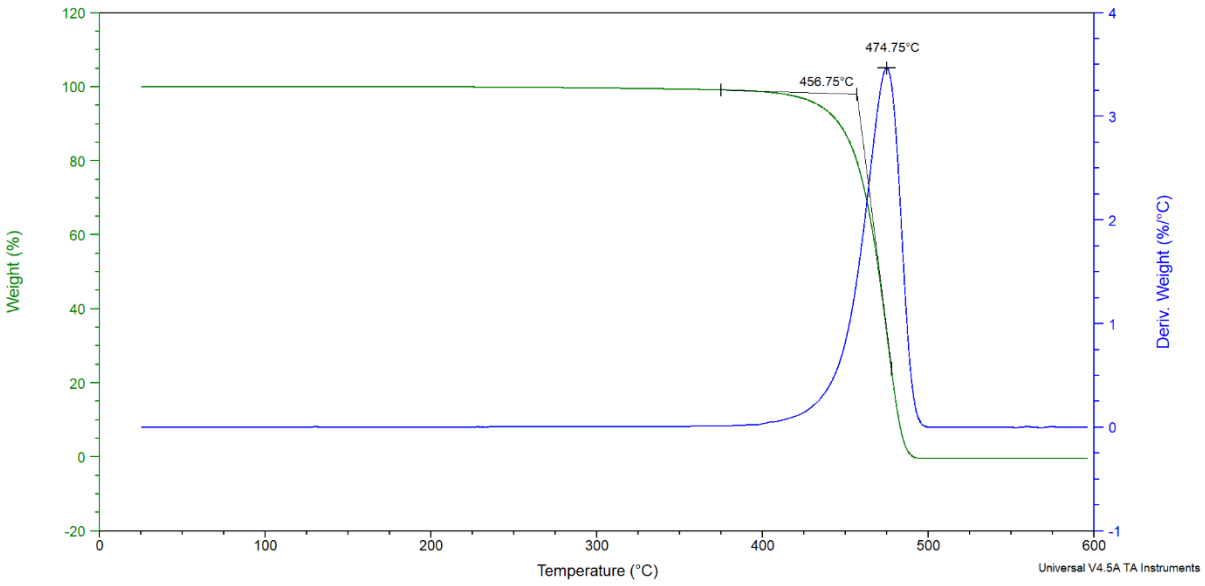

Figure 4.2: TGA thermograph for HE-Y499-AC (MHDPE), heating rate 10°C/min.

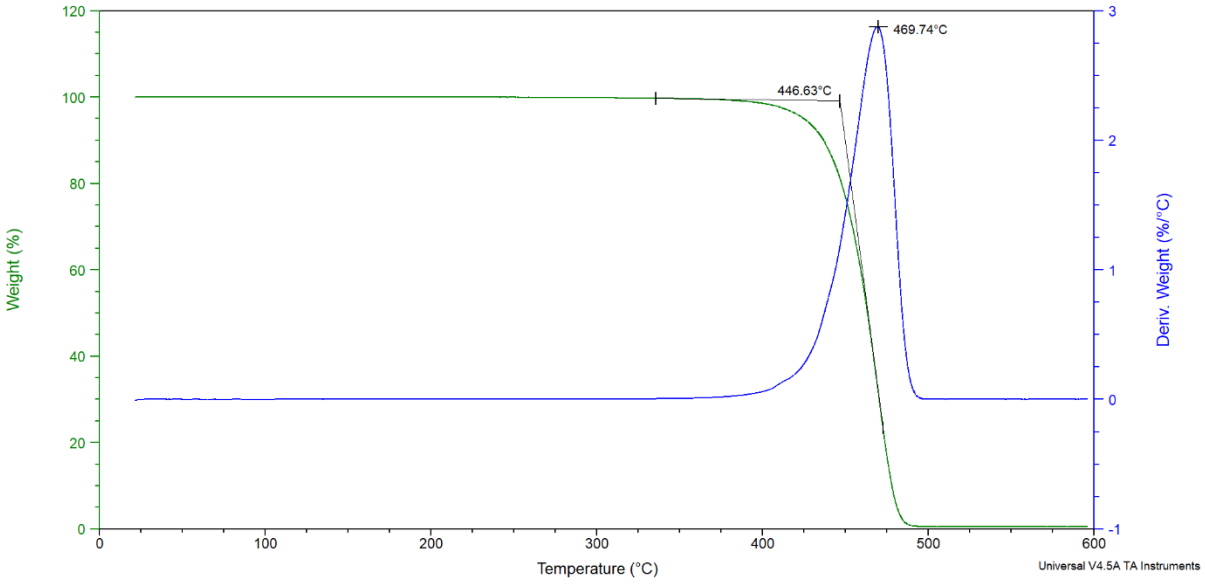

Figure 4.3: TGA thermograph for LA-0522-A (LDPE), heating rate 10°C/min.

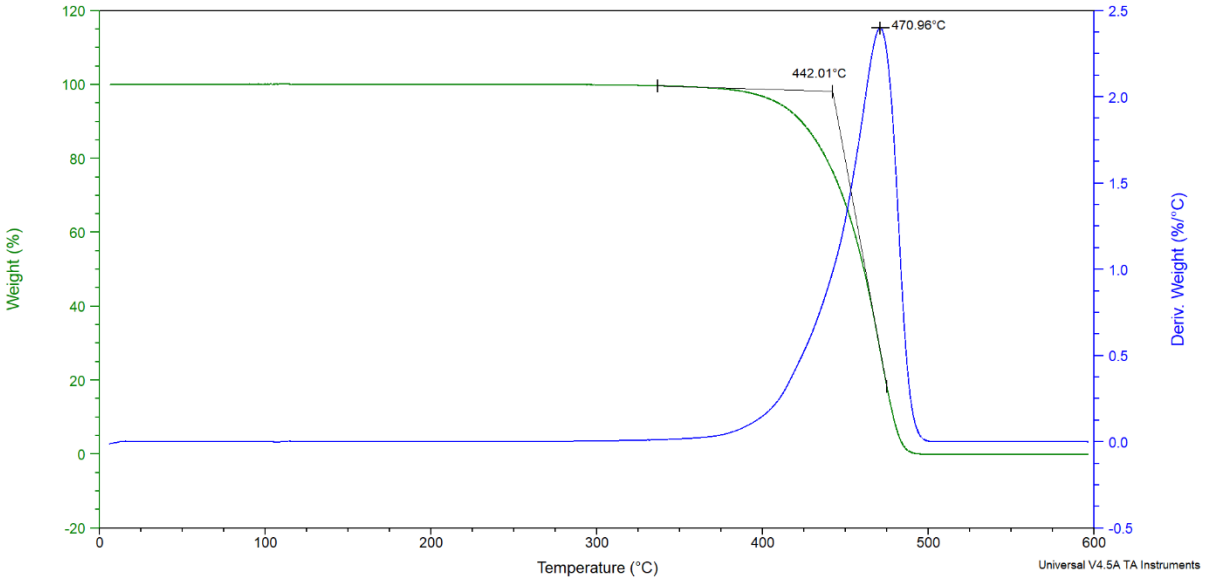

Figure 4.4: TGA thermograph for RMS-245-UG (sHDPE), heating rate 10°C/min.

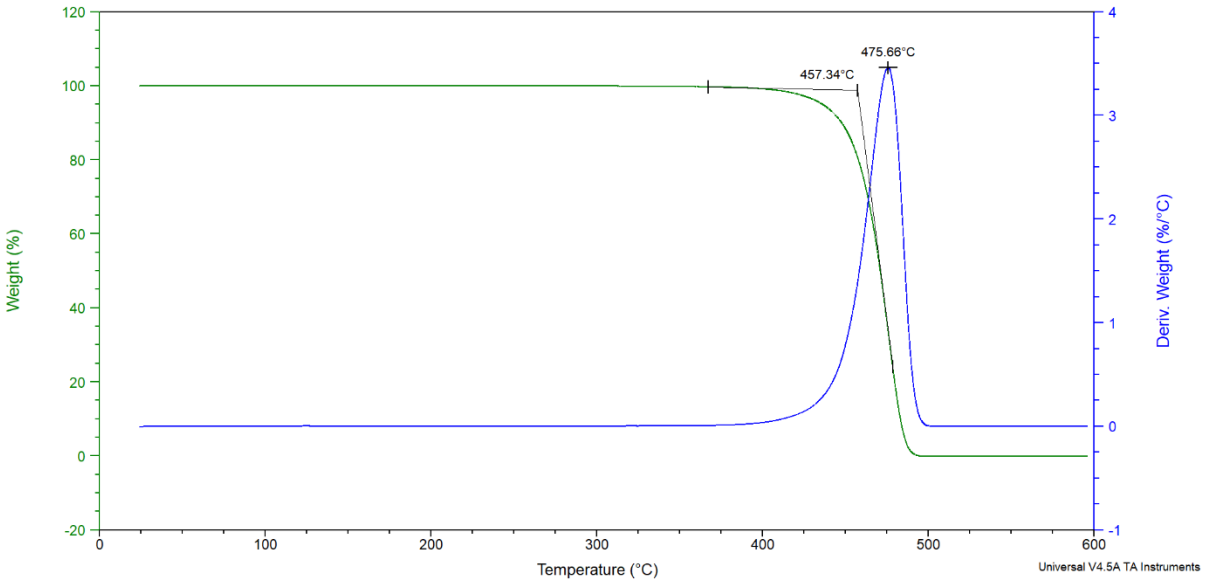

Figure 4.5: TGA thermograph for RMS-341_UG (sHDPE), heating rate 10°C/min.

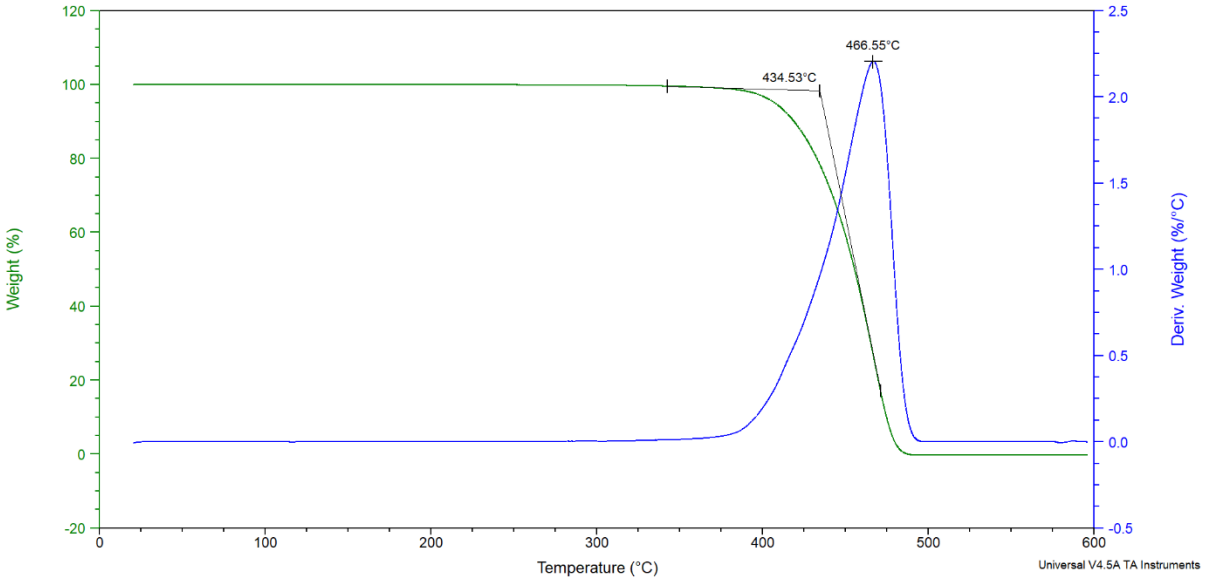

Figure 4.6: TGA thermograph for GA625662 (LLDPE), heating rate 10°C/min.

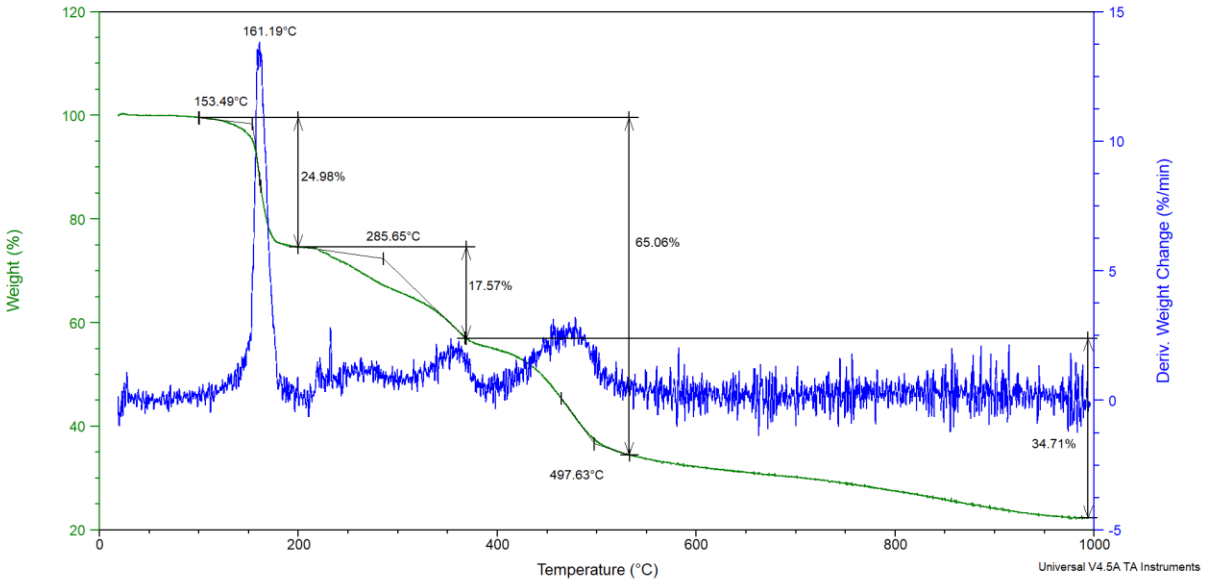

Figure 4.7: TGA thermograph for Celogen OT™, heating rate 10°C/min.

Table 4.4: Degradation temperature of PE resin.

PE Type	Onset of Degradation (°C)	DTG Peak (°C)
19C	442.74	468.37
HE-Y499-AC	456.75	474.75
LA-0522-A	446.63	469.74
RMS-245-UG	442.01	470.96
RMS-341-UG	457.34	475.66
GA625662	434.53	466.55

The melting temperature of the resin and the re-crystallization point is determined by conducting differential scanning calorimetry (DSC) analysis. The manufacture of the resin only reports the general range for the melting point and the recrystallization temperature for all PE grades. Therefore, to determine the specific melting and recrystallization temperatures, a DSC test was conducted with all relevant resin types. The DSC graph for the PE resins used in the experiments are presented in Figure 4.8 to Figure 4.13. The melting and recrystallization temperature are summarized in Table 4.5.

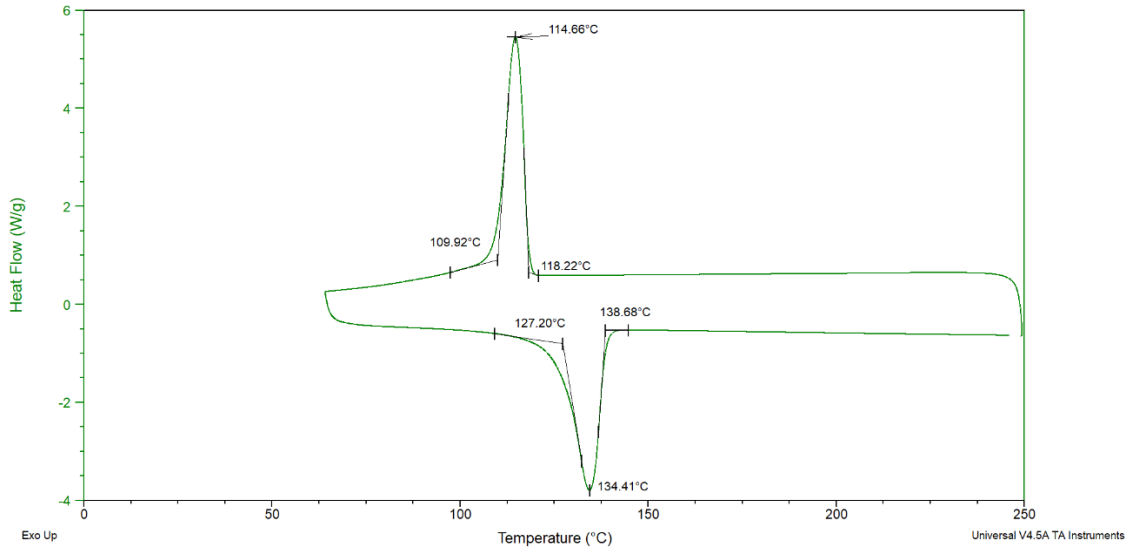

Figure 4.8: DSC thermograph for 19C (HDPE), heating rate 10°C/min.

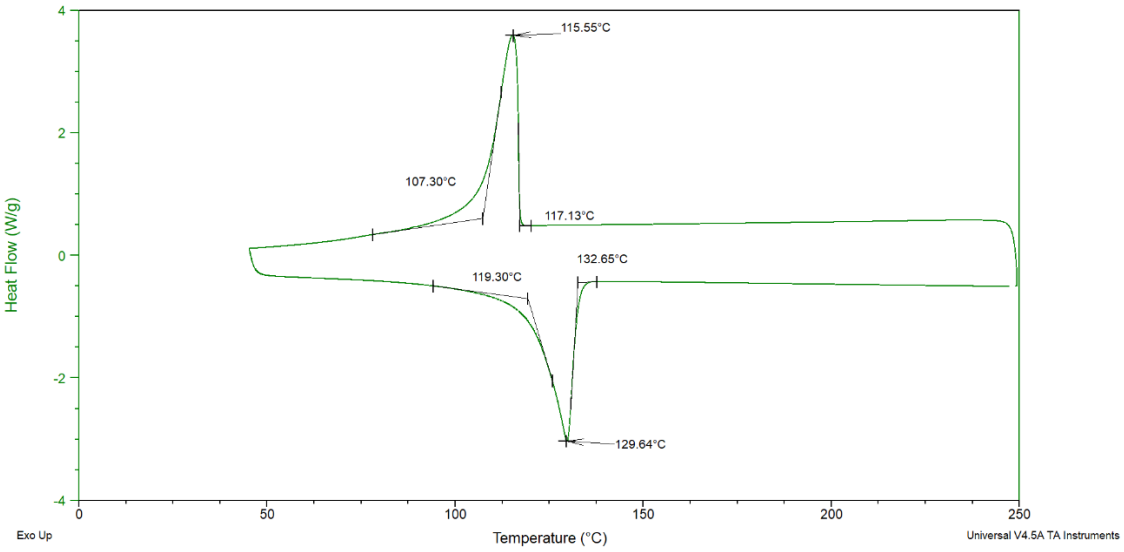

Figure 4.9: DSC thermograph for HE-Y499-AC (MHDPE), heating rate 10°C/min.

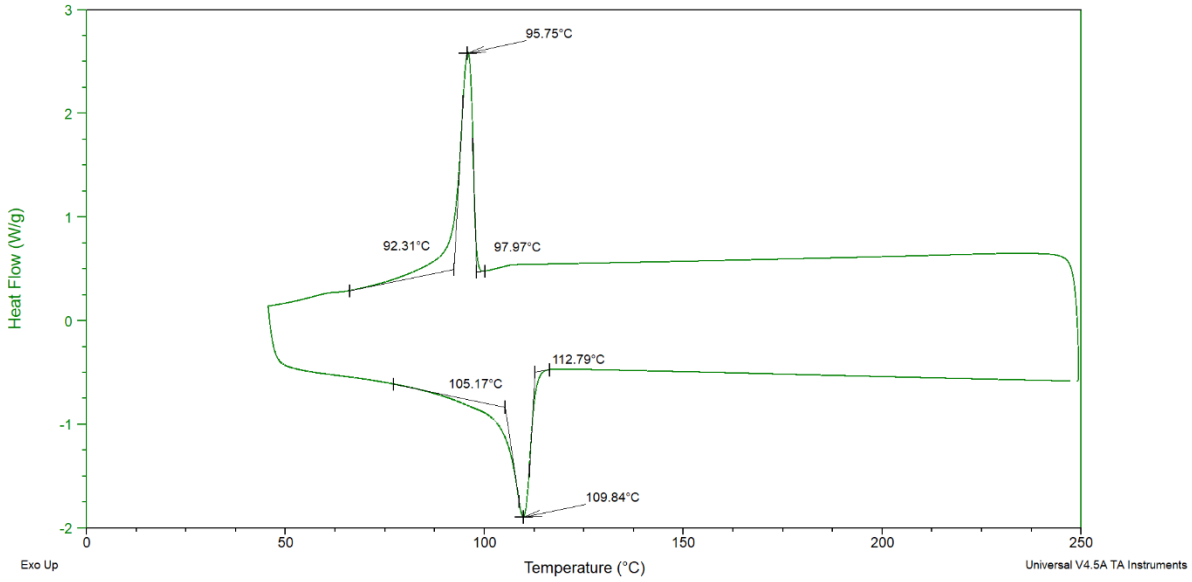

Figure 4.10: DSC thermograph for LA-0522 (LDPE), heating rate 10°C/min.

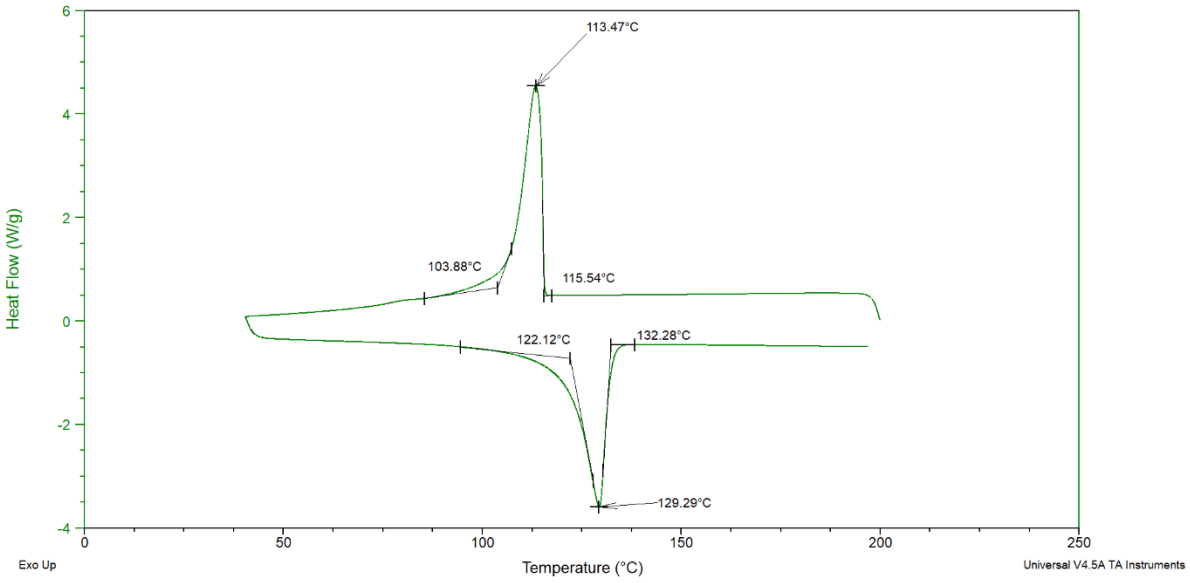

Figure 4.11: DSC thermograph for RMS-245-UG (sHDPE), heating rate 10°C/min.

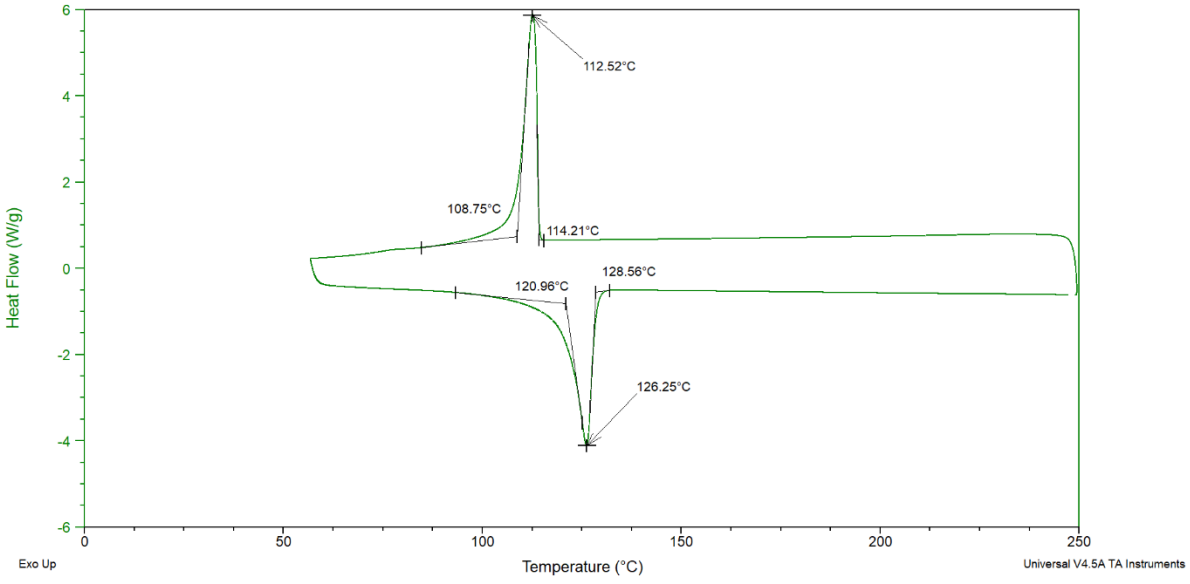

Figure 4.12: DSC thermograph for RMS-341-UG (sHDPE), heating rate 10°C/min.

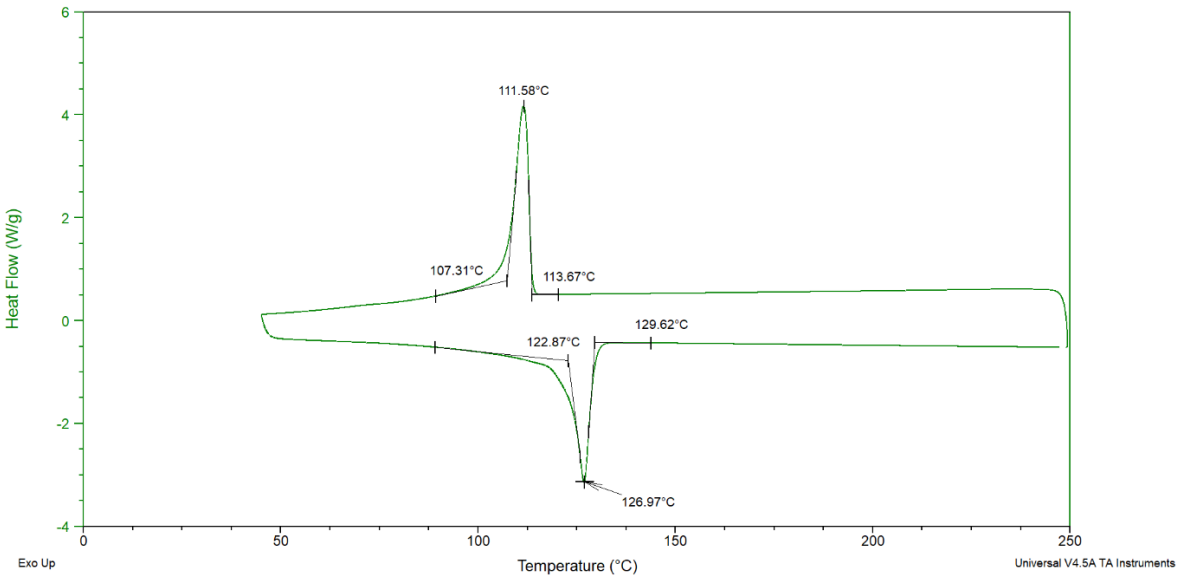

Figure 4.13: DSC thermograph for GA625662 (LLDPE), heating rate 10°C/min.

Table 4.5: Melting Temp (T_M), Recrystallization Temp (T_C) of PE resin.

PE Type	Melting Temperature (T_M) (°C)	Recrystallization Temperature (T_C) (°C)
19C	134.41	114.66
HE-Y499-AC	129.64	115.55
LA-0522-A	109.84	95.75
RMS-245-UG	129.29	113.47
RMS-341-UG	126.25	112.52
GA625662	126.97	111.58

A material's melting and recrystallization point will determine the processing temperature for foam extrusion. For instance, the resin must be completely melted within the extruder before it enters the mixing chamber. After it enters the mixer region, the melt temperature must be maintained above the recrystallization point to prevent the polymer from solidifying. The polymer can be sustained as a liquid above the recrystallization temperature. The data collected using the

TGA and DSC instruments were used as a guide for formulating the processing temperature of the resins in the extruder and the mixing chamber.

4.3. Polyethylene Foam Processing with PBA+Talc

The processing of PE resin with talc was done to evaluate the new experimental setup's ability to produce foam under different operating conditions. The polymer foam sample was immediately cooled with a water bath after leaving the die exit. Rapid cooling in water solidified the foam while preserving the cellular structure. It was assumed that the quality of the foam deteriorates at a slower cooling rate, which leads to low cell density and larger cell size. Therefore, rapidly cooling the foam prevents bubble growth and retains the maximum number of cells within a given volume. It should also be noted that PE foaming was attempted without talc. However, the final sample produced with only PBA resulted in large gas pockets within the solidified resin regardless of processing condition and PE type (Figure 4.14).

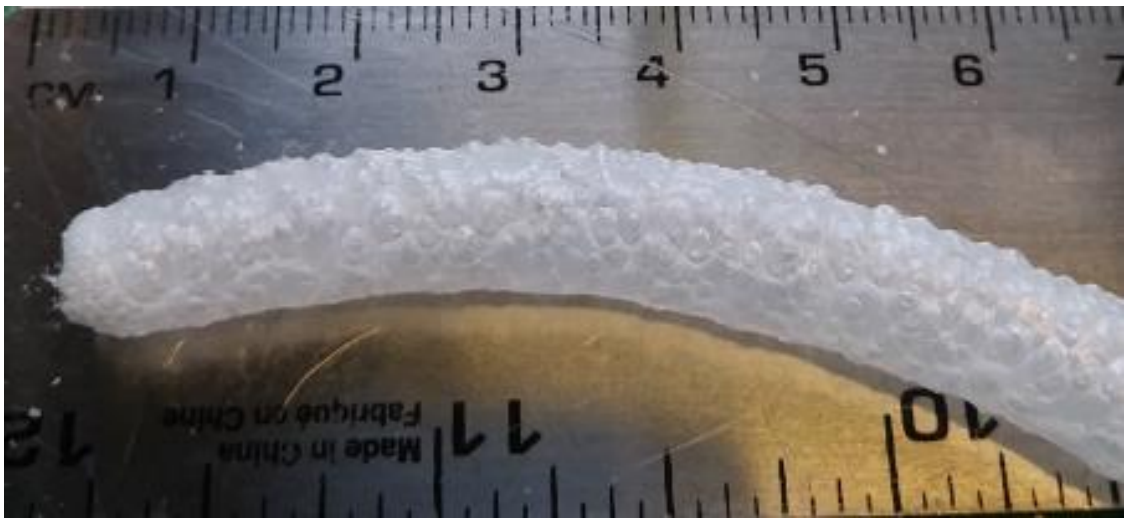

Figure 4.14: Foamed PE sample proposed in extrusion exclusively with PBA.

The first step for sample preparation was dry blending the talc powder with the polymer resin. A pre-determined quantity of PE resin was placed in a plastic bag to receive the talc powder. The talc content added into the plastic bag was 3wt % of the resin. The talc powder was thoroughly blended with the polymer resin through repeated manual agitation for five minutes. This process was identical for the PE resins supplied in both pellet and powder form.

The dry blended material was added to the extruder hopper to initiate the extrusion process. A 2-D cross-section of the experimental setup in Figure 4.15 represents the different processing zones. The experimental setup consists of seven different processing zones where the temperature can be controlled with independent external band heaters. However, the melt pressure can only be monitored with pressure transducers at zone 3 and at the exit of the static mixer (zone 5). The resin was completely melted within the extruder from zone 1 to zone 3. The extruder screw conveys the molten resin into the mixing chamber at zone 4. The processing pressure of the polymer melt is controlled with the extruder RPM.

The carbon dioxide gas was injected through the check valve and into the mixing chamber at zone 4. Before the gas enters the mixing chamber, it was heated to ensure supercritical state. The cooling shell at zone 5 is utilized to control the processing temperature at the static mixer exit. The die zone was constituted by zone 6 and zone 7. Rapid pressure drop at the die exit creates a thermodynamic instability within the gas-laden polymer melt and initiates the production of the foam. The extruded foam was immediately submerged in water to solidify the polymer. The processing parameters of talc containing PE foam is given in Table 4.6.

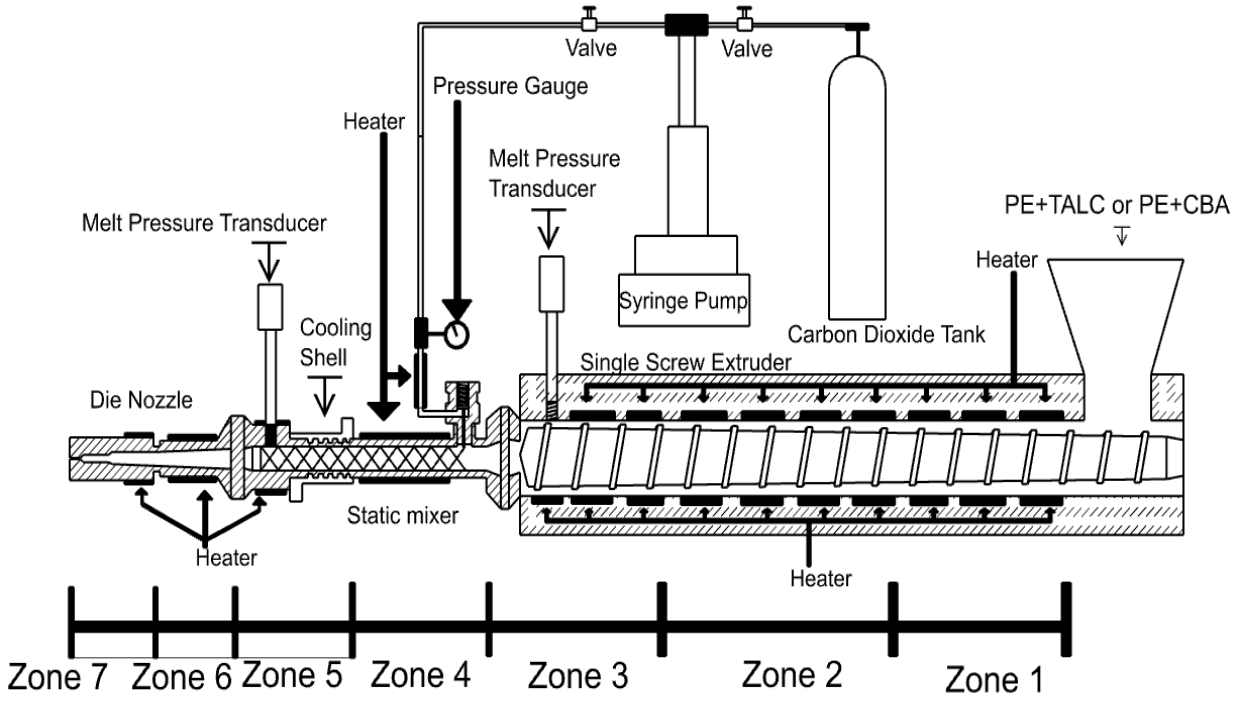

Figure 4.15: The processing zones for PBA foam extrusion.

Table 4.6: PE resin processed with 3wt % talc.

PE Resin	Z_1 °C	Z_2 °C	Z_3 °C **Psi**	Z_4 °C	Z_5 °C **Psi**	Z_6 °C	Z_7 °C	RPM	Injection Pressure (Psi)	Injection Temp °C	Gas flow rate ml/min
19C	150	160	165 **3300**	170	165 **3100**	150	125	80	3200	90	2
HE-Y449	150	160	165 **2600**	170	165 **2450**	150	125	80	3200	90	2
RMS-245	150	160	165 **2500**	170	165 **2350**	150	125	80	3200	95	2
RMS-341	150	160	165 **2100**	170	165 **2000**	150	125	80	3200	95	2
RMS-341	160	170	175 **2000**	180	165 **1850**	170	125	80	3200	95	2
19C	160	170	175 **3150**	180	165 **3000**	170	125	80	3200	95	2
HE-Y449	160	170	175 **2500**	180	165 **2400**	170	125	80	3200	95	2
RMS-245	160	170	175 **2350**	180	165 **2300**	170	125	80	3200	95	2
LA-0522	125	130	135 **1950**	135	125 **1800**	115	105	80	3000	92	2
LA-0522	130	140	145 **1600**	150	145 **1450**	115	105	80	3200	95	2
19C	145	150	155 **3150**	160	155 **3000**	145	125	80	3200	80	2
HE-Y449	145	150	155 **2900**	160	155 **2700**	145	125	80	3200	80	2
RMS-341	145	150	155 **2100**	160	155 **1950**	145	125	80	3200	80	2
RMS-245	145	150	155 **3150**	160	155 **3000**	145	125	80	3200	80	2
19C	145	150	155 **2900**	160	155 **2700**	145	125	80	3000	84	1
RMS-245	145	150	155 **2600**	160	155 **2500**	145	125	80	3000	90	1
RMS-341	145	150	155 **2300**	160	155 **2200**	145	125	80	3000	84	1
HE-Y449	145	150	155 **2700**	160	155 **2600**	145	125	80	3200	87	1
LA-0522	125	130	135 **1750**	135	125 **1600**	115	105	80	3000	88	1
LA-	130	140	145	150	145	115	105	80	3000	88	1

PE Resin	Z_1 °C	Z_2 °C	Z_3 °C **Psi**	Z_4 °C	Z_5 °C **Psi**	Z_6 °C	Z_7 °C	RPM	Injection Pressure (Psi)	Injection Temp °C	Gas flow rate ml/min
0522			**1580**		**1450**						
19C	150	160	165 **3150**	170	165 **3000**	150	125	80	3000	86	1
HE-Y449	150	160	165 **2550**	170	165 **2400**	150	125	80	3000	83	1
RMS-245	150	160	165 **2450**	170	165 **2300**	150	125	80	3000	83	1
RMS-341	150	160	165 **2050**	170	165 **1900**	150	125	80	3000	83	1
19C	160	170	175 **3100**	180	170 **3000**	160	125	80	3000	86	1
HE-Y449	160	170	175 **2550**	180	170 **2400**	160	125	80	3000	84	1
RMS-245	160	170	175 **2350**	180	170 **2200**	160	125	80	3000	83	1
RMS-341	160	170	175 **1900**	180	170 **1850**	160	125	80	3000	83	1

4.4 Polyethylene Foam Processing with PBA+Celogen OT™

The sample preparation steps are identical to the previous section. However, unlike the 3wt % of talc, the resins were dry blended with 1wt % Celogen OT™. The dispersed CBA content within the polymer melt will serve multiple functions. All the CBA particles within the polymer melt do not decompose at the same time. This is due to the inherent temperature gradient that exist within the polymer melt. Particles that decompose first will increase the overall gas concentration within the bulk fluid. CBA particles that activates after the die exit will serve as nucleating sites for gas diffusion. Finally, as the last remaining particles decompose, it will increase the overall cell density within the extruded foam. The processing parameters for resins processed with CBA are given in Table 4.7.

Table 4.7: PE resin processed with 1wt % Celogen OT™.

PE Resin	Z_1 °C	Z_2 °C	Z_3 °C Psi	Z_4 °C	Z_5 °C Psi	Z_6 °C	Z_7 °C	RPM	Injection Pressure (Psi)	Injection Temp °C	Gas flow rate ml/min
LA-0522	125	130	135 **1900**	135	125 **1800**	115	105	80	3100	90	2
LA-0522	130	140	145 **1600**	150	145 **1450**	115	105	80	3200	95	2
19C	145	150	155 **3150**	160	155 **3000**	145	125	80	3100	81	2
HE-Y449	145	150	155 **2400**	160	155 **2100**	145	125	80	3200	94	2
RMS-341	145	150	155 **1770**	160	155 **1600**	145	125	80	3200	80	2
RMS-245	145	150	155 **1800**	160	155 **1700**	145	125	80	3200	81	2
LA-0522	125	130	135 **1800**	135	125 **1700**	115	105	80	3100	90	1
LA-0522	130	140	145 **1600**	150	145 **1500**	115	105	80	3200	95	1
19C	145	150	155 **2300**	160	155 **2100**	145	125	80	3100	87	1
HE-Y449	145	150	155 **2300**	160	155 **2100**	145	125	80	3000	86	1
RMS-341	145	150	155 **2100**	160	155 **2050**	145	125	80	3100	87	1
RMS-245	145	150	155 **2400**	160	155 **2300**	145	125	80	3100	85	1

4.5 Rotational Molded Foam Composite Processing

4.5.1 *Skin Material Formulation*

The formulation for the skin material will remain unchanged from the research work conducted by Kimberly. From her work, the skin volume was determined to be 224.89 cm^3 and the total mold volume was 1467.54 cm^3. The mass of the skin material was 211 g determined from Equation 2.4. After subtracting the skin volume, the remaining volume is filled with foam (Kimberly 2009).

4.5.2 *Processing steps of Functionally Graded Foam for RRFM*

The processing steps for functionally graded rotational molded foam composite are now presented:

Step 1: The mold was charged with the non-foamable resin powder (Figure 4.16). After which, the top plate was attached to the mold to seal the mold cavity.

Figure 4.16: Mold charging with non-foamable outer skin material.

Step 2: The mold arm assembly was translated into the pre-heated oven. Inside the oven, the mold rotates bi-axially to form the outer skin (Figure 4.17). The skin formation time was 40-50 minuets depending on the resin type.

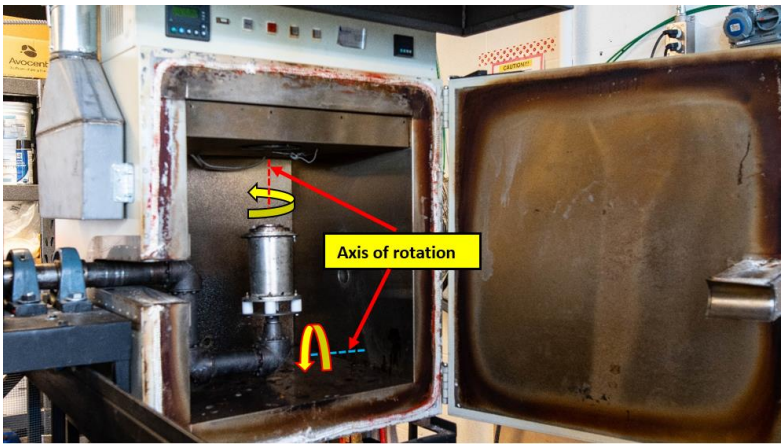

Figure 4.17: Mold translation into the Oven.

Step 3: The extruder and the static mixer was preheated to the desired processing temperature for foam extrusion. Each zone temperature can be controlled from the extruder control panel (Figure 4.15). The only exception was the cable heaters positioned at zone 5 after the cooling shell and the supercritical gas inlet port at zone 4. These heaters have independent controllers that can

increase or decrease the total wattage output. A detailed description of the cable heaters was given in chapter 3. The heating time for the static mixer section can range from one hour to two hours depending on the processing temperature that needs to be achieved.

Step 4: The foamable resin was obtained by dry blending the polymer resin as received from the manufacturer with either Celogen OT™ or talc, depending on the experiment to be performed. The dry blended material was poured into the hopper to begin the extrusion process (Figure 4.18).

Figure 4.18: Addition of dry blended material into the hopper.

Step 5: Before the extrusion process can begin, the injection line was slowly pressurized with the syringe pump at the desirable gas flowrate. This process involved gradually increasing the pressure up to the check valve pre-set opening pressure. The increasing fluid pressure compressed the spring eventually moving the needle inward to open the valve. At this point the opening allowed supercritical fluid to flow directly into the mixing chamber to mix with the polymer melt (Figure 4.19).

Step 6: The rotational mold was translated out of the oven while the outer skin was still molten. The die interphase port opening was removed along with the skin material that was sticking to the inner port surface. This created an opening for the nozzle to enter inside the mold cavity (Figure 4.20). The extruder screw RPM was increased to the desired speed to start producing the foam. The foam was extruded into the mold cavity as the mold rotated uni-axially.

Step 7: The filling process was terminated when the foam reaches the tip of the port interface plate. The Interface port is reattached to the mold to encapsulate the extruded foam with the outer skin.

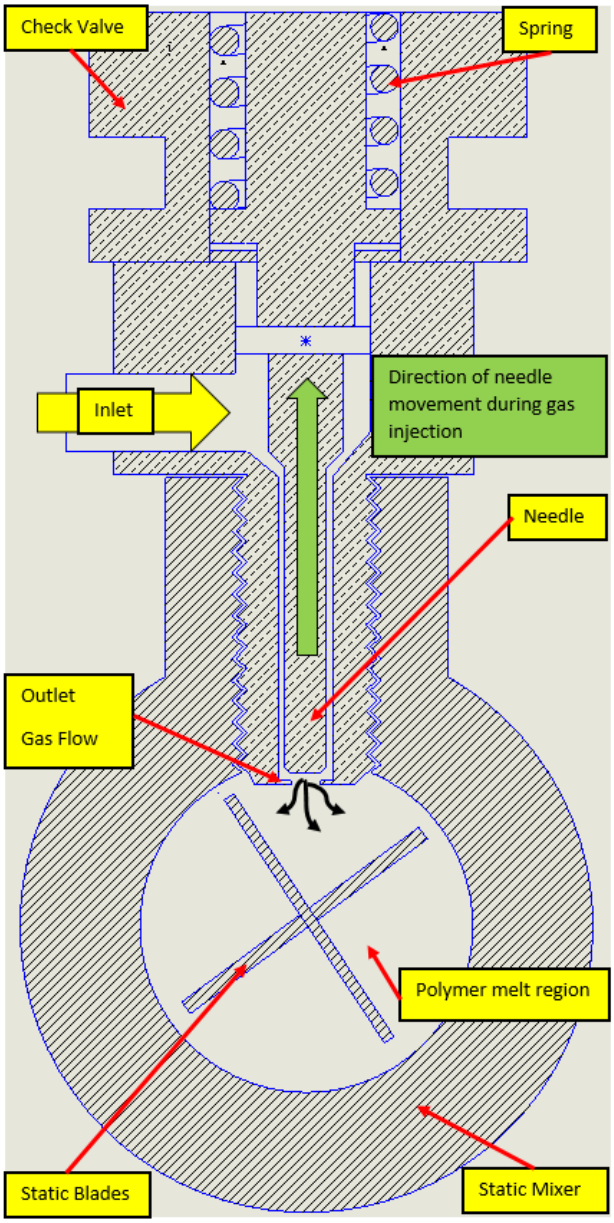

Figure 4.19: Cross-section of the static mixer and check valve.

Step 8: The mold is cooled by forced air convection as the mold arm assembly rotated bi-axially. The composite article is extracted when the outer surface of the mold reaches room temperature.

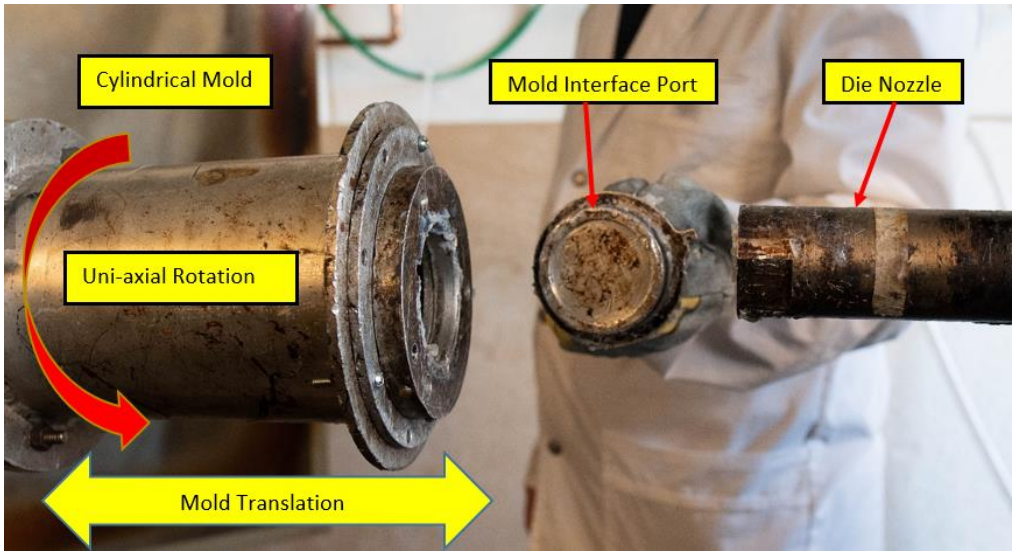

Figure 4.20: Mold interface port removed for foam injection.

4.6 Functionally Graded Foaming Processing Strategies

4.6.1 *Processing by Gradual Modification of Gas Flowrate*

In this method an attempt was made to modify the quality of the foam by gradually changing the gas flowrate into the static mixer during the extrusion phase. However, the talc content and the Celogen OT™ content within the dry blended resin was kept constant. The gas flowrate was gradually decreased from 5 ml/min to 2 ml/min at 1ml/min intervals. The gas injection time for each interval was 2 minutes where the total time to fill the mold cavity at 80 RPM was 8-9 minutes. The total quantity of dry blended material added to the hopper was 800 grams of resin. The material that remained within the static mixer after the completion of foam injection was 100 to 150 grams depending on the volume expansion ratio of the foam. The processing condition of the foam production method is presented in Table 4.8 and 4.9. The pressure at Zone 3 and Zone 5 was recorded at each gas injection rate.

Table 4.8: Foam processing method with talc.

PE Resin	Z_1 °C	Z_2 °C	Z_3 °C Psi P_1P_2 P_3P_4	Z_4 °C	Z_5 °C Psi P_1P_2 P_3 P_4	Z_6 °C	Z_7 °C	Talc wt %	Injection Pressure (Psi)	Injection Temp °C	Gas flow rate ml/min f_1, f_2 f_3 ,f_4
19C	145	150	155	160	155	145	140	3	3000	90	----------
			2800		**2500**						5
			2800		**2500**						4
			3000		**2750**						3
			3000		**2750**						2
HE-Y449	145	150	155	160	155	145	140	3	3000	87	----------
			3000		**2400**						5
			2600		**2000**						4
			2700		**2300**						3
			2800		**2600**						2
RMS-245	145	150	155	160	155	145	140	3	3000	95	----------
			2650		**2500**						5
			2500		**2200**						4
			2500		**2250**						3
			2500		**2200**						2
RMS-245	140	145	150	150	145	125	120	3	3000	92	----------
			2800		**2600**						5
			2800		**2600**						4
			2900		**2750**						3
			2900		**2750**						2
LA-0522	125	130	135	135	125	115	105	1	3000	96	----------
			2000		**1880**						5
			2000		**1880**						4
			2100		**1880**						3
			2100		**1880**						2
RMS-341	140	145	150	150	145	125	120	3	3100	95	----------
			2500		**2300**						5
			2500		**2300**						4
			2500		**2300**						3
			2500		**2300**						2

Table 4.9: Foam processing method with Celogen OT™ .

PE Resin	Z_1 °C	Z_2 °C	Z_3 °C Psi P_1P_2 P_3P_4	Z_4 °C	Z_5 °C Psi P_1P_2 P_3 P_4	Z_6 °C	Z_7 °C	CBA wt %	Injection Pressure (Psi)	Injection Temp °C	Gas flow rate ml/min f_1, f_2 f_3 ,f_4
LA-0522	125	130	135	135	125	115	105	1	3000	96	----------
			1800		**1700**						5
			1800		**1700**						4
			1800		**1700**						3
			1800		**1700**						2
RMS-245	140	145	150	150	145	125	120	1	3000	86	----------
			2600		**2200**						5
			2500		**2100**						4
			2500		**2200**						3
			2500		**2200**						2

4.6.2 *Processing by Gradually Increasing the Content of Nucleating Agent & CBA*

In this method rather than gradually modifying the gas flow rate the nucleating agent content or the CBA content was gradually increased during the extrusion process. The polymer resin was dry blended separately with different quantities of talc and CBA. In the case of talc assisted foaming process, the weight percentage of the talc powder was increased from 1 % to 3 % at 0.5 % increments. However, for the CBA assisted foaming process, the Celogen OT™ content within the resin was increased from 0.5 % to 2 % at 0.5 % increments. The foaming process for two of the resin types were carried out at three different processing temperatures and at two different gas injection rates. The extruder's RPM for all foaming experiments was kept at 80. The processing parameters implemented for these foams are presented in Table 4.10 – Table 4.11. For the final polymer type the foaming process was carried out at different gas injection rate (Table 4.12).

Table 4.10: RMS-245 foam processing method at different operating temperatures.

PE Resin	Z_1 °C	Z_2 °C	Z_3 °C Psi P_1P_2 P_3P_4	Z_4 °C	Z_5 °C Psi P_1P_2 P_3 P_4	Z_6 °C	Z_7 °C	Talc wt %	Injection Pressure (Psi)	Injection Temp °C	Gas flow rate ml/min
RMS-245	145	150	155 **2900** **2850** **2850** **2750** **2700**	160	155 **2600** **2600** **2600** **2600** **2600**	145	125	------ 1.0 1.5 2.0 2.5 3.0	2900	90	1
RMS-245	150	160	165 **2300** **2300** **2400** **2400** **2400**	170	165 **2100** **2000** **2050** **2100** **2100**	150	125	------ 1.0 1.5 2.0 2.5 3.0	3000	88	1
RMS-245	160	170	175 **2200** **2300** **2300** **2300** **2450**	180	170 **2000** **2100** **1900** **2000** **2000**	160	125	------ 1.0 1.5 2.0 2.5 3.0	3100	87	1
RMS-245	145	150	155 **2700** **2700** **2700** **2700** **2700**	160	155 **2400** **2400** **2400** **2350** **2400**	145	125	------ 1.0 1.5 2.0 2.5 3.0	3000	86	0.25
RMS-245	145	150	155 **2700** **2700** **2700** **2600**	160	155 **2400** **2400** **2400** **2400**	145	125	**CBA** 0.5 1.0 1.5 2.0	3050	89	0.25
RMS-245	150	160	165 **2550** **2550** **2550** **2550** **2550**	170	165 **2200** **2100** **2100** **2100** **2100**	150	125	------ 1.0 1.5 2.0 2.5 3.0	3050	90	0.25
RMS-245	160	170	175 **2400** **2400**	180	170 **2000** **2000**	160	125	------ 1.0 1.5	3000	90	0.25

PE Resin	Z_1 °C	Z_2 °C	Z_3 °C Psi P_1P_2 P_3P_4	Z_4 °C	Z_5 °C Psi P_1P_2 P_3 P_4	Z_6 °C	Z_7 °C	Talc wt %	Injection Pressure (Psi)	Injection Temp °C	Gas flow rate ml/min
			2350		**2000**			2.0			
			2400		**2000**			2.5			
			2400		**2000**			3.0			

Table 4.11: RMS-341 foam processing method at different operating temperatures.

PE Resin	Z_1 °C	Z_2 °C	Z_3 °C Psi P_1P_2 P_3P_4	Z_4 °C	Z_5 °C Psi P_1P_2 P_3 P_4	Z_6 °C	Z_7 °C	Talc wt %	Injection Pressure (Psi)	Injection Temp °C	Gas flow rate ml/min
RMS-341	145	150	155	160	155	145	125	------	2900	86	1
			2000		**1900**			1.0			
			2000		**1950**			1.5			
			2000		**1900**			2.0			
			2000		**1900**			2.5			
			2000		**1900**			3.0			
RMS-341	150	160	165	170	165	150	125	------	2900	87	1
			1700		**1600**			1.0			
			1800		**1700**			1.5			
			1800		**1650**			2.0			
			1800		**1700**			2.5			
			1800		**1700**			3.0			
RMS-341	160	170	175	180	170	160	125	------	2900	87	1
			1650		**1400**			1.0			
			1650		**1500**			1.5			
			1650		**1500**			2.0			
			1650		**1550**			2.5			
			1650		**1550**			3.0			
RMS-341	145	150	155	160	155	145	125	------	2900	92	0.25
			2250		**2000**			1.0			
			2250		**2050**			1.5			
			2250		**2050**			2.0			
			2250		**2050**			2.5			
			2250		**2050**			3.0			
RMS-341	145	150	155	160	155	145	125	**CBA**	3000	95	0.25
			2300		**2100**			0.5			
			2300		**2100**			1.0			
			2100		**1900**			1.5			

PE Resin	Z_1 °C	Z_2 °C	Z_3 °C Psi P_1P_2 P_3P_4	Z_4 °C	Z_5 °C Psi P_1P_2 P_3 P_4	Z_6 °C	Z_7 °C	Talc wt %	Injection Pressure (Psi)	Injection Temp °C	Gas flow rate ml/min
			2100		**1900**			2.0			
RMS-341	150	160	165	170	165	150	125	------	3000	92	0.25
			1850		**1750**			1.0			
			1850		**1750**			1.5			
			2100		**2000**			2.0			
			2100		**2000**			2.5			
			2100		**2000**			3.0			
RMS-341	160	170	175	180	170	160	125	------	3000	92	0.25
			1950		**1600**			1.0			
			1950		**1600**			1.5			
			1950		**1600**			2.0			
			1950		**1600**			2.5			
			1950		**1600**			3.0			

Table 4.12: LA-0522 foam processing method at different gas flow rate.

PE Resin	Z_1 °C	Z_2 °C	Z_3 °C Psi P_1P_2 P_3P_4	Z_4 °C	Z_5 °C Psi P_1P_2 P_3 P_4	Z_6 °C	Z_7 °C	Talc wt %	Injection Pressure (Psi)	Injection Temp °C	Gas flow rate ml/min
LA-0522	125	130	135	135	125	115	105	------	2900	84	1
			1850		**1800**			1.0			
			1750		**1700**			1.5			
			1750		**1700**			2.0			
			1750		**1700**			2.5			
			1750		**1700**			3.0			
LA-0522	125	130	135	135	125	115	105	**CBA**	2900	89	1
			1700		**1650**			0.5			
			1600		**1500**			1.0			
			1600		**1500**			1.5			
			1600		**1550**			2.0			
LA-0522	125	130	135	135	125	115	105	------	2900	87	0.25
			1750		**1680**			1.0			
			1750		**1700**			1.5			
			1750		**1700**			2.0			
			1750		**1700**			2.5			
			1750		**1700**			3.0			
LA-0522	125	130	135	135	125	115	105	**CBA**	2900	87	0.25
			1600		**1500**			0.5			

PE Resin	Z_1 °C	Z_2 °C	Z_3 °C Psi P_1P_2 P_3P_4	Z_4 °C	Z_5 °C Psi P_1P_2 P_3 P_4	Z_6 °C	Z_7 °C	Talc wt %	Injection Pressure (Psi)	Injection Temp °C	Gas flow rate ml/min
			1600		**1550**			1.0			
			1600		**1550**			1.5			
			1600		**1550**			2.0			

Chapter 5. Results & Discussion

5.1 Introduction

This chapter presents the experimental results of foaming experiments described in Chapter 4. The cellular morphology of the foamed core of rotational molded foam composites are analyzed to evaluate the new experimental setup.

5.2 Sample Preparation for Rapidly Cooled Foam

The ability of the new experimental setup to produce physical blowing agent (PBA) -based foam was investigated with different grades of PE resins. These resins were processed at various temperatures and gas injection rates to observe the differences in the resulting cell morphologies. The extruded foams were water cooled to preserve the cellular structure immediately after cell nucleation. Upon rapid cooling, the foam samples were collected from each batch to determine its quality according to foam density, volume expansion ratio (VER), cell population density, and average cell size. The internal morphology of the foam was visually inspected after fracturing each sample below its glass-transition temperature with a liquid nitrogen bath. These foamed cross-sections were analyzed by using a CT scanner, a digital microscope, and scanning electron microscopy, respectively.

The PE resins were dry blended with talc to increase the cell density by increasing the total number of nucleating sites within the polymer melt. In contrast, some samples were dry blended with Celogen OT™ to observe its effect on the final cell morphology. The residence time within the mixing chamber was kept constant for all foaming experiments and material output at extruder screw of 80 RPM was 74 g $\pm$ 3 g for one minute of continuous extrusion of pure resin. The PE residence time within the mixing chamber can range from 30 to 35 seconds. However, the residence time can vary depending on the gas injection rate. When the gas is injected into the mixing chamber, all the supercritical fluid does not completely dissolve into the polymer melt. Therefore, two different phases exist within the mixing chamber regardless of gas injection rate. The undissolved gaseous phase between the polymer phases acts as a propellant and ejects the polymer melt out of the die exit in rapid succession (Figure 5.1). The ejection rate increases as the gas flowrate into the mixing chamber is increased. Complete dissolution of gas into the polymer melt was not observed from 5 ml/min to 0.25 ml/min.

The density of each foam type was obtained by dividing the average mass of 10 samples collected from each batch by the average volume of those same 10 samples. The formula for density is given in Equation 4.1. The volume expansion ratio of the foam sample is determined from Equation 2.5 in chapter 2. The cell density and the average cell size is determined from Equation 2.9 and Equation 2.10.

$$\rho_{FOAM} = \frac{\overline{m_{10}}}{\overline{V_{10}}} \tag{4.1}$$

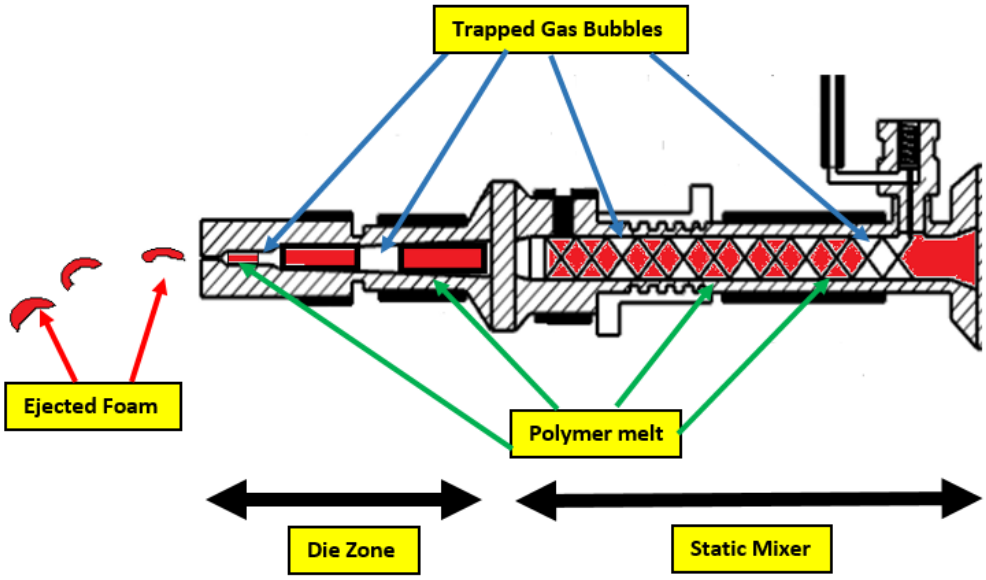

Figure 5.1: PBA foam ejection from the die exit.

5.3 Foam Quality Comparison of Different HDPE Grades

The PE resins were processed at 160°C, 170°C, and 180°C at two different injection rates (2 ml/min & 1 ml/min). However, the CBA assisted foaming process was done at 160°C, since at higher processing temperatures degradation of Celogen OT™ left scorched residue marks on the extruded resin. In contrast, foam processed with talc had light greyish hue due to the color of talc particles. To maintain constant melt temperature during the extrusion process, cooling fluid was injected through the cooling shell periodically. This was done manually for 5 to 10 seconds intervals to lower the process temperature. The melt temperature was also adjusted by controlling the band heater heat output. The die temperature was maintained at 125°C for HDPE resin and 105°C for LDPE resin to increase the melt strength of the polymer before cell nucleation at the die exit.

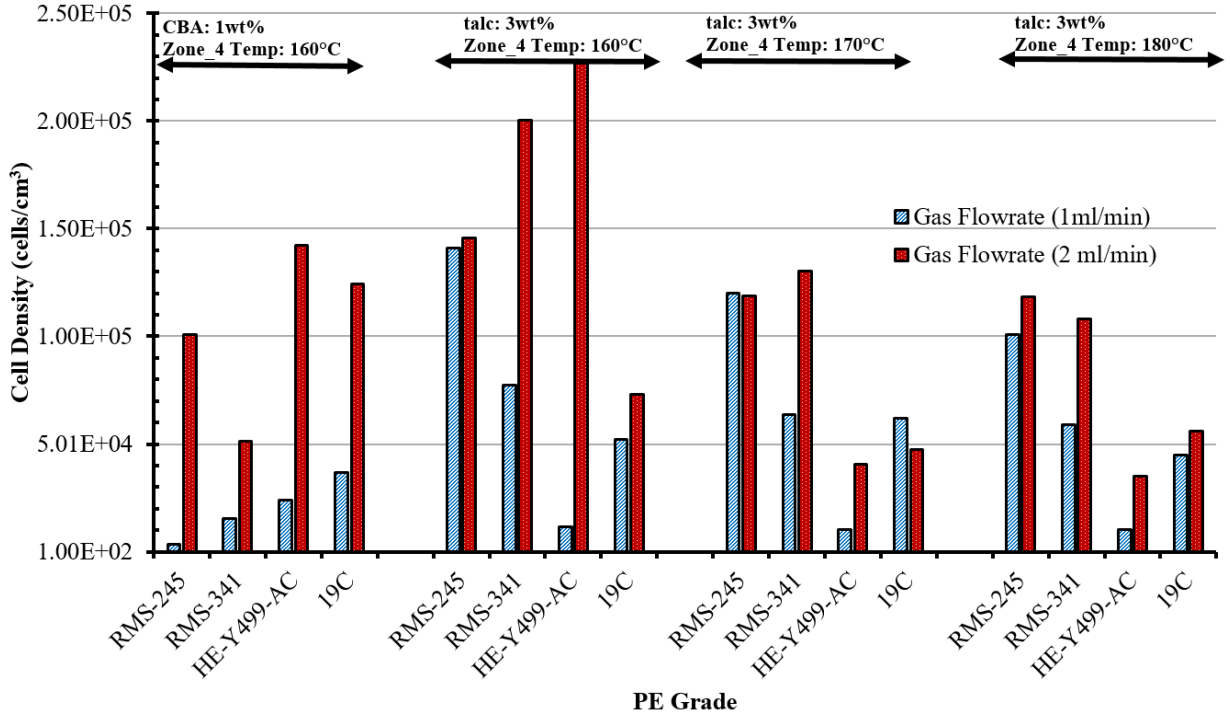

Figure 5.2: Distribution of cell density at different processing temperature and flowrate.

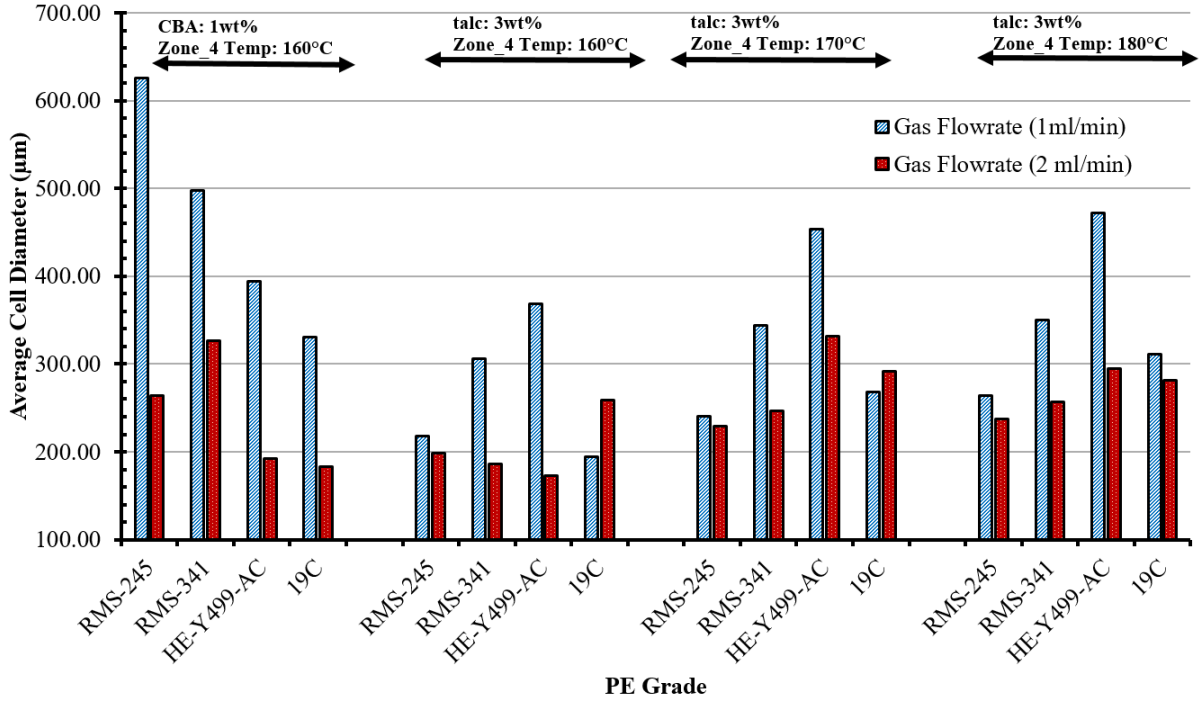

Figure 5.3: Distribution of cell diameter at different processing temperature and flowrate.

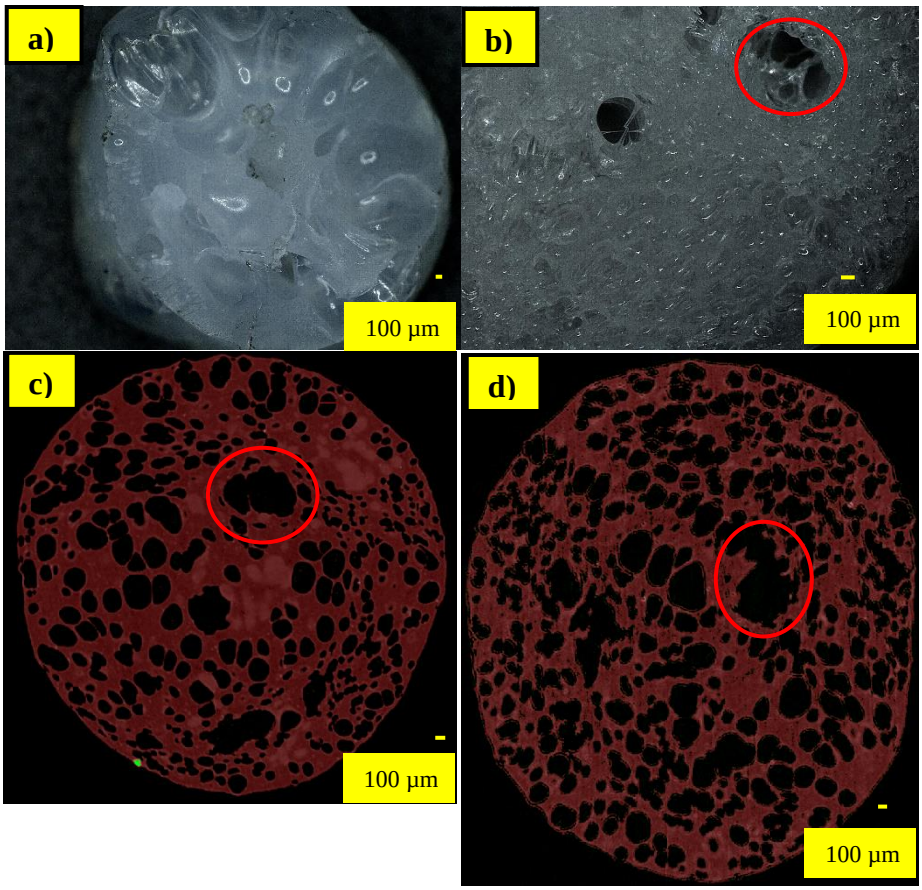

Figure 5.4: Water cooled RMS-245UG foam: a) Mixing zone temp: 160°C, 1wt% CBA, 1 ml/min gas flow rate b) Mixing zone temp: 160°C, 3wt% talc, 1 ml/min gas flow rate c) Mixing zone temp: 170°C, 3wt% talc, 1 ml/min gas flow rate d) Mixing zone temp: 180°C, 3wt% talc, 1 ml/min gas flow rate.

RMS-245UG foam processed with 1wt% Celogen OT™ had significantly lower cell density and higher average cell size compared with foams produced with talc (Figure 5.2 & Figure 5.3). However, the cell density increased when the gas injection rate was increased from 1ml/min to 2 ml/min. The change in injection rate also decreased the average cell diameter. However, the cell density did not improve at 170°C with an injection rate 2 ml/min. When comparing the foam cross-sections depicted in Figures 5.14 and 5.15, it can be observed that the cell size is smaller for foams produced at 2 ml/min. The cell density of the foams from talc containing samples decreased when processing temperature was increase from 160°C to 170°C and later to 180°C. This corresponded with increase in cell size from 217 µm at 160°C to 264 µm at 180°C. However, for talc containing samples, the cell density increased when the injection rate was increased to 2 ml/min from 1

ml/min at a given processing temperature. The foam with the best quality was observed to be at 160°C with 2 ml/min gas flow rate where the average cell diameter was 198 µm.

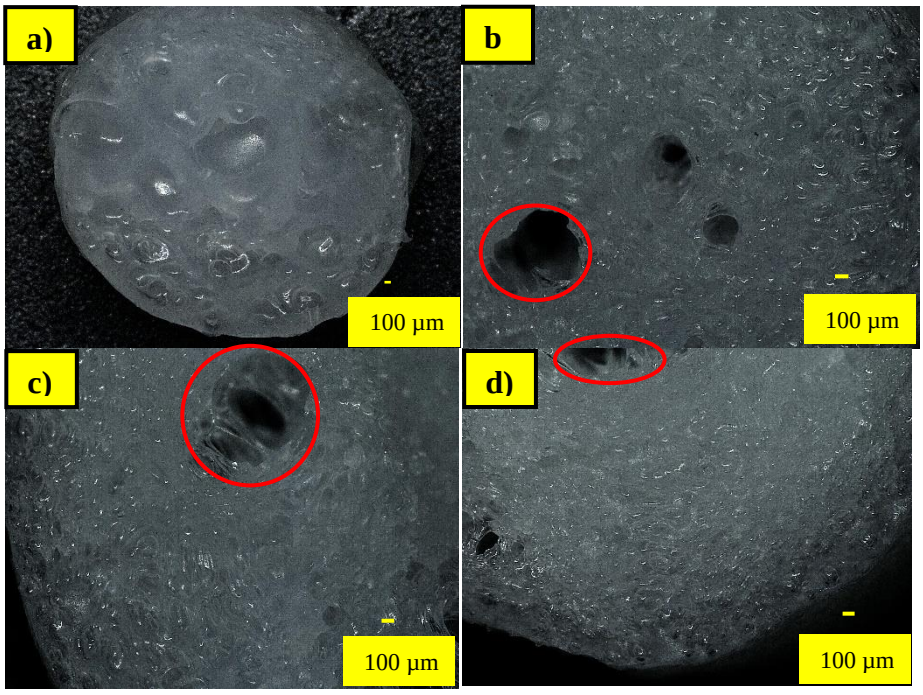

Figure 5.5: Water cooled RMS-245UG foam: a) Mixing zone temp: 160°C, 1wt% CBA, 2 ml/min gas flow rate b) Mixing zone temp: 160°C, 3wt% talc, 2 ml/min gas flow rate c) Mixing zone temp: 170°C, 3wt% talc, 2 ml/min gas flow rate d) Mixing zone temp: 180°C, 3wt% talc, 2 ml/min gas flow rate.

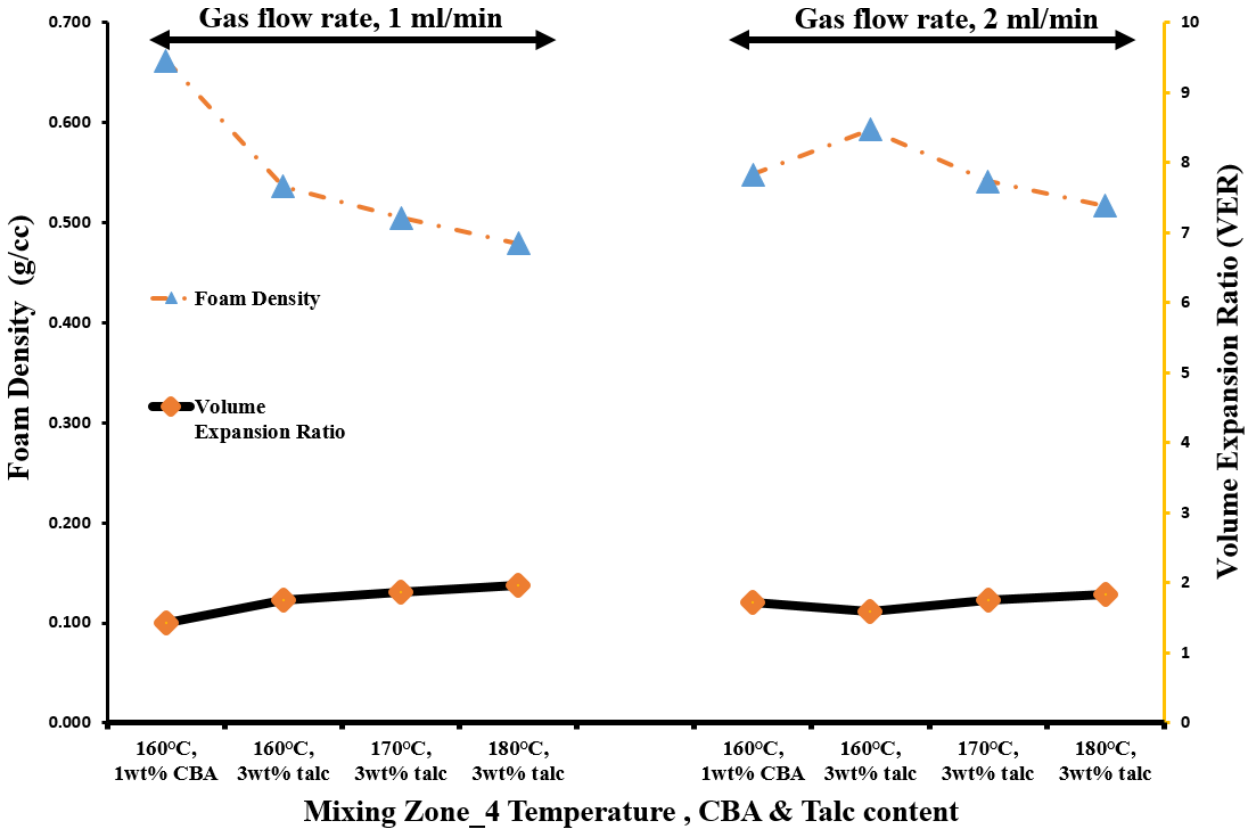

Figure 5.6: Foam density and volume expansion ratio of RMS-245-UG.

In Figure 5.4 and 5.5, the regions circled in red points out large gas pockets within the foam. This indicates that not all the injected gas was dissolved into the polymer melt before reaching the die exit. The larger gas pockets were observed at all processing temperatures and at the two different gas flowrates. From these images, it appears that the gas laden polymer solution was supersaturated at the die exit. Therefore, undissolved CO_2 produced large gas pockets adjacent to the smaller cells.

The highest foam density was observed for foam produced with Celogen OT™ at 1 ml/min gas flow rate (Figure 5.6). The foam density decreased at higher processing temperature regardless of gas flow rate. However, the foam density was higher at gas injection of 2 ml/min when comparing talc containing samples. The volume expansion ratio (VER) increased slightly at higher processing temperature. This could indicate the presence of larger voids or large gas bubbles within the foam at higher processing temperatures.

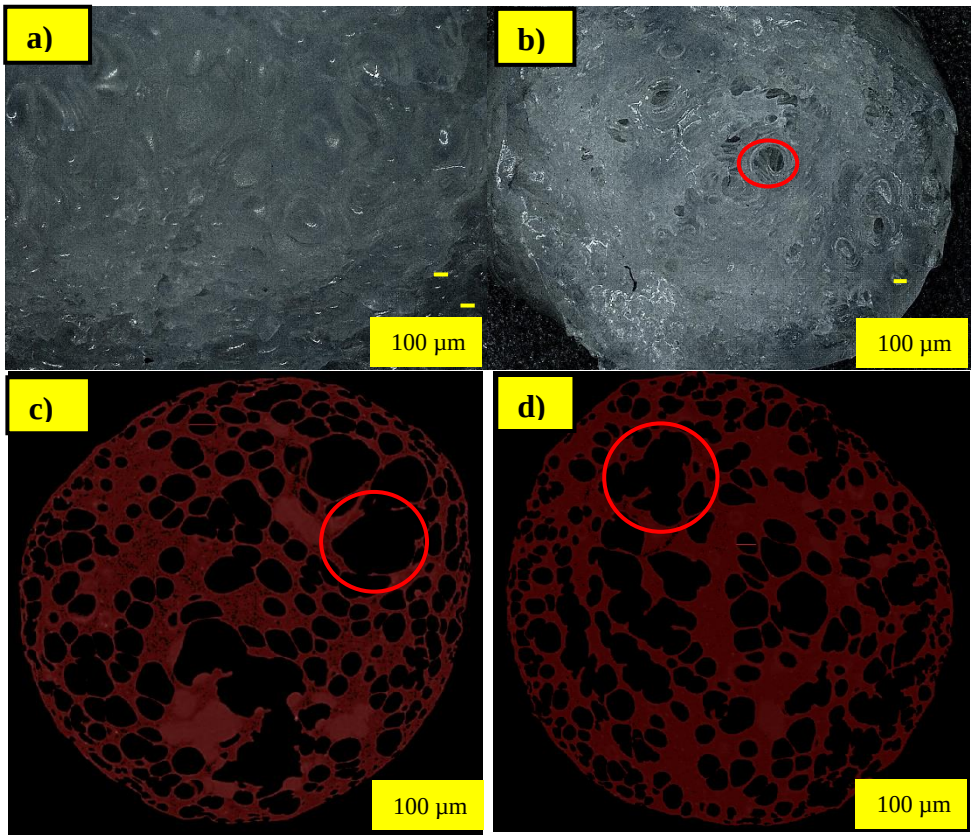

Figure 5.7: Water cooled RMS-341UG foam: a) Mixing zone temp: 160°C, 1wt% CBA, 1 ml/min gas flow rate b) Mixing zone temp: 160°C, 3wt% talc, 1 ml/min gas flow rate c) Mixing zone temp: 170°C, 3wt% talc, 1 ml/min gas flow rate d) Mixing zone temp: 180°C, 3wt% talc, 1 ml/min gas flow rate.

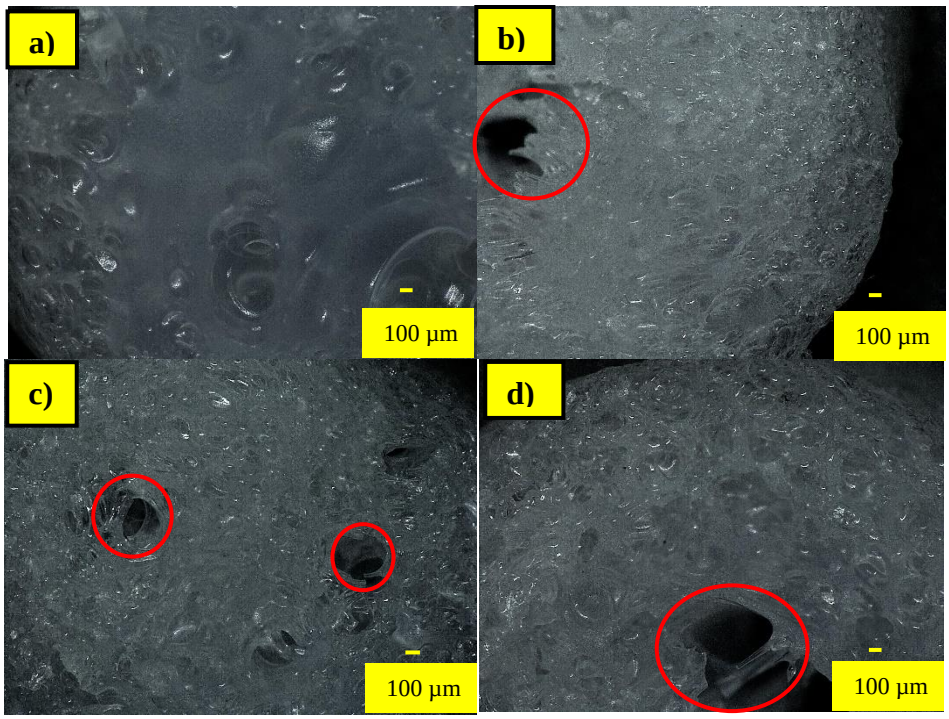

Figure 5.8: Water cooled RMS-341UG foam: a) Mixing zone temp: 160°C, 1wt% CBA, 2 ml/min gas flow rate b) Mixing zone temp: 160°C, 3wt% talc, 2 ml/min gas flow rate c) Mixing zone temp: 170°C, 3wt% talc, 2 ml/min gas flow rate d) Mixing zone temp: 180°C, 3wt% talc, 2 ml/min gas flow rate.

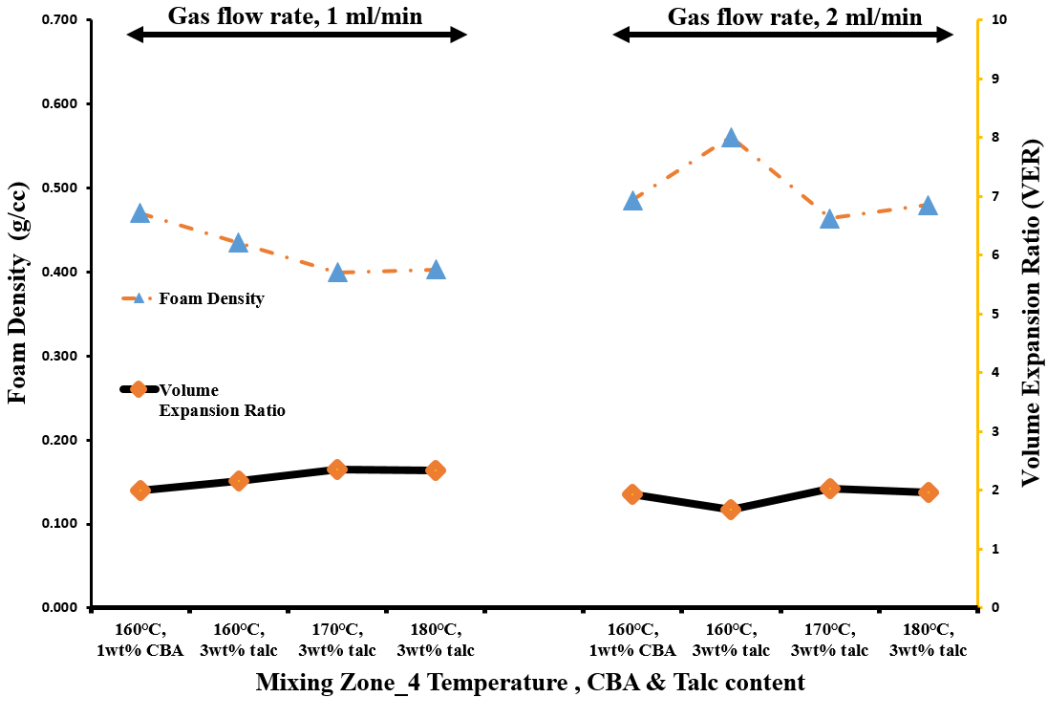

Figure 5.9: Foam density and volume expansion ratio of RMS-341-UG.

RMS-341UG is a roational molding grade resin similar to RMS-245UG. However, unlike RMS-245UG, RMS-341UG melt flow index (MFI) is higher. Therefore, at the same processing temperature the melt strength of RMS-341UG will be lower. The cell density of RMS-341UG foam processed with Celogen OT™ was lower than that corresponding to the talc assisted foaming process. However, the cell density increased and the average cell size decreased for CBA assisted foaming process when the gas flow rate was increased from 1 ml/min to 2 ml/min (Figure 5.2 & 5.3). In a similar relationship to the RMS-245Ug foam, the talc assisted foaming process had higher cell density comared to the CBA assisted foam. However, as the temperature increased, the cell density decreased for talc assisted foaming process experimental samples. This trend was observed at 1 ml/min and at 2 ml/min. However, the cell density increased and the average cell size decreased at higher gas injection rate in a given processing temperature. The highest cell density was observed when the resin was processed at 160°C and the gas injection rate was 2 ml/min with 3wt% talc. The smallest average cell dimater of 186 µm was also recored at the same processing conditions.

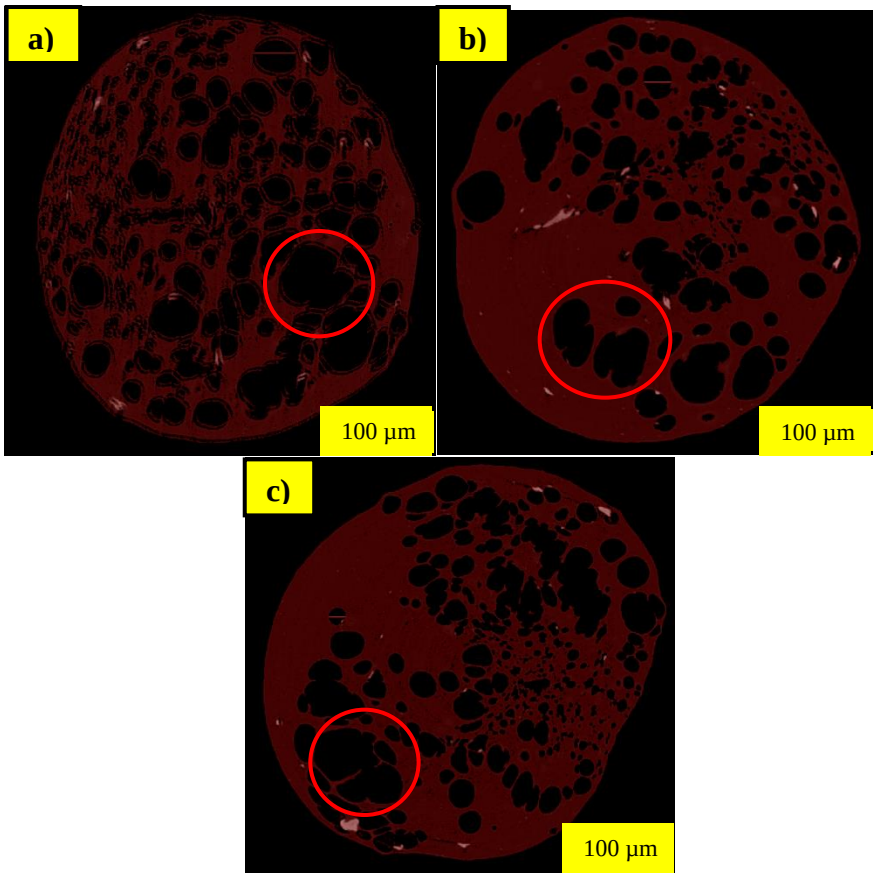

Figure 5.10: Water cooled HE-499-AC foam: a) Mixing zone temp: 160°C, 1wt% CBA, 1 ml/min gas flow b) Mixing zone temp: 170°C, 3wt% talc, 1 ml/min gas flow rate c) Mixing zone temp: 180°C, 3wt% talc, 1 ml/min gas flow rate.

In Figure 5.7 and 5.8, circled in red large gas voids are illustrated. This indicates the polymer melt was super saturated at the die exit. The foam density decreased at higher processing temperature when the gas injection rate was 1 ml/min (Figure 5.8). This corresponded with a slight increase in VER until 170°C. However, a clear trend was not observed for foam density and VER at gas injection rate of 2 ml/min. It should be noted that the formula for VER only considers the change in sample density from the pure resin, even though high VER can indicate low-density high-quality foam. However, VER in combination with overall cell density within the sample is a better indicator of foam quality.

To investigate the cell morphology of low melt flow index (MFI) PE resin, extrusion grade HDPEs were used. One of these special class of extrusion grade resin was HE-Y499-AC. From all the resins that were used for the foam production process, HE-Y499-AC had the lowest melt flow index (MFI) value and the highest flexure modulus value. The foaming characteristic of this resin

was significantly different from the other PE resins. For instance, HE-Y499-AC foam was produced in a long unbroken continuous strand from the die exit. Where the other resin types were rapidly ejected from the die exit in short segments. Unlike the rotational molding grade resin types, Celogen OT™ assisted foam produced with HE-Y499-AC resin had higher cell density compared with talc assisted foaming process for gas injection rate of 1 ml/min. The cell density increased and the average cell size reduced at a given processing temperature when the gas injection rate was increased to 2 ml/min. The CBA foam produced at the higher injection rate contained higher cell density compared to talc assisted foam at 170°C and 180°C (figure 5.2 However, the highest cell density was observed for talc assisted foaming process at 160°C with 2 ml/min gas flow rate. The average cell size at this cell density was 173.04 µm. In contrast, the cell size for CBA assisted foaming process at 2 ml/min was 191.99 µm (Figure 5.3).

From observing the foam cross-section in Figure 4.10 and 5.11 the gas pockets are observed similar to the other resin types. However, for talc containing samples, the cells are not evenly distributed throughout the cross-section. There are regions within the foam where bubbles do not exist. This could be due to the nature of recrystallization of the resin that acts as a barrier and prevents bubble migration. Similar to the other resin types, the foam density of HE-Y499-AC does decrease with temperature and the VER can range from 1.5 to 1.8 depending on the processing temperature (Figure 5.12).

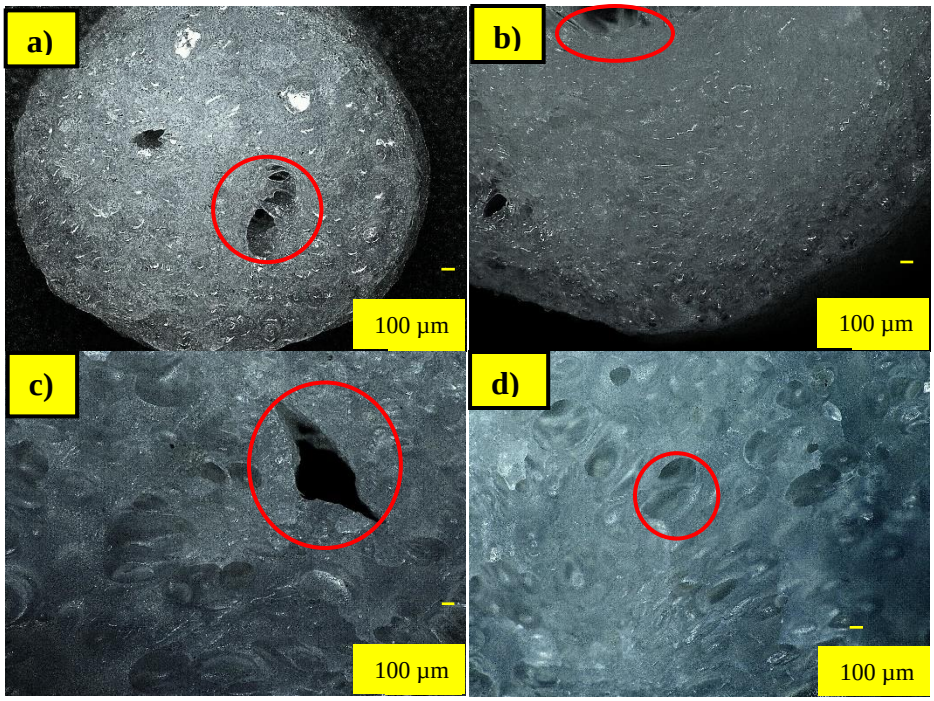

Figure 5.11: Water cooled HE-Y499-AC foam: a) Mixing zone temp: 160°C, 1wt% CBA, 2 ml/min gas flow rate b) Mixing zone temp: 160°C, 3wt% talc, 2 ml/min gas flow rate c) Mixing zone temp: 170°C, 3wt% talc, 2 ml/min gas flow rate d) Mixing zone temp: 180°C, 3wt% talc, 2 ml/min gas flow rate.

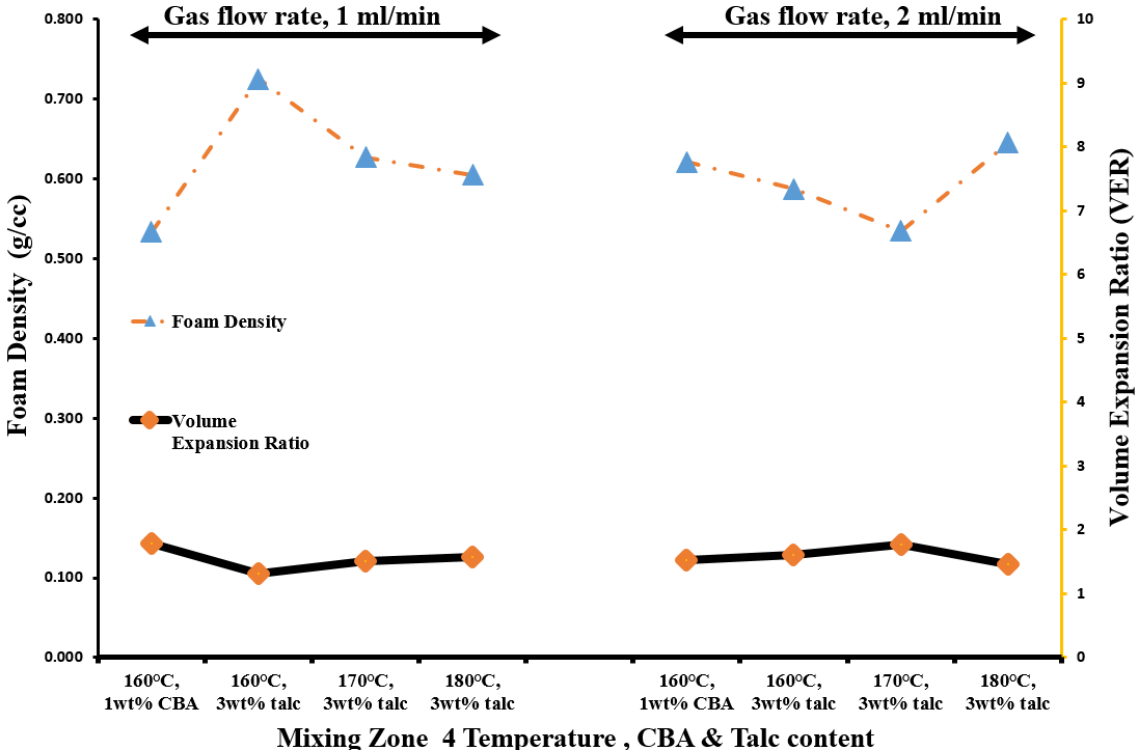

Figure 5.12: Foam density and volume expansion ratio of HE-Y499-AC.

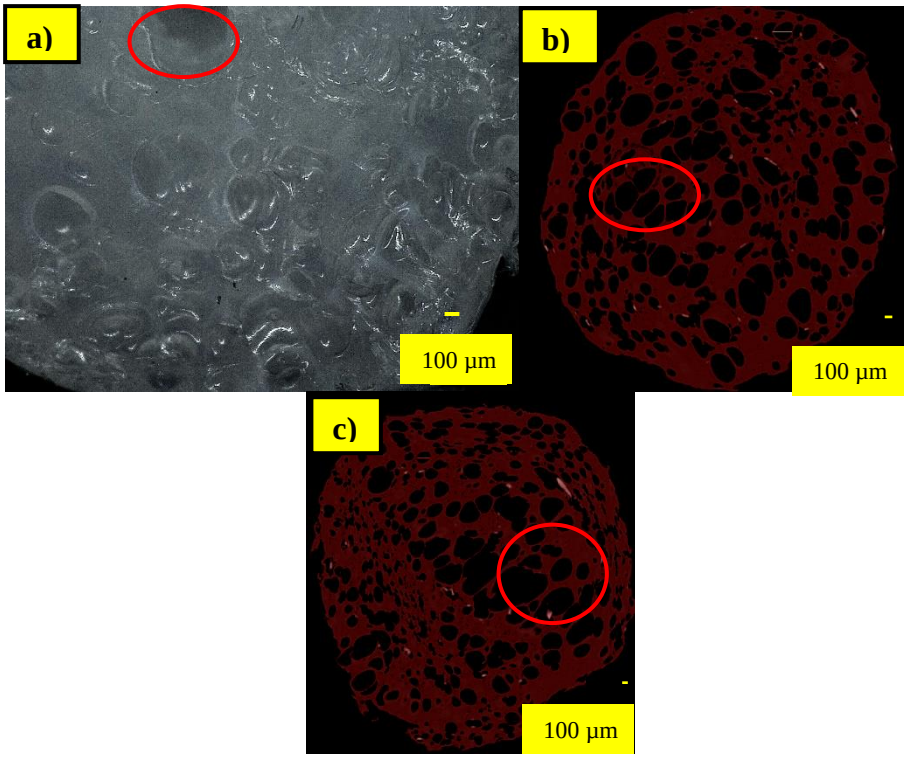

Figure 5.13: Water cooled 19C foam: a) Mixing zone temp: 160°C, 1wt% CBA, 1 ml/min gas flow b) Mixing zone temp: 170°C, 3wt% talc, 1 ml/min gas flow rate c) Mixing zone temp: 180°C, 3wt% talc, 1 ml/min gas flow rate**.**

The second extrusion grade HDPE resin that was utilized for foaming experiments was 19C. In comparison with the other resin types, 19C has the second lowest MFI value and the second highest flexure modulus value is similar to the rotational molding grade HDPEs. In a similar manner the cell density of the CBA contacting 19C foam displayed lower cell density compared with the talc containing samples at 1 ml/min gas injection rate. The cell density of the CBA assisted foaming process was improved by increasing the injection rate to 2 ml/min. The cell density was higher than samples dry blended with 3wt% talc. The average cell size at 160°C was reduced to 182 µm and the cell density was increased by a factor of 10. However, a clear trend of decreasing cell density was not observed at increasing processing temperature when the gas flow rate 1 ml/min. Also, at 170°C the cell density was higher at gas flow rate of 1 ml/min (Figure 5.2).

The foam cross section in Figures 5.23 and 5.24 reveals the presence of gas pockets in areas circled in red. These gas pockets are more likely to be present toward the interior of the foam and smaller cells are found closer to the surface. The foam density was lower at higher processing

temperature for gas flow rate of 1 ml/min. However, a similar trend was not observed for higher gas flowrate (Figure 5.15). The VER did not vary significantly for the two gas injection rates.

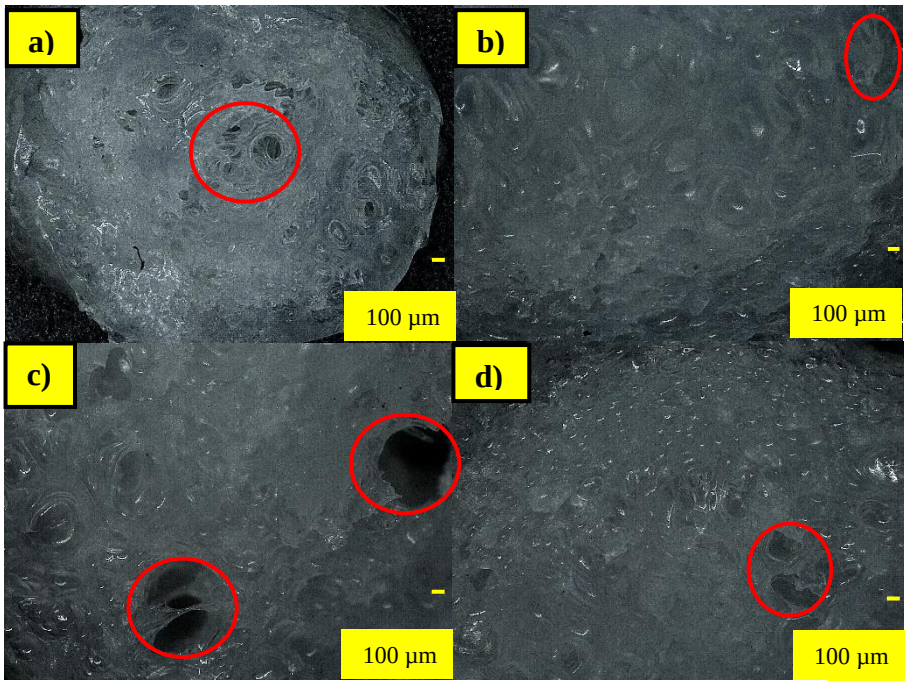

Figure 5.14: Water cooled 19C foam: a) Mixing zone temp: 160°C, 1wt% CBA, 2 ml/min gas flow rate b) Mixing zone temp: 160°C, 3wt% talc, 2 ml/min gas flow rate c) Mixing zone temp: 170°C, 3wt% talc, 2 ml/min gas flow rate d) Mixing zone temp: 180°C, 3wt% talc, 2 ml/min gas flow rate.

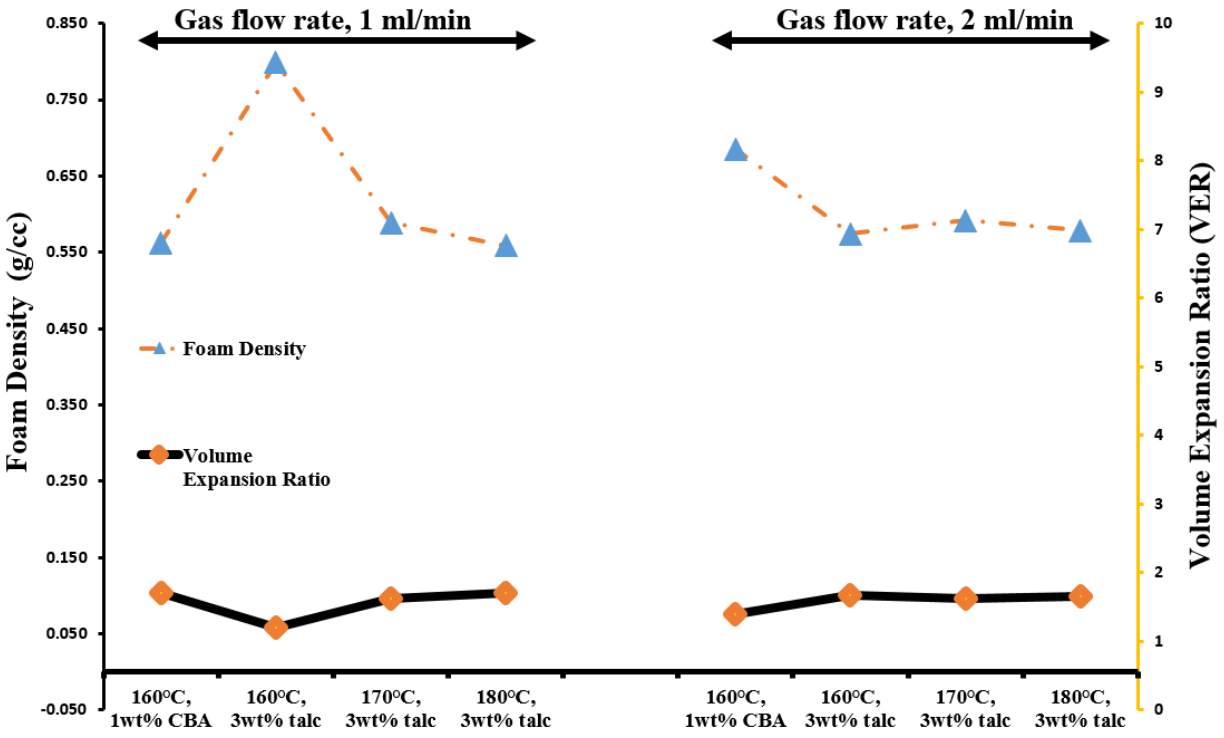

Figure 5.15: Foam density and volume expansion ratio of 19C.

The cell morphology of different grades of HDPE resins has been studied to understand their suitability for the foaming process with PBA. From the data presented in Figure 5.2 and 5.3, resins processed with 1wt% CBA at 160°C had lower cell density and higher average cell size compared with 3wt% talc at the same processing temperature. However, the cell density was higher for extrusion grade HDPE processed with CBA. In contrast, the rotational molding grade HDPEs have better suitability for foaming at higher temperatures, as the results indicates higher cell density and smaller cell size at 170°C and 180°C compared to the extrusion grade HDPE. However, higher processing temperature reduces the quality of the foam due to cell coalescence. By doubling the gas injection rate from 1 ml/min to 2 ml/min the cell density was increased.

5.3.1 *Foam Characterization of Resin LA-0522*

The final PE resin experimented with PBA foaming process was, LA-0522. The LDPE resin is a special grade of polyethylene made for polymer foaming process. The melting point and the recrystallization temperatures are lower than HDPE resin and therefore, this particular LDPE resin

can be processed at a lower temperature. All LDPE foams were produced by processing the gas laden polymer in the mixing zone at 135°C and later at 150°C. The LDPE resins were dry blended with 1wt% Celogen OT™ to produce CBA assisted foam and 3wt% talc to produce nucleating agent assisted foam. The supercritical gas was injected into the polymer melt at 1 ml/min and later at 2 ml/min to observe the differences in cell morphology.

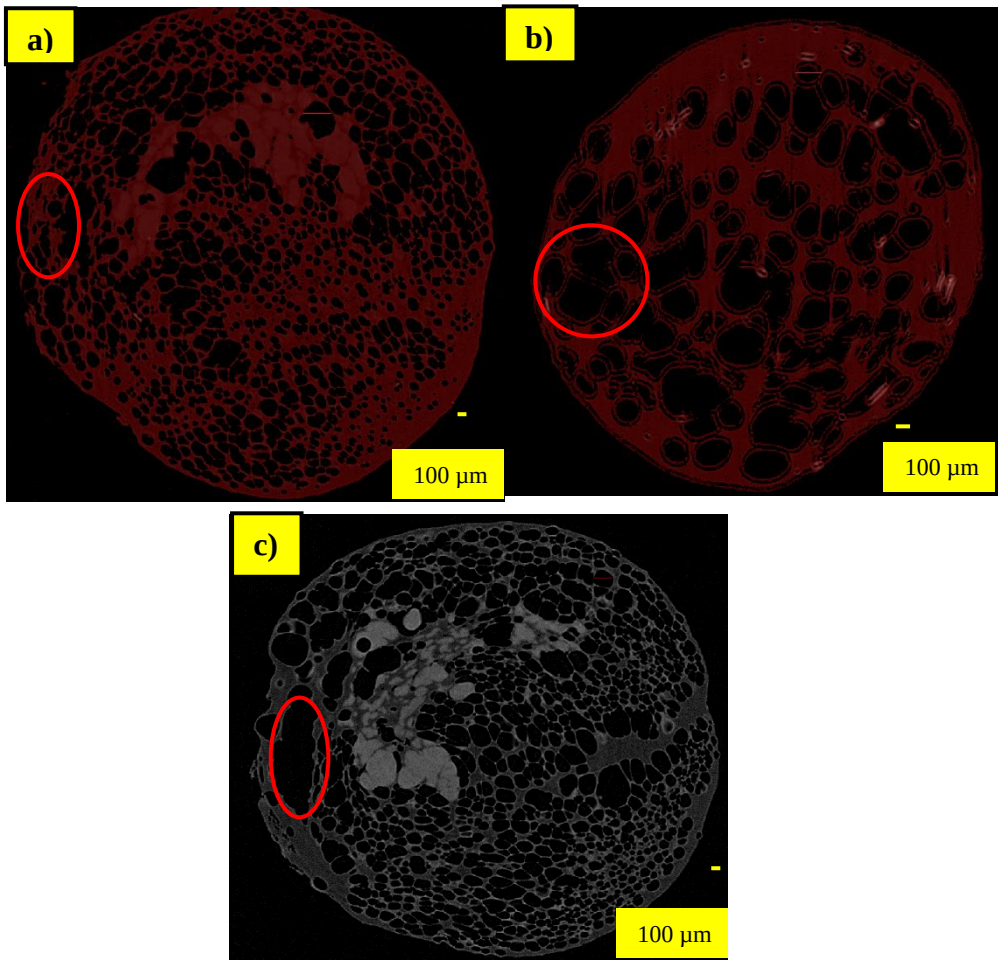

Figure 5.16: Water cooled LA-0522 foam: a) Mixing zone temp: 135°C, 1wt% CBA, 1 ml/min gas flow b) Mixing zone temp: 135°C, 3wt% talc, 1 ml/min gas flow rate c) Mixing zone temp: 150°C, 1wt% CBA, 1 ml/min gas flow rate.

The cross-section of the LDPE foam is represented in Figures 5.16 and 5.17. From the images, the cells within the CBA assisted foam is closely packed with thin walls in between adjacent cells. However, for nucleating agent assisted foaming process the cells are larger and more sparsely populated with thicker cell walls between adjacent cells. The areas circled in red identify the large gas pockets within the foam. This indicates that gas laden LDPE melt at the die

exit was supersaturated and trapped undissolved gas was present. Similar to the HDPE resin, these large gas pockets were present under all processing conditions and could not be eliminated with the current experimental setup.

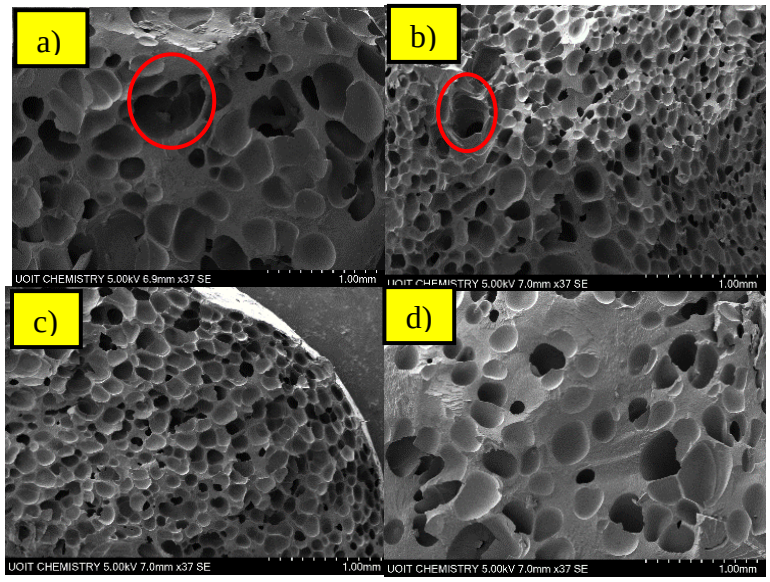

Figure 5.17: Water cooled LA-0522 foam: a) Mixing zone temp: 135°C, 3wt% talc, 2 ml/min gas flow rate b) Mixing zone temp: 135°C, 1wt% CBA, 2 ml/min gas flow rate c) Mixing zone temp: 150°C, 1wt% CBA, 2 ml/min gas flow rate d) Mixing zone temp: 150°C, 3wt% talc, 2 ml/min gas flow rate.

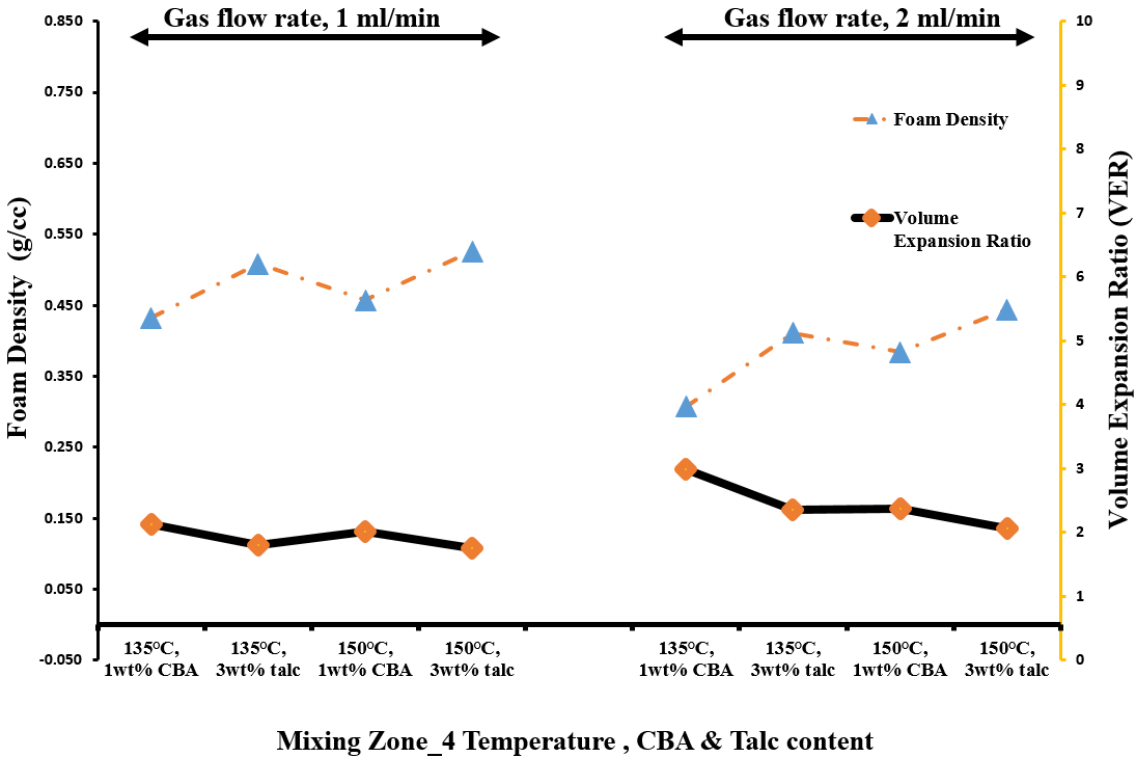

Figure 5.18: Foam density and volume expansion ratio of LA-0522.

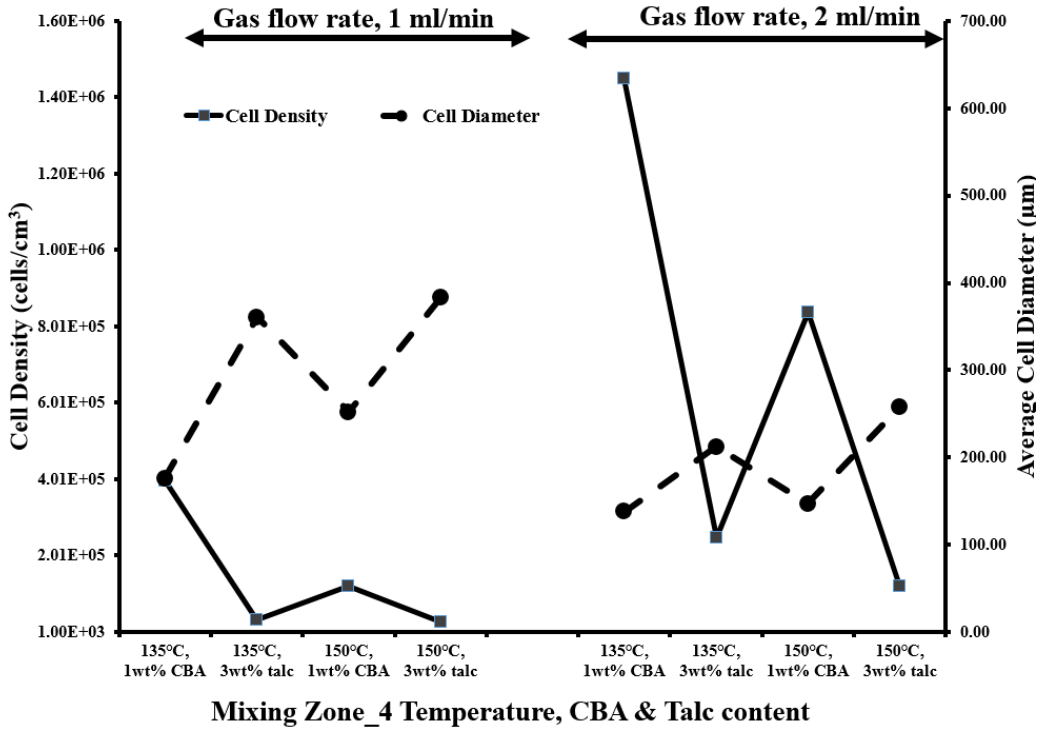

Figure 5.19: Cell density and average cell diameter of LA-0522.

The foam density of LDPE resin is given in Figure 5.18 for the two different gas injection rates. From the data, the CBA assisted foaming process has lower foam density compared with the talc assisted foaming process. By increasing the processing temperature, the foam density increases for both CBA assisted foam and talc assisted foam. However, the density of the CBA assisted foam processed at 150°C remains below the talc assisted foam produced at 135°C. The foam density was decreased regardless of processing condition when the gas injection rate was increased to 2 ml/min. At this higher injection rate the general trend remained the same, where CBA processed foam had lower foam density. The VER was closely related to the foam density. The lower the foam density the higher the expansion ratio was observed. The highest VER was recorded to be 2.99 for foam processed at 135°C with 1wt% Celogen OT™ and, the gas injection rate was 2 ml/min.

The cell density and the average cell size is presented in Figure 5.19. From the graph, foam processed with CBA had higher cell density than talc contacting foam at the same processing temperature. The cell density of both CBA and talc contacting foam decreased as the processing temperature was increased from 135°C to 150°C. The decrease in cell density corresponded with increase in average cell size. However, the cell density of CBA contacting foam was higher at 150°C compared to talc containing foam at 135°C. The cell density increased and the average cell size decreased after increasing the gas injection rate. The best quality foam was produced at mixing chamber temperature of 135°C with 1wt% CBA at 2 ml/min gas injection rate.

5.4 Sample Preparation for RRFGFM Composites

In order to analyze the cell morphology of the rotational molded foamed articles, the composites were cut in half to expose the internal structure. The height of the composite articles are 16 cm along its central axis, and the width at the narrowest section is 9 cm and 11 cm at the widest. In Figure 5.20, a cross-section of the composite article is presented. The mold filling takes place parallel to the y-axis, starting from position A_1 and it terminates at the end of D_1. The quality of the foam is determined according to its density, volume expansion ratio, cell population density, average cell size and, bonding quality with the outer skin. The foam is analyzed at four positions within the core: A_1, B_1, C_1, & D_1. These positions correspond with deliberate change in variables to modify the quality of the foam.

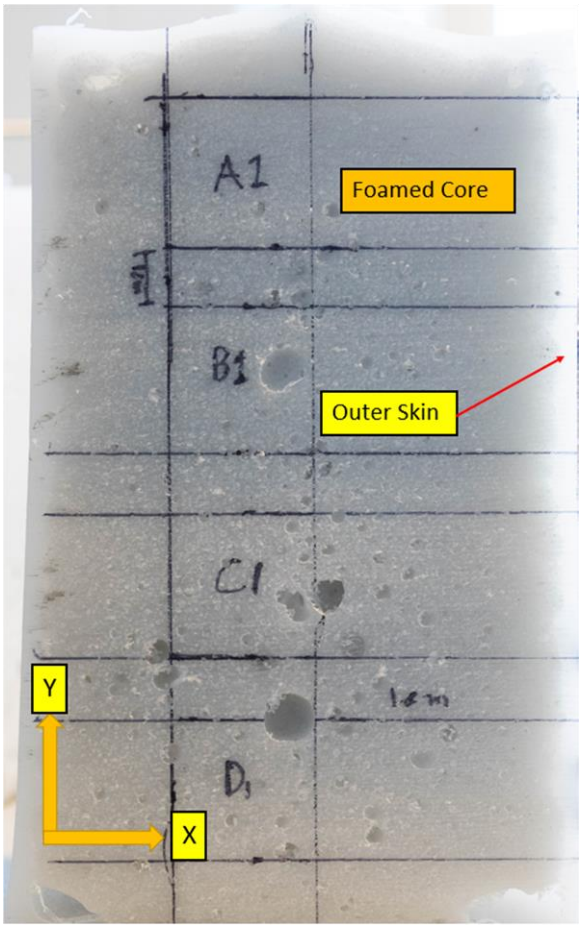

Figure 5.20: Rotational molded foam composite cross-section.

5.5 Rapid Rotational Functionally Graded Foam Molding (RRFGFM) Processing Strategies

5.5.1 *RRFGM Gradual Modification of Gas Flowrate*

5.5.1.1 RRFGFM Processing with sHDPE Resin Powder

The sHDPE resins were all processed at 150°C inside the static mixer, which is represented by zone 4 in Figure 4.15. This was the lowest allowable processing temperature for foam production with rotational molding grade resin. Bellow 150°C, continuous melt flow within the static mixer cannot be maintained without bursting the rupture disk. The foamed cores were produced by utilizing 3wt% talc with RMS-341UG resin, and RMS-245UG resin. An alternative foamed core was produced from 1wt% Celogen OT™ with RMS-245UG resin. The samples were selected for analysis according to visual inspection after cutting the RRFM composite in half. A sample was selected for further analysis if it had the fewest number of defects from a group with identical processing conditions. The quality of the defects was assed according to the foam fill amount; size and quantity of voids within the foam; and foam attachment with the integral outer skin.

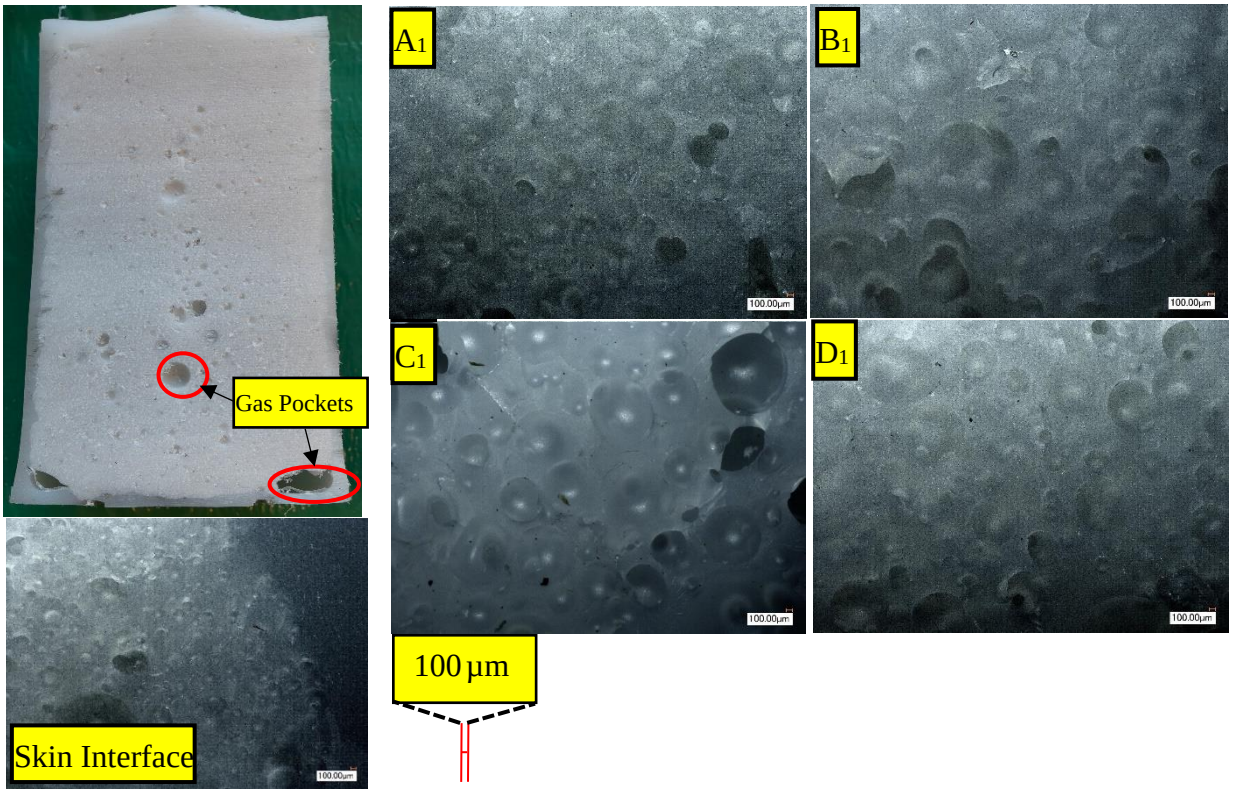

Figure 5.21: RMS-341UG foamed core processed at 150°C with talc.

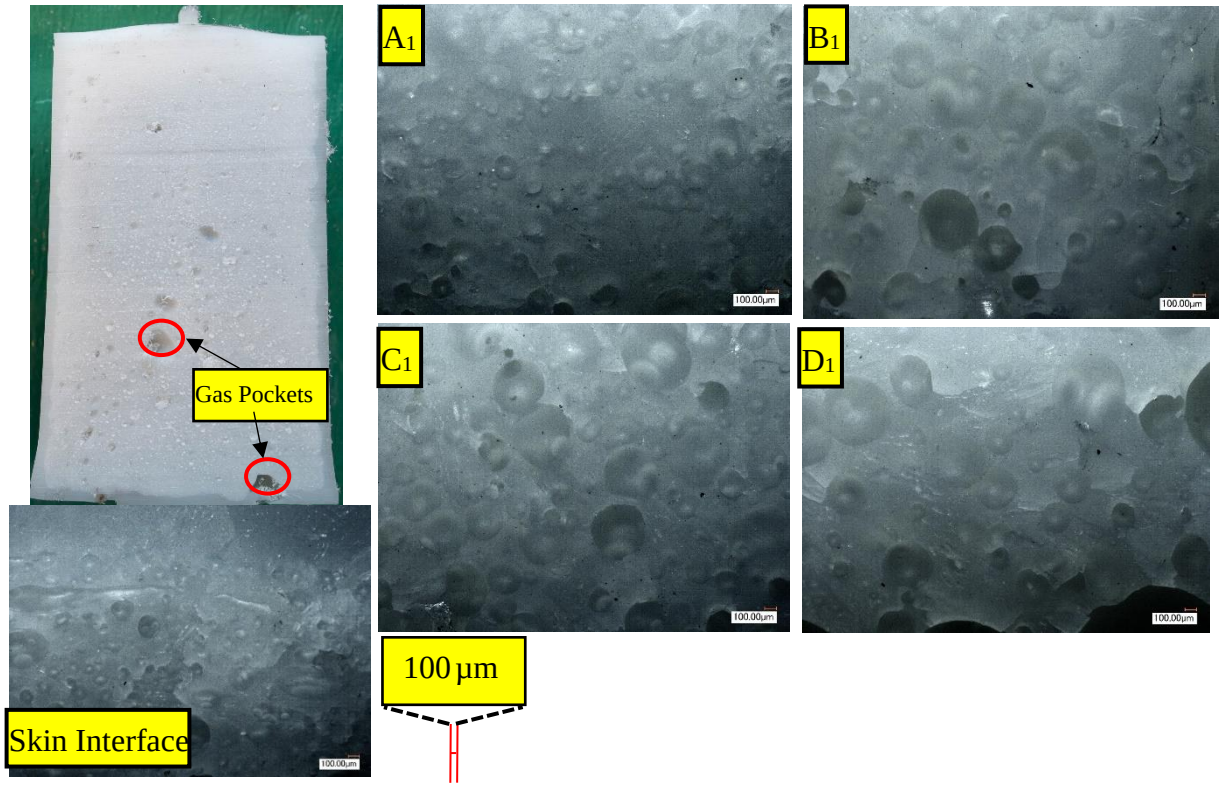

Figure 5.22: RMS-245UG foamed core processed at 150°C with talc.

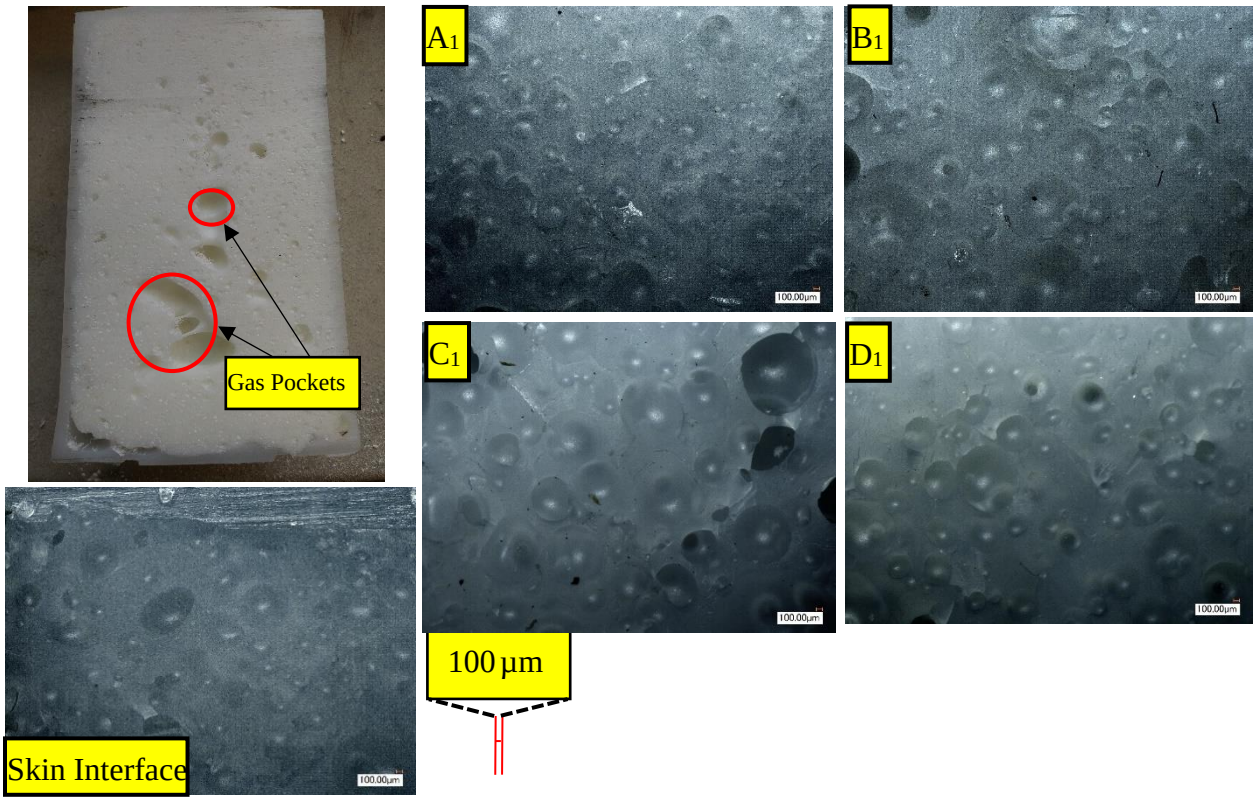

Figure 5.23: RMS-245UG foamed core processed at 150°C with Celogen OT™.

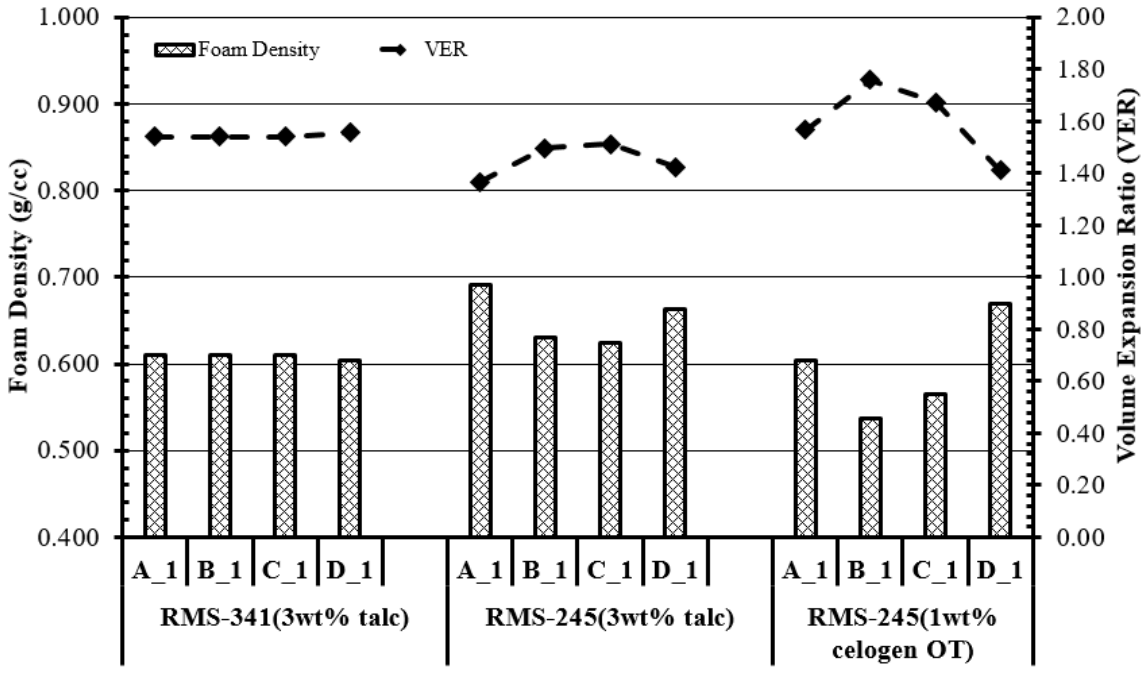

Figure 5.24: Foam density and volume expansion ratio of sHDPE resin processed at 150°C in mixing zone 4.

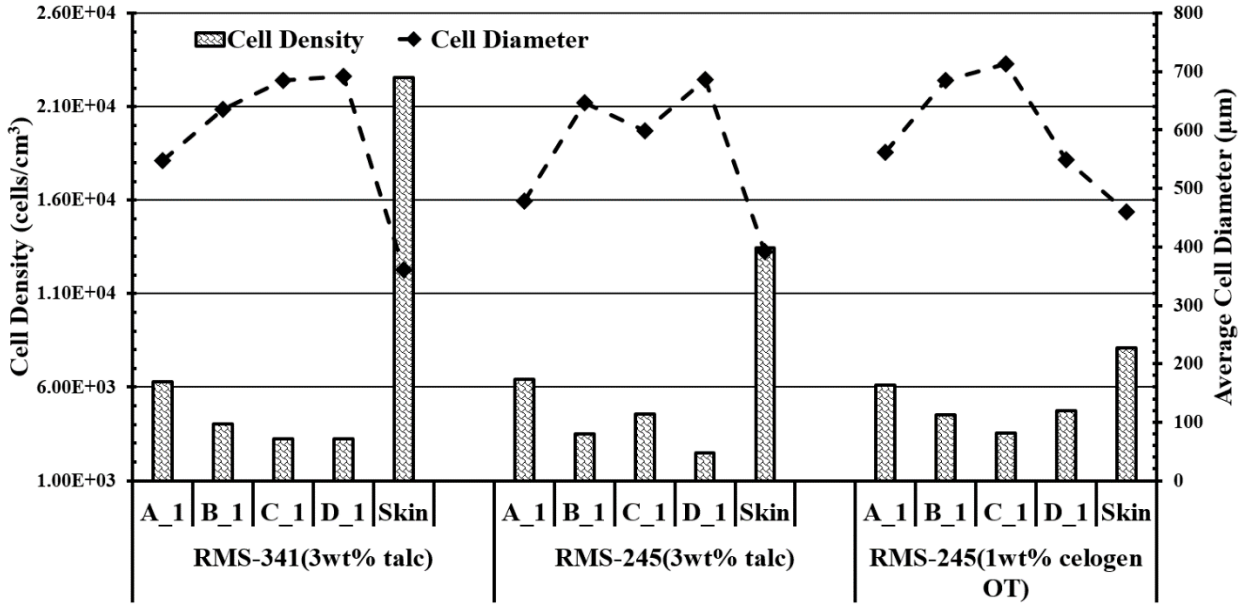

Figure 5.25: Cell density and average cell size of sHDPE resin processed at 150°C in mixing zone 4.

The foamed core cross-section of RMS-341UG is presented in Figure 5.21. From visual inspection, there are prominent gas pockets present toward the center of the foamed core. This is also observed for foamed core produced with RMS-245UG (Figure 5.22). Gas pockets are identified according to their size. An empty void larger than 5 mm in diameter is identified as a gas pocket. These pockets can be found at any region of the foamed core not just at the center of the core. However, the gas pockets are larger toward the center since the foam in this region re-crystallize later than the foam region closer to the outer skin. This allows the voids to grow to a bigger size as gas diffusion continues until the resin re-crystalizes.

Initially a gas pocket can originate when a cetin quantity of undissolved physical blowing agent is encapsulated by the molten extruded foam during the filling process. However, in some instances, entrapped air at the skin interface can form voids. Cell coalescence is another contributing factor for gas pockets to form. The merging of smaller cells into larger ones takes place between neighboring cells to reduce overall surface area of cell walls and become more stable. This process can continue until the melt strength of the resin increases to counteract cell walls from merging.

The digital microscope images of the skin interface are given for the three different foamed cores in Figures 5.21-5.22. From the images, all three samples show bubble penetration into the skin layer, a clear visual indication of foam layer bonding with the outer skin. The cell morphology was determined at four distinct layers and near the skin interface. The regions of interest are identified in Figure 5.20. The VER and the foam density did not change substantially from A_1 to D_1 for foamed core produced from RMS-341UG and 3wt% talc (Figure. 5.24). In contrast, the VER increased from A_1 to C_1 and later decreased at D_1 for foamed core produced with RMS-245UG with 3wt% talc. The corresponding foam density decreased moving from A_1 to C_1 and it increased again at region D_1. The foamed core produced with Celogen OT™ revealed a similar pattern to the foamed core produced with RMS-245UG with talc. However, the foam density was lower for any given region of interest. The VER reached its peak in region B_1 at 1.75 and it gradually decreased to 1.41 at D_1.

The cell density of RMS-341UG gradually decreased from 6.03 X 10^3 cells/cm^3 from A_1 to 3.22 X 10^3 cells/cm^3 at D_1 (Figure. 5.25). However, the cell density near the skin region reached 2.24 X 10^4 cells/cm^3. The higher cell density near the skin resulted due to faster cooling rate than the interior of the foam. Higher cell density at the skin region was observed for RMS-245UG with talc and Celogen OT™. However, the cell density near the skin region was higher for foam processed with talc rather than Celogen OT™. The cell density of RMS-245UG foam processed with talc decreased from A_1 to D_1. However, a slight increase in cell density was observed from region B_1 to C_1 and later it reduced again at D_1. The cell density of foam processed with Celogen OT™ revealed a U-shaped pattern, where the initial cell density decreased from 6.09 X 10^3 cells/cm^3 at A_1 to 3.54 X 10^3 cells/cm^3 at C_1 and it increased to 4.74 X10^3 cells/cm^3 at D_1.

The corresponding average cell diameter is presented in top of the bar graph in Figure. 5.25. For RMS-341UG, the cell dimeter gradually increased from 547 µm at A_1 to 691 µm at D_1. However, the average cell diameter at the skin interface was 391 µm because of the higher cell density near the surface. The average cell diameter for foam produced with RMS-245UG with talc also increased from A_1 to region D_1. The average cell diameter for foam processed with Celogen OT™ was higher than the other two foam types. The cell dimeter peaked at 713 µm at region B_1 and then it gradually reduced toward D_1.

5.5.1.2 RRFGM Processing with sHDPE Resin Powder & Extrusion Grade HDPE

In this section the foamed cores were produced with pipe and film extrusion grade HDPE, and a single grade of rotational molding sHDPE resin for comparison. Unlike the previous section, the minimum processing temperature for extrusion grade HDPE resin at zone 4 was 160°C. Bellow 160°C, the polymer melt viscosity is too high for the extruder to maintain continuous flow bellow the rupture disc pressure. However, the die zone temperatures were reduced to 145°C in zone 6 and 140°C in the die nozzle (zone 7). The purpose of reducing the melt temperature was to increase the melt strength of the polymer before injecting the foam into the mold cavity to minimize cell coalescence and gas diffusion out of the semi-molten foam. However, such foam processing methods with 19C and HE-Y499-AC can be very challenging. By reducing the extruded foam temperature, the surface of the foam is prone to freezing more rapidly. When the surface solidifies, further expansion of the foam seizes. This leads to improper mold filling as empty voids are encapsulated by solidified foam walls leaving gaps between adjacent foam layers. The outer surface quality of the integral outer skin is also negatively affected. The gaps between adjacent of foam layer on the internal skin surfaces causes an uneven force distribution which leads to the integral outer skin to warp as the foam cools. This effect can be minimized by increasing the die zone temperature, however it cannot be completely eliminated.

The cross-section of foamed core produced with 19C resin and 3wt% talc is presented in Figure 5.26. From this image it can be observed that larger gas pockets are present toward the center of the foamed core compared with RMS-245UG foam processed under the same condition (Figure 5.27). Unlike the two grades of HDPE resin, the foamed core produced with sHDPE did not show any signs of skin warpage at the die nozzle temperature of 140°C or 120°C.

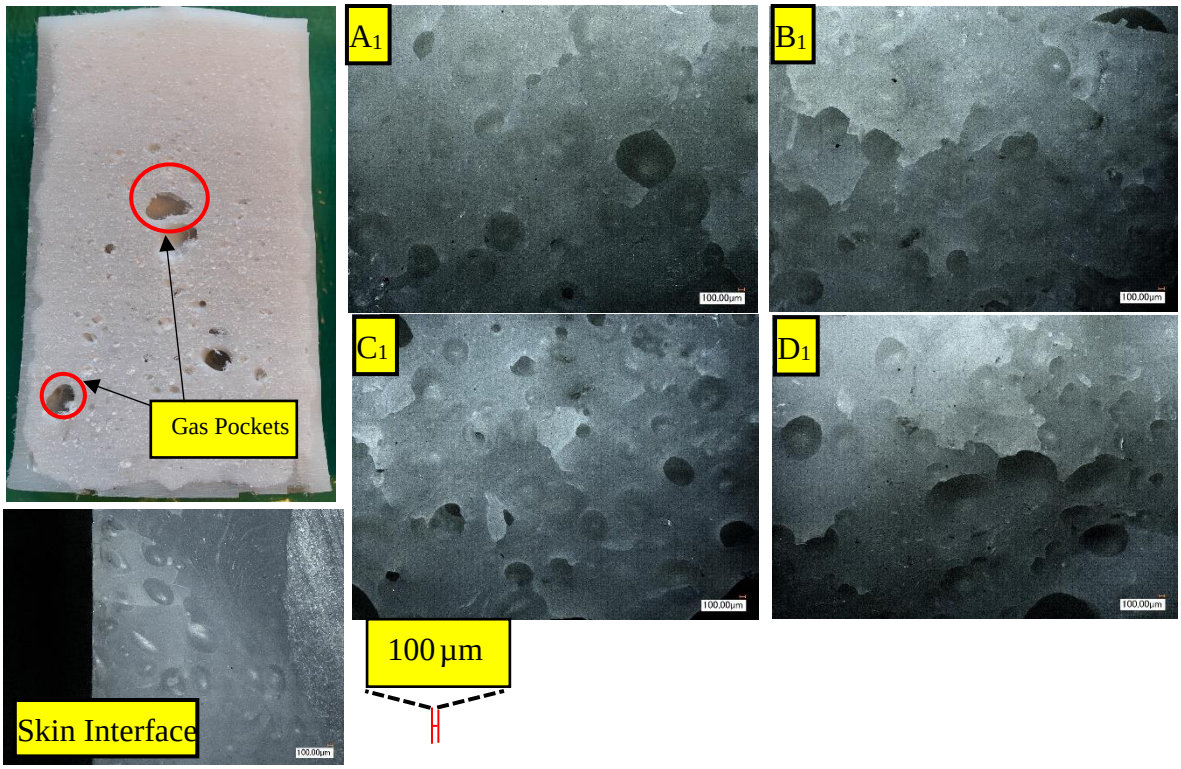

Figure 5.26: 19C foamed core processed at 160°C with talc.

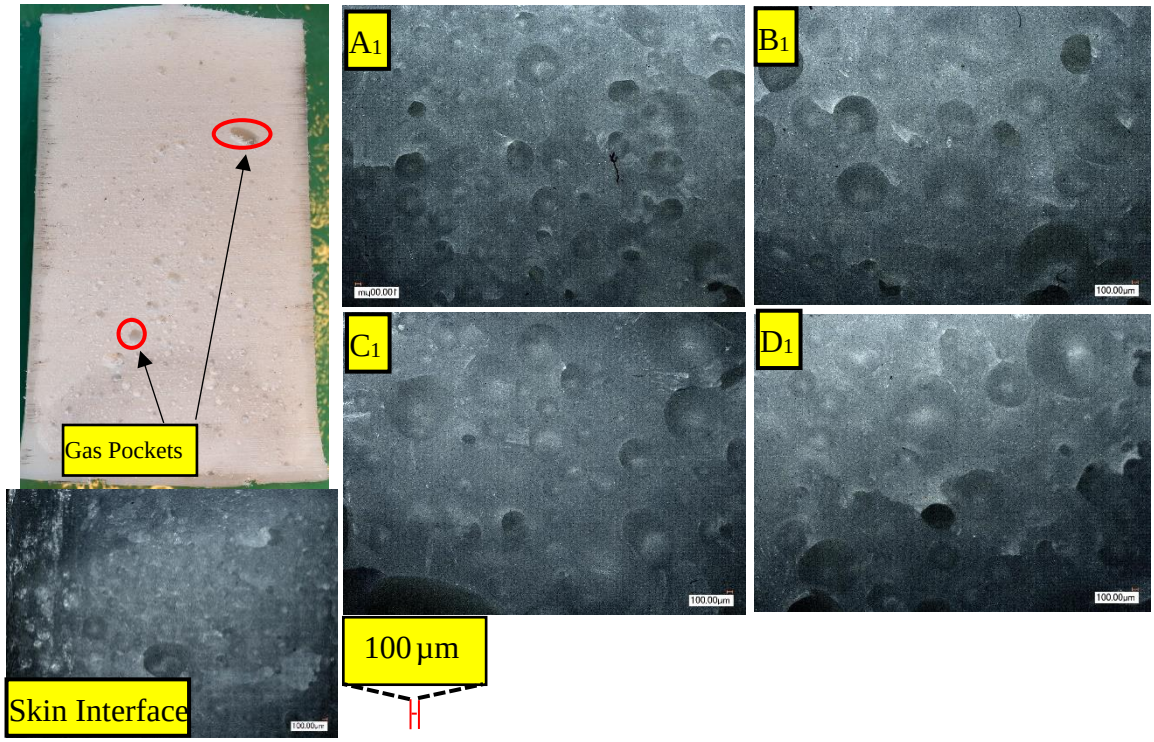

Figure 5.27: RMS-245UG foamed core processed at 160°C with talc.

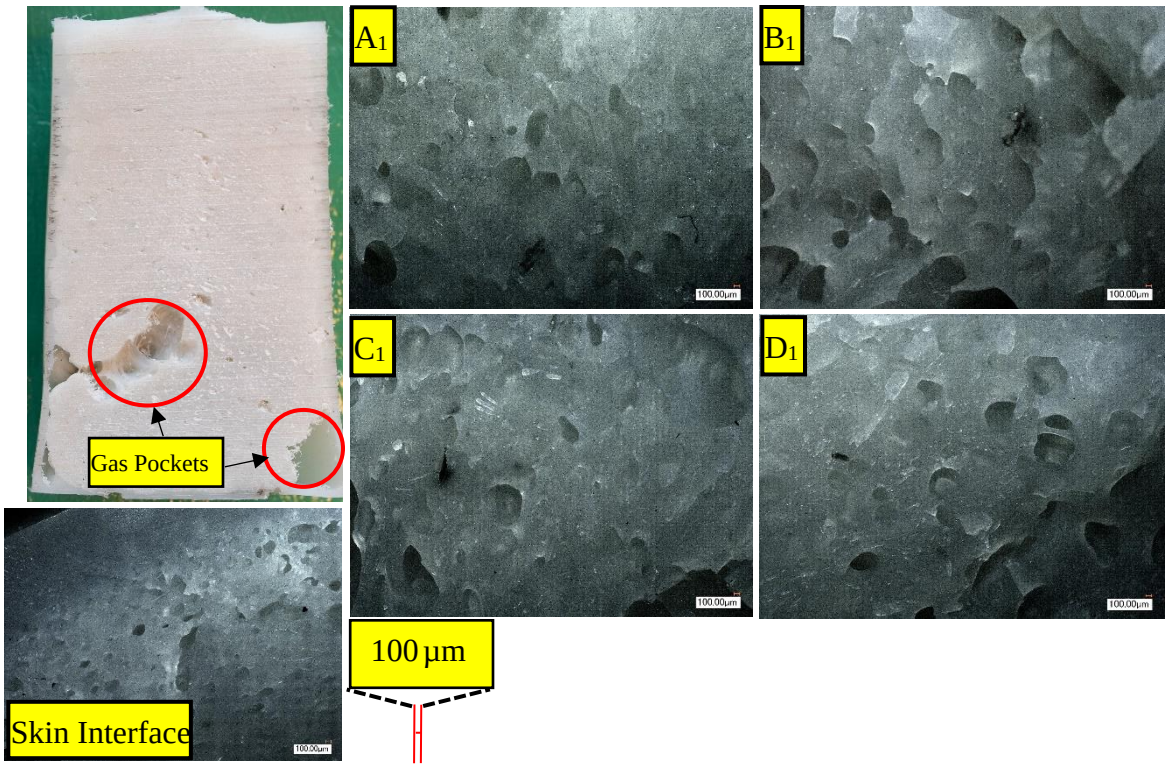

Figure 5.28: HE-Y499-AC foamed core processed at 160°C with talc.

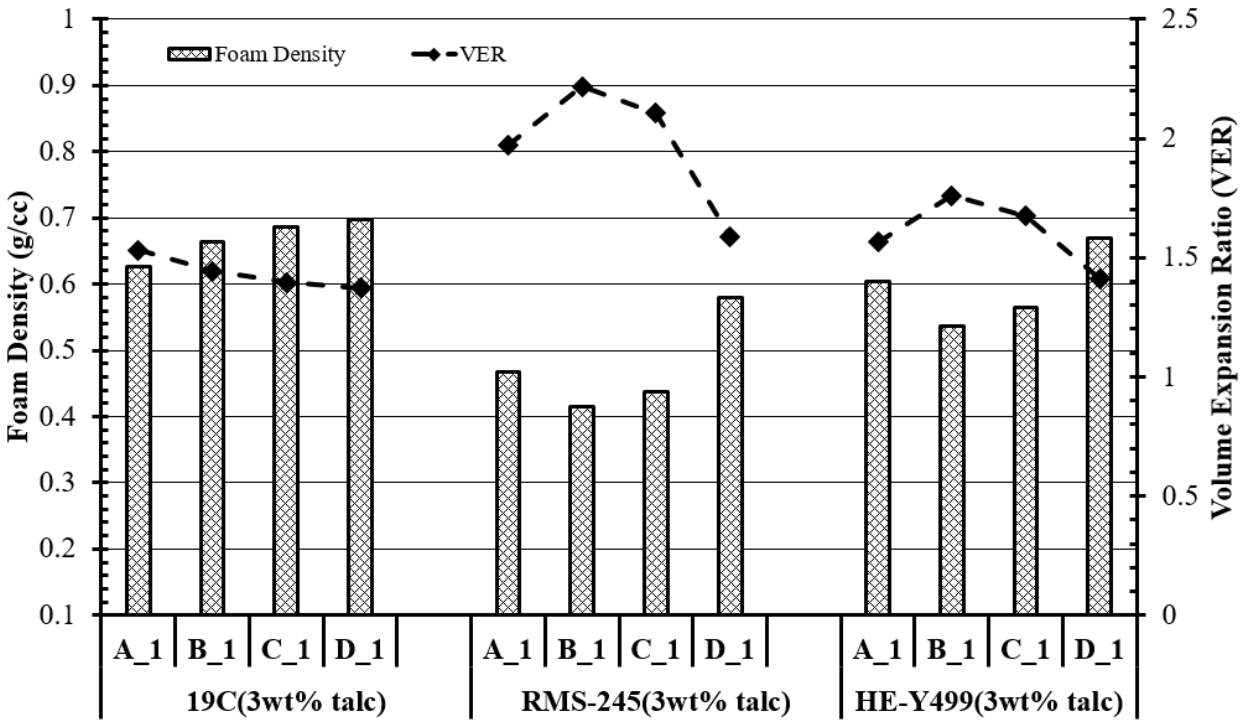

Figure 5.29: Foam density and volume expansion ratio of sHDPE & HDPE resin processed at 160°C in mixing zone 4.

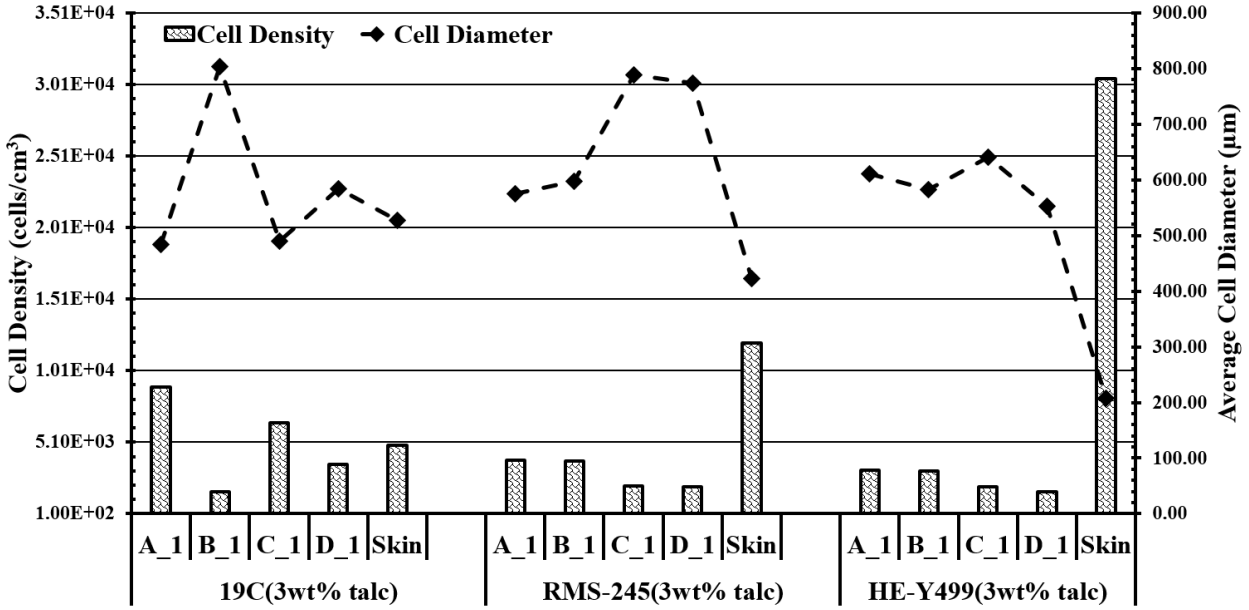

Figure 5.30: Cell density and average cell size of sHDPE & HDPE resin processed at 160°C in mixing zone 4.

From multiple foaming attempts, the foamed core sample presented in Figure 5.28 was the best quality specimen achieved with HE-Y449-AC resin. The sample cross-section has revealed improper filling near the mold interface port due to rapid cooling of the foam surface. The solidified surface prevented further expansion of the foam and creating the large voids. However, all three types of foam resins in this section demonstrate adequate foam bonding with the outer skin layer. As seen in Figures 5.26 - 5.28, cell penetration into the foam layer is observed.

The VER and foam density of the foamed cores in this section are presented in Figure 5.29. From the data the VER of the 19C foamed core decreases from position A_1 to D_1. This corresponded with an increase in foam density from region A_1 to D_1. This gradual increase in foam density was also observed for water cooled foam when the gas flow rate was reduced. However, this trend was not observed for RMS-245UG and HE-Y499-AC foamed core. This indicates gradual variation in foam quality is not only dependent on the gas injection rate, rather the thermal gradient within the foamed core that develops during the cooling process also play a significant role controlling the quality of the foam. The foam density of RMS-245UG was significantly lower in a given region of interest compared with the other two foamed cores. This also corresponded

with higher VER value compared with other two resin types. For this reason, it seems that the foamed core produced with RMS-245UG had smaller gas pockets.

The cell density and the average cell size of the foamed cores are presented in figure 5.30. For 19C foamed core, gradual change in internal structure was not observed for cell density and average cell size. In contrast, the cell density of RMS-245UG resin gradually decreased from 3.86 X 10^3 cells/cm^3 at A_1 to 1.95 X 10^3 cells/cm^3 at D_1. For HE-Y499-AC resin the cell density also decreased gradually from 3.12 X 10^3 cells/cm^3 at A_1 to 1.62 X 10^3 cells/cm^3 at D_1. However, a gradual change in cell size was not observed for HE-Y499-AC resin. The average cell size decreases to 583 µm at B_1 and increases back to 641 µm at C_1. In contrast, the average cell size gradually increased for RMS-24UG resin foamed core.

5.5.1.3 RRFGFM Processing with Foam Extrusion Grade LDPE

In this section, the foamed core was produced with LDPE resin either with 1wt% talc or 1wt% Celogen OT™. Since the LDPE resin's melting point is 109°C, the processing temperature can be lower compared with HDPE resin. The static mixer zone 4 temperature for processing the two types of foamed core was set at 135°C. It is possible to produce the foam at a lower processing temperature, however at temperatures higher than 135°C the extrusion pressure may drop below the critical point at zone 5. Therefore, the upper temperature limit for LDPE foam processing was kept at 135°C. The recrystallization temperature of this particular LDPE resin is 95°C. It is for this reason the die temperatures are decreased to 115°C in zone 7 and 105°C in zone 8 to increase the melt strength.

Unlike the HDPE resins, the surface of the LA-0522 foamed core was softer and can be easily indented. This is due to its low flexure modulus and yield strength values compared to the other resin types. The cross-section of the foamed core produced with 1wt% Celogen OT™ is given in Figure 5.31. The gas pockets within the foam resulted from trapped undissolved gas and additional nitrogen gas being released from the decomposition of CBA particle. In a similar fashion, gas pockets are also prominent in the foamed core processed with 1wt% talc (Figure 5.32). For both types of foamed core, bubble penetration into the skin layer was observed indicating good bonding with the integral outer skin.

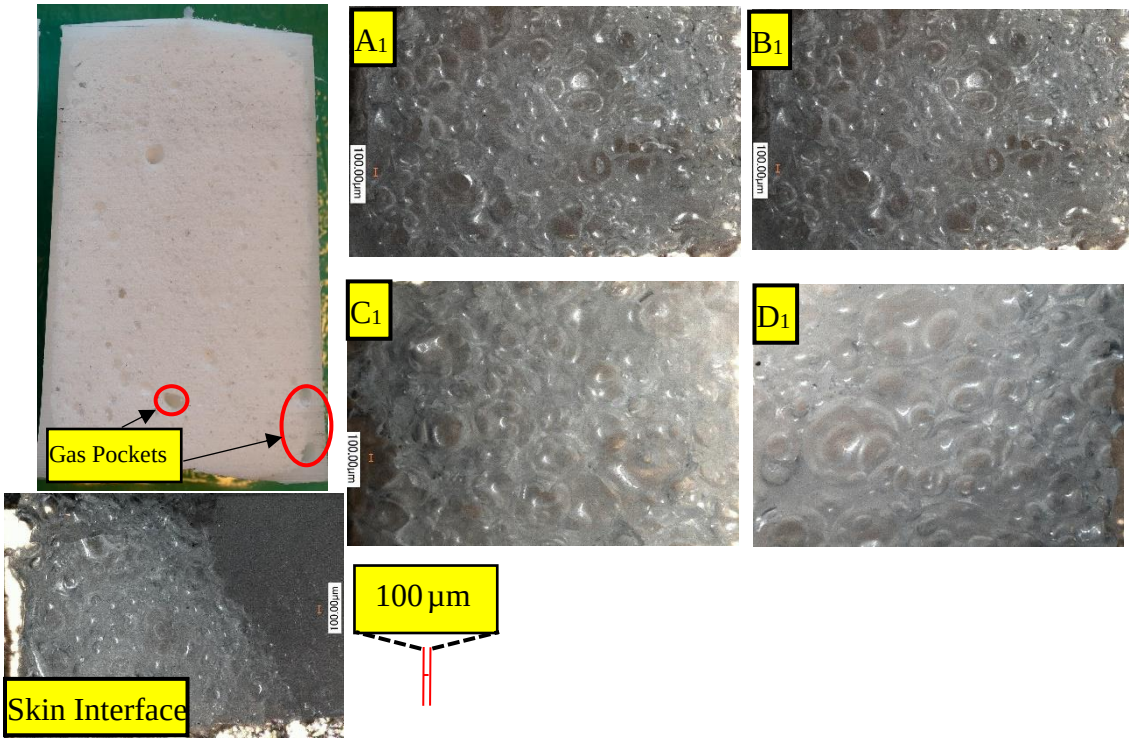

Figure 5.31: LA-0522 foamed core processed at 135°C with Celogen OT™.

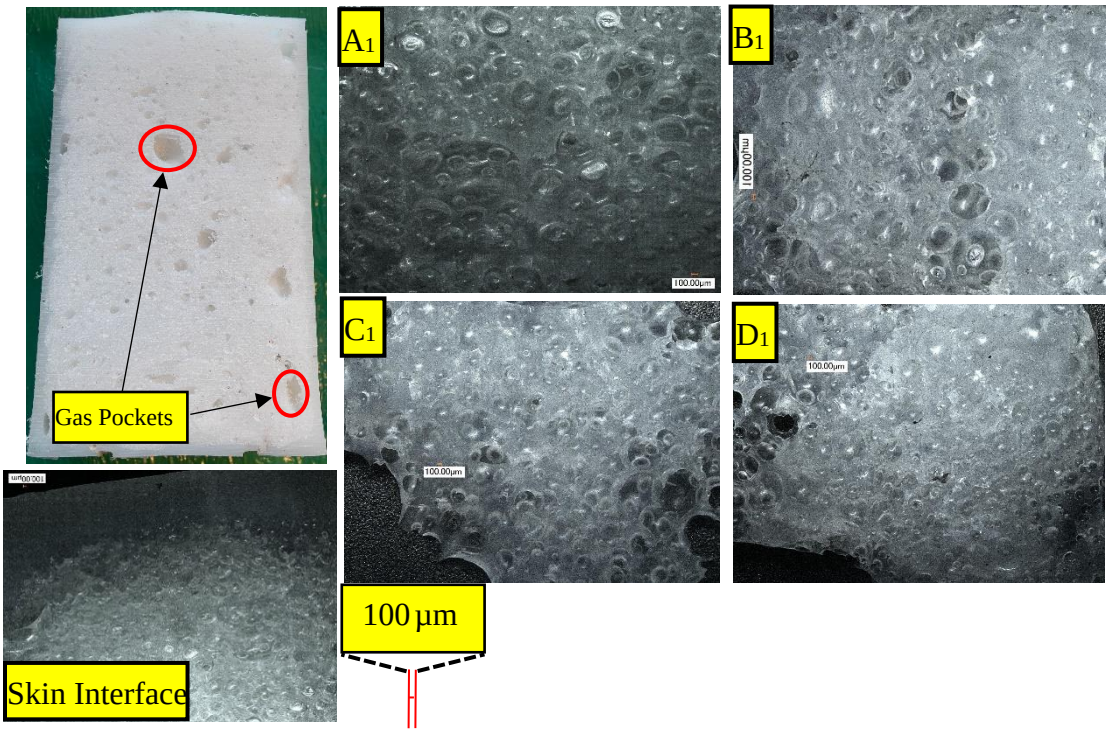

Figure 5.32: LA-0522 foamed core processed at 135°C with talc.

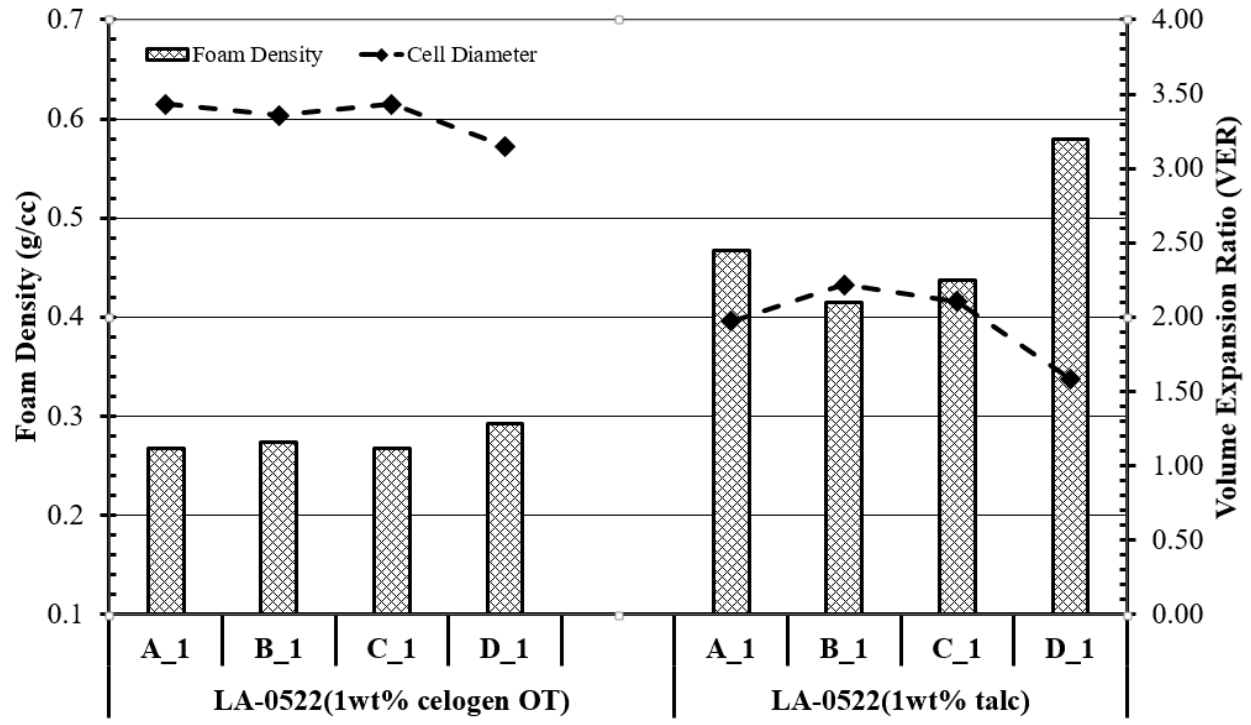

Figure 5.33: Foam density and volume expansion ratio of LDPE resin processed at 135°C in mixing zone 4.

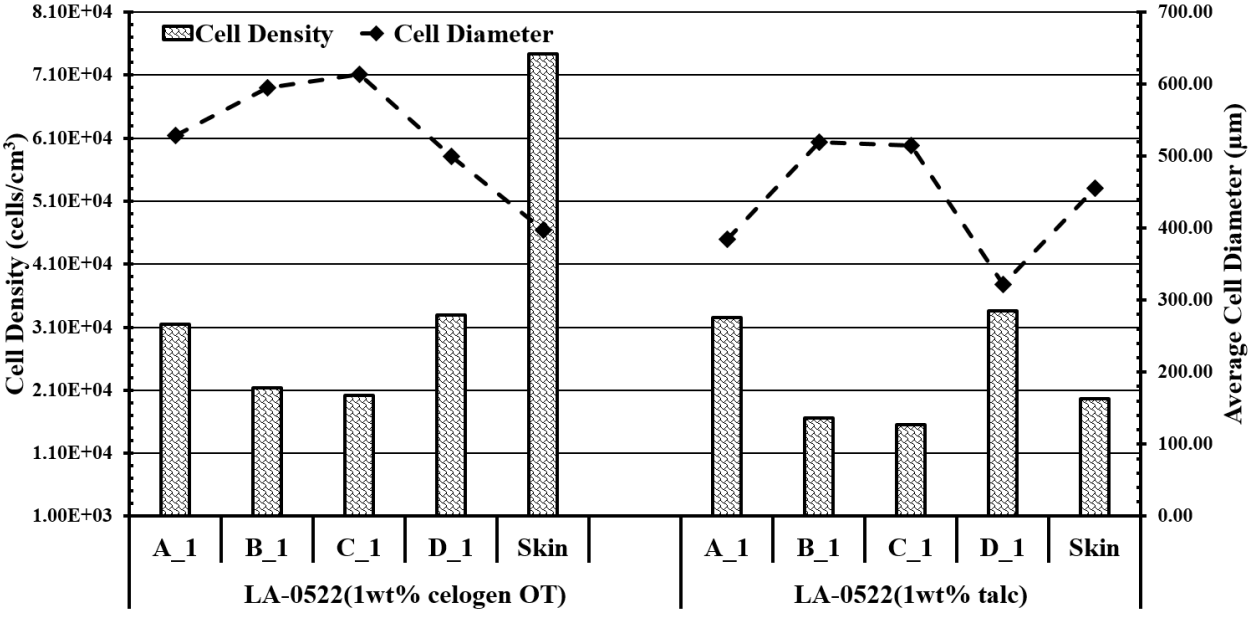

Figure 5.34: Cell density and average cell size of LDPE resin processed at 135°C in mixing zone4.

The foam density and VER is presented in Figure 5.33 for the two LDPE samples. LDPE foamed core processed with 1wt% Celogen OT™ had lower foam density compared with LDPE foamed core processed with 1wt% talc. The decomposition of CBA particles released additional gas to increase the volume expansion ratio greater than 3. By comparison the VER of talc containing foam did not exceed 2.2. The foam density was relatively constant for LDPE foamed core processed with CBA. In contrast, the foamed core processed with talc decreased toward Region B_1 and C_1 and later it increased at D_1 to a maximum value of 0.58 g/cc.

The cell density and average cell size for the foamed core is presented in Figure 5.34. For the talc containing sample the cell density gradually decreased from 3.15 X 10^4 cells/cm^3 at A_1 to 2.02 X 10^4 cells/cm^3 at C_1, however the cell density increased once more at position D_1 to 3.29 X 10^4 cells/cm^3. The cell density at the skin interface was higher due to faster cooling. The foamed core processed with 1wt% talc also had gradual decrease in cell density from 3.25 X 10^4 cells/cm^3 at A_1 to 1.55 X 10^4 cells/cm^3 at C_1 the cell density than increases at D_1 to a value of 3.35 X 10^4. The average cell size reached its peak at position C_1 for CBA containing sample. However, compared with the talc containing sample the average cell size is larger for CBA processed sample at a given region of interest. The smallest cell size was 514 μm, obtained at position C_1 in the talc containing foamed core.

5.5.2 *Processing by Gradual Modification of Nucleating Agent & Blowing Agent*

5.5.2.1 Foam Processing with RMS-245UG Resin Powder

In this section, the RMS-245UG resin was utilized to produce the foamed core at three different processing temperatures while maintaining constant injection rate. To gradually vary the composition of the foamed core, the nucleating agent content within the resin was modified during the foam extrusion process.

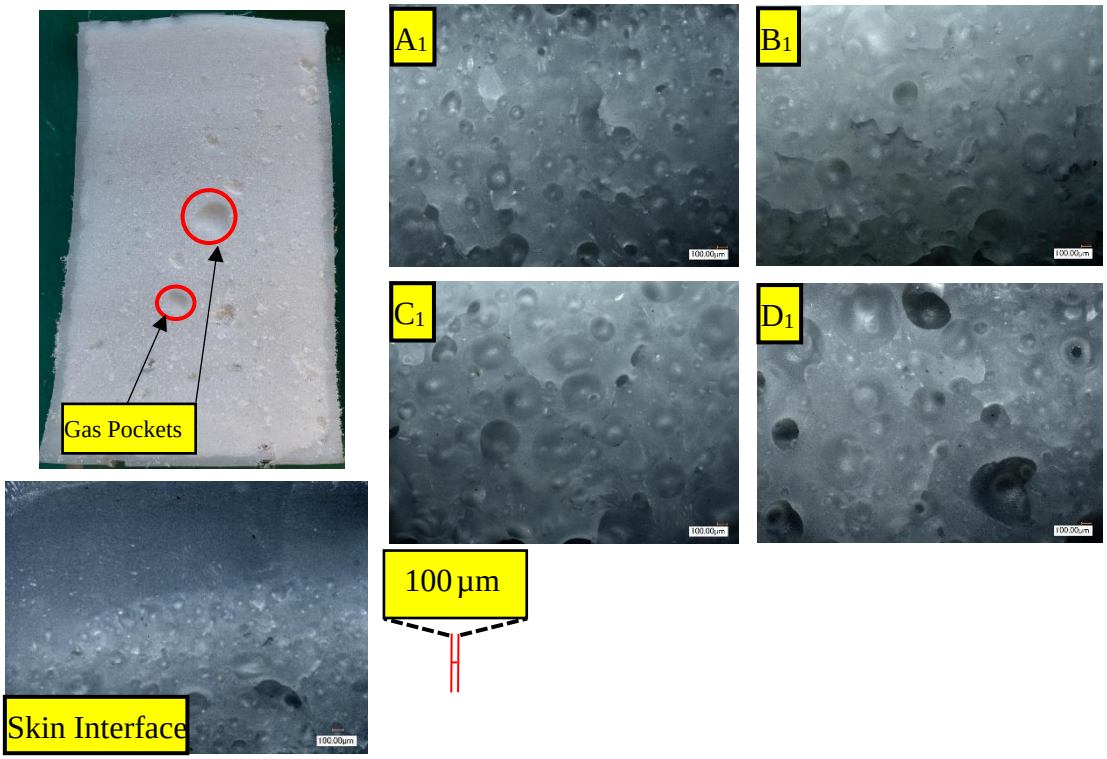

Figure 5.35: RMS-245UG foamed core processed at 160°C with talc at 1 ml/min gas injection rate.

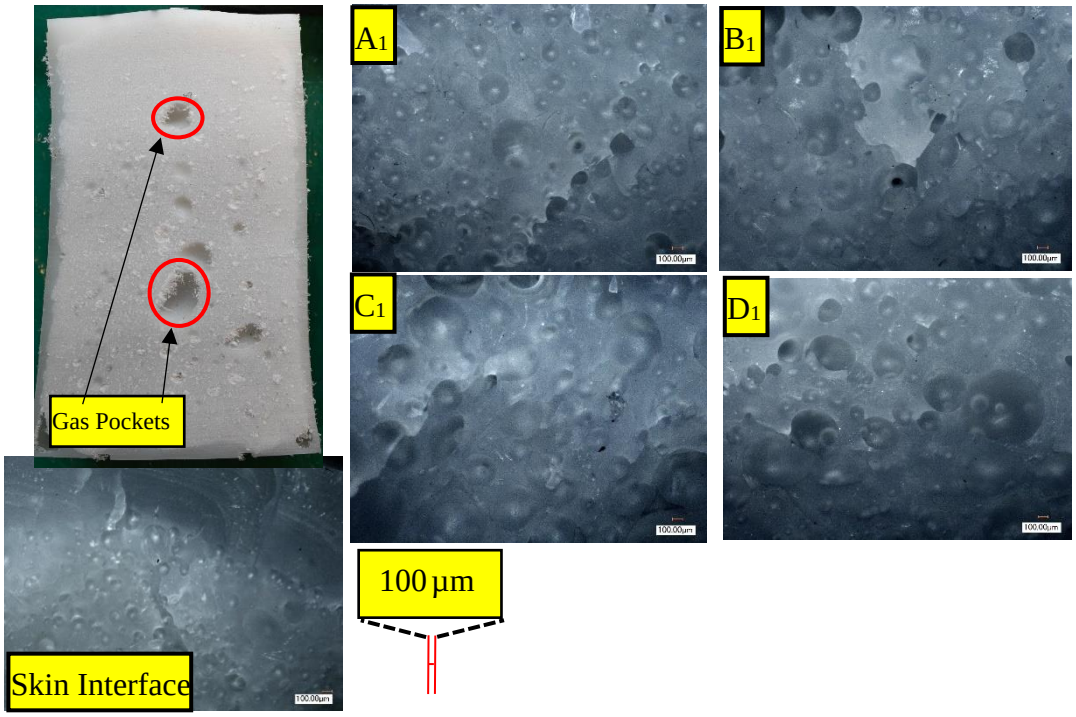

Figure 5.36: RMS-245UG foamed core processed at 170°C with talc at 1 ml/min gas injection rate.

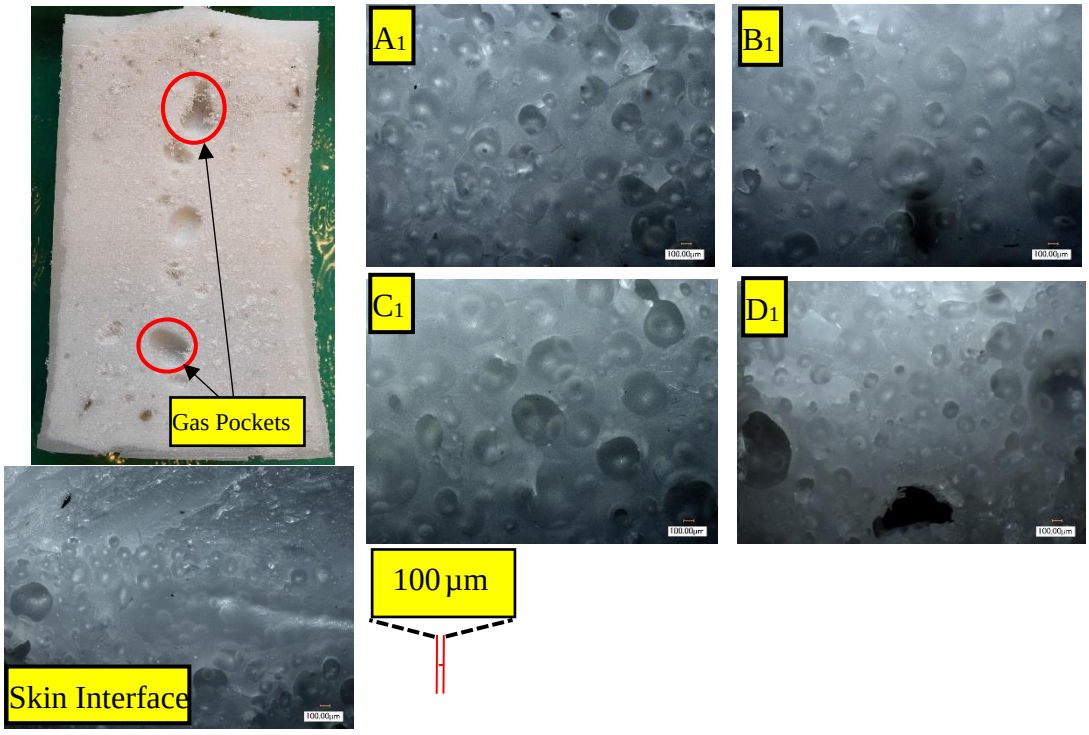

Figure 5.37: RMS-245UG foamed core processed at 180°C with talc at 1 ml/min gas injection rate.

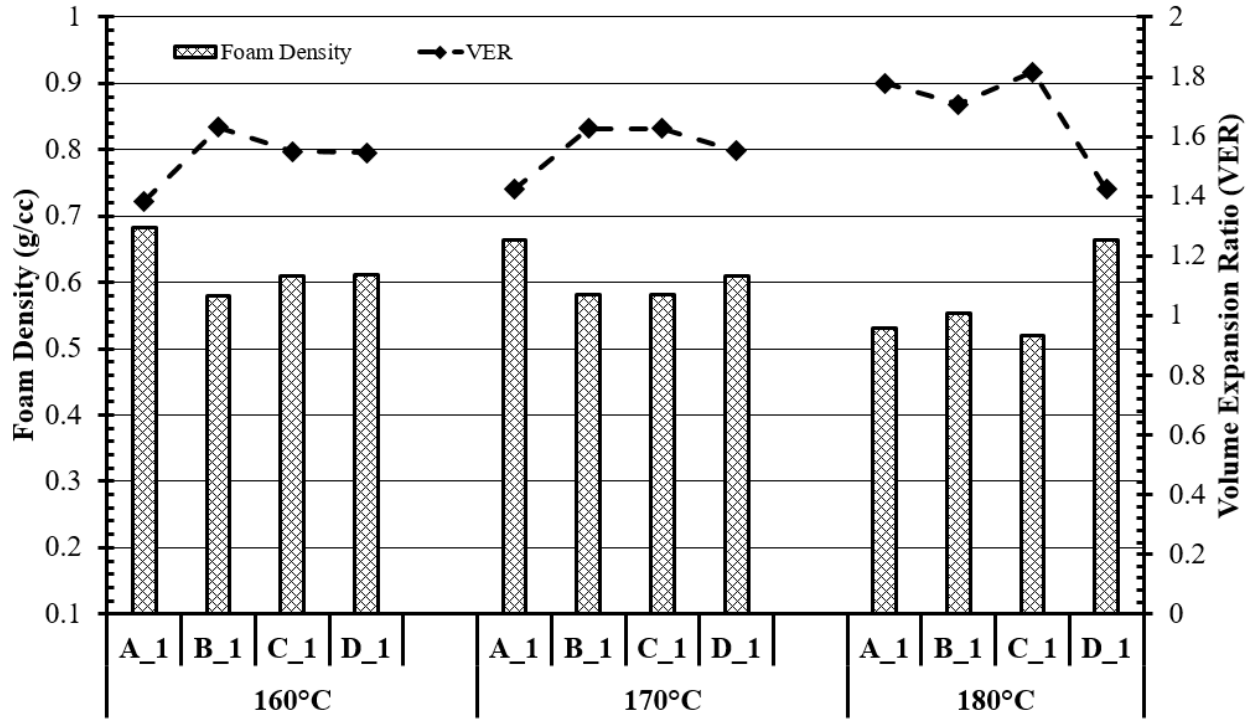

Figure 5.38: Foam density and volume expansion ratio of RMS-245UG resin produced with 1ml/min gas injection rate.

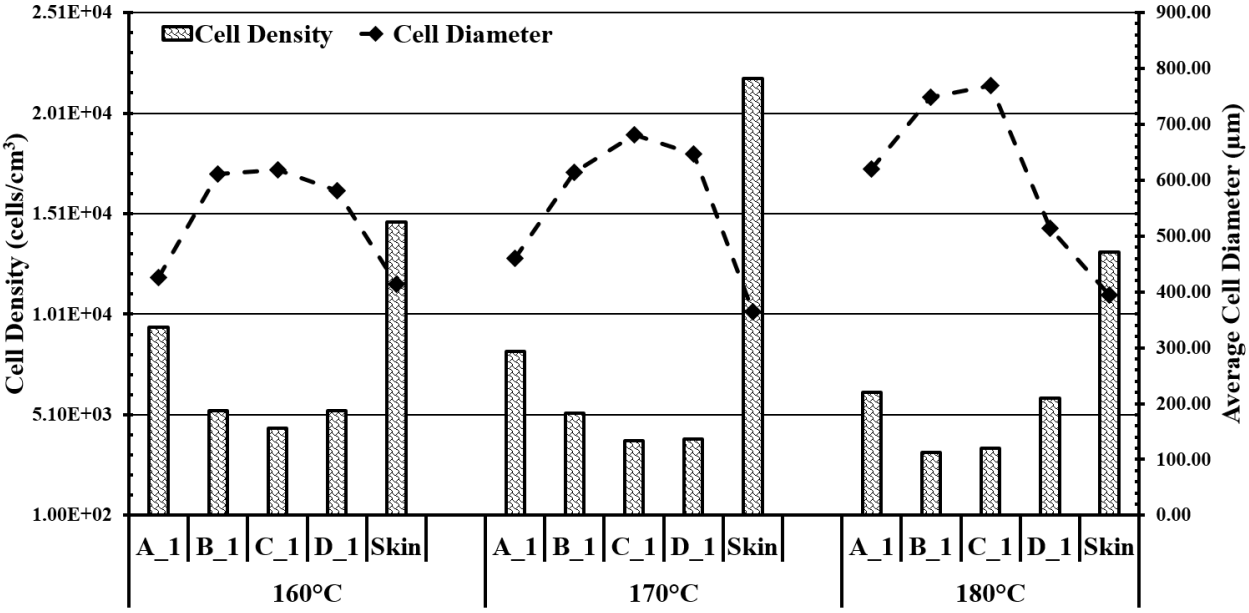

Figure 5.39: Cell density and cell size of RMS-245UG resin produced with 1ml/min gas injection rate.

The cross-sections of the foamed cores presented in Figures 5.35-5.37 were processed at 1 ml/min gas injection rate. From the images it can be observed that at higher processing temperature the gas pockets are more prominent and larger toward the center of the core. The higher processing temperatures, increase the rate of gas diffusion out of the polymer melt leading to larger voids. Also, specimen processed at higher temperatures require longer cooling time allowing the gas pockets to grow before the resin recrystallizes. All three specimen types processed with 1 ml/min gas injection rate demonstrated bubble penetration into skin layer without any gaps.

The VER and foam density of the foamed cores processed at 1 ml/min gas injection rate is presented in Figure 5.38. The foamed cores did not display a gradual change in foam density, rather the foam density was relatively stable at position B_1 to D_1 for foam processed 160°C and 170°C. For foamed core processed at 170°C the foam density remained relatively unchanged from A_1 to C_1, and then it increased to a higher value at position D_1. By increasing the processing temperature of the resin, the expansion ratio of the foam increased. However, this was probably due to the presence of greater quantities of gas pockets resulting from the higher processing temperature. As this was confirmed when observing the cell densities of the samples in Figure 5.39. Where the foamed core processed at higher processing temperature displayed lower cell density and higher average cell size.

The cell density of all foamed core produced with 1 ml/min decreased from position A_1 and reached a minimum value at C_1 before increasing at Position D_1. The average cell size peaked at position C_1 where the cell density was observed. As with cell density, the average cell diameter increased at higher processing temperatures.

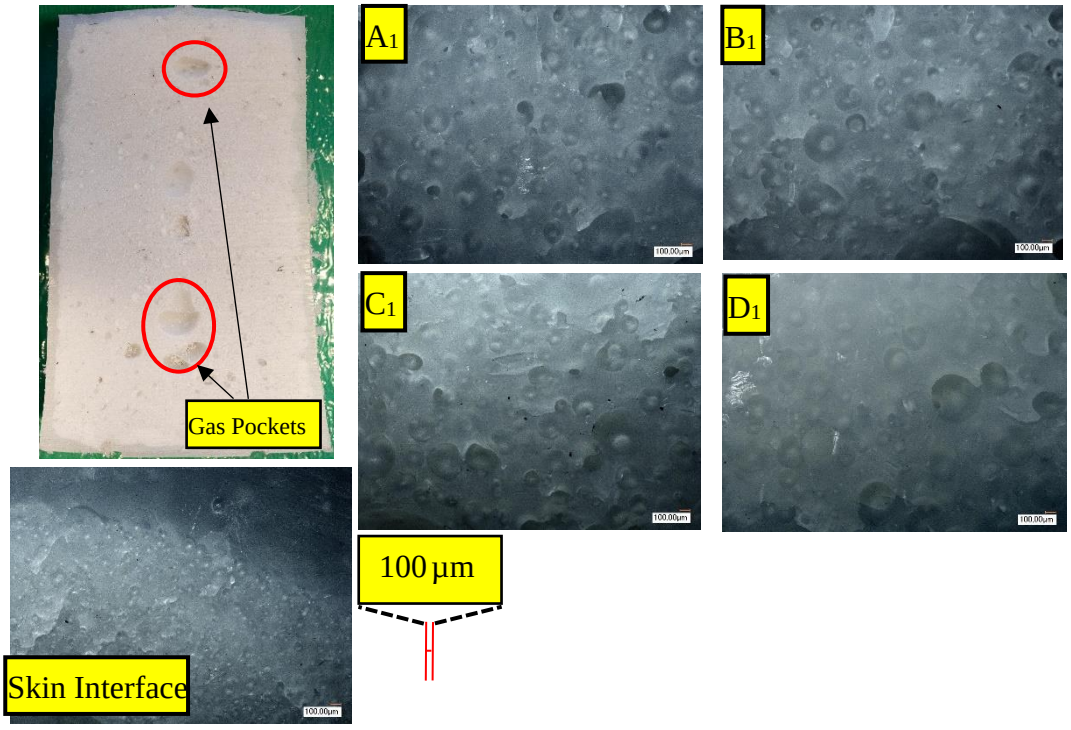

Figure 5.40: RMS-245UG foamed core processed at 160°C with talc at 0.25 ml/min gas injection rate.

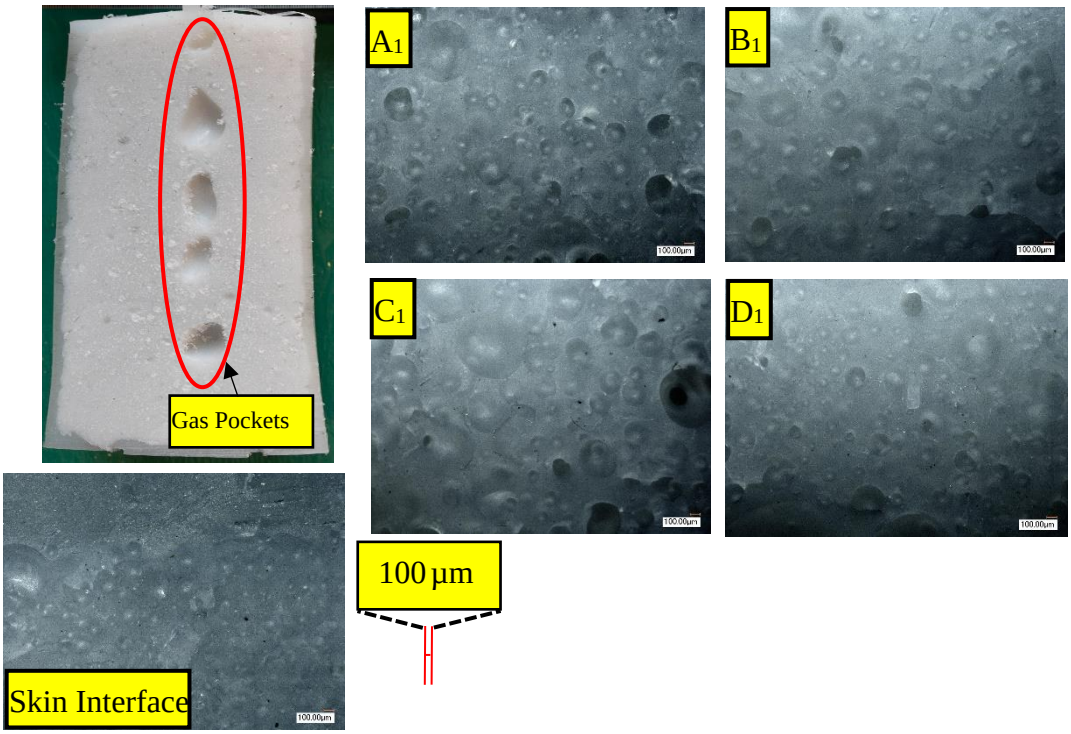

Figure 5.41: RMS-245UG foamed core processed at 170°C with talc at 0.25 ml/min gas injection rate.

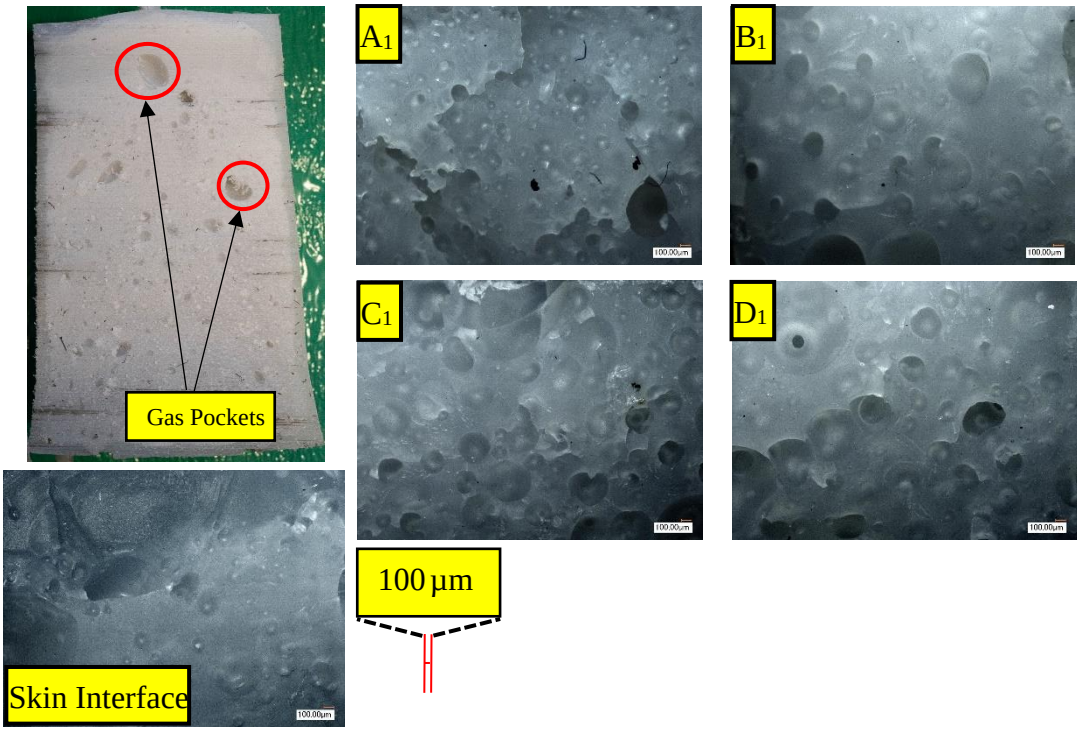

Figure 5.42: RMS-245UG foamed core processed at 180°C with talc at 0.25 ml/min gas injection rate.

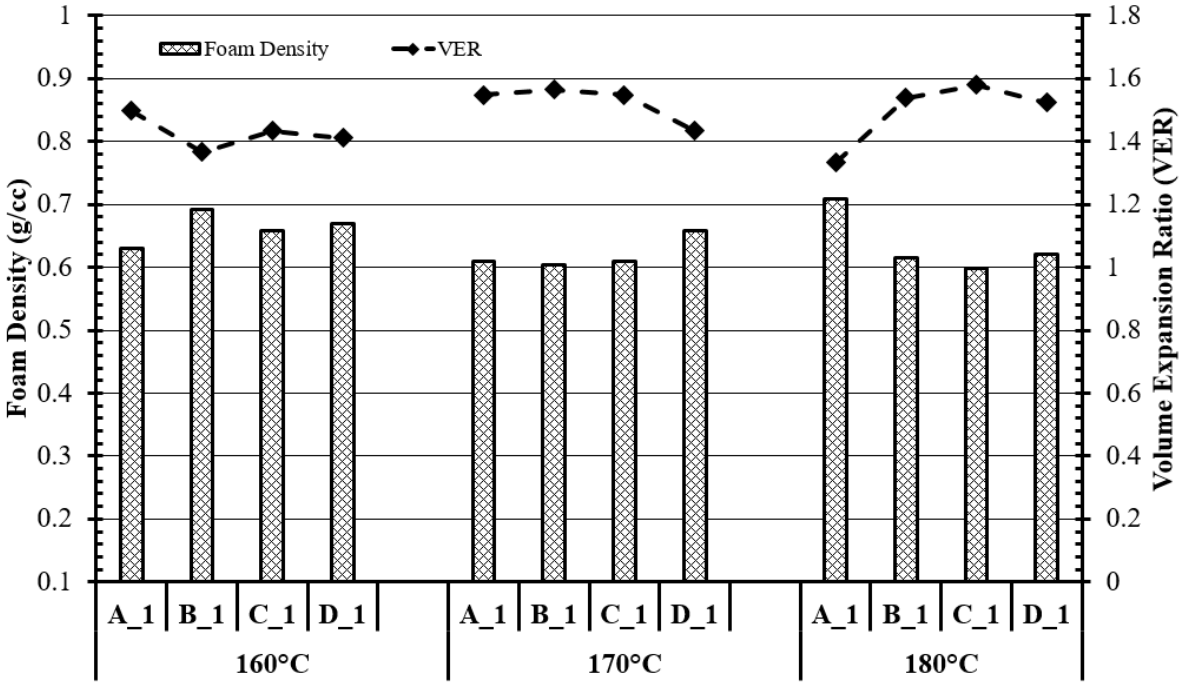

Figure 5.43: Foam density and volume expansion ratio of RMS-245UG resin produced with 0.25 ml/min gas injection rate.

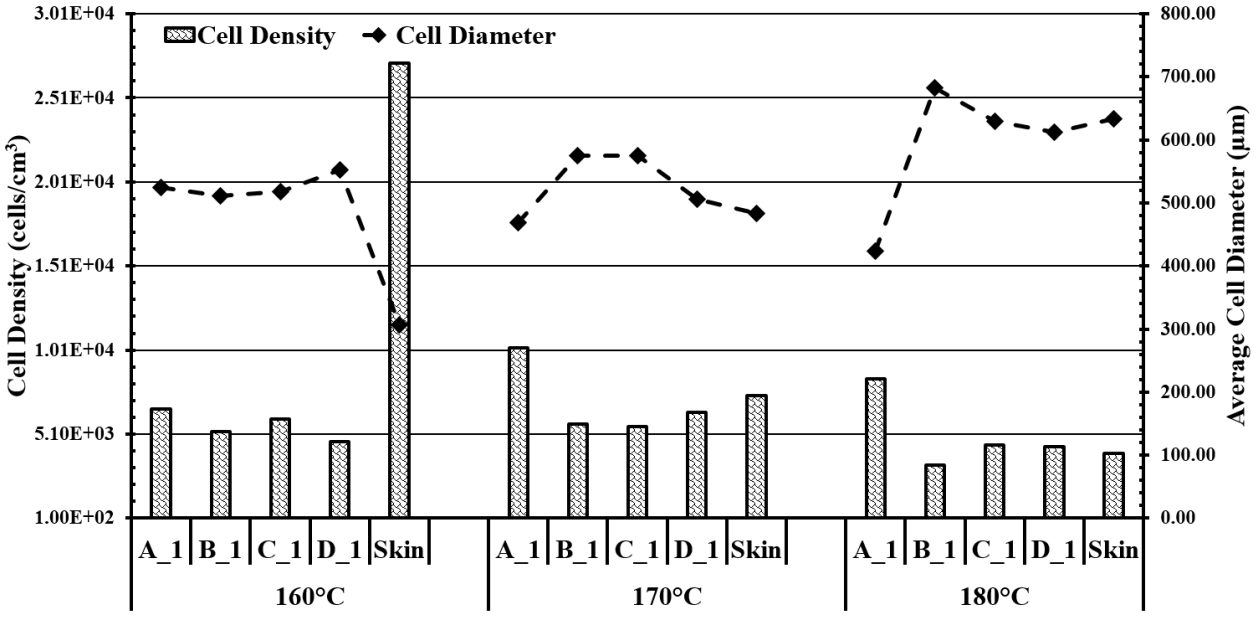

Figure 5.44: Cell density and cell size of RMS-245UG resin produced with 0.25 ml/min gas injection rate.

The foamed cores produced at 0.25 ml/min gas injection rate are presented in Figure 5.40-5.42. The gas injection rate was reduced to its minimum possible value to ensure complete dissolution of supercritical gas into the polymer melt. However, even at this lowest possible gas injection rate, complete dissolution of gas into the polymer melt was not achieved. Numerous gas pockets were observed at all locations of the foamed core for all three processing temperatures. Larger pockets were observed toward the center of the foamed cores. From the skin interface images, bubble penetration into the skin layer was observed for all three foamed cores produced with 0.25 ml/min gas injection rate. There were no differences observed between the foam bonding with the outer skin at 1 ml/min gas injection rate and 0.25 ml/min injection rate.

The foam density and the VER of the foam produced with 0.25 ml/min gas injection rate is presented in Figure 5.43. A gradual change in foam density was not observed for the foamed core. However, the volume expansion ratio was slightly higher at 170° and 180°C. In contrast the cell density and average cell size presented in Figure 5.44 also did not reveal a significant change in composition from one region of interest to another. However, the overall the cell density decreased at higher processing temperature which corresponded with higher average cell size as well.

When comparing the foamed cores of two different gas injection rate. The cell density was observed to be higher at position A_1 for foam being processed at 160°C and 170°C with 1 ml/min gas injection rate. However, higher cell density was observed at the skin interface for foam produced with 0.25 ml/min at 160°C. Otherwise the cell density was higher at the skin interface for foam processing temperature of 170°C and 180°C under 1 ml/min gas injection rate. In position B_1, the cell density did not vary significantly under all processing temperatures and gas injection rate. In contrast the cell density was observed to be higher at position C_1 for gas injection rate of 0.25 ml/min compared to 1 ml/min. In position D_1, the cell density is higher for gas injection rate of 1 ml/min at 160°C and 180°C.

5.5.2.2 Foam Processing with RMS-341UG Resin Powder

In this section a similar attempt to vary the foamed core was done by gradually increasing the nucleating agent content within the resin as it is being extruded. Similar to the previous section, the foamed cores were produced at two different gas injection rates. The first set of foamed cores were produced with RMS-341UG resin powder at 1 ml/min gas injection rate and talc as the nucleating agent.

From the images presented in Figure 5.45-5.47, gas pockets were observed throughout the foam. However, these pockets increased in size at higher processing temperature. The skin interface of all the three foamed core types produced with 1 ml/min gas injection rate demonstrated bubble penetration into the skin layer, which is an indicator of acceptable bonding with the outer skin.

The foam density and the volume expansion ratio is presented in Figure 5.48 for foamed core produced with 1 ml/min gas injection rate. From the Figure, the foamed core produced at 160°C revealed a decrease in foam density from position A_1 to C_1 and it increased at position D_1. Similar pattern of decrease in foam density is observed at 170°C. However, at 180°C the foam density remains relatively constant. The VER increased at 170°C, In contrast the VER did not fluctuate greatly for foamed core produced at 180°C.

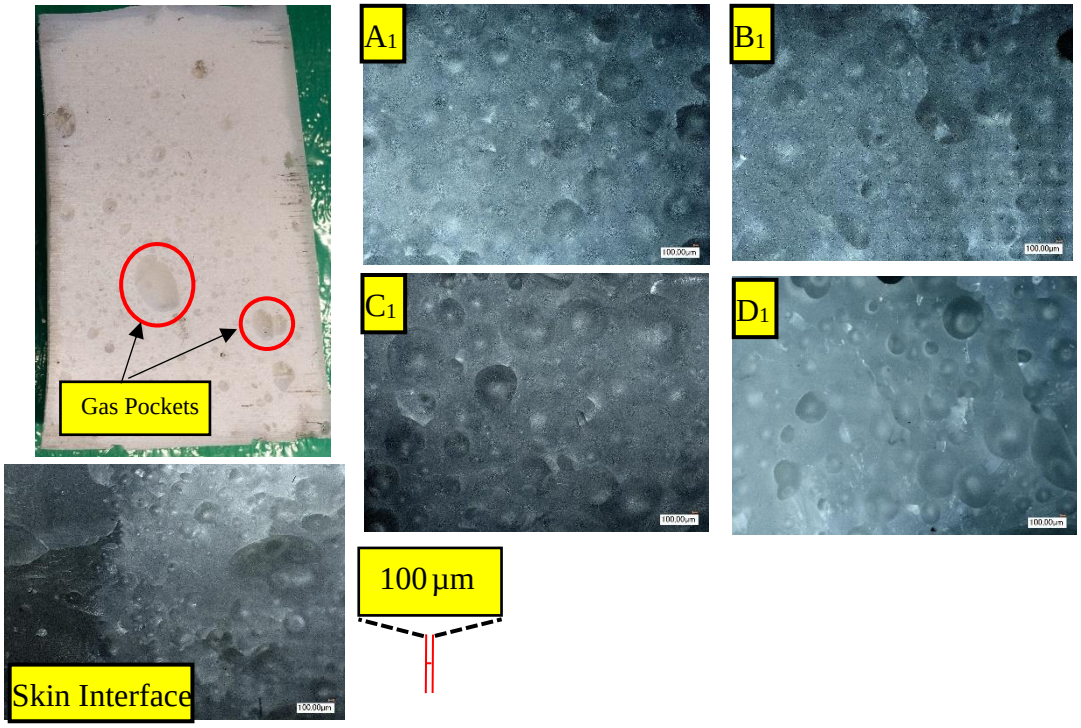

Figure 5.45: RMS-341UG foamed core processed at 160°C with talc at 1 ml/min gas injection rate.

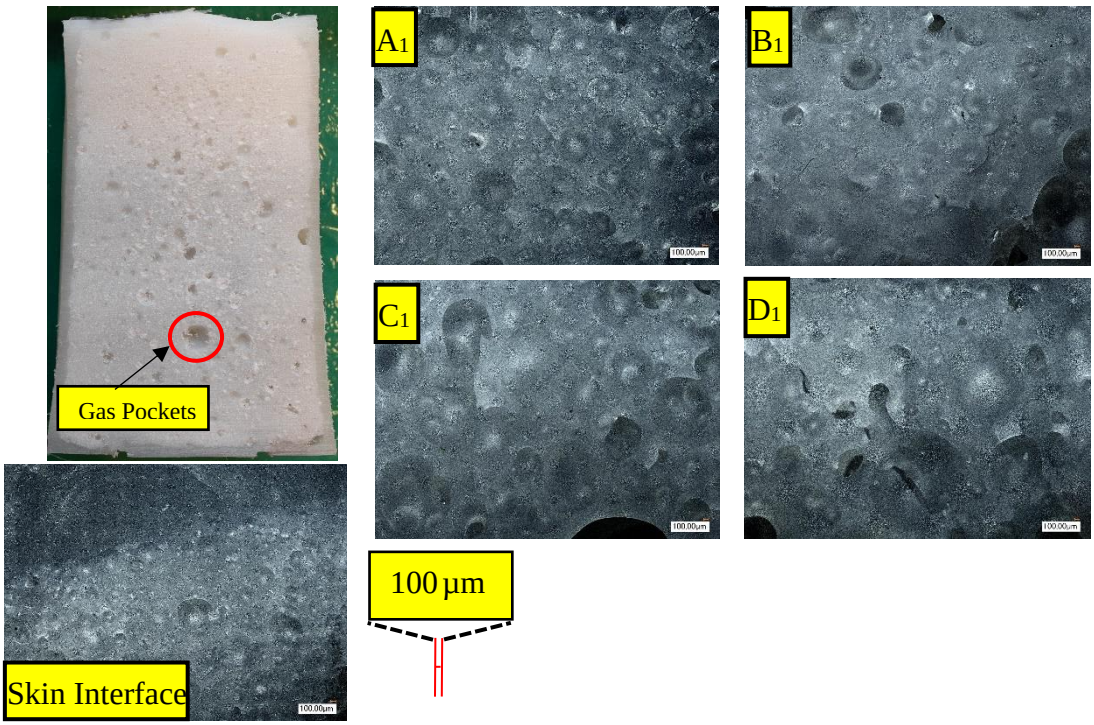

Figure 5.46: RMS-341UG foamed core processed at 170°C with talc at 1 ml/min gas injection rate.

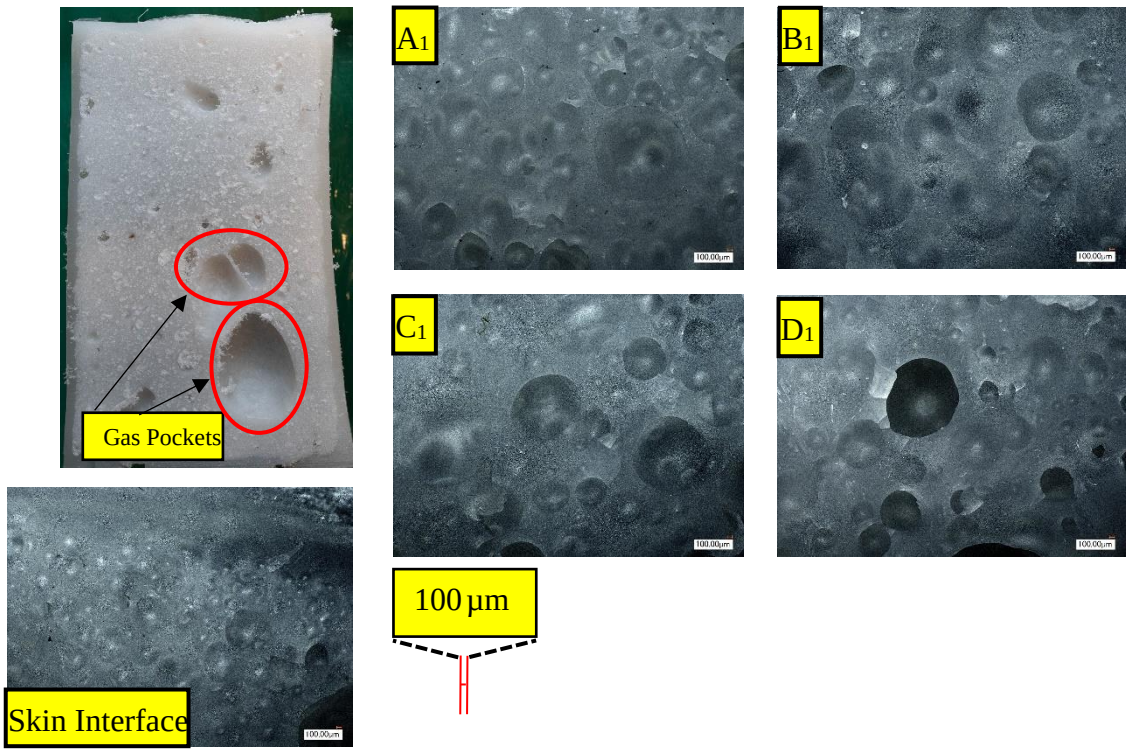

Figure 5.47: RMS-341UG foamed core processed at 180°C with talc at 1 ml/min gas injection rate.

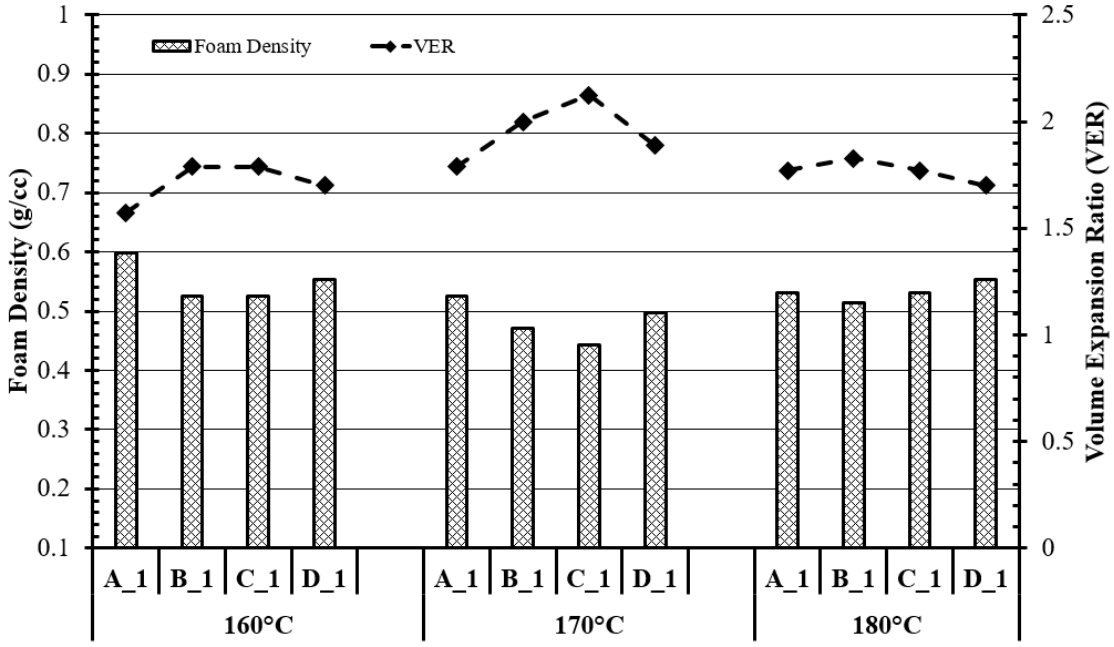

Figure 5.48: Foam density and volume expansion ratio of RMS-341UG resin produced with 1 ml/min gas injection rate.

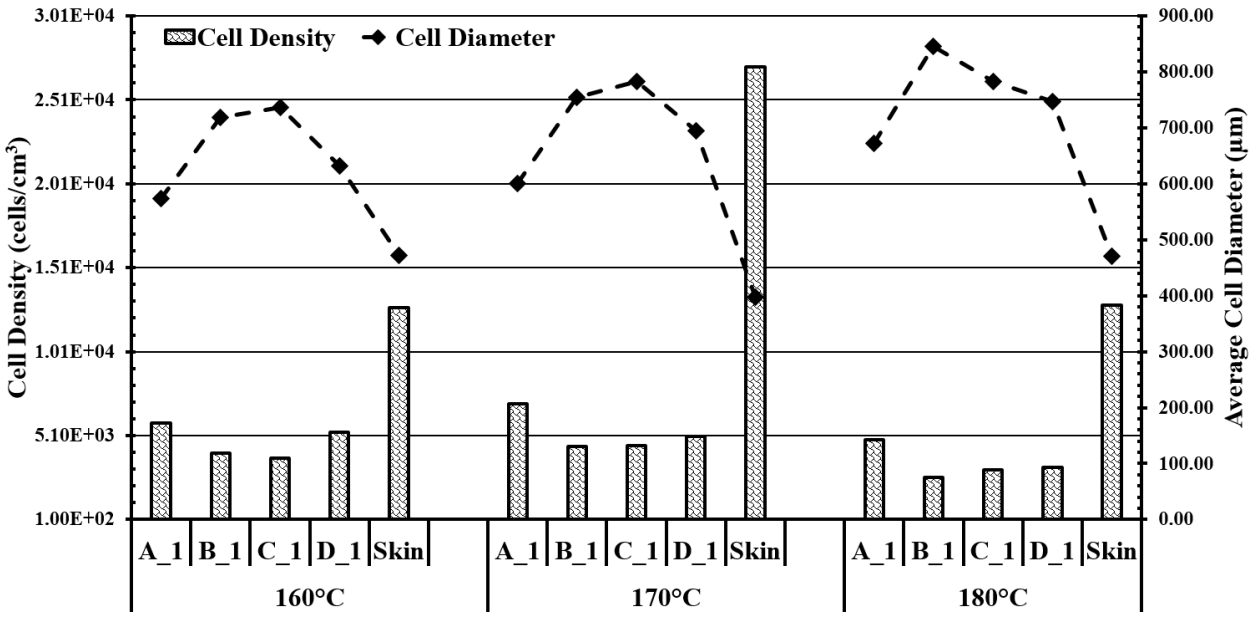

Figure 5.49: Cell density and cell size of RMS-341UG resin produced with 1 ml/min gas injection rate.

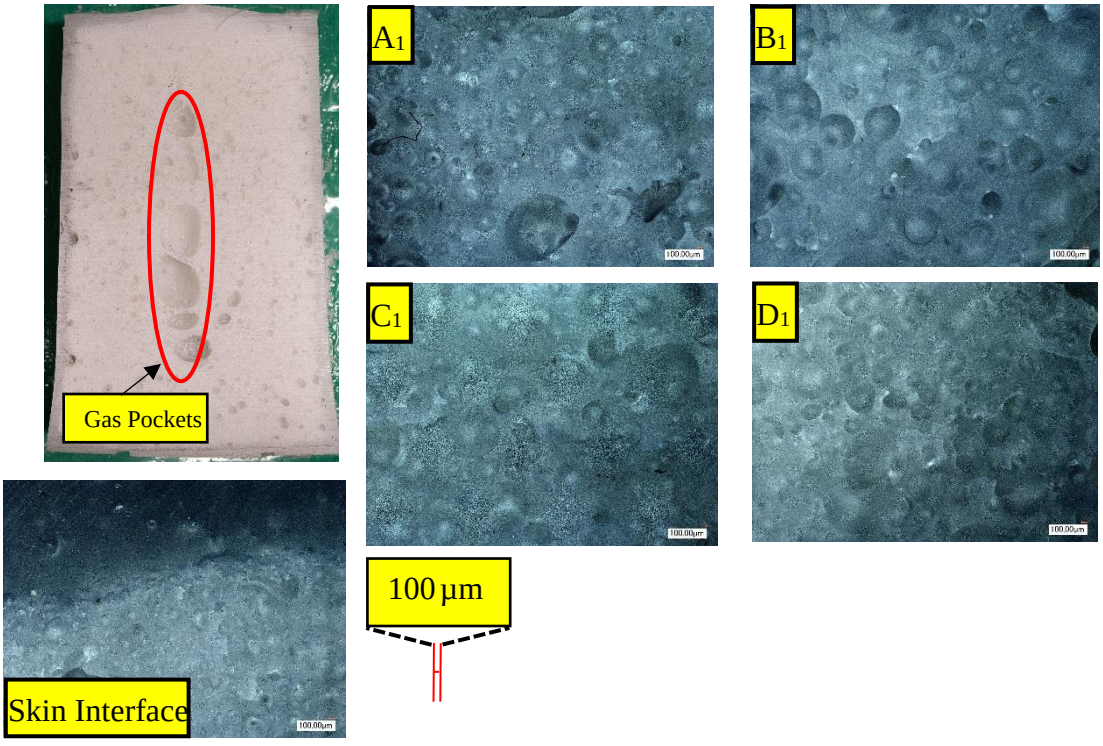

Figure 5.50: RMS-341UG foamed core processed at 160°C with talc at 0.25 ml/min gas injection rate.

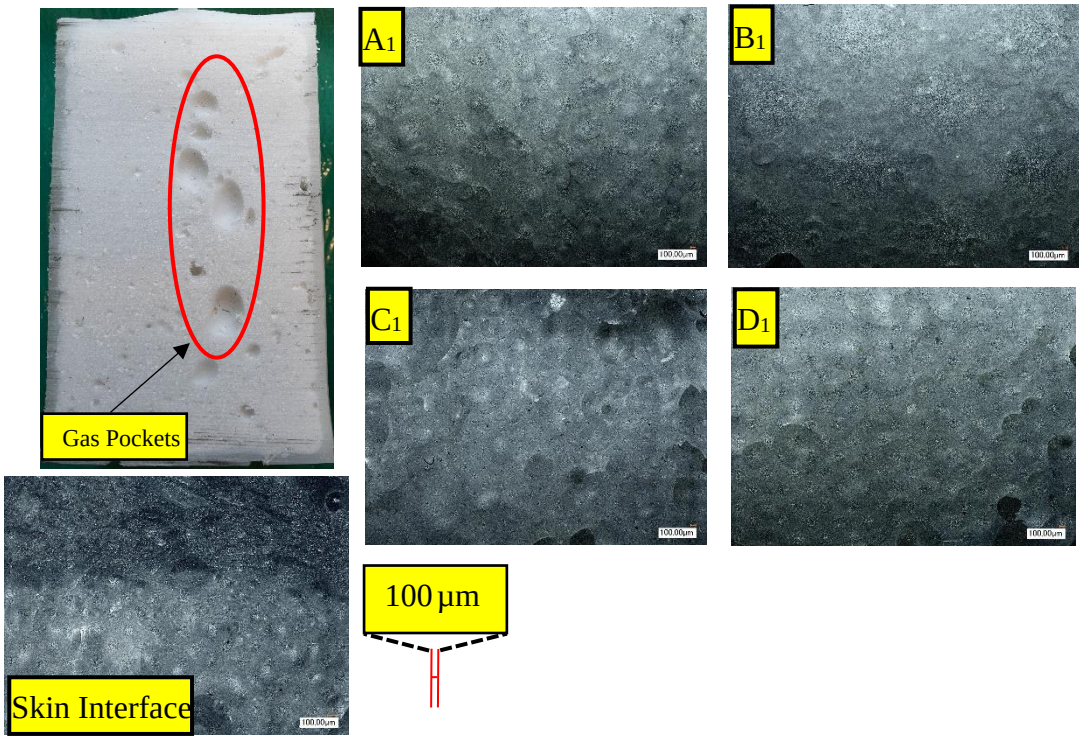

Figure 5.51: RMS-341UG foamed core processed at 170°C with talc at 0.25 ml/min gas injection rate.

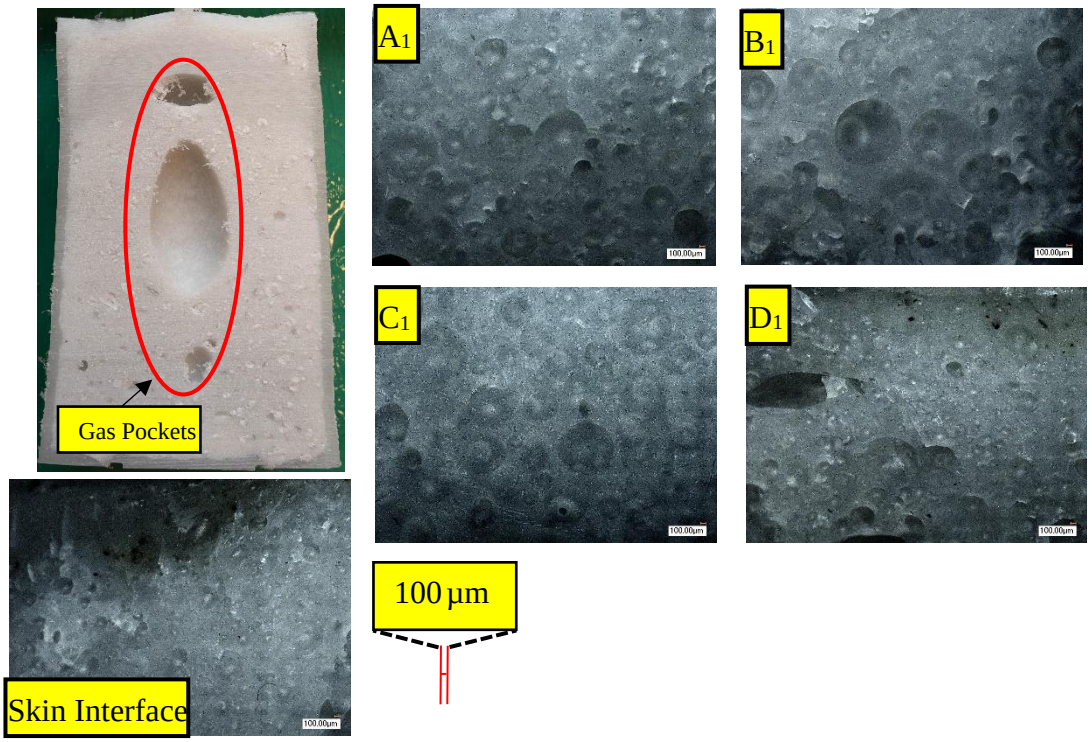

Figure 5.52: RMS-341UG foamed core processed at 180°C with talc at 0.25 ml/min gas injection rate.

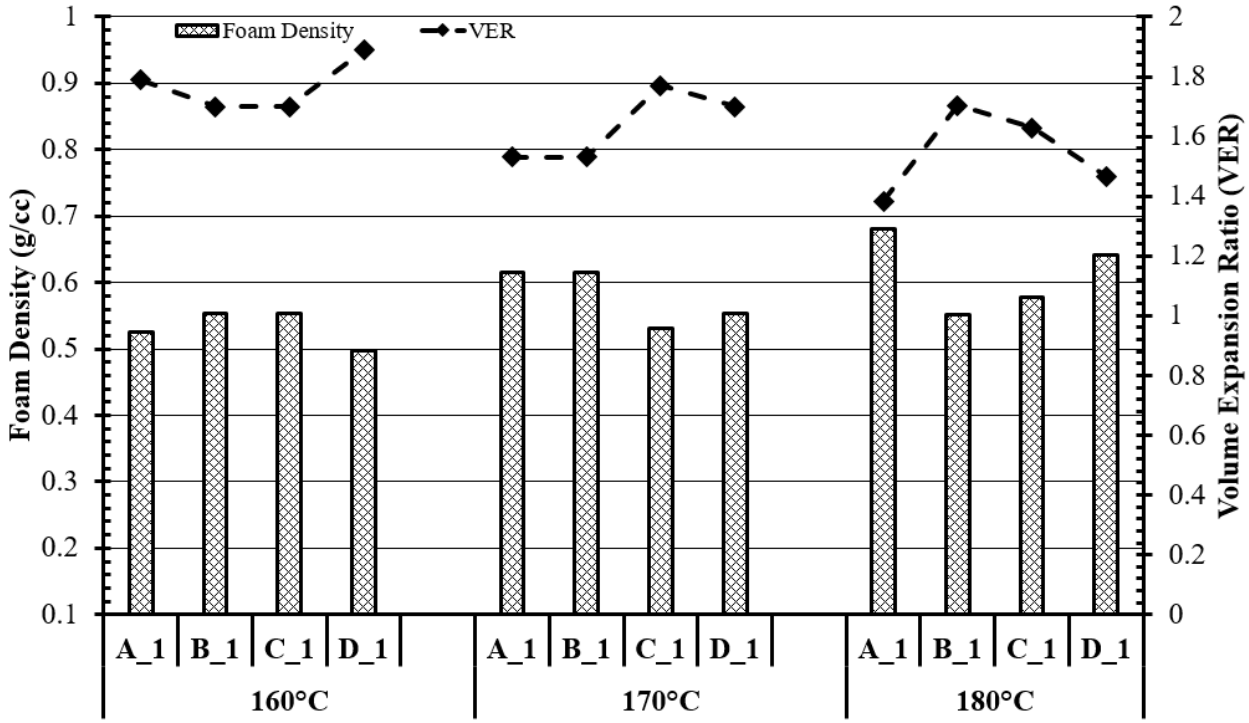

Figure 5.53: Foam density and volume expansion ratio of RMS-341UG resin produced with 0.25 ml/min gas injection rate.

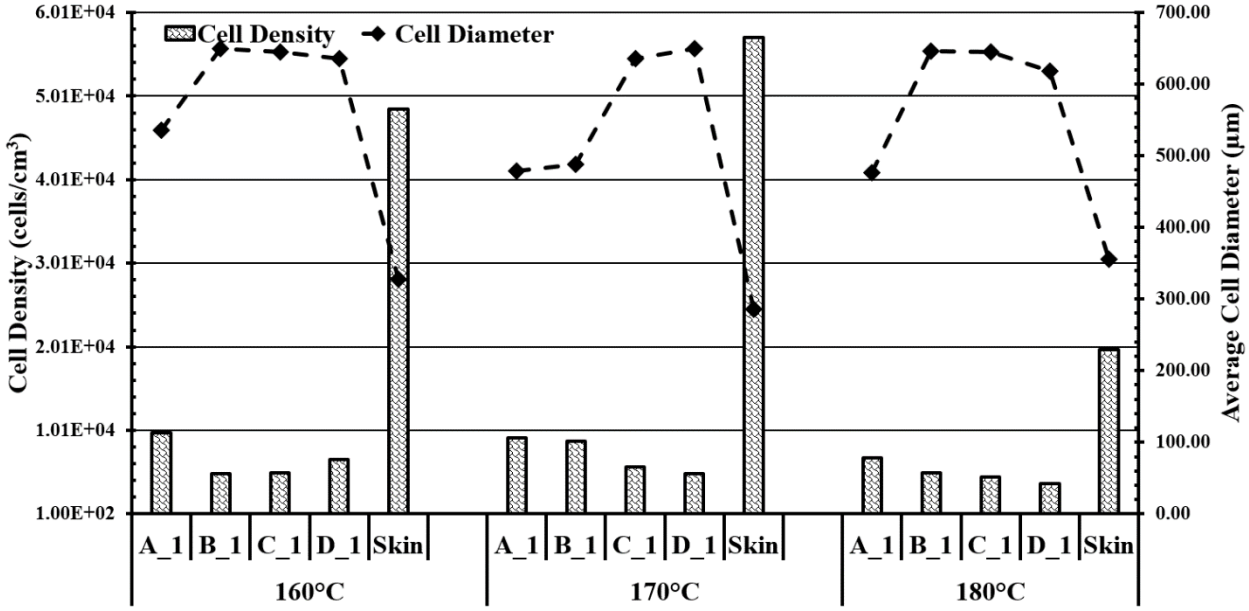

Figure 5.54: Cell density and cell size of RMS-341UG resin produced with 0.25 ml/min gas injection rate.

The cell density and he average cell size is presented in Figure 5.49 for foamed core produced with 1 ml/min gas injection rate. The cell density decreased from position A_1 to C_1 and it increased again at D_1 and the highest cell density was observed at the skin interface where cooling rate is faster. A similar pattern was observed for cell density at 170°C and at 180°C. However, at higher processing temperature overall cell density decreased and the average cell size increased. For instance, the average cell size reached its highest value at position B_1 for 180°C processing temperature.

The cross-section for the foamed core produced with 0.25 ml/min gas injection rate is presented in Figures 5.50-5.52. From the images it can be observed that gas pockets are prominent toward the center of the foam at the three processing temperatures. However, the largest gas pocket was observed at 180°C. The foamed cores demonstrated adequate bonding with the outer skin as bubble penetration into skin layer was observed at all processing temperature.

The foam density and VER for foamed core produced with 0.25 ml/min gas injection rate is presented in Figure 5.53. The foamed core processed at 160°C displayed a slight increase in foam density at position B_1 and C_1 and then the foam density decreased at position D_1. For foamed core processed at 170°C the foam density decreased after position B_1 and remained relatively unchanged up to position D_1. However, at 180°C the foamed core displayed a reduction in foam density from position A_1 to B_1 and the foam density gradually increased from B_1 to D_1. The overall VER decreased at higher processing temperature.

The cell density of the foamed core produced with 0.25 ml/min gas injection rate is presented in Figure 5.54. The cell density of the foamed core processed at 160°C initially decreased and then increased slightly from position B_1 to D_1. The cell density decreased gradually for foamed cores processed at 170°C and 180°C. The highest cell density was recorded at the skin interface for all the foam types. The average cell size of the foamed cores increased in size toward the center of the core and sharply reduced in size at the skin interface. However, a relationship between the cell size and processing temperature wasn't observed. The cell density of the foamed core produced with 0.25 ml/min exhibited lower cell density compared to the foamed cores produced with 1 ml/min gas injection rate.

5.5.2.3 Foam Processing with LA-0522 Resin

In this section the foamed core produced with LDPE resin is presented. The foamed cores have been processed with talc and elogen OT. Foams produced with 1 ml/min gas injection rate is presented in Figures 5.55-5.56. From the images of the cross-section, gas pockets are dispersed throughout foamed core, however unlike sHDPE resin, the gas pockets are smaller in size. The two types of foamed core exhibit foam bonding with the outer skin through bubble penetration into the skin layer.

The foam density and VER of the foamed core produced with 1 ml/min gas injection rate is presented in Figure 5.57. The foamed core processed with talc exhibited gradual decrease in density from position A_1 to C_1 and the density increased at position D_1. The corresponding VER increased as the foam density decreased from one region to another. In a similar fashion the foam density of Celogen OT™ processed foam exhibited a gradual decrease in density from position A_1 to C_1 and the density increased once more at position D_1. The corresponding VER also increased as the foam density decreased for the Celogen OT™ assisted foam. The foam density and VER for a given region of interest was higher for foamed core processed with talc. At it's the VER value was greater than 2.5 at position C_1 for Celogen OT™ assisted foam.

The cell density and the average cell size is presented in Figure 6.58. The cell density gradually decreased from 1.97 X 10^4 cells/cm^3 at position A_1 to 5.67 X 10^3 cells/cm^3 at C_1 and increased once more to 1.04 X 10^4 at position D_1. The cell density of the foamed core processed with Celogen OT™ increased from position A_1 to B_1. However, the cell density decreased at position C_1 and increased at position D_1. The cell density was observed to be higher for foam processed with Celogen OT™ and the average cell size was below 500 µm.

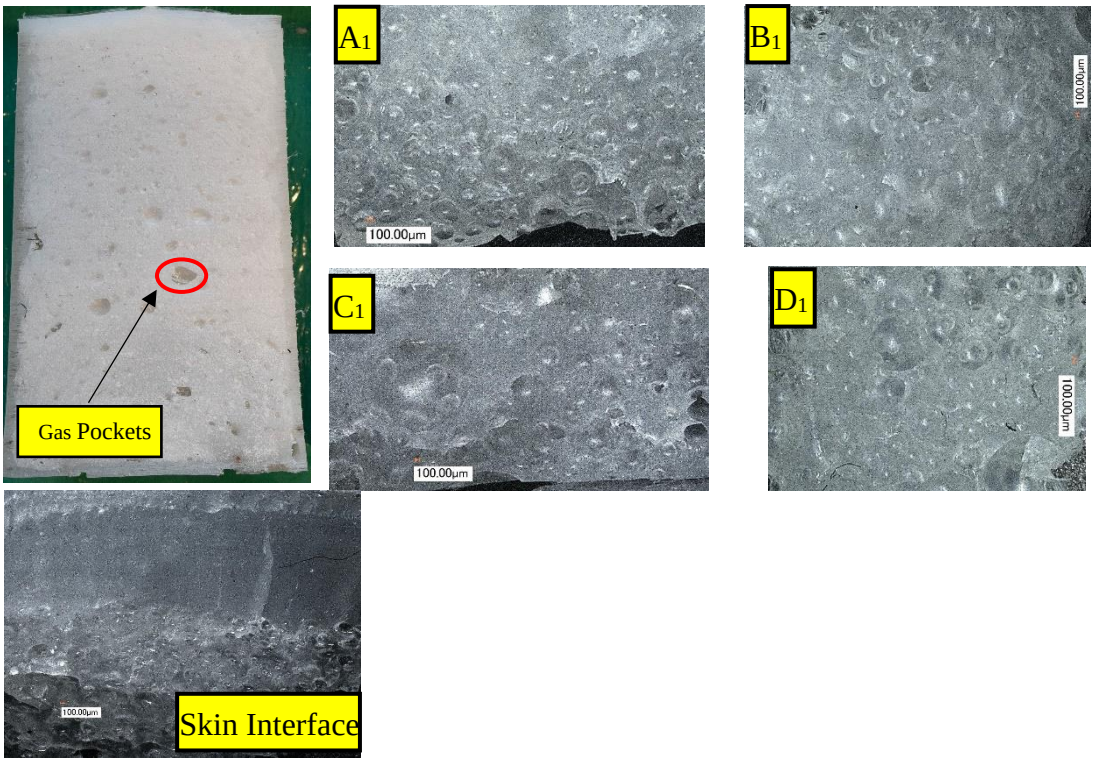

`Figure 5.55: LA-0522 foamed core processed at 135°C with talc at 1 ml/min gas feed rate.

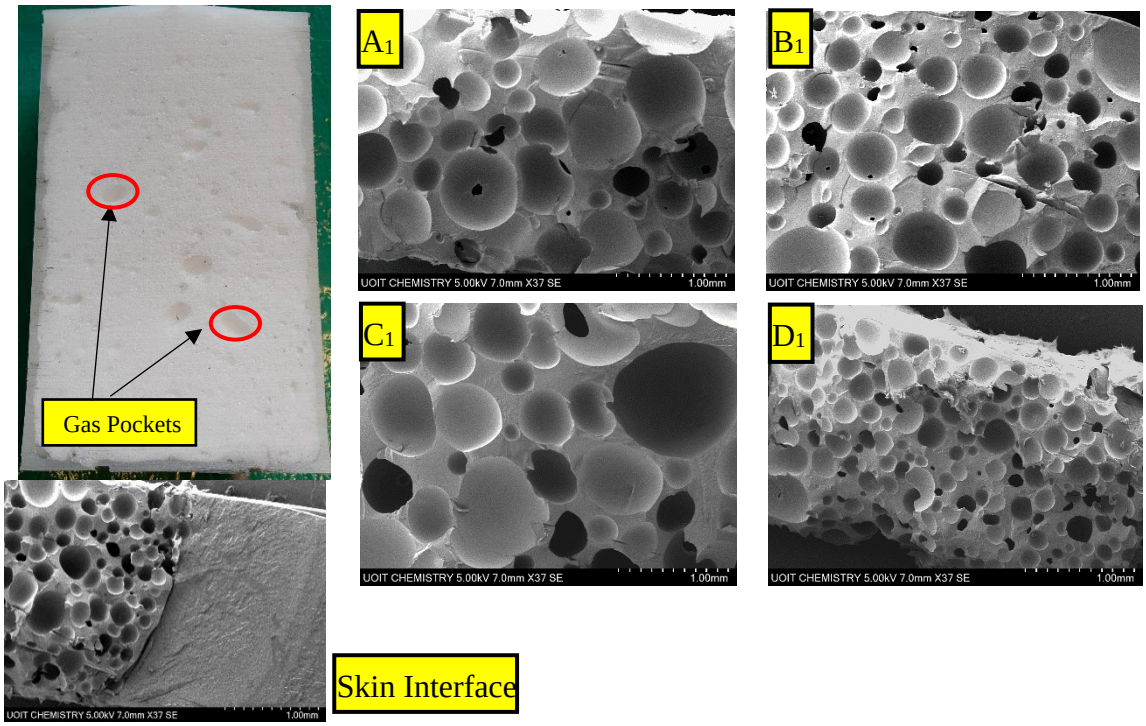

Figure 5.56: LA-0522 foamed core processed at 135°C with Celogen OT™ at 1 ml/min gas injection rate.

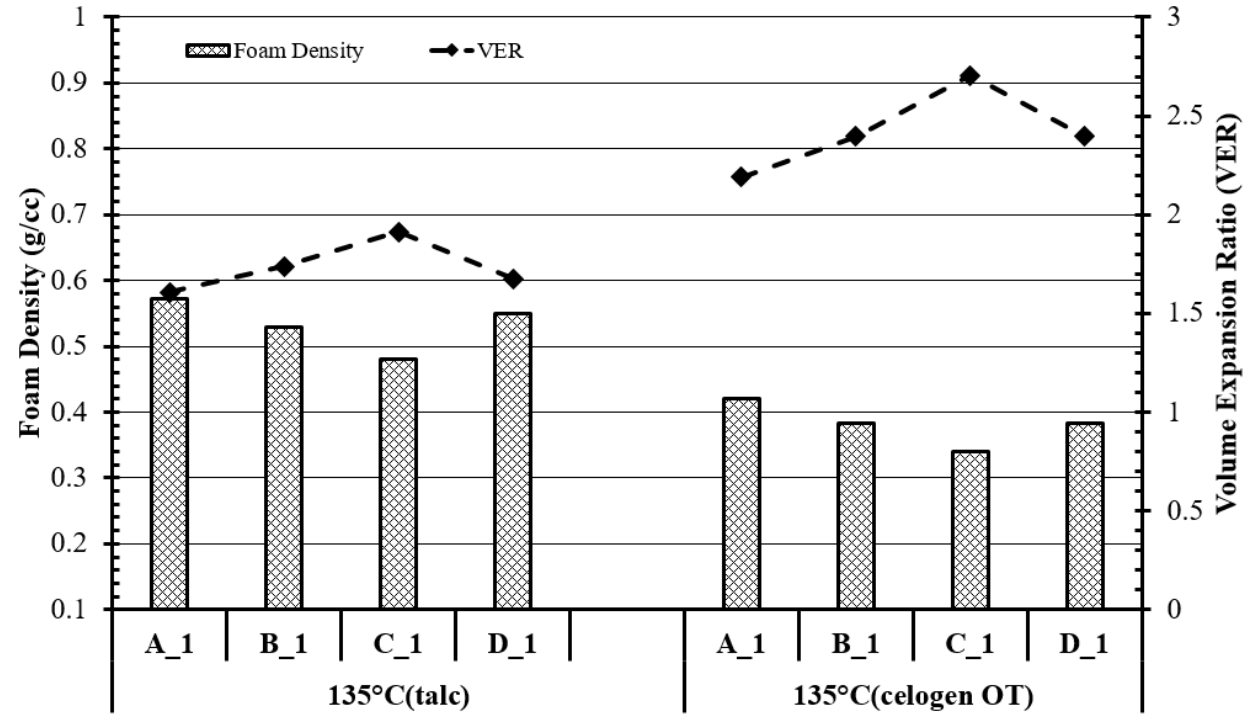

Figure 5.57: Foam density and volume expansion ratio of LA-0522 resin produced with 1 ml/min gas injection rate.

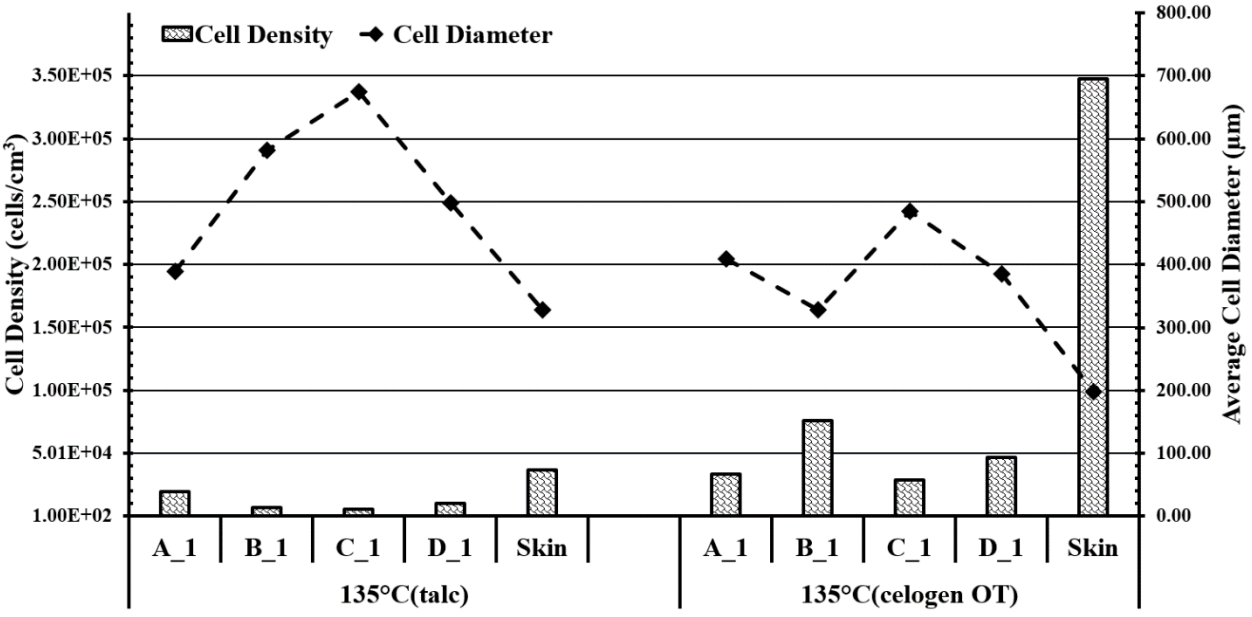

Figure 5.58: Cell density and cell size of LA-0522 resin produced with 1 ml/min gas injection rate.

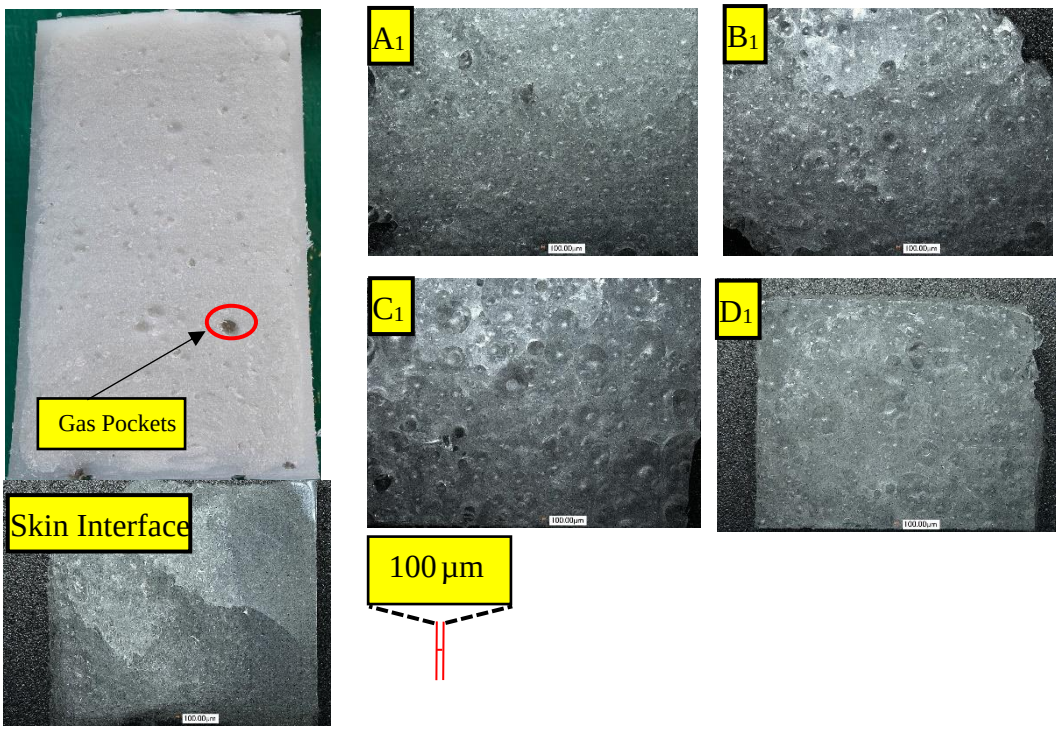

Figure 5.59: LA-0522 foamed core processed at 135°C with talc at 0.25 ml/min gas injection rate.

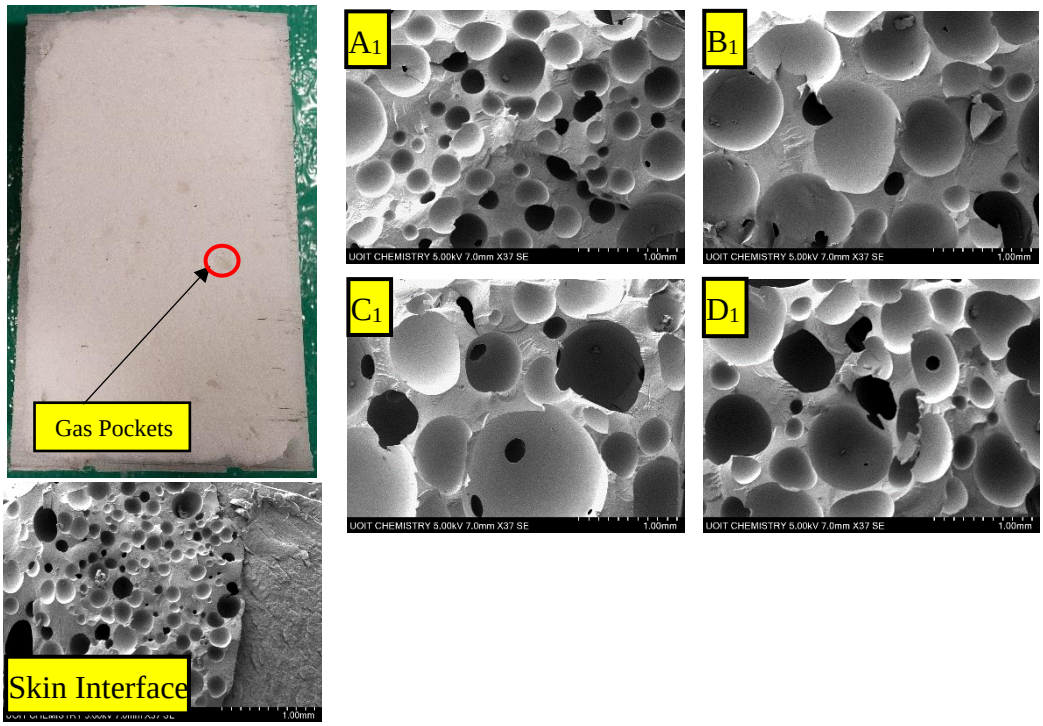

Figure 5.60: LA-0522 foamed core processed at 135°C with Celogen OT™ at 0.25 ml/min gas injection rate.

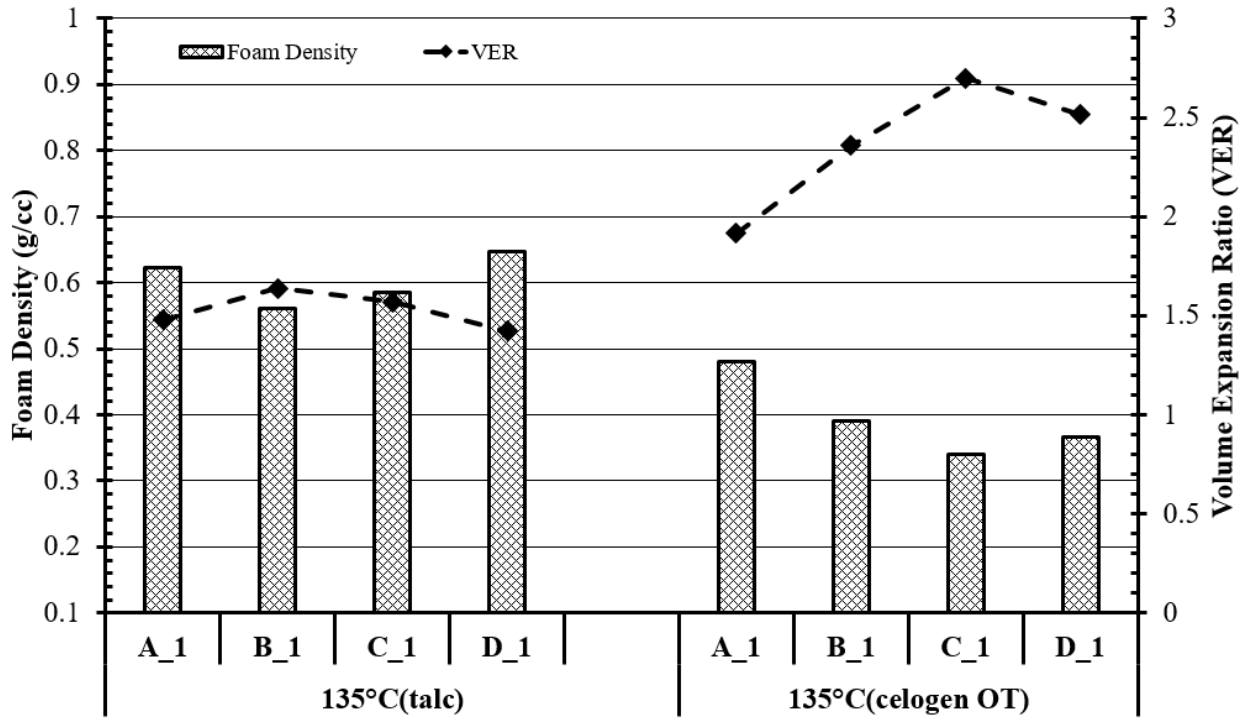

Figure 5.61: Foam density and volume expansion ratio of LA-0522 resin produced with 0.25 ml/min gas injection rate.

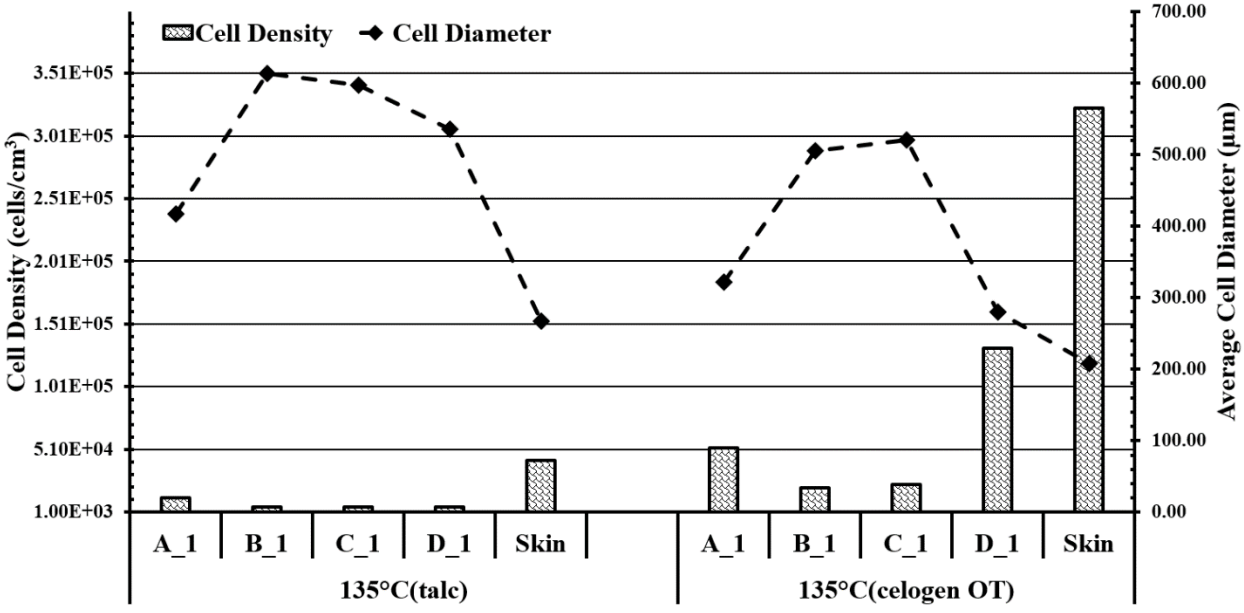

Figure 5.62: Cell density and cell size of LA-0522 resin produced with 0.25 ml/min gas injection rate.

The final set of foamed cores were produced with 0.25 ml/min gas injection rate. The cross-section of the foamed core is presented in Figures 5.59-5.60. The foamed cores are evenly filled with smaller gas pockets compared with the foamed cores of 1 ml/min gas injection rate. The foamed cores produced with 0.25 ml/min injection rate exhibited bubble penetration into the skin layer and good bond quality with the outer skin.

The foam density and the VER of foamed core produced with 1 ml/min gas injection rate is presented in Figure 5.61. The foam density of the talc containing foam is higher than the Celogen OT™ contacting foam. The talc containing foamed core exhibited an initial reduction in density at B_1, however the density increased gradually to position D_1. The Celogen OT™ contacting foamed core displayed gradual reduction in density from position A_1 to C_1 before increasing slightly at position D_1. The volume expansion ratio was observed to be significantly higher for Celogen OT™ containing foam. However, the volume expansion was comparable to the Celogen OT™ foamed core processed at 1 ml/min gas injection rate. In contrast the VER of foamed core processed with talc was lower for gas injection rate 0.25 ml/min.

The cell density and average cell size of the foamed cores processed with 0.25 ml/min gas injection rate is presented in Figure 5.62. The talc containing foamed core exhibited a reduction in cell density from 1.26×10^4 cells/ cm^3 at A_1 to 5.12×10^3 cell/cm^3 at position C_1. The cell density increased to 5.24×10^3 at cell/cm^3 D_1 and the cell density increased further close to the skin interface to a value of 4.22×10^4 cells/cm^3. The corresponding cell size gradually decreased in size from position B_1 to D_1 and further into the skin interface region. The foamed core produced with Celogen OT™ experienced a reduction in cell density from position A_1 to C_1 and then cell density increased After C_1 to the skin interface region. The corresponding average cell size reached its peak at position C_1 and reduced in value from D_1 to the skin interface. Finally, the foamed core processed with 1 ml/min gas injection rate exhibited higher cell density than the foamed cores produced from 0.25 ml/min gas injection rate.

Chapter 6. Conclusion, Summary & Suggestions for Future Improvements

6.1 Conclusion

Unlike homogeneous or conventional composite materials, Functionally Graded Materials (FGMs) represent a class of advanced heterogeneous materials that exhibit different position-dependent property gradients and functional performances over their volume due to the gradual spatial variation of their composition, chemical and/or structural features that are deliberately designed, generated and controlled during their manufacturing process for specific function and applications. Because of the functional gradation the global mechanical, physical, or thermal properties of FMGs are unique and different from the properties of any of their constituent materials, which makes them attractive for an extensive range of engineering applications. However, in spite of their importance and applicability, compared to analog metal-based systems, the knowledge on processing methods for functionally graded cellular polymeric composites is quite limited. The targeted compositional and microstructural gradients of these composites by design will allow for an optimum combination of component properties such as weight, material density, surface hardness, wear resistance, impact resistance, toughness, mechanical strength, impact energy absorption, cushioning, shock mitigation, acoustic and thermal insulation, which would qualify them to serve as multifunctioning components in a wide variety of industries.

In this context, the research work presented in thesis represents a significant contribution to the development of novel processing technologies for manufacturing functionally graded integral-skin cellular polymeric composites based on a previously patented melt extrusion-assisted rotational foam molding process, referred to as Rapid Rotational Foam Molding (RRFM). These functionally graded integral-skin cellular polymeric composites will represent a unique class of advanced lightweight multi-constituent and multi-phase engineering materials. They can be deliberately engineered with spatially varied gradients of composition that is essentially governed by the inhomogeneous, interchanging, or adjacent solid and cellular macro, micro, or nano morphological structures. The existence of this morphological non-uniformities introduces specific advantageous material properties that vary smoothly and continuously in preferred directions or orientations. Hence, the resulting integral-skin cellular systems can be intentionally designed for specific purposes and applications where having varying properties in different regions of a single component is a requirement.

A new lab-scale Rapid Rotational Functionally Graded Foam Molding (RRFGFM) experimental setup was successfully designed and built and its functionality was fully validated through extensive experimental trials. It has thereby been proven that the proposed processing concept for fabricating integral-skin functionally graded cellular composite artifacts in rotational molding is founded on solid scientific and engineering grounds and feasible. In addition, it has been proven and documented in an unprecedented manner that physical blowing agent (PBA) based foam production can successfully and effectively be integrated in the rotational foam molding process when aiming to produce integral-skin functionally graded rapid rotational molded foam composites. As such, the research work presented in this thesis has not only completely fulfilled its intended scope and purpose, but it has also paved the way and created the potential to be derived into a family of technologies that will be capable of generating new classes of functionally graded polymeric composites.

It is very important to recognize that until the development of the RRFM process, chemical blowing agents (CBAs) were exclusively utilized in rotational foam molding foaming operations because of the intrinsic atmospheric nature of the process that uses vented molds. As melt extrusion foaming has been successfully integrated into the RRFM process, it advantageously becomes feasible to implement physical blowing agents (PBAs) in RRFM for the first time. Consequently, processing functionally graded polymeric composite structures becomes possible because it can synergistically involve melt extrusion foaming while using chemical and physical blowing agents exclusively or concurrently. Since different polymers develop distinctly different cellular morphologies when using different kinds of blowing agents at different processing parameters, it is possible to introduce property gradients into the components by varying the processing parameters. A smooth cellular morphology gradient can be produced by adjusting the uni-axial centrifugation speed of the rotating mold containing the solid skin and the structure of the injected foam.

The impact of the proposed research work related to RRFGFM is expected to advance Canada’s processors of polymeric cellular composites to the forefront of the international competition because these technologies will provide the means for manufacturing advanced new classes of ultra-lightweight integral-skin functionally graded cellular composites the properties of which will reach currently not conceivable levels. It is certain that this research work will have the

potential to be derived into a family of technologies that will be capable of generating new classes of functionally graded polymeric composites that will be characterized with a complex anisotropic structure made of an outer solid skin and an inner cellular region or core.

6.2 Summary and Suggestions for Future Improvements

In the first set of experiments, various grades of resins were foamed by injecting supercritical gas directly into the polymer melt in the mixing chamber. The foams were rapidly cooled to preserve the cell morphology immediately after cell nucleation. However, from the experimental results microcellular foam was not produced with any of the PE grades being tested. The highest cell density and the lowest average cell size was produced with LDPE resin processed with both 1wt% Celogen OT™ and 2 ml/min PBA injection rate at 135°C mixing zone temperature. The cell density can be improved at higher gas injection rate and by reducing the processing temperature. However, with higher gas injection rate the foam layering process with rotational molding becomes more difficult due to faster foam ejection rate from the die exit. The acceptable upper limit for gas injection rate was 5 ml/min. However, complete dissolution of all the supercritical gas into the polymer melt was not observed at any gas injection rate.

To vary the quality of the foamed core, two types of foaming strategy were employed. In the first attempt, the gas injection rate was gradually decreased as the mold filled with foam along the central axis of the mold. The second attempt involved gradually increasing the nucleating agent or the blowing agent content within the extruded resin to vary the foam quality. From the experimental results, talc with supercritical CO_2 was more suitable as a nucleating agent for HDPE and sHDPE resin and Celogen OT™ + supercritical CO_2 was more suitable for foaming application with LDPE resin. Regardless of resin type, bubble penetration into the skin layer was observed for all the different foaming experiments. However, extrusion grade HDPE with MFI value less than 1 was discovered to be unsuitable for foaming application with the RRFGFM process. The cell density within the foamed core of the rotational molded composite decreased at positions further away from the skin interface region. This pattern of cell morphology was observed for both types of foaming strategy. The variation in cellular structure was strongly related to the thermal gradient within the foamed core rather than just the gas injection rate or the nucleating agent content. Foam region further away from the integral outer skin take longer to solidify which promotes cell coalescence and gas diffusion out of the polymer melt into growing bubbles and reducing the

overall cell density. Higher processing temperatures did not improve the quality of the foam rather at higher processing temperature larger gas pockets are more likely with reduced cell population and higher cell size. By decreasing the processing temperature, higher pressure drop can be induced at the die exit and increasing the overall cell density and reducing the cell size.

To improve the quality of the foam further, multiple modification to the experimental setup could be performed. One improvement to the experimental setup would be to exchange the die nozzle with a die that has a smaller orifice. The diameter of the nozzle opening can be modified from 3 mm to 1 mm to induce a higher pressure drop to generate greater quantities of bubble nucleation sites. Through this modification the cell density of the foam can be improved at higher processing temperatures. Another major modification to the experimental setup will be to change the mixing blade design. Currently with helical blades, complete single-phase polymer-gas solution was not achieved. By increasing the blade surface area the dissolution of large gas bubbles into small ones will be more rapid to form the single-phase polymer-gas solution. Finally, the extrusion process can be modified to produce functionally graded chemical blowing agent (CBA) and PBA foam simultaneously utilizing a co-extrusion system. This new design will be a new evolution for the RRFGFM process. In this new design two extruders can be used simultaneously. A single extruder is only responsible for either producing CBA or PBA-based foam. An especially designed nozzle could then deliver which ever foam is desired to produce functionally graded foamed cores.

References

Adxchiri, Tadfumi, et al. *Supercritical Fluid Technology in Materials Science and Engineering.* New York: Marcel Dekker, 2002.

Aerogel. *Product Documents of Pyrogel.* 2020. https://www.aerogel.com/products-and-solutions/product-documents/?addFilter=28 (accessed January 15, 2020).

Amazon. *PowerMax PM4 100A 110V AC to 12V DC 100 Amp Power Converter with Built-in 4 Stage Smart Battery Charge.* 2020. https://www.amazon.ca/gp/product/B01ER3LH5W/ref=ppx_yo_dt_b_asin_title_o09_s00?ie=UTF8&th=1 (accessed January 15, 2020).

Ashcroft. "Type 100 Series Threaded Capsule Diaphragm Seal." *Viking Instruments & Control LTD.* 2011. https://vikinginstrument.com/wp-content/uploads/files/products/diaphragm-seal-type-100.pdf (accessed January 15, 2020).

Ashcroft. "Type 1009 Stainless Steel Gauge." *Viking Instruments.* January 1, 2012. http://vikinginstrument.com/wp-content/uploads/files/products/gauge-stainless-steel-type-1009-4-1-2.pdf (accessed January 15, 2020).

ASTM-D1622-08. *Standard Test Method for Apparent Density of Rigid Cellular Plastics.* 2008. http://www.astm.org/cgi-bin/resolver.cgi?D1622 (accessed August 8, 2019).

Aubee, Norman, Patrick Lam, and Sarah Marshall. "A New Family of sHDPE Polymers for Enhanced Moisture Barrier Performance." *JOURNAL OF PLASTIC FILM & SHEETING* 22 (2006): 315-330.

Autoclave. *Low Pressure Fittings, Check Valve, and Tubing.* 2020. http://www.autoclave.com/products/fittings_and_tubing/low/low.html (accessed January 15, 2020).

Barzegari, Mohamad, Jiaolian Yao, and Denis Rodrigue. "Compression Molding of Polyethylene Foams Under a Temperature Gradient: Morphology and Flexural Modulus." *Cellular Polymers* 28, no. 4 (2009): 237-248.

Brunner, Gerd. "Applications of Supercritical Fluids." *The Annual Review of Chemical and Biomolecular Engineering* 1 (2010): 321-341.

Chaudhary, Bharat, and Andy Jhons. "Solubilities of Nitogen, Isobutane and Carbon Dioxide in Polyethylene." *Journal of Cellular Plastics* 34 (1998): 312-328.

Chauvet, Margot, Martial Sauceau, and Jacques Fages. "Extrusion Assisted by Supercritical CO2: A Review on Its Application to Biopolymers." *The Journal of Supercritical Fluids* 120 (2017): 408-420.

Crawford, R. "Chapter 5 - Analysis of Polymer Melt Flow." In *Plastics Engineering Third Edition*, by R Crawford, 344-345. Oxford: Butterworth-Heinemann, 1998.

Crawford, R.J. "Chapter 1: Introduction to Rotational Moulding." In *Rotational Moulding of Plastics Second Edition*, by R.J Crawford, 1-31. Somerset: Research Studies Press LTD., 1996.

Cui, Liang, Stephen Kiernan, and Michael Gilchrist. "Designing The Energy Absorption Capacity of Functionally Graded Foam Materials." *Materials Science and Engineering A* 507 (2009): 215-225.

El-Desouky, Ahmed, Samuel Kassegne, Kee Moon, J McKittrick, and K Morsi. "Rapid Processing & Characterization of Micro-scale Functionally Graded Porous Materials." *Journal of Materials Processing Technology* 213 (2013): 1251-1257.

Fradette, Louis, Huai Li, Lionel Choplin, and Philippe Tanguy. "Gas/Liquid Dispersions with a SMX Static Mixer in the Laminar Regime." *Chemical Engineering Science* 61 (2006): 3506-3518.

Funami, Eita, Kentaro Taki, and Masahiro Ohshima. "Density Measurement of Polyme/CO2 Single-Phas Solution at High Temperature and Pressure Using a Graviometric Method." *Journal of Applied Polymer Science* 105 (2007): 3060-3068.

Gefran. *W9 Pressure and temperature monitoring set (1/4 DIN).* 2020. https://www.gefran.com/en/products/183-w9-pressure-and-temperature-monitoring-set-1-4-din#downloads (accessed January 2020, 2020).

Goodship, V, and E.O Ogur. *Polymer Processing with Supercritical Fluids.* Shorpshire: Rapra Technology , 2004.

Greenwood, Wim. "Chapter 1: Differential Scanning Calorimetry & Chapter 2: Thermogravimetry ." In *Characterisation of Polymers by Thermal Analysis*, by Wim Greenwood, 10-12, 61-63. Amsterdam: Elsevier Science B.V. , 2001.

Jacobs, Leon, Maartje Kemmere, and Keurentjes. "Sustainable Polymer Foaming Using High Pressure Carbon Dioxide: A Review on Fundamentals, Process and Applications." *Green Chemestry* 10 (2008): 731-738.

Kieback, B, A Neubrand, and H Riedel. "Processing Technique for Functionally Graded Materials." *Materials Science and Engineering* 362 (2003): 81-105.

Kim, S, J Lee, C Park, and Sain M. "Enchancing Cell Nucleation of Thermoplastic Polyolefin Foam Blown with Nitrogen." *Journal of Applied Polymer Science* 118 (2010): 1691-1703.

Kimberly, Christian. *Rapid Rotational Foam Molding of Polyethylene Integral-Skin Foamed Core Molding.* Masters Thesis, University of Ontario Institute of Technology: ProQuest Dissertations, 2009.

Lee, Patrick, et al. "Effect of Die Geometry on Foaming Behaviour of High-Melt-Strength Polypropylene with CO2." *Journal of Applied Polymer Science* 109 (2008): 3122-3132.

Mahmood, Rasheedat M, and Esther Akinlabi. "Chapter 1: Introduction to Functionally Graded Materials." In *Functionally Graded Materials*, by Rasheedat M Mahmood, & Esther Akinlabi, 1-8. Cham: Springer International Publishing, 2017.

Mapleston, Peter. "Rotational Moulding: Rotomoulders Take Control." *Plastics Engineering*, October 1, 2008: 10-16.

Matuana, L. "Solid State Microcellular Foamed Poly(Lactic Acid): Morphology and Property Characterization." *Bioresource Technology*, 2008: 3643-3650.

MatWeb. *LyondellBasell Microthene® MP625662 Linear Low Density Polyethylene.* n.d. http://www.matweb.com/search/datasheet.aspx?matguid=de76e0c99fb7486eb04b472525efc857 (accessed January 15, 2020).

Meijer, Han, Mrityunjay Singh, and Patrick Anderson. "On the Performance of Static Mixers: A Quantitative Comparison." *Progress in Polymer Science* 37 (2012): 1333-1349.

Menczel, Joseph, R Prime, and P Gallagher. "Chapter 1: Introduction." In *Thermal Analysis of Polymers*, by Joseph Menczel, & R Prime, 1-6. Hoboken: John Wiley & Sons Inc, 2009.

MilliporeSigma. *Talc.* 2020. https://www.sigmaaldrich.com/catalog/product/sial/86257?lang=en&region=US&cm_sp=Insite-_-prodRecCold_xviews-_-prodRecCold10-1 (accessed January 15, 2020).

Mills, Nigel. *Polymer Foams Handbook Engineering and Biomechanics Applications and Design Guide.* Burlington: Butterwort-Heinemann, 2007.

Naguib, Hani, Chul Park, and Patrick Lee. "Effect of Talc Content on the Volume Expansion Ratio of Extruded PP Foams." *Journals of Cellular Plastics* 39 (2003): 499-511.

Nalawade, Sameer, Francesco Picchioni, and L Janssen. "Supercritical Carbon Dioxide as a Green Solvent for Processing Polymer Melts: Processing Aspects and Applications." *Progress in Polymer Science* 31 (2006): 19-43.

Nobelen, M, S Hoppe, C Fonteix, F Pla, M Dupire, and Jacques B. "Modelling of the Rehological Behaviour of Polyethylene/Supercritical CO2 Solutions." *Chemical Engineering Science* 61 (2006): 5334-5345.

NovaChemicals. *Polyethylene Product Finder.* 2020. https://www.novachem.com/polyethylene/product-finder/?pg=1 (accessed January 15, 2020).

O'Connor, Leo. "Rotational Molding." *Advanced Manufacturing Technology* , August 15, 2003: 11-12.

Ogila, K, M Shao, W Yang, and J Tan. "Rotational Molding: A Review of the Models and Materials." *Express Polymer Letters* 11 (October 2017): 778-798.

Park, Chul, Amir Behravesh, and Ronald Venter. "Low Density Microcellular Foam Processing in Extrusion Using CO2." *Polymer Engineering and Science* 38, no. 11 (1998): 1812.

Park, Chul, and N Suh. "Rapid Polymer/Gas Solution Formation for Continuous Production of Microcellular Plastics." *Journal of Manufacturing Science and Engineering* 118 (1996): 639-645.

Park, Chul, Patrick Lee, Jin Wang, and Valentina Padareva. "Strategies for Achieving Microcellular LDPE Foams in Extrusion." *Cellular Polymers* 25, no. 1 (2006): 1-25.

Peacock, Andrew. "Introduction: The Essence of Polyethylene." In *Handbook of Polyethylene Structures, Properties, and Applications*, by Andrew Peacock, 1-7. New York: Marcel Dekker, Inc, 2000.

Pop-Iliev, Remon. "Processing of Integral-Skin Cellular Polymeric Composites in Rapid Rotational Foam Molding." *Acta Physica Polonica A* 120 (2011): 292-297.

Pop-Iliev, Remon, and Chul B Park. "Processing of Polypropylene Foams in Melt Compounding Based Rotational Foam Molding." *Journal of Reinforced Plastics and Composites* , 2002: 1079-1100.

Pop-Iliev, Remon, and Chul B Park. "Single-step Rotational Foam Molding of Skin-surrounded Polyethylene Foams." *Cellular Plastics* 39 (2003): 49-58.

Pop-Iliev, Remon, Donglai Xu, and Chul B Park. "Manufacturability of Fine-celled Cellular Structures in Rotational Foam Molding." *Journal of Cellular Plastics* 40 (2004): 13-25.

Pop-Iliev, Remon, Kimbery Christian, and Emad Abdalla. Rapid Rotational Foam Molding Process . United States of America Patent US 8,628,704 B2. January 14, 2014.

Pop-Iliev, Remon, Kyoung-Ho Lee, and Chul B Park. "Manufacture of Integral Skin PP Foam Composites in Rotational Molding ." *Journal of Cellular Plastics* , 2006: 139-152.

Pop-Iliev, Remon, Ning Dong, Donglai Xu, and Chul B Park. "Visualization of the Foaming Mechanism of Polyethylene Blown by Chemical Blowing Agents under Ambient Pressure." *Advances in Polymer Technology*, 2007: 213-222.

Princessauto. *12V DC Double-Acting Lifting Hydraulic Power Unit.* 2020. https://www.princessauto.com/en/detail/12v-dc-double-acting-lifting-hydraulic-power-unit/A-p8582769e (accessed January 15, 2020).

Raktim, Isha, and Remon Pop-Iliev. "New Experimental Setup Design For Applying Physical Blowing Agent In Rapid Rotational Foam Molding Technology." *Canadian Society for Mechanical Engineering.* Toronto: CSME-SCGM, 2018.

Ramirez, Yendery, Luis Cisternas, and Andrzej Kraslawski. "Application of House of Quality in Assessment of Seawater Pretreatment Technologies." *Journal of Cleaner Production* 148 (2017): 223-232.

Rauwendaal, Chris. "Chapter 1: Introduction & Chapter 5: Single Screw Estruder." In *Polymer Mixing A Self-Study Guide*, by Chris Rauwendaal, 1-7, 91-93. Cincinnati: Hanser/Gardner Publications, 1998.

Rizvi, S. "Microcellular Foam Injection Molding of Thermoplastics Using Green Physical Blowing Agent." *Materials Science Forum* 875 (2016): 77-111.

Sato, Yoshiyuki, Koji Fujiwara, Tado Takikawa, Sumarno, Shigeki Takishima, and Hirokatsu Masuoka. "Solubilities and Diffusion Coefficients of Carbon Dioxide and Nitrogen in Polypropylene, High-Density Polyethylene, and Polysyrene Under High Pressure and Temperatures." *Fluid Phase Equilibria* 162 (1999): 261-276.

Sauceau, Martial, Jacques Fages, Audrey Common, Clemence Nikitine, and Elisabeth Rodier. "New Challenges in Polymer Foaming: A Review of Extrusion Process Assisted by Supercritical Carbon Dioxide." *Progress in Polymer Science* , 2011: 749-766.

Schneider, Gottlieb. "Static Mixing Technology for Extrusion and Injection Molding ." *Stamixco.com.* n.d. https://www.stamixco.com/downloads/Stamixco_Technical_Presentation.pdf (accessed January 1, 2018).

Selvakumar, P, and Naresh Bhatnagar. "Studies on Polypropylene/Carbon Fiber Composite Foams by Nozzle-Based Microcellular Injection Molding System." *Materials and Manufacturing Process* 24 (2009): 533-540.

Shakoor, A, and N Thomas. "Talc as a Nucleating Agent and Reinforced Filler in Poly(lactic acid) Composites." *Polymer Engineering and Science*, 2014: 64-70.

Soman, Sudhanshu, and Chandra Madhuranthakam. "Effects of Internal Geometry Modifications on the Dispersive and Distributive Mixing in Static Mixers." *Chemical Engineering & Processing: Process Intensification* 122 (2017): 31-43.

Speyer, Robert. "Chapter 3: Differential Thermal Analysis & Chapter 5: Themograviometric Analysis." In *Thermal Analysis of Materials*, by Robert Speyer, 35-40, 111-120. New York: Marcel Dekker, 1994.

Srinivas, Siripurapu, Gay Yvon, Joseph Royer, Joseph DeSimone, Richard Spontak, and Saad Khan. "Generation of Microcellular Foams of PVDF and Its Blends using Supercritical Carbon Dioxide in a Continuoius Process." *Polymer* 43 (2002): 5511-5520.

Strong, Brent. "Chapter 4: Mechanical Properties." In *Plastics Material and Processing*, by Brent Strong, 124-125. Columbus: Pearson Education, 2006.

Sun, Guangyong, Guangyao Li, Shujuan Hou, Shiwei Zhou, Wei Li, and Li Quing. "Crashworthiness Design for Functionally Graded Foam-filled Thin-walled Structures." *Materials Science and Enginerring A* 527 (2010): 1911-1919.

Teledyne. *260D Syringe Pump.* 2020. https://www.teledyneisco.com/en-us/pumpproducts/Pages/260D.aspx (accessed January 10, 2020).

Thakur, R, C Vial, K Nigam, E Nauman, and G Djelveh. "Static Mixers in the Process Industries- A Review." *Institution of Chemical Engineering* 81 (2003): 787-825.

"Theory of Inventive Problem Solving." *University of Michigan, Department of chemical Engineering* . 2011. http://umich.edu/~scps/html/07chap/html/powerpointpicstriz/Chapter%207%20TRIZ.pdf (accessed January 27, 2020).

Throne, James. "Chapter 4: Foaming Agents." In *Thermoplastic Foams*, by James Throne, 125-179. Hinckley : Sherwood Publishers, 1996.

Todd, Clifford, and Valentina Kuznetsova. "Closed-Cell Foam Skin Thickness Measurement Using a Scanning Electron Microscope." *Microscopy and Microanalysis* 17 (2011): 772-778.

Tomasko, David, et al. "Development of CO2 for Polymer Foam Applications." *The Journal of Supercritical Fluids* 47 (2009): 493-499.

Tsivintzelis, Ioannis, Anastasia Angelopoulou, and Costas Panayiotou. "Foaming of Polymers with Supercritical CO2: An Experimental and Theoretical Study." *Polymer* 48 (2007): 5928-5939.

Utkarsh, Isha Raktim, R Pop-Iliev, and G Rizvi. "3-Dimensional Characterization Of The Quality Of Foam-To-Skin Bonding Of Rapid Rotationally Foam Molded Integral-Skin Cellular Composites." *ANTEC.* Orlando: Society of Plastics Engineers, 2018.

Valco. *Valco Fittings.* 2019. https://www.vici.com/vfit/vfit.php (accessed January 15, 2020).

Viachopoulos, J. *Society of Plastics Engineers Extrusion Division 1-0-Wiki.* January 31, 2015. http://www.extrusionwiki.com/wiki/CC-V25-1-D.ashx (accessed January 22, 2020).

Walter, Michaeli. *Extrusion Dies for Plastic and Rubber Design and Engineering Computation 3rd Edition* . Munchen: Carl Hanser Verlag, 2003.

Wang, Jing, Weli Zhu, Hongtao Zhang, and Chul Park. "Continuous Processing of Low-Density, microcellular Poly(Lactic acid) Foams with Controlled Cell Morphology and Crystalinity." *Chemical Engineering Science* 75 (2012): 390-399.

Wang, K, et al. "Effect of Talc Content on the Degeneration of Re-extruded Polypropylene/talc Composites." *Polymer Degradeation and Stability* 98 (2013): 1275-1286.

Xiang, Xu, Chul Park, Donglai Xu, and Pop-Iliev Remon. "Effects of Die Geometry on Cell Nucleation of PE Foam Blown with CO2." *Polymer Engineering and Science* 43, no. 7 (2003): 1378-1390.

Xiang, Xu, Park, Chul, Xu Donglai, and Remon Pop-Iliev. "Effects of Die Geometry on Cell Nucleation of PS Foams Blown With CO2." *Polymer Engineering and Science* 43, no. 7 (2003): 1378-1390.

Xu, Donglai, Remon Pop-Iliev, Chul B Park, and R. G Fenton. "Fundamental Study of CBA-blown Bubble Growth and Collapse Under Atmospheric Pressure." *Journal of Cellular Plastics* 41 (2005): 519-538.

Yao, Jiaolian, and Denis Rodrigue. "Density Graded Polyethylene Foams Produced by Compression Moulding Using a Chemical Blowing Agent." *Cellular Polymers*, 2012: 189-205.

Yao, Jiaolian, Mohamad Barzegari, and Denis Rodrigue. "Density Graded Linear Medium Density Polyethylene Foams Produced Under a Temperature Gradient With Expancel Microbeads." *Cellular Polymers* 30, no. 4 (2011): 157-185.

Zhang, Jingjing, Ghaus Rizvi, and Chul Park. "Study on cell nucleation behavior of HDPE–wood composites/supercritical CO2 solution based on rheological properties." *Journal of Material Science* 46 (2011): 3777-3784.

Zhang, Xiaoxue, Saara Heinonen, and Erkki Levanen. "Applications of Supercritical Carbon Dioxide in Materials Processing and Synthesis." *Royal Society of Chemestry* 4 (2014): 61137-61152.

Appendices

Appendix A

A1. House of Quality for polyethylene foam extrusion with physical blowing agent.

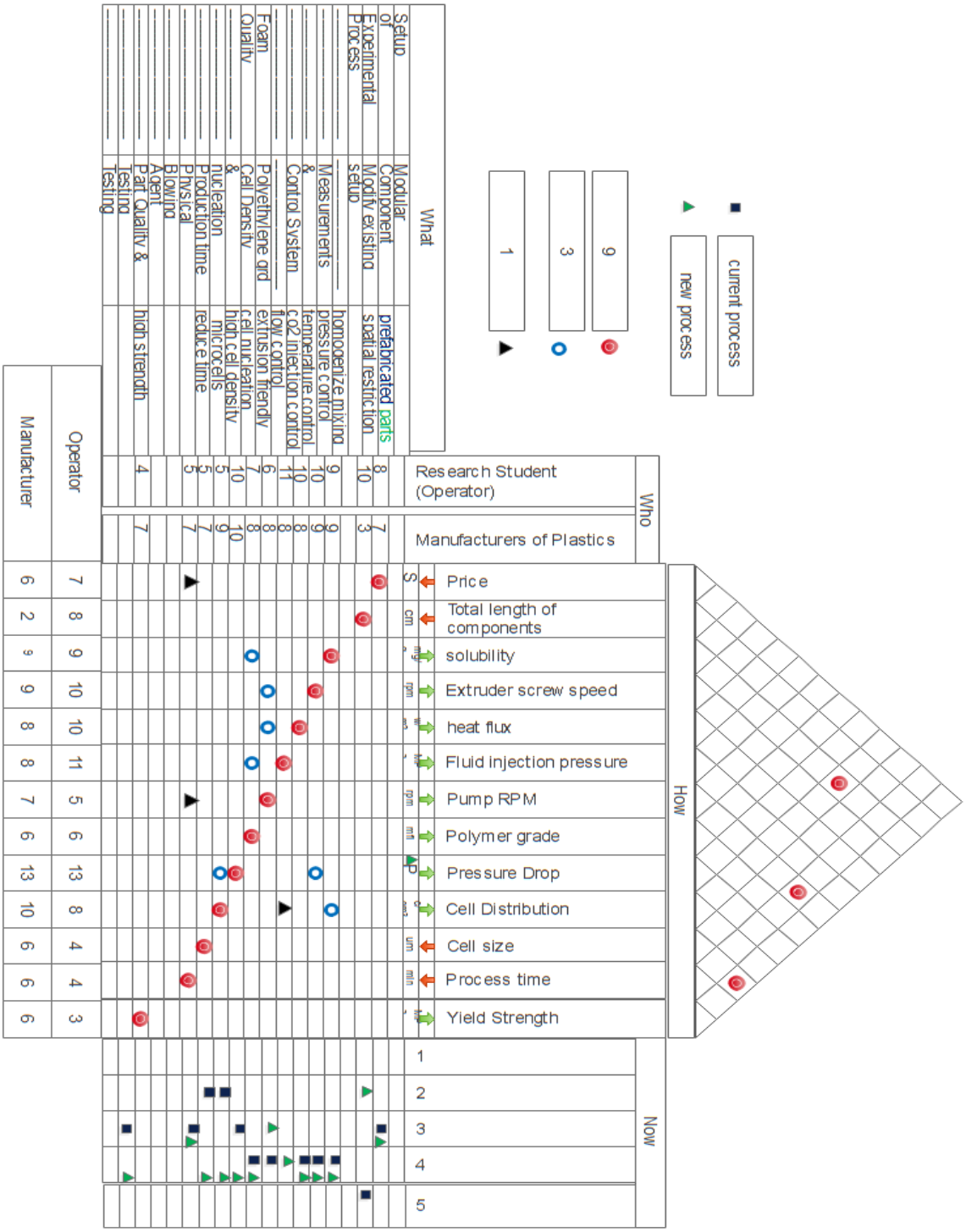

A2. StamixCo drawing of the static mixer mixing chamber.

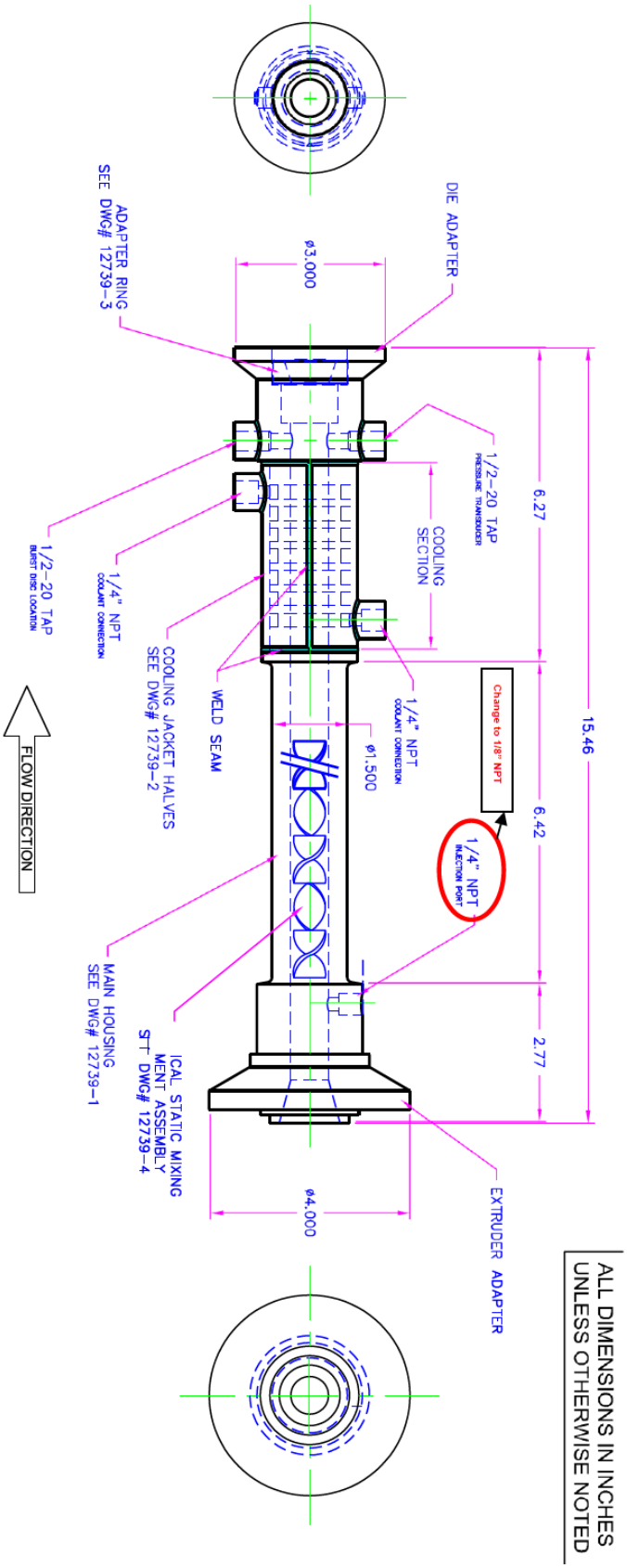

A3. StamixCo helical blade dimensions.

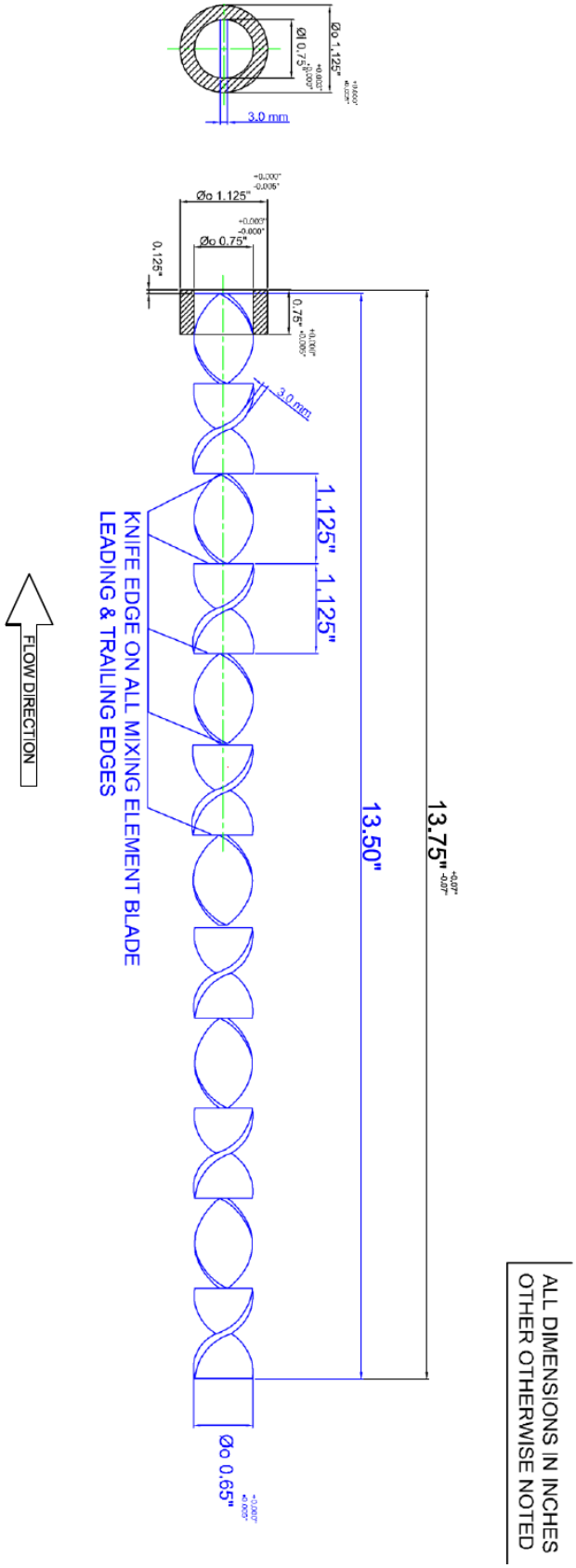

Appendix B.

B1. Homopolymer HDPE 19C material properties.

SCLAIR® 19C Resin

Homopolymer HDPE Film Resin

Property		ASTM	Typical Values	
Melt Index[3]		D 1238	0.95 g/10 min	
Density		D 792	0.958 g/cm³	
Hardness, Shore D		D 2240	68	
			METRIC UNITS	ENGLISH UNITS
Vicat Softening Point		D 1525	131 °C	268 °F
Film Properties[4]				
Thickness			38 µm	1.5 mil
Tear Strength	MD	D 1922	26 g	
	TD		711 g	
Dart Drop Impact, F_{50}		D 1709/A	44 g	
Low Friction Puncture[5]			20 J/mm	4 in-lb/mil
Tensile Strength	MD	D 882	42 MPa	6,100 psi
	TD		40 MPa	5,800 psi
Yield Strength	MD	D 882	25 MPa	3,600 psi
	TD		27 MPa	3,900 psi
Elongation	MD	D 882	560 %	560 %
	TD		890 %	890 %
Haze		D 1003	36 %	36 %
Gloss @ 45°		D 2457	23	23
1% Secant Modulus	MD	D 882	840 MPa	121,800 psi
	TD		1,180 MPa	171,100 psi
OTR[6]		D 3985	1,488 cm³/m²/day	96 cm³/100in²/day
MVTR[7]		F 1249	2.64 g/m²/day	0.17 g/100 in²/day

B2. HDPE resin HE-Y449-AC material properties.

NOVAPOL® HE-Y449-AC Resin

Hexene Copolymer HDPE Pipe Extrusion Resin

Property	ASTM [1]	Typical Values[2]	
Melt Index [3]	D 1238	0.3 g/10 min	
Density	D 792	0.949 g/cm³	
Hardness, Shore D	D 2240	61	
		METRIC UNITS	ENGLISH UNITS
Vicat Softening Point	D 1525	124 °C	255 °F
Low Temperature Brittleness Point	D 746	< -70 °C	< -94 °F
Flexural Tangent Modulus	D 790	1,140 MPa	165,300 psi
Melting Point (DSC)		130 °C	266 °F
Yield Strength [4]	D 638	24 MPa	3,500 psi
Elongation [4]	D 638	650 %	650 %
ESCR, (F_{50}) [5]	D 1693	> 1 000 h	
Izod Impact		1.1 J/cm	2.0 ft-lb/in
Oxidative Induction Time [6]		10 min	

B3. sHDPE rotational molding grade powder RMS-245UG material properties.

SURPASS® RMs245-U(UG) Resin

Octene Copolymer sHDPE Rotational Molding Resin

Property		ASTM (1)	Typical Values (2)			
Melt Index (3)		D 1238	1.7 g/10 min			
Density		D 792	0.945 g/cm³			
			METRIC UNITS		ENGLISH UNITS	
Melting Point (DSC)			127	°C	261	°F
Flexural Modulus	(4)	D 790	1,030	MPa	149,400	psi
Yield Strength	(5)	D 638	23	MPa	3,300	psi
Elongation at Yield	(5)	D 638	11	%	11	%
ESCR, (F_{50})	(6)	D 1693	> 1 000	h		
Heat Distortion Temperature						
- 66 psi (4.64 kg/cm²)		D 648	63	°C	145	°F
- 264 psi (18.56 kg/cm²)		D 648	43	°C	109	°F
ARM Low Temperature Impact	(7)					
- 0.125" (3.17 mm)		ARM Method	75	J	55	ft-lb
- 0.250" (6.35 mm)		ARM Method	> 245	J	> 180	ft-lb

B4. sHDPE rotational molding grade powder RMS-341UG material properties.

SURPASS® RMs341-U(UG) Resin

Octene Copolymer sHDPE Rotational Molding Resin

Property	ASTM (1)	Typical Values(2)	
Melt Index(3)	(3) D 1238	3.5 g/10 min	
Density	D 792	0.941 g/cm³	
		METRIC UNITS	ENGLISH UNITS
Melting Point (DSC)		126 °C	259 °F
Flexural Modulus	(4) D 790	827 MPa	119,900 psi
Yield Strength	(5) D 638	20.2 MPa	2,900 psi
Elongation at Yield	(5) D 638	12 %	12 %
ESCR, (F_{50})	(6) D 1693	> 1 000 h	
Heat Distortion Temperature			
- 66 psi (4.64 kg/cm²)	D 648	62 °C	144 °F
- 264 psi (18.56 kg/cm²)	D 648	43 °C	109 °F
ARM Low Temperature Impact	(7)		
- 0.125" (3.17 mm)	ARM Method	67 J	49 ft-lb
- 0.250" (6.35 mm)	ARM Method	230 J	170 ft-lb

B5. Foam extrusion grade LDPE resin LA-0522 material properties.

NOVAPOL® LA-0522-A Resin

Homopolymer LDPE Extrusion Resin

Property	ASTM	Typical Values			
Melt Index[3]	D 1238	4.5	g/10 min		
Density	D 792	0.920	g/cm³		
		METRIC UNITS		ENGLISH UNITS	
Coating Properties					
Minimum Coating Weight[5]	D 539	8.0	g/m²	5.0	lb/ream
Drawdown Speed[4]		8.1	m/s	1,590	ft/min
Neck-in @ 1 000 ft/min[4,6]		5.1	cm	2.0	in
Heat Seal Strength[5,7]	D 517	1,400	g/25 mm		lb/in
Hot Tack Strength[4,7]		450	g/50 mm		lb/2 in
MVTR[7]	F 1249	17	g/m²/day	1	g/100 in²/day
Plaque Properties					
1% Flexural Secant Modulus	D 790	276	MPa	40,000	psi
Yield Strength	D 638	9.4	MPa	1,400	psi
Elongation	D 638	650	%	650	%

B6. Rotational molding grade powder LLDPE resin GA625662 material properties.

LyondellBasell Petrothene® GA625662 Linear Low Density Polyethylene (Unverified Data)**

Categories: Polymer; Thermoplastic; Polyethylene (PE); Linear Low Density (LLDPE); Linear Low Density Polyethylene (LLDPE), Rotational Molding Grade

Material Notes:

Applications
PETROTHENE GA 625-662, a hexane LLDPE, pelletized rotational molding resin with excellent flow properties, can be used to produce a variety of objects such as toys, playground equipment, drums and agricultural and chemical storage containers.

Processing Techniques
Specific recommendations for conditions under which GA 625-662 should be processed can be made only when the end use and type of processing equipment are known.

Regulatory Status
GA 625-662 meets the requirements of the Food and Drug Administration regulation, 21 CFR 177.1520. This regulation allows the use of this olefin polymer in "...articles or components of articles intended for use in contact with food..." Specific limitations or conditions of use may apply.

Physical Properties
GA 625-662 exhibits excellent ESCR, low temperature impact strength and warp resistance. It is UV-stabilized and available in a 35-mesh powders MICROTHENE® MP 625-662.

Other Information
UV Stabilized.

This product is from the former Equistar product line.

Vendors: No vendors are listed for this material. Please click here if you are a supplier and would like information on how to add your listing to this material.

Physical Properties	Metric	English	Comments
Density	0.935 g/cc	0.0338 lb/in³	Compression molded; ASTM D1505
ESCR 100% Igepal®	>= 1000 hour @Thickness 3.17 mm	>= 1000 hour @Thickness 0.125 in	Rotomolded, F_{50}; ASTM D1693
ESCR 10% Igepal®	350 hour @Thickness 3.17 mm	350 hour @Thickness 0.125 in	Rotomolded, F_{50}; ASTM D1693
Melt Flow	5.0 g/10 min	5.0 g/10 min	190/2.16; Pellets; ASTM D1238

Mechanical Properties	Metric	English	Comments
Tensile Strength, Yield	17.2 MPa @Thickness 3.17 mm	2490 psi @Thickness 0.125 in	2"/min, Rotomolded; ASTM D638
Flexural Modulus	0.601 GPa @Thickness 3.17 mm	87.2 ksi @Thickness 0.125 in	1% Secant, Rotomolded; ASTM D790
Impact Test	61.0 J @Thickness 3.17 mm, Temperature -40.0 °C	45.0 ft-lb @Thickness 0.125 in, Temperature -40.0 °F	Rotomolded; ARM STD
	203 J @Thickness 6.35 mm, Temperature -40.0 °C	150 ft-lb @Thickness 0.250 in, Temperature -40.0 °F	Rotomolded; ARM STD

Thermal Properties	Metric	English	Comments
Deflection Temperature at 0.46 MPa (66 psi)	52.0 °C @Thickness 3.17 mm	126 °F @Thickness 0.125 in	Rotomolded; ASTM D648
Deflection Temperature at 1.8 MPa (264 psi)	39.0 °C @Thickness 3.17 mm	102 °F @Thickness 0.125 in	Rotomolded; ASTM D648

B7. Data sheet for Celogen OT™.

CELOGEN® OT for Plastics

Low-Temperature Chemical Foaming Agent

CELOGEN OT is a low-temperature foaming agent suitable for operating temperatures of 300-350°F (149-177°C). It is recommended for rubber, LDPE, EVA, and soft vinyl compounds. It generates a polymeric, non-polar residue that does not interfere with electrical properties in wire insulation applications. Process temperatures should not exceed 350°F (177°C) when using CELOGEN OT. Materials such as triethanolamine and urea are strong decomposition activators. Zinc oxide and similar materials provide moderate to weak activation. CELOGEN OT is oil-treated to reduce dustiness. It has three FDA sanctions for use in food-contact applications.

- **Product Description**

Chemical Composition:	p,p'-oxybis(benzenesulfonylhydrazide)
Appearance:	White to off-white powder
Decomposition Point:	320°F (160°C)
Gas Yield:	125 cc/g
Gas Composition:	Nitrogen, steam
Specific Gravity:	1.55
Bulk Density:	31 lbs./cu.ft. (496 kg/m^3)

- **Solubility**

Soluble with reaction in ketones; very soluble in DMSO and DMF; moderately soluble in ethanol and polyalkylene glycols; insoluble in benzene, ethylene dichloride and water.

- **Storage Stability**

Good under normal conditions.

- **Flammability**

This product will burn rapidly when ignited. It should be stored in a cool, dry place away from hot steam pipes, free flames, direct sunlight, and any source of static or spark.

B8. Data Sheet for magnesium silicate.

SAFETY DATA SHEET

Version 6.1
Revision Date 15.04.2019
Print Date 20.10.2019

SECTION 1: Identification of the substance/mixture and of the company/undertaking

1.1 Product identifiers

Product name : Talc

Product Number : 86257
Brand : Sigma-Aldrich
CAS-No. : 14807-96-6

1.2 Relevant identified uses of the substance or mixture and uses advised against

Identified uses : Laboratory chemicals, Synthesis of substances

1.3 Details of the supplier of the safety data sheet

Company : SIGMA-ALDRICH CANADA CO.
2149 WINSTON PARK DRIVE
OAKVILLE ON L6H 6J8
CANADA

Telephone : +1 905 829-9500
Fax : +1 905 829-9292

1.4 Emergency telephone number

Emergency Phone # : +1-703-527-3887 (CHEMTREC)

SECTION 2: Hazards identification

2.1 Classification of the substance or mixture

Not a hazardous substance or mixture.

2.2 GHS Label elements, including precautionary statements

Not a hazardous substance or mixture.

2.3 Hazards not otherwise classified (HNOC) or not covered by GHS - none

SECTION 3: Composition/information on ingredients

3.1 Substances

Synonyms : Hydrous magnesium silicate
Talcum

Formula : $H_2Mg_3O_{12}Si_4$
Molecular weight : 379.27 g/mol